UNIVERSITY OF SOUTHAMPTON

Methods to Assess CSF Dynamics and the Mechanical Properties of the Cerebral Mantel in Hydrocephalus

Helen Eleri Whitehouse

Doctor of Philosophy

Institute of Sound and Vibration Research, University of Southampton and the Department of Academic Neurosurgery, University of Cambridge

April 1999

UNIVERSITY OF SOUTHAMPTON

ABSTRACT

FACULTY OF ENGINEERING

INSTITUTE OF SOUND AND VIBRATION RESEARCH

Doctor of Philosophy

Methods to Assess CSF Dynamics and the Mechanical Properties of the Cerebral Mantel in Hydrocephalus

by Helen Eleri Whitehouse

This thesis describes the use of modern engineering and computational techniques to investigate the complex biomechanical relationships between the main cerebral components in normal pressure hydrocephalus and other complex disorders of cerebrospinal fluid (CSF) circulation.

CSF infusion tests and overnight intracranial pressure (ICP) monitoring were combined with simultaneous transcranial Doppler ultrasongoraphy (TCD) to investigate the relationship between CSF dynamics and cerebral haemodynamics. ICP increases induced during CSF infusion studies, provoked an increase in the pulsatility of the haemodynamic waveform. As the increase was significantly greater in patients with increased resistance to CSF outflow TCD may be used to enhance or replace ICP monitoring during CSF infusion studies. Overnight ICP and TCD monitoring demonstrated that haemodynamic fluctuations are the driver for hydrodynamic B waves seen in some hydrocephalic patients during sleep. This study also demonstrated that the transmission of haemodynamic fluctuation to the CSF is dependent on changes in compliance of the cerebral mantle.

The relationship between increased CSF volume and the properties of the cerebral mantle was explored using image analysis and mathematical modeling. An innovative technique was developed for the quantitative assessment of hyperintensities on magnetic resonance images. The results from this study demonstrated that patients with minimal disruption to the brain tissue are more likely to improve with insertion of a CSF shunt. A finite element model was established to investigate the stress-strain relationship in the brain tissue as CSF volume increases. The tissue changes simulated in the model correlated well with the pathopyhsiological and anatomical changes seen in hydrocephalus, providing insight into the possible biomechanical process that may produce these changes.

TABLE OF CONTENTS

Chapter 1:

BACKGROUND AND AIMS

Chapter 2:

A STUDY OF TRANSCRANIAL DOPPLER FLOW VELOCITY DURING LUMBAR CEREBROSPINAL FLUID INFUSION TESTS

ACKNOWLEDGMENTS

I would like to thank all the academic and clinical staff in the Department of Academic Neurosurgery, University of Cambridge, for their support. In particular Dr Marek Czosnyka for his help and support relating to the hydrodynamic studies and Dr Hugh Richards for performing the surgery described in Appendix 1 and providing statistical advice.

I would also express my gratitude to:

Dr Malcolm Bolton and Dr Alonso Pena from the Department of Engineering, University of Cambridge, for their advice regarding the production of the finite element model described in Chapter 6

Dr Wilkinson formally of the Applied Psychology Unit, University of Cambridge, for help in setting up the sleep laboratory and advice regarding sleep scoring techniques.

Finally I would like to express my sincere appreciation to my supervisors Professor Maurice Petyt, Institute of Sound and Vibration Research, University of Southampton and Professor John Pickard, Department of Academic Neurosurgery, University of Cambridge, for their guidance and encouragement.

ABBREVIATIONS AND DEFINITIONS

Abbreviations and definitions in alphabetical order for each chapter.

Chapter 1

BIH	Benign intracranial hypertension
CSF	Cerebrospinal Fluid
CT	Computerised tomography
ICP	Intracranial pressure
MRI	Magnetic resonance image
NPH	Normal pressure hydrocephalus
R_{csf}	Resistance to CSF outflow
TCD	Transcranial Doppler ultrasonography

Chapter 2

ABP	Arterial blood pressure
AMP	Fundamental component of the pressure pulse wave
C_{out}	Conductance to CSF outflow
CPP	Cerebral perfusion pressure
CSF	Cerebrospinal Fluid
CT	Computerised tomography
CVR	Cerebrovascular resistance
FV	Cerebral blood flow velocity
FVa	The amplitude of the flow velocity pulse wave
FVd	Cerebral blood flow velocity diastolic
FVs	Cerebral blood flow velocity systolic
ICP	Intracranial pressure
ICP_b	Baseline ICP
NPH	Normal pressure hydrocephalus
MAP	Mean arterial pressure

PI	Goslings pulsatility index
PI_b	Baseline pulsatility index
PVI	Pressure volume index
R_{csf}	Resistance to CSF outflow
RI	Resistive index
SJO_2	Jugular oxygen saturation
TCD	Transcranial Doppler ultrasonography
V_{abs}	Volume of CSF absorbed
V_{in}	Infusion rate
V_{out}	Surplus CSF volume

Chapter 3

CSF	Cerebrospinal fluid
EEG	Electroencephalography
EEGf	Power of EEG fast waves
EEGs	Power of EEG slow waves
EMG	Electromyogram
EOG	Electro-oculogram
FFT	Fast fourier transform
FV	Cerebral blood flow velocity
ICP	Intracranial pressure
LEs	Power of slow waves in left eye channel
NPH	Normal pressure hydrocephalus
NREM	Non rapid eye movement sleep
REM	Rapid eye movement sleep
REMS	Rapid eye movements
REs	Power of slow waves in right eye channel
TCD	Transcranial Doppler ultrasonography

Chapter 4

ABP	Arterial blood pressure
AMP	Is the fundamental component of the ICP pulse wave
BIH	Benign intracranial hypertension
CSF	Cerebrospinal fluid
CT	Computer tomography
EEG	Electroencephalography
FVa	Amplitude of cerebral blood flow velocity waveform
FV_{Bwave}	Amplitude of B waves in the TCD signal
ICP	Intracranial pressure
ICP_{Bwave}	Amplitude of B waves in the ICP signal
ICP_{open}	The initial ICP recorded before fluid infusion
MRI	Magnetic resonance imaging
NPH	Normal pressure hydrocephalus
PI	Goslings pulsatility index
PVI	Pressure/volume index
R_{csf}	Resistance to CSF absorption
REM	Rapid eye movement sleep
TCD	Transcranial Doppler ultrasonography

Chapter 5

CSF	Cerebrospinal fluid
CT	Computerised tomography
DWML	Deep white matter lesions
MRI	Magnetic resonance image
NPH	Normal pressure hydrocephalus
PVH	Peri-ventricular hyperintensities
tiff	Tagged image file format

Chapter 6

$\frac{\partial \varepsilon_v}{\partial t}$	Rate of volumetric strain.
υ	Poisson's ratio
σ	Normal stress
τ	Shear stress
ε	Normal strain
γ	Shear strain.
σ'	Effective normal stress
CT	Computed tomography
γ_w	Bulk modulus
CSF	Cerebrospinal fluid
E	Young's modulus.
FEM	Finite element method
GPD	Geometry program
i	Hydraulic gradient
k	Coefficient of permeability
K	Bulk modulus
MPD	Main program
MRI	Magnetic resonance image
Pv	Intraventricular CSF pressure
u	Displacements in the x direction
U_w	Fluid pressure
V	Flow rate per unit area
v	Displacements in the y direction

Chapter 7

CSF	Cerebrospinal Fluid
ICP	Intracranial pressure

MRI	Magnetic resonance image
NPH	Normal pressure hydrocephalus
PI	Goslings pulsatility index
R_{csf}	Resistance to CSF outflow
TCD	Transcranial Doppler ultrasonography

Appendix 1

ABP	Arterial blood pressure
CBF	cerebral blood flow
CPP	Cerebral perfusion pressure
CSF	Cerebrospinal Fluid
CVR	Cerebrovascular resistance
FV	Cerebral blood flow velocity
FVa	The amplitude of the flow velocity pulse wave
FVd	Cerebral blood flow velocity diastolic
FVs	Cerebral blood flow velocity systolic
ICP	Intracranial pressure
LDF	laser Doppler flowmetry
MCA	middle cerebral artery
NPH	Normal pressure hydrocephalus
PI	Goslings pulsatility index
R_{csf}	Resistance to CSF outflow
TCD	Transcranial Doppler ultrasonography

Appendix 2

p	Acoustic pressure of the ultrasound beam
α	Coefficient of ultrasonic energy absorption
ρc	Characteristic of acoustic impedance of the ultrasound beam
d	Diameter of the ultrasound beam

f	Percentage of ultrasound energy absorbed
I	Time averaged intensity of ultrasound beam
i	Intensity of the ultrasound beam
K	Thermal conductivity
p_0	Pressure amplitude of the ultrasound beam
qv	Heat production rate per unit volume,
SAPA	Spatial - average pulse- average intensity. Of the ultrasound beam
SATA	Spatial - average temporal - average intensity of the ultrasound beam
SPPA	Spatial - peak pulse- average intensity of the ultrasound beam
SPTA	Spatial - peak temporal - average intensity of the ultrasound beam
SPTP	Spatial - peak temporal - peak intensity of the ultrasound beam
TCD	Transcranial Doppler ultrasonography
Tdif	Bone temperature
Tref	Reference temperature
W	Total Power of ultrasound beam

CHAPTER 1

BACKGROUND AND AIMS

BACKGROUND AND AIMS

1. INTRODUCTION

Hydrocephalus is one of the most common neurological disorders requiring neurosurgical intervention [1]. It is defined as an increase in cerebrospinal fluid (CSF) volume which may result from increased CSF secretion, decreased CSF absorption or an obstruction within the CSF pathways. Acute hydrocephalus is often reversible resulting in no neurological deficit implying that excess fluid may be accommodated in the extended ventricles without inducing ischaemia, tissue degeneration or other permanent changes, provided the CSF is diverted early. However there are more chronic forms of CSF disturbance where effects are not so readily reversible.

In adults the rigid skull maintains a constant intracranial volume, therefore reciprocal changes must occur in the brain tissue (cerebral mantle), cerebral blood volume or subarachnoid CSF to compensate for increased ventricular CSF volume. In more complex disturbances of the CSF circulation, the interaction between the main intracranial components is not fully understood.

The studies described in this thesis focus on methods to assess the effects of increased CSF volume on CSF hydrodynamics, cerebral haemodynamics and cerebral mantle in patients with complex disorders of CSF circulation.

2. BACKGROUND

2.1 Physiology of CSF

CSF is found within the ventricular cavities and the subarachnoid space and acts as a buoyancy support for the brain and spinal cord, cushioning the nervous tissue and bone, to prevent mechanical trauma. The bulk of CSF (80%) is formed by active secretion by the choroid plexus within the ventricles [2,3]. The remaining extrachoroidal CSF begins as interstitial fluid that is produced at the brain endothelium and seeps through the brain tissue

in to the ventricles via the ependyma [4] or into the subarachnoid space via the pia membrane. In man the CSF volume is approximately 140ml. As CSF is secreted at a rate of 0.35ml every minute [5] there is a total renewal of fluid every 5-7 hours. CSF slowly circulates through the ventricular system, subarachnoid space and over the cerebellum and is absorbed into the venous system by the arachnoid villi that project into the dural venous sinus [6].

2.2 Pathophysiology of Hydrocephalus

In acute experimental hydrocephalus induced by the injection of kaolin to obstruct CSF flow, ventricular dilation is seen within hours, as the resistance to CSF outflow and intracranial pressure (ICP) increases. As the ventricles enlarge the reserve capacity of the venous system and CSF spaces reduces and the ependymal cells become stretched and flattened to match the increase in the surface area of the ventricles. The ependyma may or may not become disrupted depending on the degree of ventriculomegaly and the rate of dilatation [7,8,9,10]. Computed tomography (CT) and magnetic resonance imaging (MRI) studies have demonstrated that CSF accumulates in the subependymal white matter [11,12], as the result of either the reversal of fluid flow across the ependyma or the accumulation of interstitial fluid that can no longer drain into the ventricles. As the hydrocephalus becomes chronic the periventricular tissue may become gliotic and scarred. White matter demyelination and axonal degeneration may also be features of the hydrocephalic brain [13,14]. Early treatment may prevent these white matter changes [15].

2.3 Treatment of Hydrocephalus

Hydrocephalus is usually treated by the surgical insertion of a CSF shunt. This is a mechanical device which provides an additional route through which CSF may flow, effectively reducing the resistance to CSF outflow. A less common treatment is a third ventricolostomy, where free communication between the third ventricle and the cisterna interpeduncularis is surgically established.

3. RATIONALE

Although some cases of hydrocephalus with known aetiology, and obvious symptomology may be simple to diagnose and treat, difficulties are encountered with some patient groups. The studies described in this thesis focus primarily on patients with normal pressure hydrocephalus (NPH) and other patients with complex disorders of the CSF circulation.

3.1 Normal pressure hydrocephalus

Normal pressure hydrocephalus was first described by Hakim and Adams in 1965 [16]. They described a clinical triad of gait disturbance, dementia and urinary incontinence, occurring in this order. Gait disorder may range from mild disturbances to complete inability to walk or stand. Mental symptoms include the slowing of thoughts, actions and forgetfulness especially effecting the recent memory. Incontinence is usually of urine and is present only when gait and mentation are disturbed.

Ventricular enlargement is seen on CT or MRI, however at lumbar puncture ICP appears normal. This paradox was addressed by Hakim and Adams who proposed that a period of increased CSF pressure initially produced ventricular dilation, increasing the surface area of the ventricular walls. As force is the product of pressure and surface area, a given CSF pressure would produce a greater force if applied over an increased area. This explanation is probably an over simplification, and numerous other theories have been proposed [17,18], however, the pathophysiology remains unclear.

Normal pressure hydrocephalus is primarily a disease of the elderly and accounts for 0-6% of all cases of dementia [19]. It can occur following subarachnoid haemorrhage, head injury, intracranial surgery or infection, however, up to 50% of cases are idiopathic [20,21]. A literature review demonstrated that 50-70% of patients with NPH of known aetiology improved with shunting, however, only 10-39% of those with idiopathic NPH demonstrated significant improvement [22, 23]. Comparing these success rates with a 30-50% rate of post

surgical complications and a 1-12% morbidity rate [22,24,25] demonstrates the importance of differential diagnosis.

Assessment of signs and symptoms demonstrated that patients are more likely to improve if they have a short clinical history and gait disturbance precedes impaired mentation [25, 26, 27]. Gjerris et al suggested that patients who demonstrate the triad of symptoms, have known aetiology and short history, should be considered for shunting without further diagnostic tests [28]. However, many patients do not fall in to this category and further investigations are required. A battery of diagnostic tests has evolved to investigate markers which may predict favorable outcome with shunting. These investigations primarily focus on the assessment on CSF hydrodynamics, cerebral blood volume or neuroimaging, however, as yet no definitive diagnostic criteria exist. This is partly because the pathophysiology of this chronic condition is not fully understood and the relationship between the intracranial components have not been established. Consequently, the complex biomechanical interdependencies between CSF, cerebral blood flow and brain tissue remains one of the most important questions in hydrocephalus research.

3.2 Patients with other Complex Disorders of the CSF Circulation

Although the emphasis of this thesis is placed on chronic normal pressure hydrocephalus in the elderly, disorders such as benign intracranial hypertension (BIH) and suspected shunt malfunction with normal ICP are difficult to diagnose and are also included.

BIH is an uncommon disorder, characterised by numerous symptoms including headache, visual disturbance, diplopia, intracranial noises, photopsia and nausea and vomiting [29]. Common signs are papilloedema with visual loss and VIth nerve palsies. The causes and pathophysiology of BIH remain unclear, however, it is primarily associated with obesity and recent weight gain. Diagnostic tests include neuroimaging, to exclude arteriovenous malformations and abnormalities of venous drainage, haematology assessments to exclude myeloproliferative or lymphoproliferative disorders, and CSF hydrodynamic studies. In

typical BIH cases ICP is increased at lumbar puncture, however, the ventricles are normal or reduced in size. In exceptional cases, where ICP is unexpectedly normal, assessment of CSF hydrodynamics may be useful. BIH is self limiting, however, treatment may include serial lumbar punctures, diuretics and corticosteroids. Surgical subtemporal decompression or insertion of a CSF shunt is performed in exceptional cases where vision is deteriorating on referral or drug therapy has not been successful.

A further group considered in this thesis are patients with suspected CSF shunt malfunction. Post-surgical complications following the insertion of a CSF shunt are common in all patient groups. The rate of shunt failure is between 20-30% during the first year after implantation and subsequently continues at a rate of 5% per year [30]. Often shunt function deteriorates over a period of time and therefore is not characterised by a rapid onset of clinical symptoms. In cases where shunt blockage or overdrainage is suspected assessment of CSF hydrodynamics is useful.

4. AIMS

The aim of this thesis was to use modern engineering and computational techniques to investigate the complex biomechanical interrelationship between CSF dynamics and cerebral haemodynamics and CSF volume and the cerebral mantle.

The studies described in this thesis explore the 'dynamic' and 'static' biomechanical interdependencies between the main intracranial components. The physical properties of CSF and blood within the cranial vault may change rapidly (within seconds) and are therefore considered to be 'dynamic' parameters. As hydrocephalus is associated with abnormal CSF hydrodynamics it is probable that cerebral haemodynamics are also disrupted, but this relationship has not been explored. Increases in CSF volume may also affect the physical properties of brain tissue. These changes occur more slowly, over days, weeks or even years, therefore these parameters are considered to be 'static'. Anatomical changes may be

investigated using neuroimaging techniques, but this does not provide information on the biomechanical changes occurring within the cerebral mantle.

Engineering and computational techniques were used to address the following questions regarding CSF dynamics and cerebral haemodynamics:

- Are changes in CSF dynamics related to changes in cerebral haemodynamics and/or vice versa?
- Is the relationship between CSF hydrodynamics and cerebral haemodynamics the same in all patients?
- Can the information provided by non-invasive haemodynamic measurements enhance or replace invasive hydrodynamic assessments?

The following questions regarding CSF volume and the cerebral mantle were addressed using image analysis and mathematical modeling:

- What is the stress-strain relationship in the cerebral mantle when CSF volume increases?
- Does the distribution of stresses and strains reflect anatomical changes observed with neuroimaging?
- Is the degree of white matter damage revealed using MRI a good predictive marker of outcome after shunting?

5. SUMMARY AND AIMS OF EACH STUDY PERFORMED

This thesis has been divided into chapters, each describes a stand-alone study. Chapters 2, 3 and 4 investigate the relationship between CSF hydrodynamics and cerebral haemodynamics. Chapters 5 and 6 investigate the changes in the cerebral mantle during hydrocephalus.

Chapter 2 combines two established techniques, CSF infusion studies and transcranial Doppler ultrasonography (TCD). CSF infusion studies are an accepted means of determining CSF hydrodynamics in hydrocephalus with normal pressure. The addition of TCD allowed cerebral blood flow velocity to be assessed during controlled ICP increases. The specific questions addressed in this study were:

- Are haemodynamic parameters indicative of ICP?
- Do cerebral haemodynamic parameters change in response to increasing ICP during CSF infusion tests?
- Is haemodynamic behavior during CSF infusion tests different in patients with normal and increased resistance to CSF outflow (R_{csf})?
- Is there potential for TCD to replace direct ICP measurement during CSF infusion studies providing a non-invasive method for the assessment of R_{csf}?

Chapter 3 describes the use of TCD to assess and quantify the physiological haemodynamic changes during sleep in normal volunteers. These results were then compared to overnight ICP and TCD recordings in patients with hydrocephalus in chapter 4.

Chapter 4 describes two clinical studies. The first study used TCD during routine overnight ICP monitoring allowing prolonged simultaneous recording of cerebral haemodynamic and CSF hydrodynamic changes during sleep. The second study compared the relationship between B wave activity recorded during overnight ICP monitoring and CSF hydrodynamic parameters. The aims of these studies were to provide further understanding of the pathophysiology of B wave activity and address the following questions:

- Are B wave type haemodynamic fluctuations demonstrated with TCD in patients with complex disorders of the CSF circulation?
- Are the properties of the haemodynamic B waves observed in normal volunteers different to those observed in the patient group?

- What are the pathophysiological conditions required for haemodynamic B waves to be transmitted to the CSF?
- Could non-invasive TCD monitoring enhance or replace invasive ICP monitoring?

Chapter 5 presents a new quantitative approach to the assessment of magnetic resonance images. The aim of this study was to quantify white matter changes on a series of magnetic resonance images from patients with suspected NPH and address the following questions:

- Does the quantified area of white matter hyperintensities relate to outcome after shunting?
- Is the location of the white matter changes related to outcome?
- Does this data provide evidence to support the 'watershed' zone theory for the position of the deep white matter hyperintensities?

Chapter 6 describes the development of a innovative two dimensional finite element model to determine the distribution of stress and strain in the cerebral mantle during hydrocephalus.

CHAPTER 2

A STUDY OF TRANSCRANIAL DOPPLER FLOW VELOCITY DURING LUMBAR CEREBROSPINAL FLUID INFUSION TESTS

A STUDY OF TRANSCRANIAL DOPPLER FLOW VELOCITY DURING LUMBAR CEREBROSPINAL FLUID INFUSION TESTS

1. INTRODUCTION

The low incidence of normal pressure hydrocephalus (NPH) amongst elderly patients with ventriculomegaly, necessitates rigorous patient selection to ensure the possibility of benefit for the few is not outweighed by the risk of intervention for the majority. It is important that patients with a high probability of improvement are treated and those with other disorders are not exposed to the short and long term perils of shunt surgery. In patients with the characteristic triad of symptoms with known aetiology, up to 70% of patients may improve after shunting. Results in the idiopathic group varies from 10-39% [1] depending on the severity of the selection process. Commonly associated risks are shunt malfunction requiring revision or removal, infection and subdural haematoma [2, 3].

Publications suggest various clinical and diagnostic protocols for patient selection, but some means of cerebrospinal fluid (CSF) hydrodynamic assessment is usually recommended. Although typically patients have no signs or symptoms suggestive of raised intracranial pressure (ICP) and have normal CSF pressure at lumbar puncture, an increase in resistance to CSF outflow (R_{csf}) produced by the obstruction of CSF circulation or impairment of CSF absorption is usually seen. An implanted shunt provides an alternative route for CSF outflow, effectively lowering outflow resistance.

The value of these tests has been clearly demonstrated, however, the extent to which they are used in routine clinical practice is lower than the quantity of publications may suggest [4]. One of the reasons for this is that the techniques to measure CSF hydrodynamic parameters (discussed in detail later in this chapter) are usually invasive, requiring intrathecal access. As with all invasive diagnostic techniques, it is desirable to maximise the clinical information acquired. In this study non-invasive transcranial Doppler ultrasonography (TCD) was performed during CSF infusion studies allowing haemodynamic changes to be assessed during increasing ICP.

TCD has been applied to hydrocephalus research in the past, exploiting the mutual dependence between intracranial pressure, blood volumes and cerebral haemodynamics in an attempt to measure ICP non-invasively. These studies, discussed later in this chapter, have had limited success. This study was performed to explore the clinical potential of TCD parameters recorded during increasing ICP induced by CSF infusion.

The assessment of CSF hydrodynamic parameters is also useful in the assessment of shunt malfunction. In this study a group of patients with suspected NPH or shunt malfunction were investigated.

1.1 Aims

The aims of this study were to assess whether:

- haemodynamic parameters (measured using TCD) are indicative of ICP
- cerebral haemodynamic parameters change in response to increasing ICP during infusion
- haemodynamic behaviour during infusion is different in patients with normal and increased R_{csf}.
- there is potential for TCD to replace direct ICP measurement during CSF infusion studies. This may provide a less invasive one needle infusion test, or if a non-invasive method of raising ICP were available, a completely non-invasive method to assess R_{csf}.

2. TECHNIQUES AVAILABLE FOR THE ASSESSMENT OF R_{CSF}

The measurement of R_{csf} in patients was first introduced by Katzman and Hussey in 1970 [5] and has subsequently become a feature of many assessment protocols. Two techniques may be used in the clinic to quantify R_{csf}: Infusion tests [5,6] and bolus injections [6,7].

2.1 Infusion tests

Infusion tests are performed by measuring intracranial pressure during infusion of mock CSF, Ringer's lactate or saline. The test can be performed using constant pressure, lumboventricular perfusion or constant infusion rate. Although these techniques vary in complexity the basic principles and assumptions are the same. R_{csf} is calculated as the reciprocal of the gradient of the flow rate (infusion rate) versus ICP regression curve. This assumes that the CSF production rate and blood volumes are constant.

2.1.1 Constant Pressure Infusion Tests

Constant pressure infusion tests were first described by Davson et al [8] and have been developed by Ekstedt [9] and Portnoy and Croissant [10]. Following 12 hours bed rest two lumbar needles are inserted which are connected to a pressure transducer and a servo-controlled infusion pump. Mock CSF is then infused at a series of constant pressures and the resultant flows measured. This technique allows the assessment of R_{csf}, sagittal sinus pressure and the pressure/volume relationship, however it is time consuming and technically complex.

2.1.2 Lumboventricular Perfusion Tests

Lumboventricular perfusion tests may be performed using 3 different techniques:

(i) Lumboventricular: pressure measurement and fluid removal is via a ventricular cannula. Infusion is via a lumbar cannula.

(ii) Ventricular: pressure measurement, fluid removal and infusion are all via the ventricular route.

(iii) Lumbar: pressure measurement, fluid removal and infusion are all via the lumbar route.

These techniques are based on the same principles [11,12,13]. For the lumboventricular technique a cannula is inserted into the lateral ventricle via a burr hole and connected to a pressure monitor. ICP is monitored for 24 hours and a baseline level found. During a constant rate lumbar infusion the cannula end which is open to the atmosphere, is elevated in small steps to change ICP. The surplus CSF volume is measured for each pressure step. The volume of CSF absorbed (V_{abs}) is calculated using the equation

$V_{abs} = V_{in} + 0.4 - V_{out}$, where V_{in} is the infusion rate, 0.4 is the presumed rate of CSF production (ml/min) and V_{out} is the surplus volume. R_{csf} is calculated from the linear regression of ICP and V_{abs}. For the ventricular infusion method [12] a ventricular infusion is performed after the baseline ICP has been determined. For the lumbar infusion method the pressure monitor is connected to the same lumbar cannula as the infusion pump [13]. A baseline value is recorded for 30 minutes before the position of the lateral ventricular cannula is changed.

2.1.3 Constant Rate Infusion Tests

Constant rate infusion tests first described by Katzman and Hussey [5] are quick and simple to perform. ICP is monitored during a constant rate infusion until equilibrium is reached. A defined criteria allows the curves of pressure versus time to be classified as normal or abnormal. This technique has been developed further by Czosnyka et al [14,15] using computer analysis of the ICP signal. The computerised infusion test provides a quick, simple and reliable technique to determine hydrodynamic parameters including R_{csf}, pressure volume index (PVI), baseline ICP and CSF formation rate. R_{csf} is calculated as the total increase in pressure divided by the infusion rate (mmHg/ml/min). The pressure volume index can be defined as the volume necessary to increase the ICP by a factor of 10 and is an indicator of brain compliance. It is calculated from the increase in volume, ICP at baseline and at the end of infusion and a reference ICP. The reference pressure is taken as the point at which the ICP-AMP (AMP is the fundamental component of the ICP pulse wave) regression line crosses the ICP axis. The CSF formation rate is calculated from R_{csf}, baseline ICP and the reference pressure.

Critical evaluation of the infusion techniques highlights the clinical problems and the reliability and reproducibility of results for each technique. A problem which may affect all techniques is fluid leakage which underestimates R_{csf}. The lumboventricular perfusion test can be performed quickly and gives reliable and reproducible results [11,16] but requires a frontal burr hole which increases the risk of infection, epilepsy and haemorrhage, albeit only slightly. The constant pressure servo-controlled test is complicated, requiring sophisticated equipment and the results from the ordinary constant rate infusion test are difficult to interpret [11]. Børgesen et al [17] compared the result of

lumboventricular perfusion with the computerised infusion tests [14] in 15 patients. They found that the R_{csf} values measured for each patient did not differ for the two techniques. They therefore concluded that the computerised infusion test offers an accurate and reliable means for the assessment of R_{csf} which is quick, simple and less invasive than lumboventricular perfusion. This is the technique chosen for this study and it will be described in further detail in section 5.

2.2 Bolus Injection

Although R_{csf} can be estimated quickly using the bolus injection test first described and evaluated by Marmarou et al in 1978 [7], the principle is based on complex mathematics. A small volume is rapidly injected into the intrathecal cavity producing an immediate increase in ICP. A rapid rate of injection is required to ensure that a minimal amount of injected fluid is reabsorbed during the procedure. The bolus injection induces a sudden increase in pressure which is then followed by a gradual decrease in pressure. The initial increase in ICP is dependent on the compliance of the system, and the rate of decrease is dependent on compliance and outflow resistance. The correlation between the increase in volume and the resulting pressure rise is the pressure volume index. This value is calculated from the gradient of the bolus volume versus log ICP curve. R_{csf} is calculated from the change in pressure, the bolus volume and the pressure volume index. Comparison of the bolus injection test with other techniques [18] has demonstrated that R_{csf} is underestimated using bolus injections when compared to infusion tests.

3. THE PREDICTIVE VALUE OF R_{CSF}

Although there are many publications relating to R_{csf} measurement in NPH, the predictive value of CSF infusion tests is still somewhat confused. Børgesen and Gjerris [16] investigated 80 patients who met rigorous inclusion criteria for NPH. All patients demonstrated the typical triad of symptoms, dilated ventricles and a resting ICP of <12mmHg with no plateau waves during long term monitoring. Further criteria were that the history should not exceed 3 months and there should be no signs of cerebral infarction or tumour on computed tomogrphy (CT) scan. Sixty four patients with conductance to CSF outflow ($C_{out}=1/R_{csf}$) less than 0.12ml/min/mmHg (assessed using the

lumboventricular perfusion technique) were shunted. Comparison of C_{out} with outcome after shunting demonstrated a significant correlation between C_{out} below 0.08ml/min/mmHg and improvement after surgery. Forty nine out of a total of 51 with C_{out} below 0.08ml/min/mmHg improved after shunting demonstrating a predictive value of 96% (confidence intervals 66%-100%). Unfortunately not all groups have reported such promising results [19,20]. Vorstup et al [21] investigated a group of 17 patients and found a predictive value for C_{out} of 57% (confidence intervals 29%-82%). This was thought to be due the idiopathic nature of the disease in the patients assessed. Vanesste et al [22] questioned the use of ancillary tests and assessed the predictive value of combined clinical and CT data on which many clinicians still rely. The use of C_{out} increased the diagnostic predictive power by an additional 8%. The main advantage of measuring C_{out} would have been to avoid missed improvements in 10% of the patients. Although the power of this procedure appears to be user and selection criteria dependent, a more recent study using the computerised lumbar infusion test reiterated that R_{csf} it is the best predictor for outcome after shunting [23]. Maksymowicz et al [23] conducted a prospective study of 102 patients with suspected hydrocephalus to determine which diagnostic factors gave the best prediction of outcome after surgery. All patients underwent a selection protocol including neurological and psychological examinations, CT scan, CSF pressure monitoring and lumbar CSF infusion tests. All patients with $R_{csf} >$ 8mmHg/ml/min or resting CSF pressure > 15mmHg were shunted. The most important factors for good outcome were increased R_{csf}, increased resting CSF pressure, short history and known aetiology. More recently constant rate infusion studies in 101 patients with suspected idopathic NPH demonstrated a positive predictive value of 80% in patients with $R_{csf} <$ 18mmHg/ml/min and 90-100% with $R_{csf} \geq$ 18mmHg/ml/min [24].

Although the assessment of CSF hydrodynamics appears to have an important role in the assessment of NPH patients, a study in Holland [4] suggests that these tests are rarely performed in clinical practice. Thirty three neurologists and thirteen neurosurgeons were interviewed to determine disparities in the diagnostic procedure for NPH and to assess opinions concerning the clinical value of recently described ancillary tests. The most commonly used diagnostic tools were the CSF tap test (n=36), neuropsychological tests (n=30) and isotope cisternography (n=23). Only four of those questioned performed

lumbar infusion studies on a routine basis. When asked whether they would consider CSF infusion tests provided that sufficient time and technical facilities were available, only six responded positively. Reluctance to use these tests was mainly due to the unfamiliarity, complexity and invasiveness of the tests.

The computerised infusion test provides a quicker and more simple technique than the lumbventricular perfusion test. Although it is also less invasive, two lumbar needles are still required. Given the fragile state of many of these patients, a less invasive one needle technique would be of great benefit.

4. NON-INVASIVE INDICATORS ICP

Non-invasive assessment of ICP has been explored with numerous techniques which exploit the complex interrelationship between ICP and other physiological parameters.

4.1 Ultrasonography

TCD is a non-invasive ultrasound technique for the continuous assessment of cerebral haemodynamics. Although blood flow velocity (FV) cannot be easily be translated into cerebral blood flow volume [25], additional information may be derived from the pulsatility of the haemodynamic waveform.

Studies in laboratory models have demonstrated that the pulsatility of the flow velocity waveform is affected by changes in proximal and distal vascular resistances. Increases in proximal resistance were shown to decrease pulsatility, whereas increases in distal resistance increased pulsatility [26,27]. Clinical ultrasound studies of the peripheral circulation have confirmed that pulsatility increases when distal vascular resistance increases [28]. Although this finding has been applied to the cerebral circulation for the diagnosis of carotid artery stenosis and cerebrovascular disease, unique features of the cerebral circulation may allow further exploitation of this finding.

A close mutual dependence between intracranial pressure, blood volumes and cerebral haemodynamics has been demonstrated [29,30,31,32]. Changes in ICP are reflected in

cerebral perfusion pressure (CPP), according to the equation CPP = arterial blood pressure (ABP) - ICP. In normal healthy humans changes in CPP provoke autoregulatory adjustments of the cerebrovascular resistance (CVR) to maintain cerebral blood flow. Accordingly cerebral blood flow is calculated as CBF = CPP/CVR when autoregulation is in tact. Although the relationship between pulsatility and CVR has not been quantified, it has been suggested that because of the complex interdependencies of CVR and ICP, pulsatility of the flow velocity waveform may indirectly provide information on the CSF hydrodynamics.

Pople [33,34] was one of the first investigators to use TCD in hydrocephalus research. Children with suspected blocked shunts, were assessed using TCD, in an attempt to determine shunt function non-invasively. These investigations were based on the principle that Goslings pulsatility index (PI) is related to CVR and therefore ICP. PI was calculated as:

PI =(flow velocity systolic - flow velocity diastolic)/flow velocity mean

Although a significant correlation between PI and intraventricular pressure was found in a group of 10 patients who underwent TCD examination and invasive ICP monitoring and the test sensitivity was high (97%), specificity was low (56%). Similar problems of low specificity have been encountered by other groups. Chadduck et al [35] measured the percentage resistive index (RI) to evaluate shunt function in hydrocephalic paediatric patients. RI was calculated as:

RI % = (flow velocity systolic - flow velocity diastolic)/(flow velocity systolic x 100)

Sequential studies in individual patients prior to shunt malfunction, at the time of malfunction and post revision demonstrated a significant increase in RI for each individual during shunt malfunction compared to when the child was asymptomatic. However,a non-diagnostic range of RI values of 45-60% was found where patients may have a normally functioning or malfunctioning shunt. More recently, other groups performing studies in hydrocephalic patients have demonstrated similar results [36]. As PI and RI are influenced by heart rate, it has been suggested that the measurement of arterial blood pressure [37] or use of new Doppler indices, may provide a more accurate assessment of ICP [38].

Although ultrasonography may be a useful screening procedure for suspected shunt malfunction and increased ICP, few studies have explored its use in the assessment of CSF hydrodynamics. One study compared TCD cerebral blood flow velocity parameters with CSF hydrodynamic properties in patients with suspected hydrocephalus of various aetiologies [39]. TCD examinations were performed just prior to lumbar infusion and bolus injection tests. A significant correlation between PI and R_{csf}, amplitude of ICP pulsations and opening pressure were found. TCD was not performed during or immediately after the assessment of CSF hydrodynamics to determine the effects of CSF manoeuvres on FV. A study using TCD, pre and post controlled CSF drainage, in patients with NPH demonstrated that the patients who improved following drainage had lower baseline FV compared to those without improvement [40]. However no change in FV in patients who improved was observed. A more informative approach, may have been to monitor FV during the drainage period.

4.2 Audiology

A second non-invasive approach to ICP assessment measures tympanic membrane displacement during reflex movement of the stapes and is based on the principle that ICP is normally transmitted into the perilymph of the cochlear via the cochlear aqueduct [41]. Although useful in the sequential assessment of some hydrocephalic patients [42, 43, 44] dynamic assessment is not permitted and recordings can not be made in elderly patients where the cochlear aqueduct is no longer patent. This technique was not used in this study.

5. CLINICAL MATERIALS AND METHOD.

5.1 Patients

Computerised infusion tests and simultaneous transcranial Doppler studies were performed in 26 patients, 17 males and 9 females with an age range of 25 to 78 years. The patients had either been previously shunted and were assessed for shunt malfunction (n=7), or they had suspected NPH with ventricular enlargement confirmed by CT (n=19). For the majority of patients the decision to shunt or revise a shunt was made on

the basis of the test result. In borderline cases overnight ICP monitoring was also performed.

5.2 Infusion test methodology

The patients were put into a lateral recumbent position with a pillow under the head (figure 1). After local anaesthesia with 1% lignocaine, two 18 gauge lumbar needles were inserted into the subarachnoid space between L3/L4, and L4/L5. Flexible plastic manometer catheters were attached to both needles. The L4/L5 lumbar catheter was connected to an infusion pump with 50ml of sterile 0.9% saline solution. The L3/L4 catheter was connected to a pressure transducer set at the same height as the lumbar needle. The transducer was connected to an amplifier and monitor. The analogue lumbar CSF pressure signal from the amplifier was acquired, converted (with an analogue-to-digital converter) and stored on computer hard disc. The Computerised Infusion Test software [45] was used allowing the pressure time trend and the fundamental component of the pressure pulse wave (AMP) to be plotted on-line, with off-line calculation of R_{csf} and other cerebrospinal compensatory parameters.

Blood flow velocity was measured during the entire infusion test using TCD. The Sci-Med PC Dop equipped with a 2MHz probe was used to insonate the middle cerebral artery via the temporal window. The electronic gain and depth of insonation were adjusted to give a good quality spectrum. During the test, the probe position was maintained using an elasticated head band. The analogue flow velocity maximum and flow velocity mean signals from the TCD were recorded with the ICP signal using the Biomedical Signal Recorder (Zabolotny, Warsaw University of Technology, Poland). The TCD and ICP signals were simultaneously acquired at a frequency of 50Hz.

A constant baseline lumbar pressure measurement was recorded for over 8 minutes before the start of lumbar infusion. The rate of infusion chosen was dependent on the baseline lumbar pressure. For pressures within the normal range ($\leq$ 13mmHg), an infusion rate of 1.5 ml/min (90ml/hr) was selected.

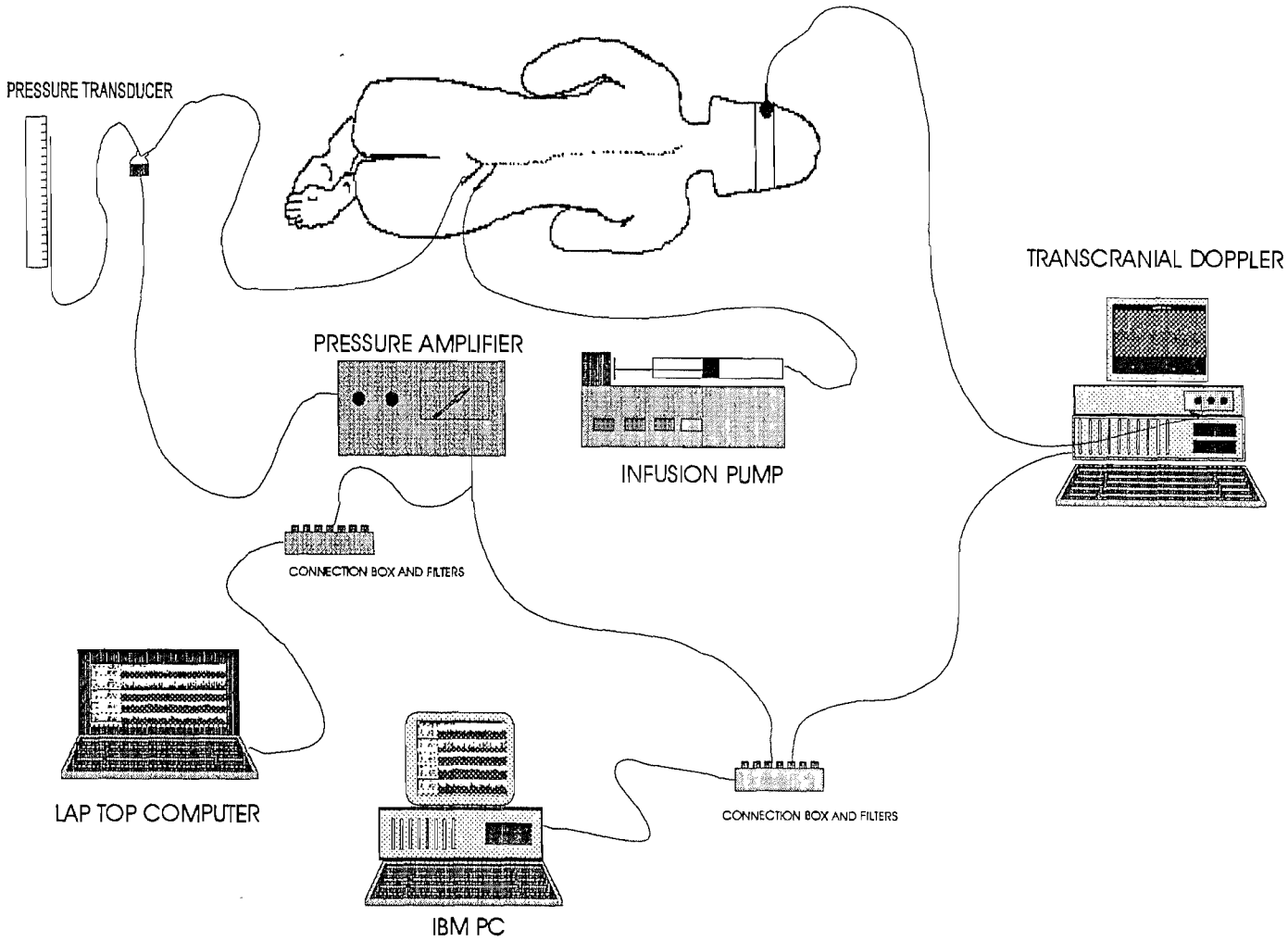

Figure 1: Set-up for infusion tests with TCD recording

For increased pressure, the infusion rate was 1.0 ml/min (60ml/hr). The infusion was continued until a plateau ICP was reached or the ICP exceeded 40 mmHg.

No patients had symptoms of increased ICP. After the infusion the TCD and pressure signals were recorded for a further 10 minutes to analyse the return of the ICP signal to a steady state.

5.3 Data analysis

The ICP signal input to the Computerised Infusion Test Program was analysed on-line every 4 or 8 seconds. During this period the signal was sampled at a frequency of 18Hz and spectrum analysis was performed to calculate the ICP power spectrum and the fundamental component of the pressure pulse amplitude (AMP). Off-line analysis of the ICP signal gave a complete set of cerebrospinal compensatory parameters. The resistance to CSF absorption was calculated as the total increase in pressure divided by the infusion rate (mmHg/ml/min). The pressure volume index was calculated from the increase in volume, ICP at baseline and at the end of infusion and a reference ICP. The reference pressure was taken as the point at which the ICP-AMP regression line crossed the ICP [45].

The TCD and ICP data recorded with the Biomedical Signal Recorder were analysed using the off-line analysis program ICMR (Czosnyka, University of Cambridge). The following TCD wave form parameters were calculated: flow velocity diastolic (FVd), flow velocity systolic (FVs), flow velocity mean time averaged (FV), the amplitude of the flow velocity pulse wave (FVa=FVs-FVd) and Goslings pulsatility index. These TCD parameters were noted for each patient at baseline ICP ($ICP_{baseline}$) and at the plateau ICP during infusion. These data and the computerised infusion test results were imported to the statistics package Statgraphics Plus for analysis. All data are presented as the mean $\pm$ standard deviation.

6. RESULTS

In this group of patients, the mean ICP before lumbar infusion was 10 $\pm$ 4mmHg (range 0mmHg to 18mmHg); the mean R_{csf} was calculated as 11.7 $\pm$ 7.1mmHg/ml/min (range 2.9mmHg/ml/min to 29.0mmHg/ml/min) and the mean PVI was 14.0 $\pm$ 9.0ml (range 8.5ml to 36.0ml). The TCD parameters were determined for each patient at baseline ICP and increased ICP. The mean values are shown in table 1.

TCD parameter (mean)	At baseline ICP	During infusion	p value
FV (cm/s)	50.0 $\pm$ 16	47.0 $\pm$ 16	p<0.0002
FVs(cm/s)	72.8 $\pm$ 19	70.9 $\pm$ 19	p<0.0490
FVd(cm/s)	35.3 $\pm$ 14	31.8 $\pm$ 13	p<0.0004
PI	0.79 $\pm$ 0.23	0.88 $\pm$ 0.25	p<0.0003

Table 1. TCD Parameters at baseline ICP and during the plateau phase of infusion

In all patients an increase in CSF volume during infusion produced a gradual increase in ICP. As ICP increased, FV decreased and the amplitude of the flow velocity pulse wave (FVs-FVd) increased, producing a significant increase in PI (table 1). A regression analysis demonstrated that neither the mean PI nor the percentage change in PI correlated well with baseline ICP ($p < 0.64$). Correlation of the change in PI with increased ICP during infusion was better ($p < 0.0014$), but not as significant as the relationship between percentage change in PI and R_{csf} ($p < 0.0001$). To determine whether the changes in PI were dependent on R_{csf}, the patients were divided into two groups: Group I with normal R_{csf} (R_{csf} < 13mmHg/ml/min) and group II with increased R_{csf} ($R_{csf} \geq$ 13 mmHg/ml/min) [16]. The cerebrospinal compensatory and TCD parameters for the two groups are shown in table 2. FV and baseline PI are not significantly different. If however, a typical simultaneously recorded ICP and TCD trace for each group (figures 2 and 3) were considered certain trends became apparent:

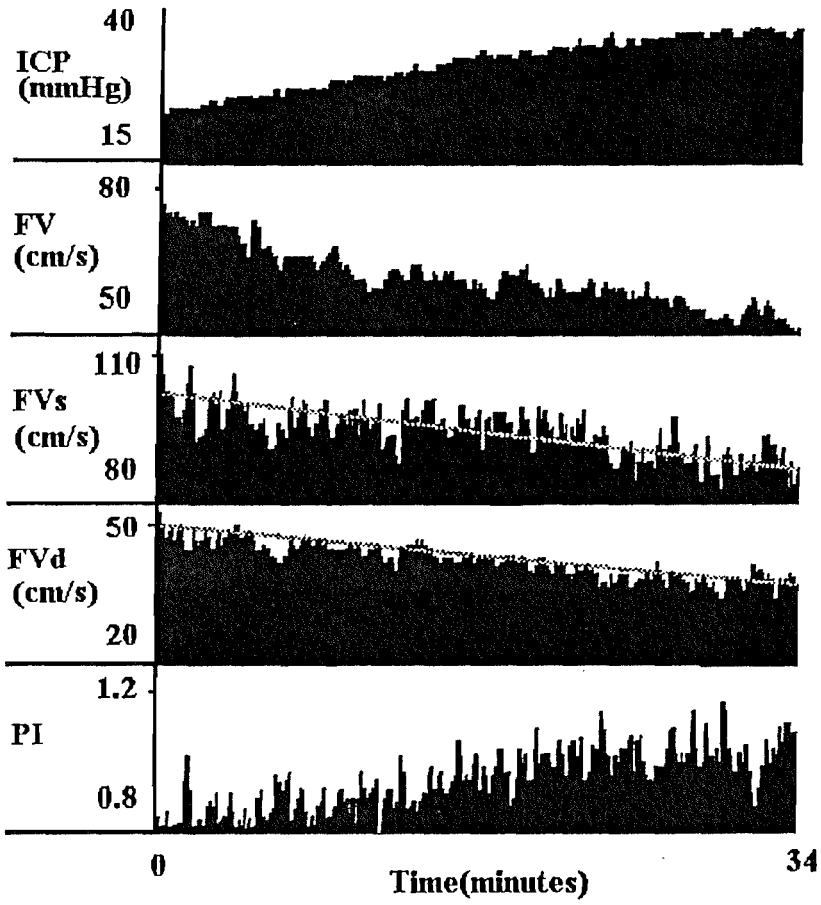

Figure 2: A typical recording for a group I patient R_{csf} < 13mmHg/ml/min demonstrating the parallel decrease in FVs and FVd during increasing ICP.

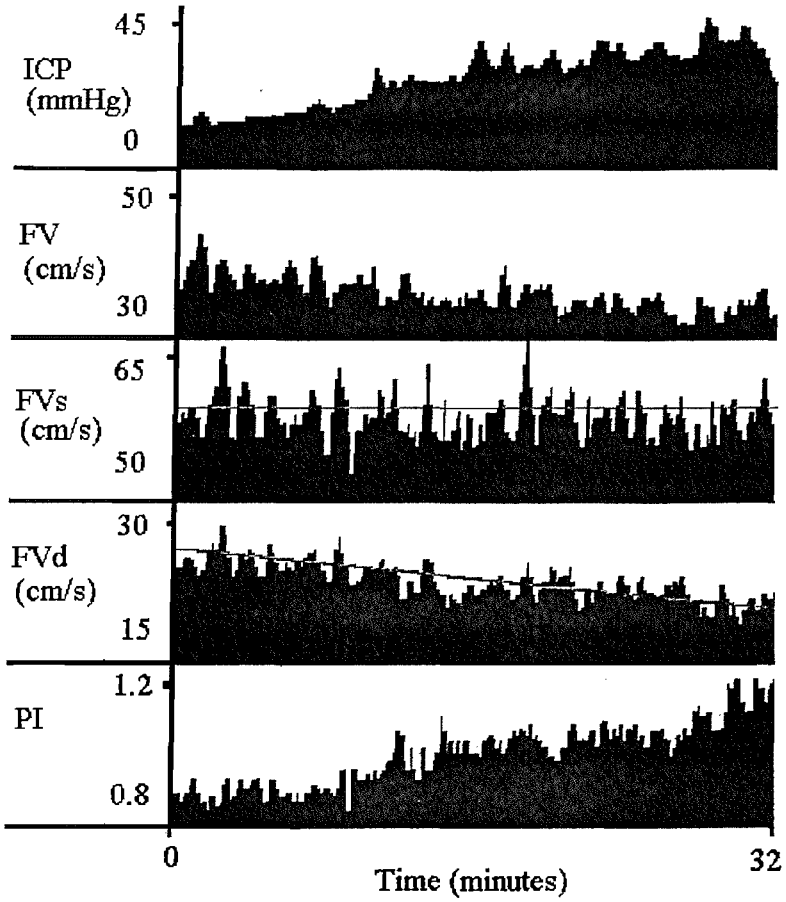

Figure 3: A typical recording for a group II patient $R_{csf} \geq$ 13mmHg/ml/min demonstrating the divergent behaviour of FVs and FVd during increasing ICP.

- In group I, where R_{csf} < 13mmHg/ml/min, FVs and FVd were well correlated. As ICP increased FVs and FVd both decreased. Hence although PP remained constant, PI increased due to a decrease in FV.

- In group II, where $R_{csf} \geq$ 13 mmHg/ml/min, FVs and FVd were less well correlated. As ICP increased FVs remained almost constant and FVd decreased giving an increase in PP. This coupled with a decrease in FV gave a greater increase in PI than seen in group I.

In both groups there was a significant increase in PI during infusion ($p < 0.05$). Table 2 shows a significant difference between the two groups for both the ratio of PI at baseline ICP and during infusion (PI/ $PI_{baseline}$).

In some cases close examination of the simultaneously recorded TCD and ICP signals revealed vasogenic B wave fluctuations in the ICP. These waves occurred at a frequency of approximately 1 per minute as ICP was increased during the infusion. During each B wave the increase in ICP corresponded with an increase in both FVs and FVd (figure 4).

ICP and TCD Parameters	Group I R_{csf} <13 mmHg/ml/min (N=16)	Group II $R_{csf} \geq$13 mmHg/ml/min (N=10)	p
$ICP_{baseline}$ (mmHg)	9.0 ± 4.4	12.7 ± 2.9	p<0.05
FV (cm/s)	48.6 ± 14.6	54.1 ± 20.3	ns
$PI_{baseline}$	0.81 ± 0.27	0.76 ± 0.15	ns
PI (during infusion)	0.87 ± 0.27	0.90 ± 0.20	ns
Increase in FVs-FVd	0.24 ± 2.39	3.76 ± 5.23	p<0.05
Decrease in FV	3.44 ± 3.5	3.99 ± 3.4	ns
PI/ $PI_{baseline}$	1.08 ± 0.06	1.20 ± 0.23	p<0.05

Table 2. Cerebrospinal compensatory parameters and TCD parameters for normal and increased R_{csf} compared using a t-test (ns = not significant)

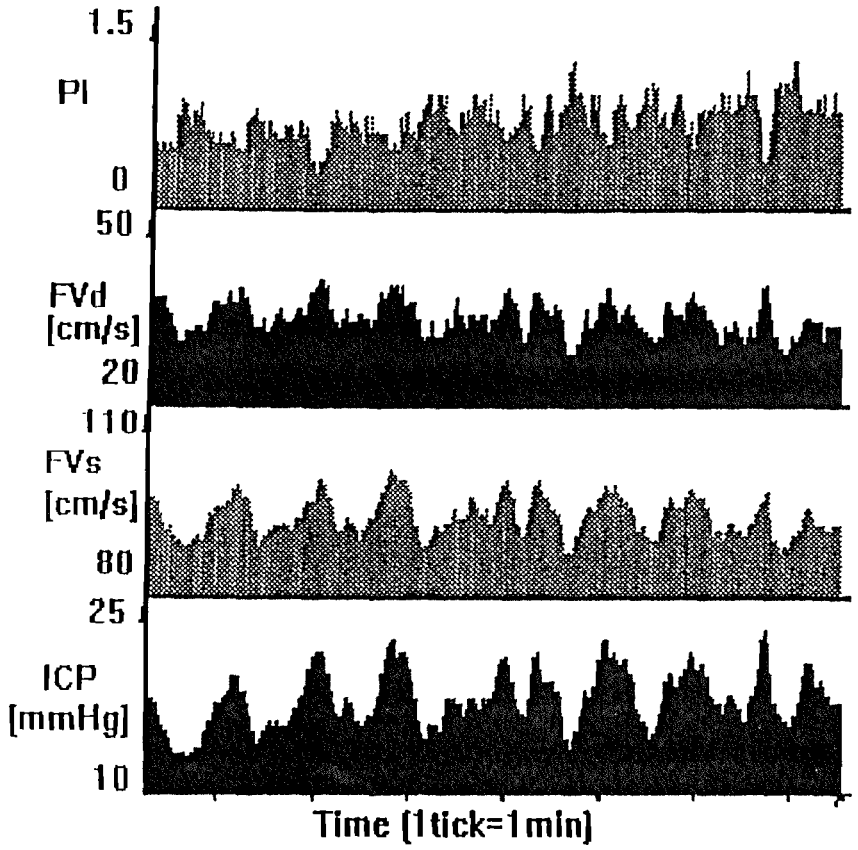

Figure 4: An example of B wave activity observed during an infusion. During each B wave the increase in ICP corresponded with an increase in both FVs and FVd and a decrease in PI.

The patients were divided according to baseline ICP to determine whether TCD parameters may be used as an indicator for ICP (table 3). A threshold of 13mmHg was used as this is considered to be the upper limit of normal resting lumbar pressure [46]. No significant difference between the TCD parameters was found between the two groups.

	$ICP_{baseline}$ <13mmHg (N=18)	$ICP_{baseline}$ ≥ 13 mmHg (N=8)	p
FV (cm/s)	46.7 ± 14	59.7 ± 19	p>0.05
Increase in FVs-FVd	1.00 ± 2.39	2.92 ± 6.45	p>0.05
PI/ $PI_{baseline}$	1.12 ± 0.12	1.13 ± 0.13	p>0.05

Table 3. TCD parameters for patients with baseline ICP < 13mmHg and baseline ICP ≥ 13mmHg compared using a t-test

7. DISCUSSION

No significant difference in PI was found for groups with normal (<13mmHg) and increased (≥13mmHg) baseline ICP (table 3) suggesting that PI is not a good indicator of ICP in this group of patients. This poor correlation may be attributed to several factors:

- The majority of patients in this group had normal or only moderately increased ICP. Other studies where PI measurements have been used to assess shunt function in hydrocephalic patients [33,34,35,47] have shown that the relationship between PI and ICP was not reliable unless ICP was significantly increased. Although TCD continues to be used as a screening tool for ICP assessment in paediatric hydrocephalus [48,49], the relationship between, PI and RI, and ICP appears to be more complex. In a recent study, Hanlo et al [36,38] measured ICP and TCD in 2 groups of paediatric patients with suspected hydrocephalus. Pre and post shunt monitoring in one group demonstrated a postoperative decrease in PI and RI. Long term monitoring in the second group demonstrated poor correlation between PI, RI and ICP. They concluded that PI and RI were inadequate for the direct assessment of ICP.

- The increases in ICP may not have been reflected in the cerebral perfusion pressure (CPP). Monitoring of TCD, ICP and mean arterial blood pressure in an early study in head injured patients, showed a significant correlation between PI and CPP. When CPP was severely compromised due to changes in arterial blood pressure or ICP, an increase in PI was observed [50]. As increases in ICP not associated with reductions in CPP produced no appreciable change in PI, CPP was found to correlate better with PI than ICP.

- Investigations using PI to assess ICP are based on the principle that PI is directly related to CVR and assume that the autoregulatory reserve is intact. Evidence now suggests this may be an over simplification of the significance of PI. For example CVR would be expected to behave similarly during a decrease in CPP and during inhalation of increased CO_2 concentrations. However an increase in PI is seen with a decrease in CPP and a decrease in PI is seen with increased CO_2 . A recent study in rabbits [51] demonstrated that PI is more dependent on vascular compliance than on CVR.

- The patients in group I have dilated ventricles and clinical symptoms with R_{csf} within the normal range. These patients therefore have some other disorder, probably of vascular origin, which may affect the autoregulatory reserve.

Although the complexity surrounding the interpretation of PI may appear to cast a shadow over its potential significance and usefulness, we have found that by considering a ratio of PI in two different states the person to person differences in the physiological and physical parameters affecting PI become less significant.

The more significant increase in PI during infusion in patients with increased R_{csf} (table 3) results from the relative fall in FVd compared with FVs at increased ICP demonstrated in figure 3. In patients with normal R_{csf}, the decrease in FVd was well correlated with a decrease in FVs, thereby maintaining FVa. Consequently a significantly smaller decrease in PI was observed. Similar cerebral haemodynamic responses have been noted in head injured patients [31] and animal models [30]. Nelson et al [30] investigated the relationship between FV and cerebral autoregulation in rabbits. Changes in TCD

parameters were recorded during increasing ICP induced by lumbar infusion into the subarachnoid space. On the basis of the experimental results and theoretical modelling three specific haemodynamic phases were described: Phase 1, where FV is maintained during changes in CPP indicating a fully preserved autoregulatory reserve. Phase 2, a transitional period where CPP in the diastolic phase is close to the critical closing pressure producing decreasing FVd and increasing FVa. Phase 3 where the autoregulatory reserve is exhausted, FV and FVa decrease rapidly as a result of diminishing FVs and FVd. Similar haemodynamic events in rabbits have been observed when a reduction in CPP is induced by controlled haemorrhage [52]. Multimodal monitoring in head injured patients [50,31] has demonstrated phase 1 and 2 haemodynamic behaviour. Decreasing FVs indicating the exhaustion of the autoregulatory reserve was not observed. This may be the result of carefully managed CPP in the intensive care unit or it may be a result of physiological changes in the autoregulatory capacity resulting from intracranial hypertension.

This evidence suggests that both the divergent behaviour of FVs and FVd seen in group II and the well correlated decrease in FVs and FVd seen in group I during increasing CSF volume is indicative of abnormal autoregulatory reserve. If the conclusions drawn from the animal models and head injured patients may be extrapolated to this group then the implication are:

- In group I (R_{csf} < 13mmHg/ml/min) the autoregulatory reserve is rapidly exhausted during infusion

- In group II (R_{csf} > 13mmHg/ml/min) autoregulation is in the transitional period where CPP in the diastolic phase is close to the critical closing pressure.

It is considered to be highly unlikely that any of the patients investigated in this study experienced either of the above scenarios. Had this been the case the majority of patients would have experienced unacceptable side effects during the infusion and this was not the case. Therefore it may be suggested that the pathophysiology in this group of patients and

head injured patients is not the same and care should be taken comparing across patient groups.

It may be that patients with suspected NPH have haemodynamic and hydrodynamic changes that affect the autoregulatory system in a way specific to this patient group. Meyer et al [53] demonstrated that the vasomotor responsiveness to CO_2 is impaired in patients with normal pressure hydrocephalus. More recently [54] cerebral blood flow and vascular response to acetazolamide was measured in 21 patients with NPH pre and post shunting. This study demonstrated all patients had decreased CBF preoperatively. Those who responded well to shunting also had an impaired vascular response to acetazolamide in the white matter that recovered post shunting. These patients also demonstrated restored CBF post shunt. In comparison CBF continued to decrease in patients who did not respond to shunting. The authors concluded that the underlying disease in the improved patients was ischaemia with a loss of autoregulatory capacity in the periventricular white matter caused by cerebrospinal fluid diffusion.

Other possible complicating factors in elderly patients include chronic hypertension which may increase the lower limit of autoregulation and/or a reduce the autoregulatory reserve as seen in severe cerebrovascular disease. Prolonged chronic hypertension shifts the classical CBF and CPP curve towards higher levels of CPP [55]. This protective mechanism provides additional defences against further increases in ABP and CPP which may exceed the upper limit of autoregulation which is accompanied by increasing CBF and decreasing cerebrovascular resistance. The adaptation mechanism may result from physiological or morphological changes. Early studies by Short [56] demonstrated that chronic hypertension induces thickening of the arteriole walls. The wall to lumen ratio is decreased reducing the cross sectional area at maximum dilatation and increasing the ability to constrict in response to increased hypertension. More recently Xie et al investigated the activity of the baroreceptors in normotensive and hypertensive rabbits [57]. In chronic hypertension the baroreceptors reset with less nerve activity at the equivalent level of ABP compared with that of normotensive rabbits. The mechanism of the resetting is not fully understood, but it may also be due to the thickening of the vascular walls as described above. Decreased distendibility of the vessel wall will result in

decreased deformation of the baroreceptors nerve endings and decreased nerve activity. Xie et al conclude that mechanical characteristics alone cannot account for these changes and suggest that biochemical factors are implicated.

The autoregulatory reserve may be exhausted early in cerebrovascular disease. Stenosis or occlusion of a major or branch vessel may activate haemodynamic mechanisms which result in insufficient CBF. The initial response is activation of the autoregulatory response. Therefore part of the autoregulatory reserve is expended to maintain normal flow in resetting conditions. Further haemodynamics events such as decreasing MAP during cardiac arrhythmia during normal sleep or physiological increases in ICP may result in the exhaustion of the autoregulatory reserve, insufficient blood supply and ischaemic events. The problem then becomes compounded as ischaemia is associated with acidosis which paralyses the vasomotor response and effectively deactivates autoregulation in the effected area during acute insults. These pathological conditions may provide an explanation for the unexpected haemodynamic changes observed in some of the patients in this study.

Although the state of the autoregulatory reserve has been discussed no firm conclusion may be drawn. Changes in CPP were not be determined as continuous invasive ABP monitoring was not considered to be clinically appropriate at that time. Intermittent ABP measurements with an inflatable cuff before infusion and during infusion in subsequent patients indicated little variation in ABP during increasing CSF volume. This is confirmed by unpublished data from the study of autoregulation in rabbits. Figure 5a shows the change in ICP, ABP, CPP and TCD parameters during a typical study in a normal rabbit. The regression plot (figure 5b) demonstrates that ABP remains constant until ICP increases to 90-100mmHg. Therefore, although this suggests that ABP remains constant during these experiments, all discussion related to autoregulation during CSF infusion studies remains tentative.

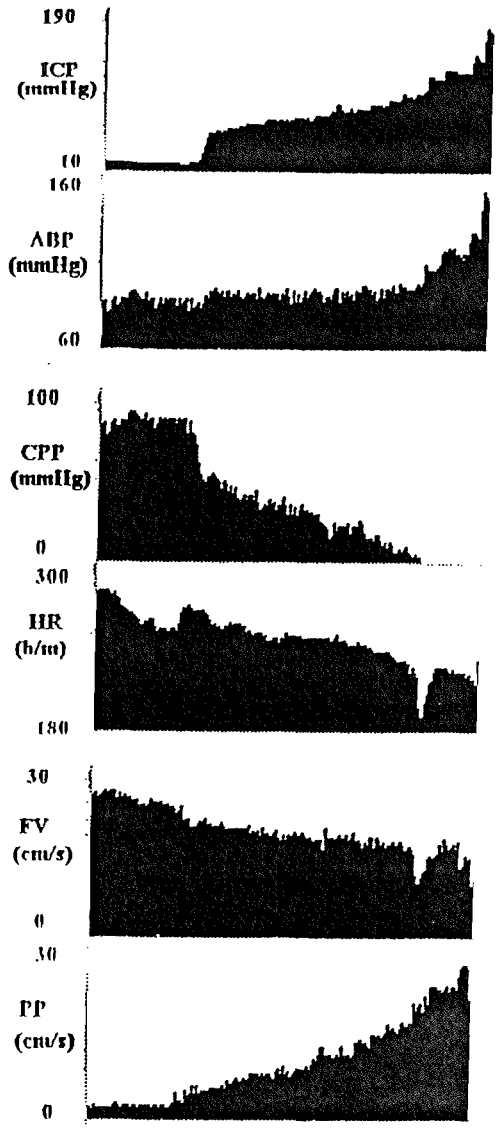

Figure 5a ICP, ABP, CPP and TCD parameters during an infusion study in a normal rabbit demonstrating that ABP remains constant until ICP reaches 90-100mmHg.

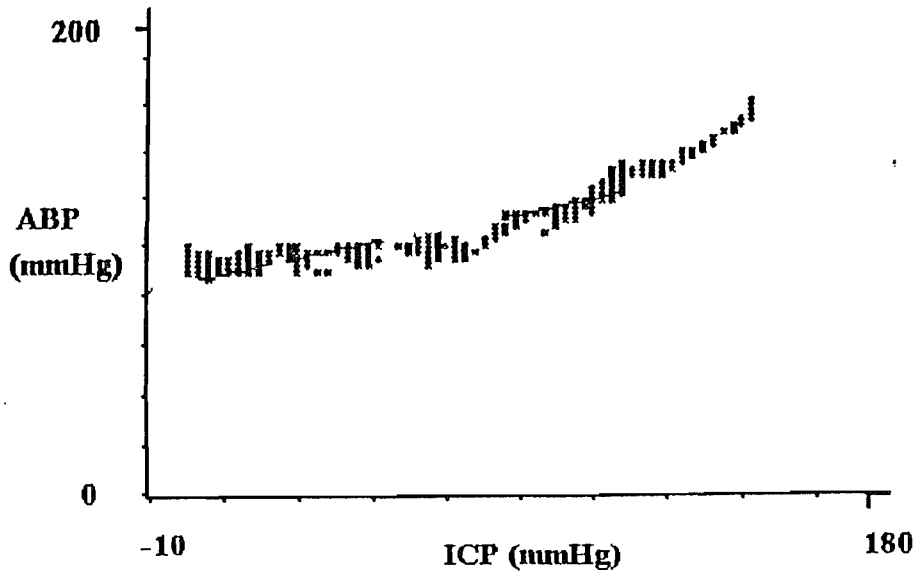

Figure 5b Regression plot of ABP and ICP for data in figure 5a.

During some recordings vasogenic B wave activity was observed. In a recent study of head injured patients ICP, ABP and jugular oxygen saturation (SJO_2) were monitored during A and B wave activity to investigate the pathophysiology of transient ICP increases [58]. A synchronised increase in SJO_2 and ICP was seen during B wave activity and a decrease was seen during A wave activity. As dynamic changes in SJO_2 reflect changes in cerebral blood flow [59], unless cerebral circulation is severely impaired [60,61], then it may be suggested that the underlying mechanism for B wave increases is increased blood flow. During B wave activity in this group, ICP increased and PI decreased (figure 6). Increases in ICP resulting from infusion correlate with increases in PI (figure 7).

Similar observations have been made in head injured patients (unpublished observation). This data shows that transient haemodynamically induced changes in ICP are accompanied by an increase in CPP and a decrease PI, where as CSF volume induced increases in ICP are reflected by a decrease in CPP and an increase in PI. Although the contrary behaviour of PI appears to reflect changes in CPP it may prove to be useful in determining a source of increased ICP is of vasomotor origin or due to changes in the CSF compartment.

The presence of B waves in ICP has been shown to be a good prognostic factor with regard to response to a shunt in patients with normal pressure hydrocephalus [62,63] but their aetiology is not fully understood. The strong correlation between the TCD signals and ICP during B waves is consistent with the findings reported by other workers [64,65].

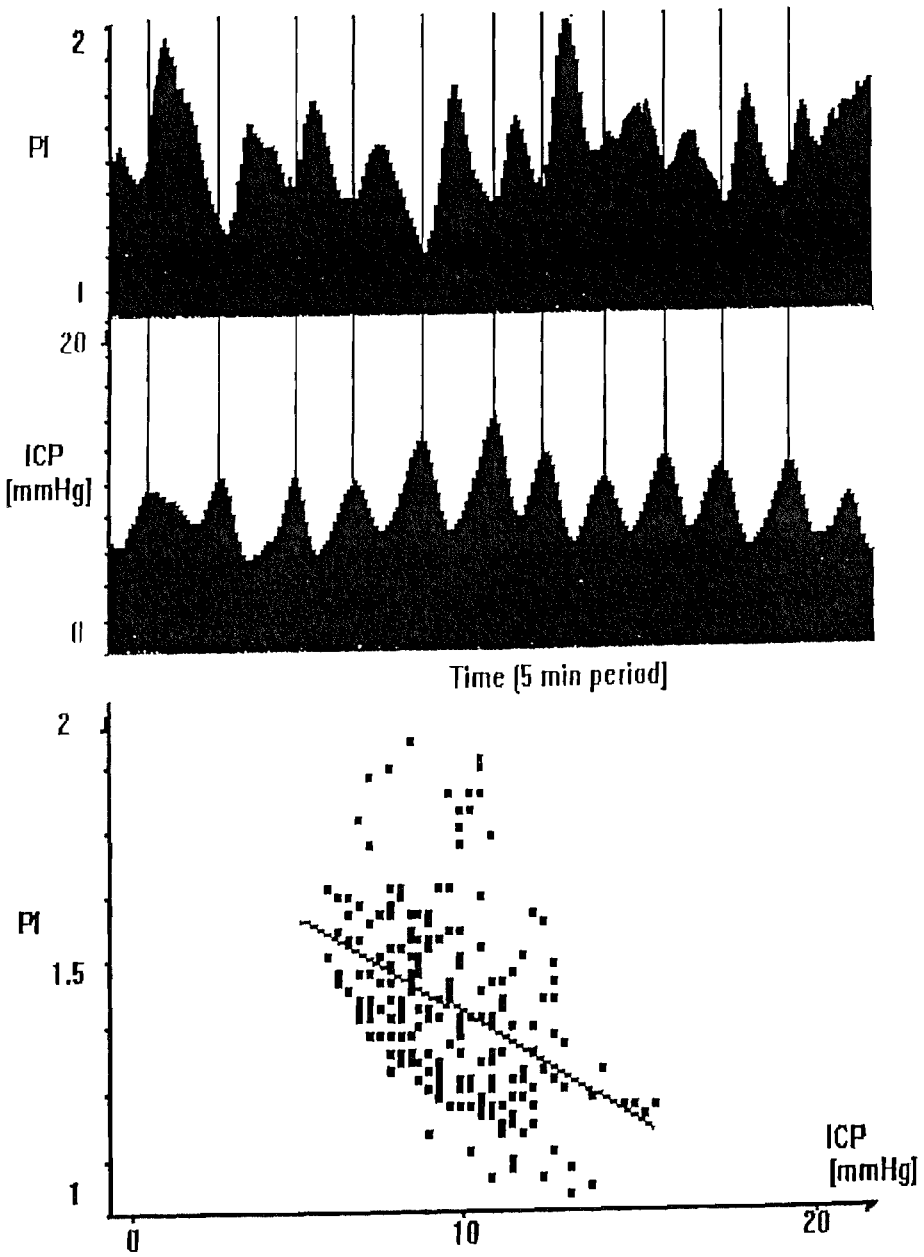

Figure 6: A decrease in PI was observed during transient increases in ICP resulting from haemodynamic changes associated with B wave activity. This suggests that increased CPP is associated with decreased PI.

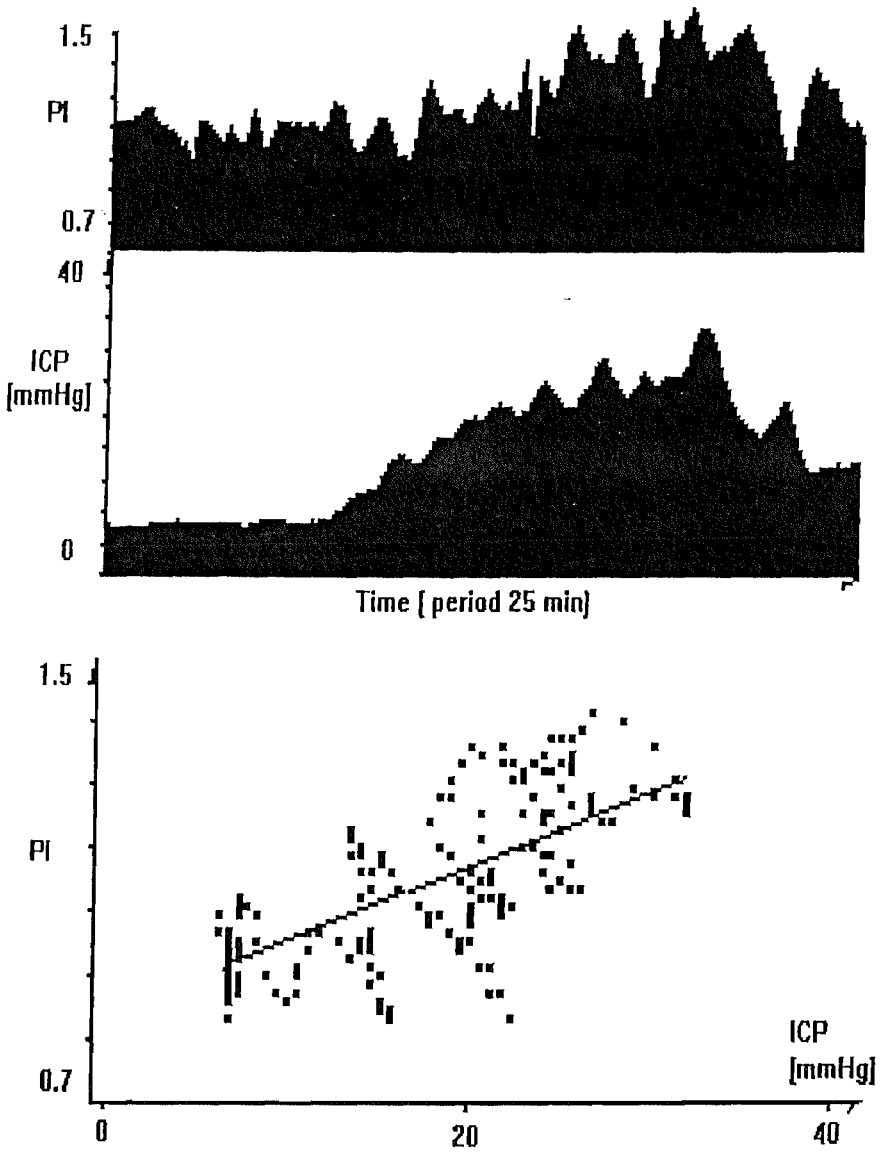

Figure 7: An increase in PI was observed during infusion induced increases in ICP resulting from increased CSF volume. This suggests that decreased CPP is associated with increased PI.

8. CONCLUSION

This study has shown that there is a significant correlation between the change in PI during CSF infusion studies and R_{csf}. This correlation is better than the change in PI and baseline ICP or ICP during infusion. This suggests that TCD may have the potential to replace direct ICP measurement during infusion tests, providing a less invasive 1 needle technique.

The assessment of hydrodynamics in hydrocephalic patients using PI appears to be more accurate if PI is measured at rest and during some form of controlled stress test. By considering the change in PI the physical and physiological parameters affecting PI become less significant.

The ratio of PI before and during infusion ($PI/ PI_{baseline}$) is considered to be a reliable parameter for the classification of normal and disturbed absorption capacity. Many investigations have been performed to correlate PI with baseline ICP. From these results we have shown that in this group of patients there was no correlation between PI and $ICP_{baseline}$.

TCD is a convenient technique which may improve the interpretation of infusion test results. It allows better identification of B waves as other fluctuations in ICP not related to B waves will not be reflected in the FVs and FVd signals.

9. FURTHER PROGRESS

Following on from this work two additional studies were performed:

- A study in rabbits was performed to assess whether changes in TCD parameters during infusion tests may be related to the state of autoregulation. The results of this study is presented in Appendix 1.

- A further study was performed by the group to investigate the hypothesis that autoregulation may be disrupted in some patients who undergo CSF infusion studies

[66]. TCD, ABP (using a non-invasive finger cuff) and ICP were recorded during CSF infusion studies in 43 patients with suspected NPH. An index of autoregulation based on the correlation coefficient between FVs and CPP [67] was found to correlate well with R_{csf}. The results from this study demonstrated that patients with increased R_{csf} are more likely to have preserved autoregulation compared with those with a low R_{csf} confirming the interpretation of the PI data earlier in this chapter.

CHAPTER 3

BLOOD FLOW VELOCITY IN NORMAL VOLUNTEERS DURING SLEEP: A STUDY OF B WAVE ACTIVITY.

BLOOD FLOW VELOCITY IN NORMAL VOLUNTEERS DURING SLEEP: A STUDY OF B WAVE ACTIVITY.

1. INTRODUCTION

Overnight intracranial pressure (ICP) monitoring in patients with suspected normal pressure hydrocephalus (NPH) has revealed periods of fluctuating ICP waves with a frequency of 1 per minute. These so-called B waves have been observed during sleep and may be particularly prominent during REM sleep. Patients that demonstrate these waves for more than 5% of the time have a greater probability of improvement following the insertion of a cerebrospinal fluid (CSF) shunt [1,2,3,4]. Although overnight ICP monitoring and CSF infusion studies are the gold standard for the selection of patients for shunting, ICP monitoring is associated with risk of infection, epilepsy and haemorrhage. Recently transcranial Doppler ultrasonography (TCD) has revealed that B waves in ICP are associated with corresponding fluctuations in middle cerebral artery blood flow velocity.

The analysis and interpretation of clinical data from patients with suspected pathology, requires insight into physiological processes and quantification of normal physiological parameters as a comparative baseline. However, as ICP monitoring is highly invasive, it is not an acceptable technique for use in normal volunteers. Therefore a normal baseline for the comparison with studies performed in patients is not available. Furthermore it would be useful to have a noninvasive screening test for elderly patients with suspected NPH.

1.1 Aims

The aim of this study was to use transcranial Doppler ultrasonography to determine whether blood flow fluctuations occur during sleep in normal volunteers, to quantify these fluctuations and to provide a comparative baseline for B wave activity seen in ICP and TCD studies in NPH patients (Chapter 4) .

2. NORMAL SLEEP

Electrophysiological parameters of electroencephalography (EEG) and electro-oculogram (EOG) have been used to define the cyclic stages of normal sleep [5]. There are two basic types of sleep: rapid eye movement sleep (REM sleep) and non rapid eye movement or slow wave sleep (NREM sleep). In humans, NREM sleep is subsequently divided into four stages each with distinctive levels of altered consciousness. At sleep onset there may be an intermediate period of drowsiness where the frequency of the EEG slows and eye rolling occurs. During light sleep (stages I and II) and deep sleep (stages III and IV) brain activity reduces until almost absent. In contrast REM sleep is associated with a high level of brain activity. The classification of sleep into various stages is complex, but is scored for each 30 second epoch using the Rechtschaffen and Kales criteria [5]. The most prominent features of these stages are:

- Stage W (wakefulness) - The EEG contains alpha activity and or low voltage mixed frequency activity.
- Movement Time - Epochs where the polygraph record is obscured due to body movement, preventing accurate scoring of the epoch.
- Non-REM sleep which is classified into:

a) Stage I - A relatively low voltage, mixed frequency EEG without rapid eye movements (REMS)

b) Stage II – Waves of 12-14 cycles per second, sleep spindles and K complexes on a background of relatively low voltage, mixed frequency EEG activity.

c) Stage III - Moderate amounts of high amplitude, slow wave activity.

d) Stage IV - Large amounts of high amplitude, slow wave activity..

- REM sleep- A relatively low voltage mixed frequency EEG in conjunction with episodic REMs and low amplitude electromyogram (EMG).

During the sleep-wake cycle the level of brain activity and consciousness are constantly changing. The subsequent fluctuating metabolic requirements are reflected by changes in cerebral blood flow. During waking restfulness it is now generally accepted that there is a close coupling between the cerebral metabolic rate and cerebral blood flow [6,7]; during sleep, the relationship is less well defined. It has been demonstrated that cerebral blood

flow and cerebral metabolism decrease with sleep onset and during stages I and II, and reaching minimum levels during stages III and IV [8,9,10]. However, during REM sleep both parameters rise to, or exceed waking levels [8,11]. Recent studies using $H_2{}^{15}O$ PET methodology have facilitated global and regional CBF assessment during multiple sleep stages in the same subject during a single night [12,13,14]. These studies demonstrated that compared with wakefulness, sleep stages III and IV, were characterised by a decrease in global blood flow. During the transition from NREM to REM a significant increase in global CBF was observed. Comparing regional blood flow in distinct brain regions demonstrated that flow is not homogenous during sleep stages III and IV [13] and during REM [14].

Until recently, dynamic changes in cerebral blood flow during sleep could not be detected due to technical limitations. A continuous, real time cerebral blood flow monitoring technique which is suitable for use in normal volunteers and compatible with sleep is required.

3. TRANSCRANIAL DOPPLER ULTRASONOGRAPHY DURING SLEEP

The introduction of transcranial Doppler ultrasonography provided a convenient, non-invasive technique for the prolonged continuous assessment of cerebral blood flow velocity (FV) in the basal arteries [15]. The technique is on-line allowing dynamic momentary changes in cerebral blood flow velocity to be observed and does not interfere with natural sleep.

As TCD is non-invasive and has a good safety record it is ideal for use in normal subjects, and has been used in several studies investigating FV changes during sleep. A simple early study, recording FV before sleep, during NREM sleep and after sleep in healthy adults and children demonstrated a significant decrease in FV during NREM sleep [16]. More recently studies of continuously monitored FV in healthy adults during wakefulness and all sleep stages, concluded that FV was higher during REM and lower during slow wave sleep when compared to the waking state [17,18]. These findings are in accordance with other global techniques [8,9,10,11]. Dynamic fluctuations in FV lasting several seconds, which were most intense during REM sleep and diminished in

intensity with the onset of NREM sleep, have also been observed [17,18]. Droste et al [18] used spectrum analysis to reveal fluctuations in the FV with a wavelength of between 20 and 75 seconds. These fluctuations were prominent during REM sleep, visible during wakefulness and sleep stages I,II and III and almost absent during sleep stage IV. Similar oscillations with a period of 30 seconds to 2 minutes were described by Mautner et al [19] in 8 out of 10 normal healthy volunteers. Healthy preterm [20] and full term new-borns [21] have also demonstrated similar phenomena.

4. MATERIALS AND METHODS

Eight healthy adults (3 males and 5 females), average age 31 years were investigated during spontaneous sleep according to a protocol accepted by the local ethics committee. Each volunteer was previously supplied with detailed information regarding the study and written consent was obtained. No volunteer had a history of vascular disease, transient ischemic attacks, circulatory disorders, diabetes or sleep disorders. Volunteers were asked to avoid substances which may affect normal sleep patterns e.g. tobacco, alcohol and caffeine for at least 12 hours prior to the investigation. Low levels of tobacco in the blood may have a sedative effect, however, as concentrations increase this is replaced by arousal which may result in delayed sleep onset [22]. Although alcohol is a sedative and promotes sleep, the normal sleep architecture is disrupted [22,23]. Like other sedatives, alcohol promotes slow wave sleep and depresses REM sleep. When the blood alcohol level drops during the course of the night there is a rebound effect, with arousal occurring as blood alcohol concentrations approach zero. Caffeine may also increase the number of arousals and decrease the periods of REM sleep [24].

Each volunteer was asked to spend only one night in the laboratory. This may lead to changes in sleep architecture described as the 'first night effect' which occurs when sleeping conditions change. However, as this data was a baseline comparator, for data from patients sleeping in an unfamiliar hospital environment, one night's recording was considered adequate.

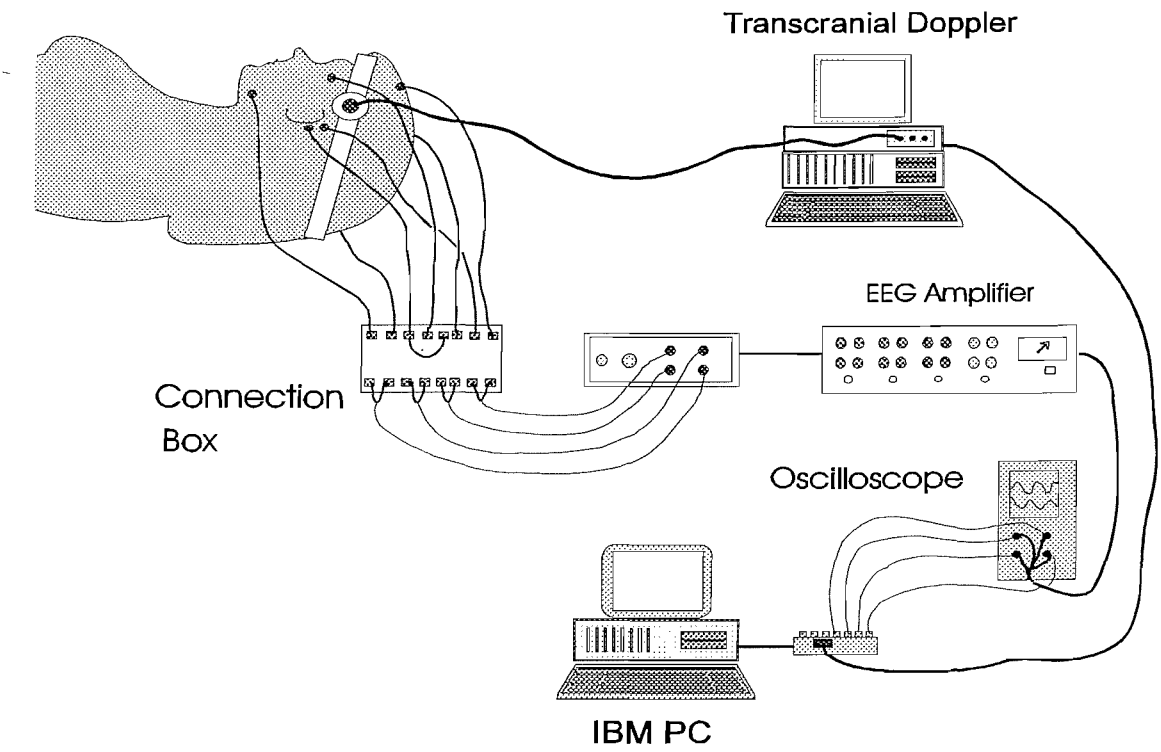

Figure 1. The sleep laboratory equipment set-up

The studies were performed in a sleep laboratory set-up to provide a relaxing, homely atmosphere to promote undisturbed natural sleep (figure 1). Domestic bedding and bed linen was used, blinds were used to exclude external light and a radio and television were provided. The studies began and ended according to the natural sleep patterns of the volunteer. Volunteers were asked to arrive at the sleep laboratory at least an hour before they wanted to sleep to allow ample time for setting up.

Four channels of electrodes were attached to the volunteer to record eye movements (2 channels), muscle tone (1 channel) and EEG (1 channel) according to Rechtschaffen and Kales guidelines [5]. Disposable adhesive silver/silver chloride paediatric electrodes (Medicotest), were used to record the EOG and the EMG channels as they provided a low resistance connection with the skin without the need for scarification. The skin was prepared with abrasive paste and cleaned before electrode application.

The EOG electrodes were attached 1cm lateral and 1cm up from the outer canthus of one eye and 1cm lateral and 1cm down from the outer canthus of the other eye. Both electrodes were then connected to a common reference behind an ear (A1, A2). This set up allowed the detection of eye rolling and rapid eye movements in both horizontal and vertical directions. During eye movement the EOG signals were out of phase providing a means of distinguishing between eye movement and noise. The submental EMG electrodes were positioned bilaterally under the chin. Conventional silver-silver chloride, EEG electrodes were applied at C3 and C4 with collodion to record EEG activity. Although only one EEG channel was recorded the second electrode was applied in case of electrode failure. The EEG electrode was referenced to an electrode behind the contralateral ear (i.e. C3 to A2 or C4 to A1). Conducting gel was injected into the electrodes and the skin scarified to reduce the resistance between the electrodes to less than 5 KΩ. The electrodes were connected via a purpose built connection box (figure 2) to the Biodata amplifier adjusted to give good quality signals observed on the 2 channel storage oscilloscope (figure 3). The length of the electrode leads was kept to a minimum to minimise electromagnetic interference yet allow movement of the subject whilst asleep.

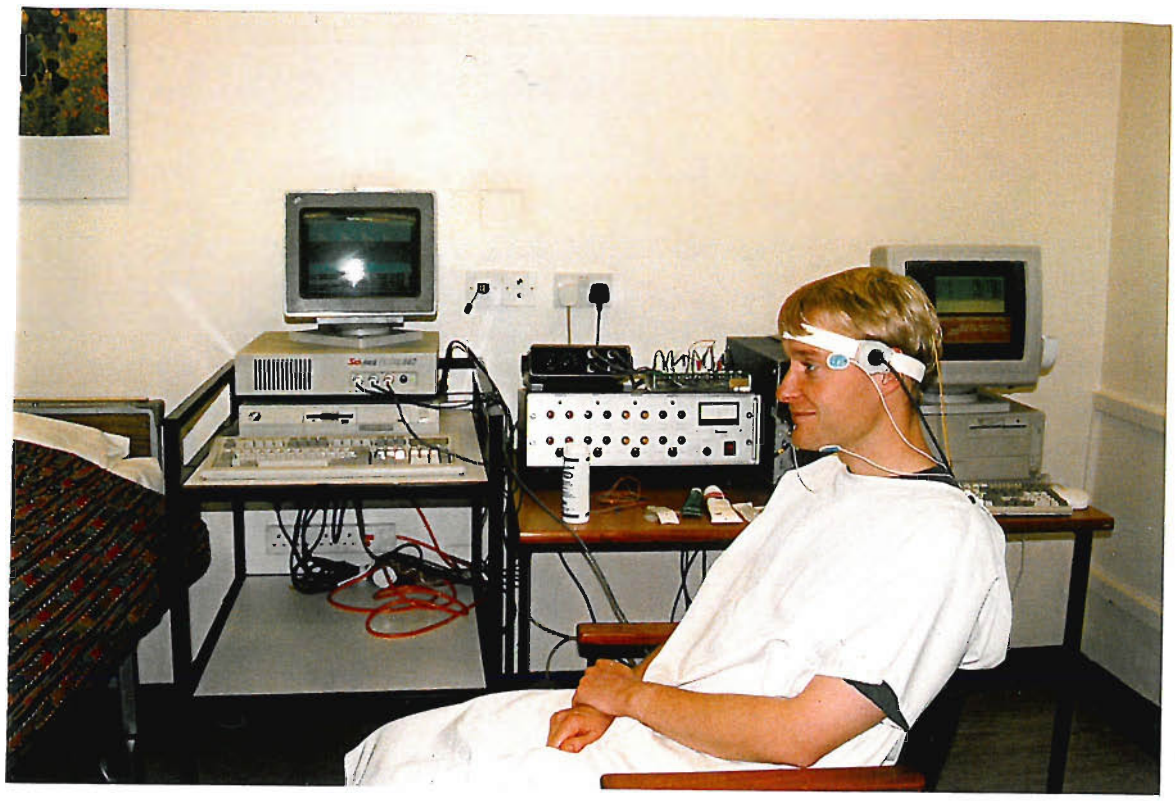

Figure 2: A volunteer with the TCD probe held in position with an elasticated headband and EEG electrodes connected to the junction box

Figure 3: The TCD machine, EEG amplifier, oscilloscope and computer for data acquisition as set-up in the sleep laboratory

The middle cerebral artery was insonated at a depth of 5-6cm via the temporal window using a 2MHz TCD probe (Sci-Med, Bristol, UK). Once the artery was located and the signal optimised the position of the probe was maintained with an elasticated head band and probe holder and the power reduced to at least 25% of the maximum power.

Although TCD is a widely used clinical tool, safety studies were performed to ensure the risks associated with long term ultrasound exposure were minimised (Appendix 2). This study investigated the heating effects which may occur due to the absorption of ultrasound energy by the skull in the insonation pathway. The results demonstrated that for long term exposure, ultrasound power should be reduced to 25% of the total (approx. 20-30mW/cm^2) to minimise any possible heating effects.

During the recording the volunteers were asked to sleep on their backs or contra-lateral side to the TCD probe and to restrict movement as much as possible. Unknown to the subjects the author observed the subject throughout the night and recorded whether the subject appeared to be asleep or awake and body movement. The recordings were continued through the night until the volunteer awoke naturally in the morning.

4.1 Data Analysis

The EEG and TCD signals were sampled at a frequency of 50Hz and stored on the hard disc of a laptop computer equipped with an analogue to digital converter. The software - ICM Biomedical Recorder (Zabolotny, Warsaw University of Technology) was specifically adapted for this purpose.

To aid sleep scoring, the signal from the EEG channel was analysed to determine the spectral power of slow waves (30-100 cycles per minute or 1/2-2Hz) and fast waves (400 - 700 cycles per minute or 6-11Hz). The frequency of eye movements with a frequency of between 20 and 180 cycles per minute or 0.3-3 Hz was calculated from the EOG signal. The prominence of a signal in an epoch may be described in terms of spectral power. Therefore a frequency of high peak to peak amplitude which occurs continually throughout an epoch will have a greater power than a frequency of low amplitude that is

intermittent. The power of the frequencies within these bandwidths was determined with spectral analysis by performing fast fourier transforms (FFT) on epochs of data 256 samples long using adapted software (ICMOFF - Czosnyka, University of Cambridge).

This data used in conjunction with the raw data displayed using the Signal Viewer for Windows (Zabolotny, Warsaw University of Technology) and the observational records in 30 second epochs to distinguish NREM and REM sleep. NREM sleep was defined when the volunteer appeared asleep (eyes closed, minimal movement, regular breathing), low frequency EEG activity was present and eye movement was absent. REM sleep was defined when the patient appeared asleep with no body movement on observation, relatively low EEG activity, rapid eye movements on the EOG and submental EMG atonia/hypotonia

For analysis of the FV data, a frequency divider was used to give an effective acquisition frequency of 0.5 Hz. The TCD recordings were also analysed using ICMOFF to determine the amplitude of B wave activity. An FFT was performed on epochs of 256 data samples. The bandwidth of interest was 1-10 cycles per minute.

The analysed EEG and FV data was converted into ASCII files and merged in an Excel (Microsoft) file. As different sampling frequencies had been used for the EEG and FV analysis the data required manipulation to provide the corresponding power of the EEG signals, FV and B wave amplitude which were then plotted with time (figure 4a,4b 5a and 5b).

Data was input into Statgraphics for analysis. Parameters were compared during REM and NREM sleep using paired t-tests

5. RESULTS

The recordings continued for a period of between 5hrs 7mins to 6hrs 40mins (mean 5hrs 48mins) depending on the natural sleep pattern of the volunteer (table 1). The time spent awake varied from 19-43 minutes (mean 31mins). REM sleep was observed in all volunteers for between 2 and 4 periods which together lasted 21-56 mins (mean 44 mins).

The mean FV during the overnight period for all the volunteers was 56cm/s with a range of 39-73 cm/s. In all volunteers a decrease in FV was observed at sleep onset. FV remained below waking levels except during REM sleep where FV increased and sometimes reached or exceeded the waking values (figures 4b and 5b).

Visual inspection revealed B wave activity in some recording; however, in other recordings the fluctuating flow velocity was less obvious. Figures 6a and 6b demonstrate sections of EEG and TCD recordings with and without B wave activity. Frequency driven analysis allowed B wave amplitude to be quantified on a minute by minute basis for each recording. This demonstrated that in the majority of volunteers, B wave activity was present throughout the recording increasing in intensity periodically. The average B wave amplitude for the whole recording varied between 2.6-3.5cm/s with a mean of 3.1cm/s.

Volunteer Number	Sex	Age	Side FV Measured	Total time recorded	Total time awake	Total time in REM sleep
1	M	26	L	5 hrs 17 mins	28 mins	48 mins
2	F	30	L	6 hrs 20 mins	33 mins	55 mins
3	M	27	L	6 hrs 15 mins	19 mins	56 mins
4	F	29	L	6 hrs 40 mins	27 mins	43 mins
5	F	30	L	5 hrs 44 mins	37 mins	53 mins
6	M	45	L	5 hrs 7 mins	43 mins	39 mins
7	F	31	L	5 hrs 20 mins	34 mins	21 mins
8	F	30	L	5 hrs 28 mins	26 mins	35 mins

Table 1: The volunteer characteristics and sleep statistics

To compare the relative amplitude of B wave activity during REM and NREM, two approaches were taken:

(i) The period of REM was compared to a paired period of NREM sleep within a 20 minute range either before or after the REM period. This is displayed graphically in figure 7. The NREM periods were carefully selected according to observational criteria (appeared to be asleep, eyes closed, minimal movement, regular breathing) and EEG criteria (low frequency EEG activity present and eye movement absent). During REM the average amplitde of B waves was 3.1cm/s and during NREM 2.7cm/s. A paired t test demonstrated a significant difference between the 2 states ($p=0.0072$).

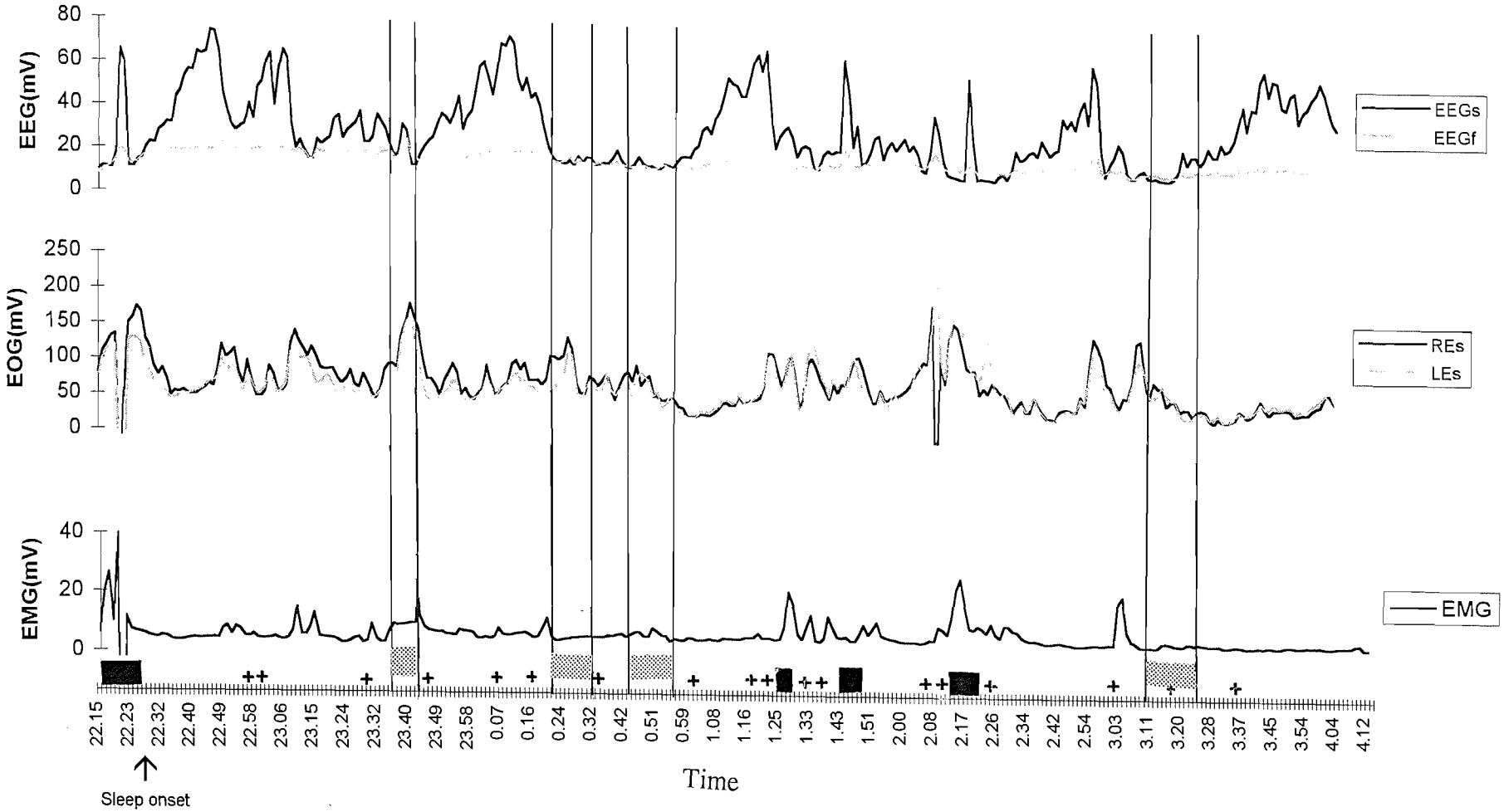

Figure 4a: The analysed EEG, EOG and EMG signals, used with the raw data and observational records to classify REM and NREM sleep for volunteer 4. (EEGs = power of EEG slow waves, EEGf = power of EEG fast waves, REs = power of slow waves in right eye channel, LEs = power of slow waves in left eye channel)

\+ Movement

Periods of wakefulness

Periods of REM sleep

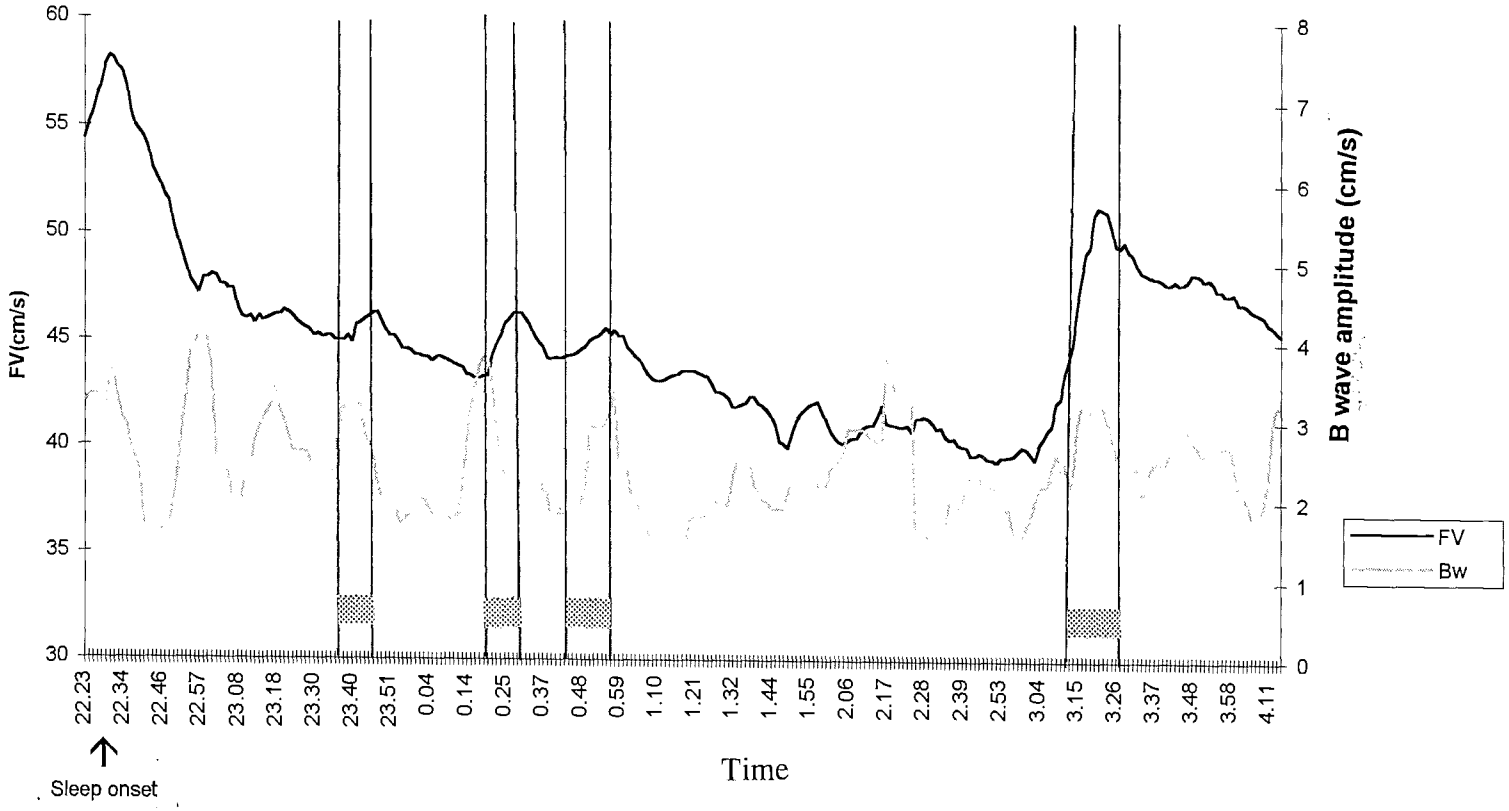

Figure 4b: The variability in flow velocity and B wave amplitude for volunteer 4 during the nights recording.

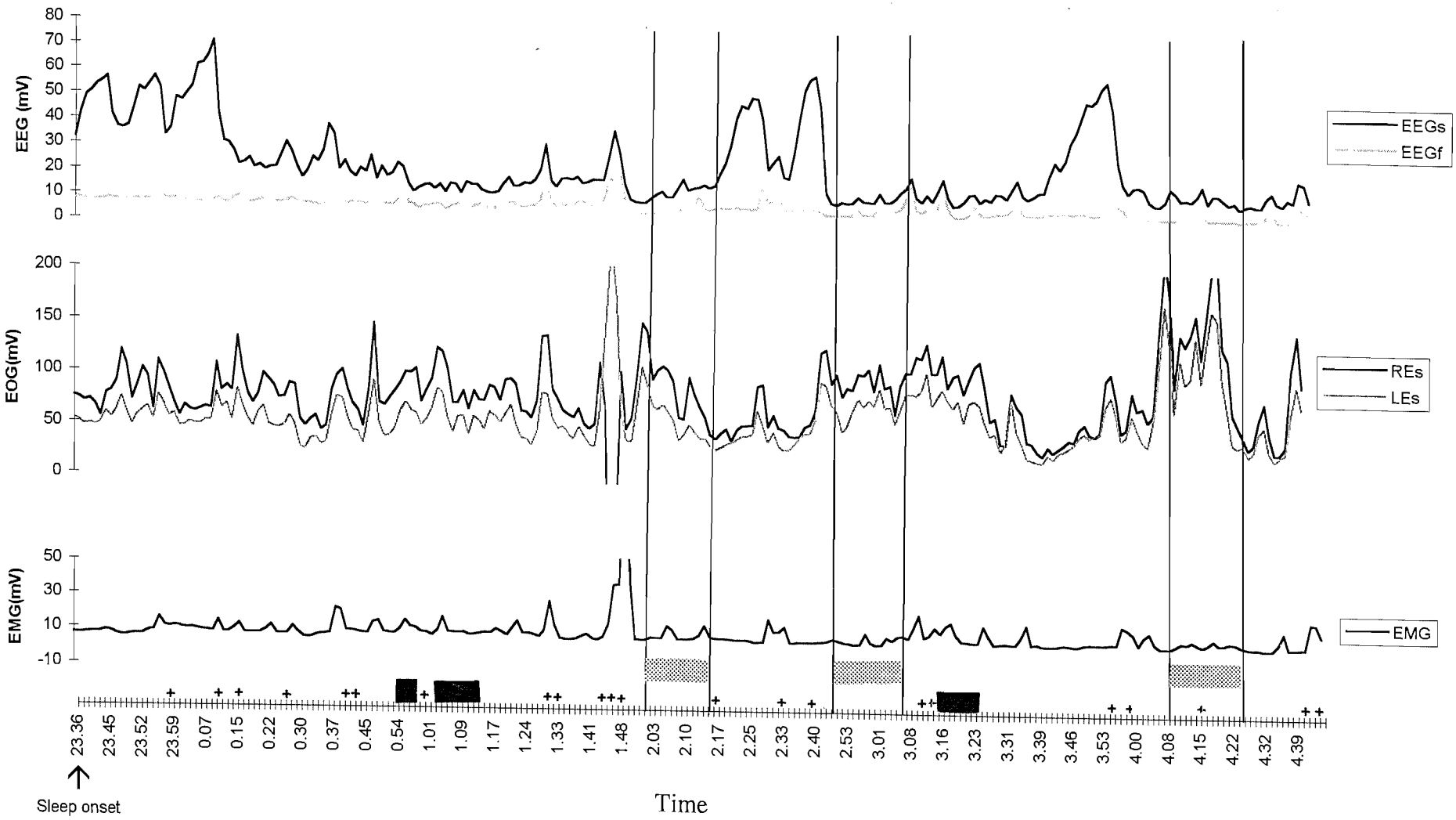

Figure 5a. The analysed EEG, EOG and EMG signals, used with the raw data and observational records to classify REM and NREM sleep for volunteer 1. (EEGs = power of EEG slow waves, EEGf = power of EEG fast waves, REs = power of slow waves in right eye channel, LEs = power of slow waves in left eye channel)

\+ Movement

Periods of wakefulness

Periods of REM sleep

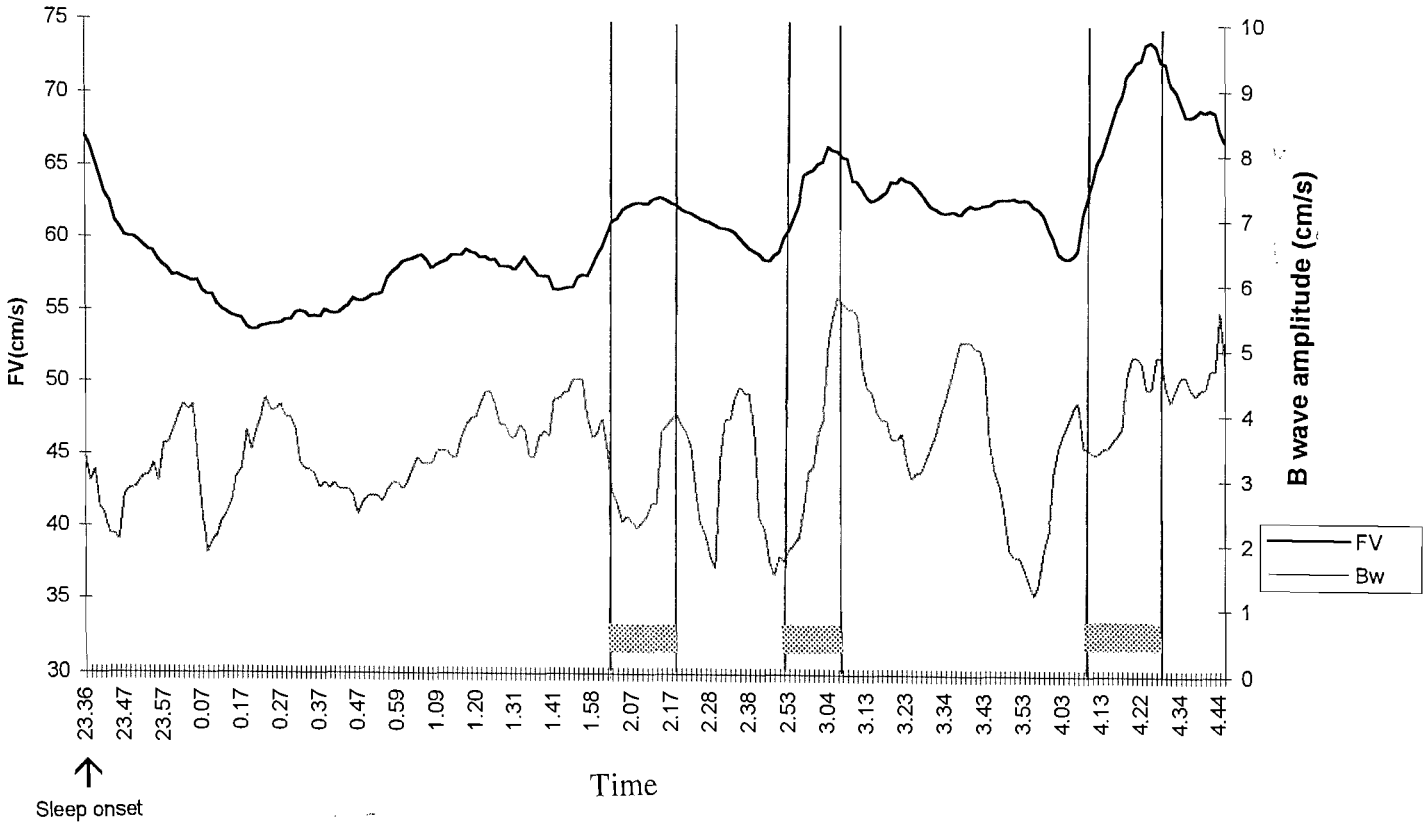

Figure 5b. The variability in flow velocity and B wave amplitude for volunteer 1 during the nights recording.

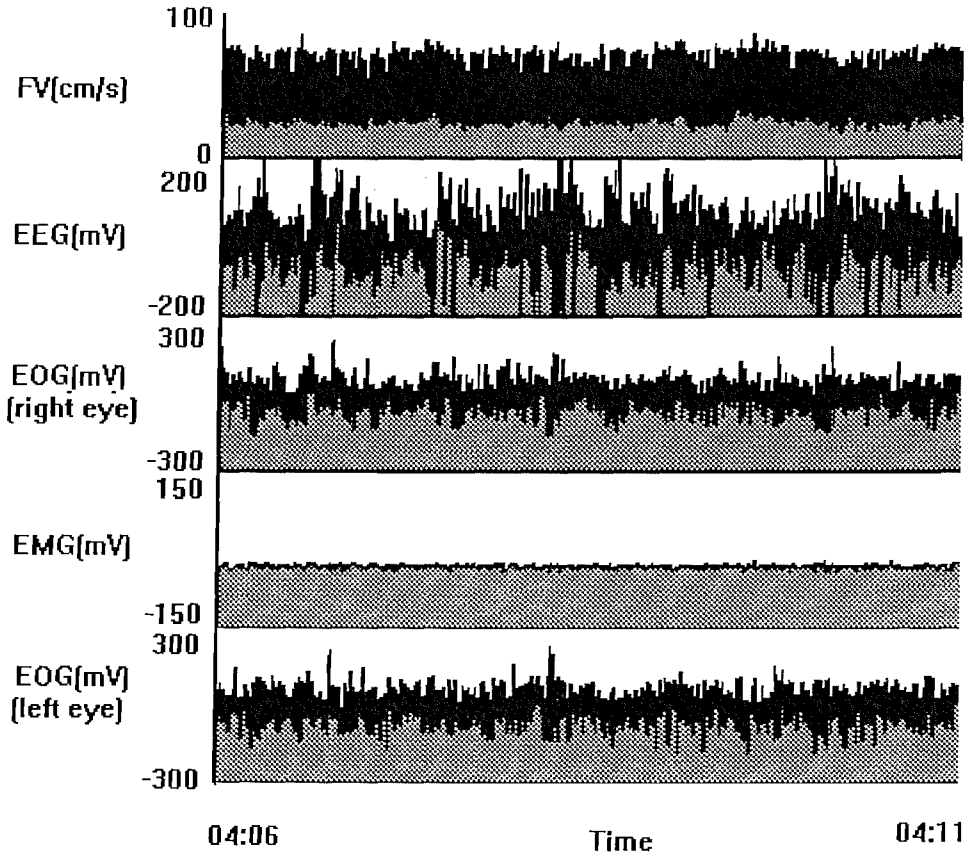

Figure 6a. A 5 minute section of raw data during NREM sleep. No B wave activity is present.

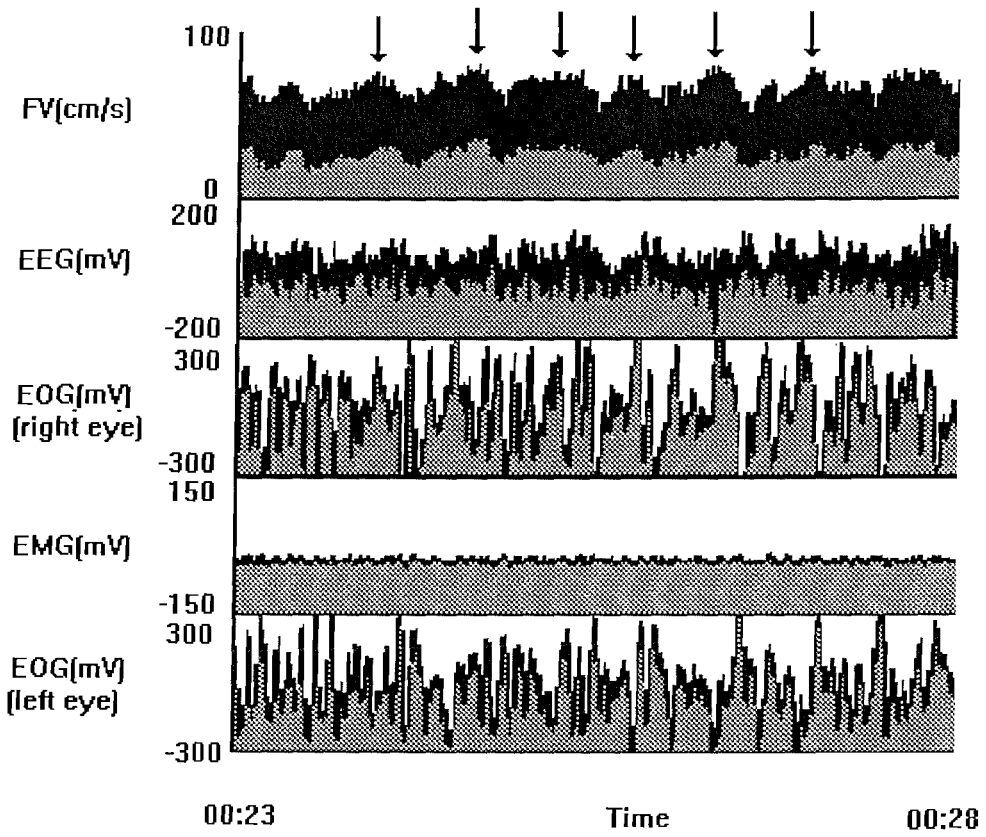

Figure 6b. A 5 minute section of raw data during REM sleep. B wave activity is present (each arrow indicates a B wave).

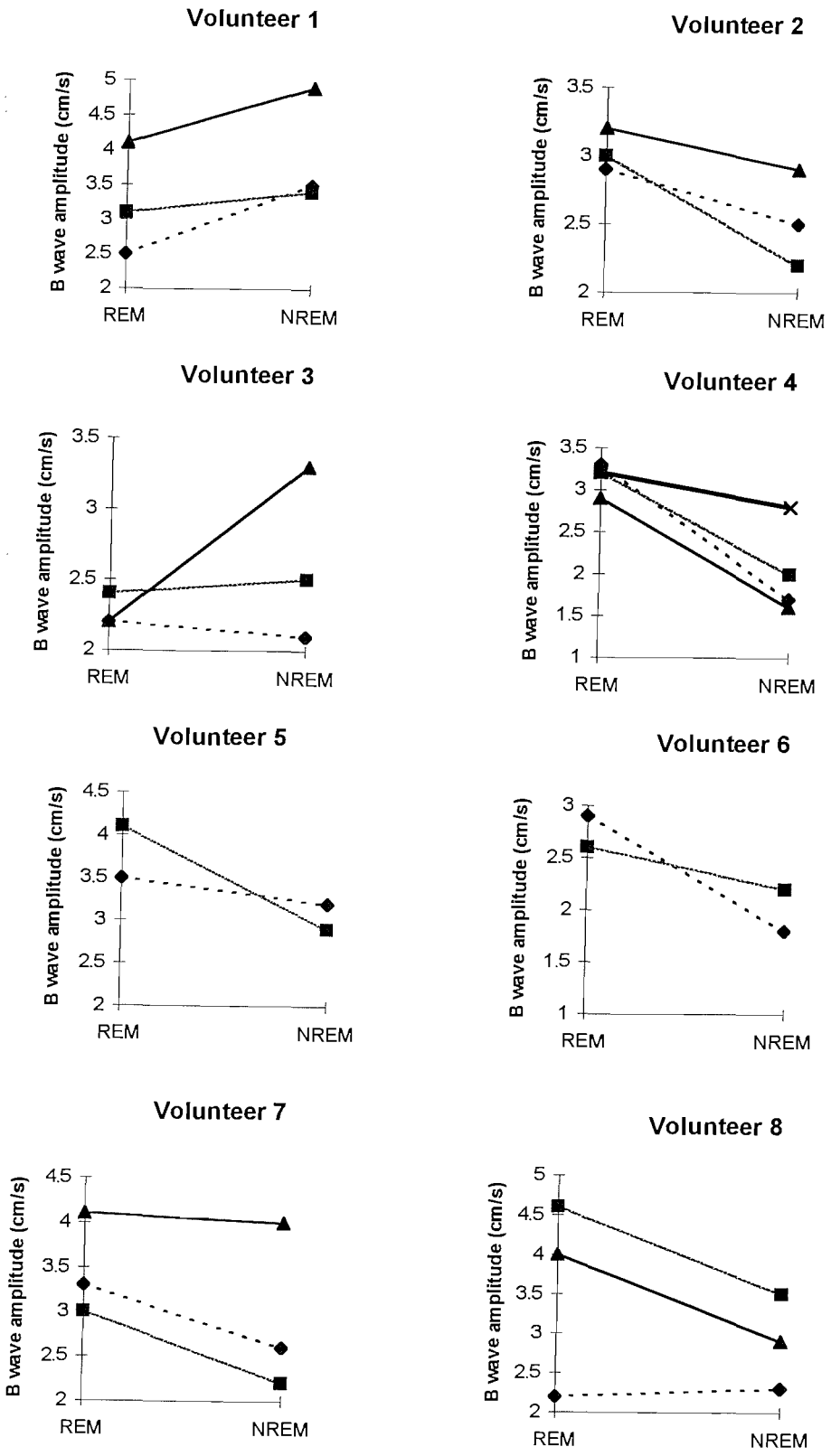

Figure 7. The B Wave amplitude during REM sleep compared to the B wave amplitude during a 20 minute NREM period pre or post REM

◆ REM period 1 ▲ REM period 3

■ REM period 2 ✖ REM period 4

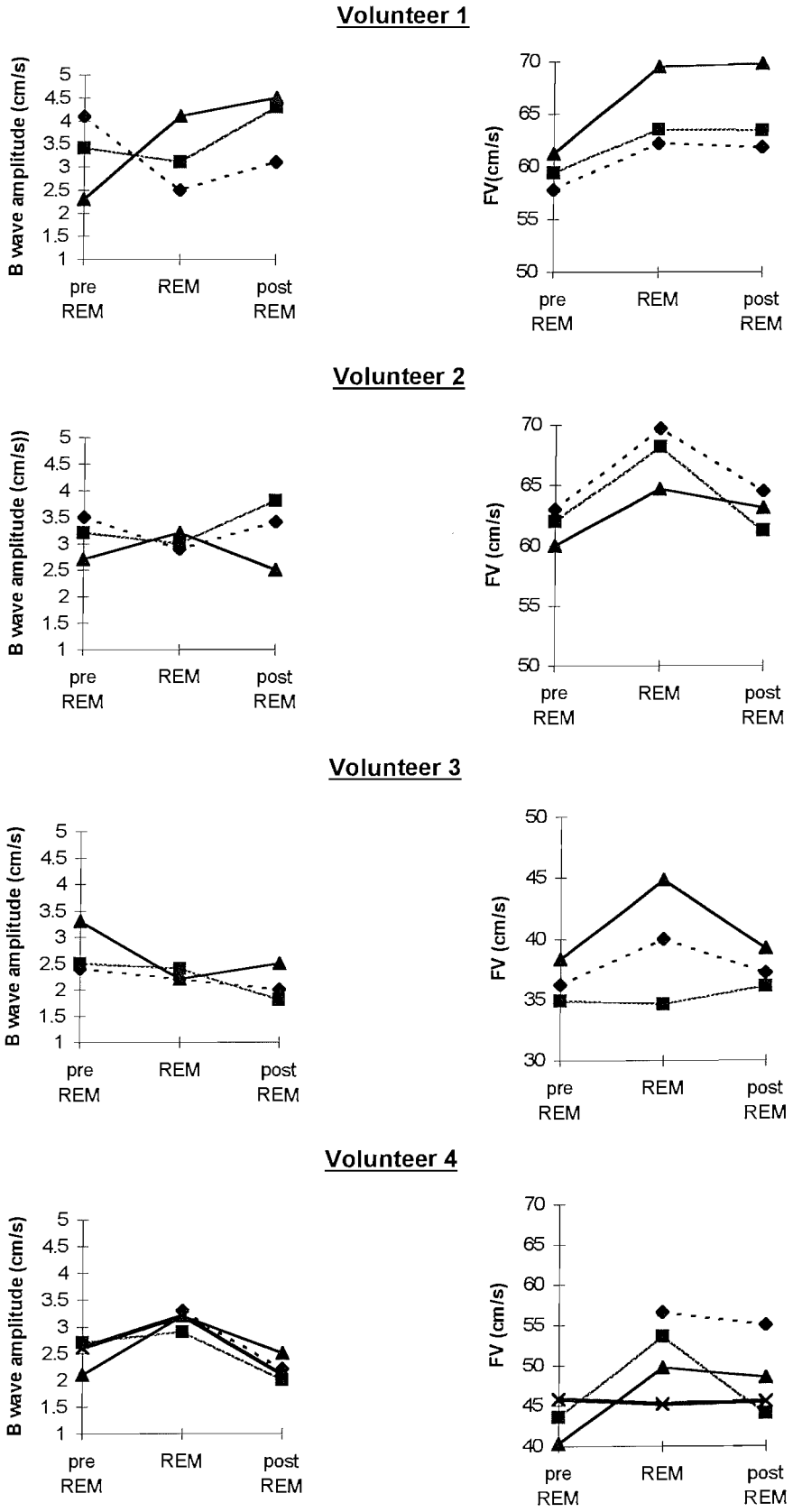

Figure 8. The B wave amplitude and FV 5 minutes before REM (NREM), during REM and 5 minutes after REM (NREM)

◆ REM period 1 ▲ REM period 3

■ REM period 2 ✖ REM period 4

Volunteer 5

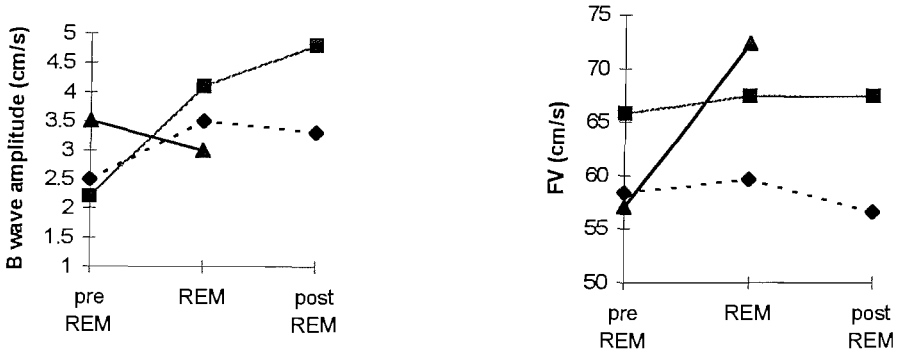

Volunteer 6

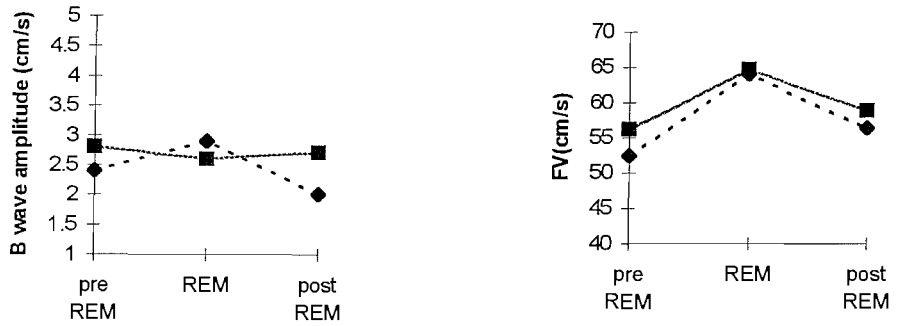

Volunteer 7

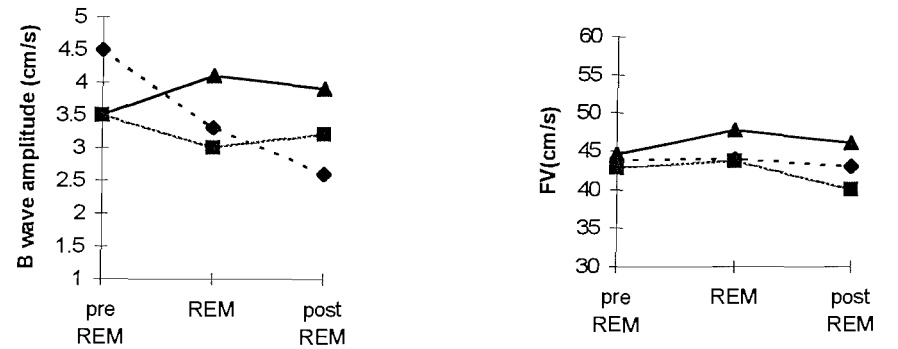

Volunteer 8

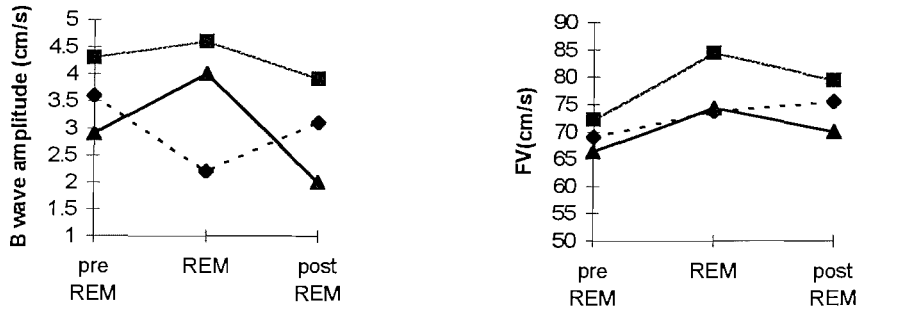

Figure 8 continued. The B wave amplitude and FV 5 minutes before REM (NREM), during REM and 5 minutes after REM (NREM)

◆ REM period 1 ▲ REM period 3

■ REM period 2 ✖ REM period 4

(ii) FV and B wave amplitude during REM were compared with ten minute periods of NREM were selected pre-REM (ending 5 minutes before the start of REM) and post-REM (starting 5 minutes after the end of REM) (figure 8) . For this analysis the period of NREM selected may or may not have contained eye movement. Eye movement that was present during the NREM period was relatively low in amplitude compared with the REM period. Comparison of FV in these three epochs (using a paired t-test) demonstrated that FV increased from an average of 53.5cm/s during pre-REM (NREM) to 59cm/s during REM ($p<0.0001$) and decreased to 55.7cm/s post-REM (NREM) ($p<0.0001$). However, no significant difference was seen in B wave power in the pre-REM and REM periods ($p<0.68$) or the REM and post-REM periods ($p<0.43$) (figure 8).

Therefore in the first approach where the period of NREM was carefully selected to contain minimum eye movement, a significant difference was found in B wave activity during REM and NREM sleep. However, in analysis two when the NREM periods were very close to the REM period and may or may not contain some eye movement, no difference was found between the two states. As a result of this finding, B wave amplitude during REM (3.1cm/s) and NREM periods with eye movement (3.3cm/s) were compared. No significant difference demonstrated in the two states ($p=0.26$).

There was a close correlation between eye movement and B wave amplitude (figure 9). Regression curves of eye movement and B wave amplitude were produced for all data with periods of arousal removed. A positive correlation was seen in 7 out of the 8 volunteers. The average of these correlation's was $R=0.44$. The volunteer with negative correlation had the lowest average B wave activity during the recorded period.

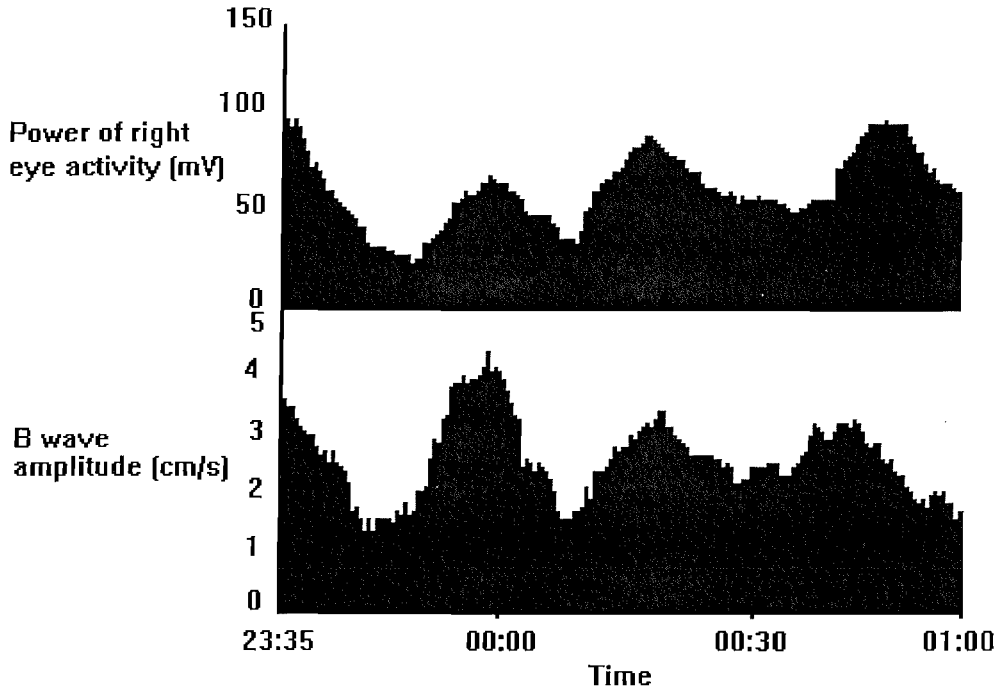

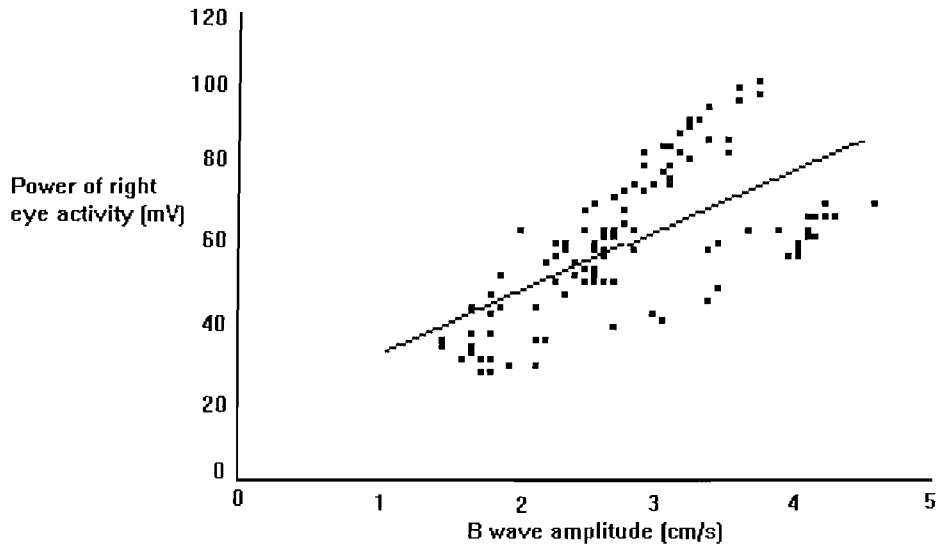

Figure 9: A 1 ½ hour section of data from one volunteer demonstrating the close correlation between B wave amplitude and eye movement

6. DISCUSSION

During this study a sleep laboratory was established for safe long term TCD monitoring during sleep. Specifically adapted computer software allowed the large quantities of EEG and TCD data to be stored digitally. Visual analysis demonstrated that B waves were present in the recordings. The author therefore concludes that periodic fluctuations in FV during sleep is a normal phenomenon. Complex, purpose written software allowed the amplitude of the B wave activity to be quantified, providing a normal baseline for overnight TCD studies in patients with NPH.

As this study was performed to assess blood flow velocity changes during REM sleep the EEG data were sampled at a frequency of 50Hz. This provides sufficient detail to allow REM sleep to be accurately identified, however it was not possible to score the NREM sleep stages.

In accordance with other authors [25,26] a decrease in cerebral blood flow velocity was observed in all the volunteers at sleep onset. During NREM sleep, FV remained well below the level recorded when fully alert. However, during periods of REM sleep FV increased to and in some cases exceeded the level recorded when awake. Low amplitude oscillations of cerebral blood flow velocity at a frequency of approximately 1 per minute were observed. These findings are in agreement with other studies [16,17,18]. Although these waves were prominent during REM sleep they were also seen during NREM when some eye movement may be present.

B wave activity during REM was significantly greater than during NREM when the NREM period was carefully selected, according to a defined criteria and was within a 20 minute window either side of the REM period. However, when the NREM period was within a 5 minute window before and after REM there was no significant difference. This may reflect the gradual increase in B wave activity seen before REM occurs increasing during REM to a plateau and then declining, in contrast to FV which increased sharply at REM onset. The gradual increasing prominence of B wave activity before REM may be explained if B waves are present during other sleep stages as suggested by previous authors [17,18]. Klingelhöfer and Sander [17] demonstrated prominent cyclic fluctuations

in FV during REM and moderate fluctuations during stage II. As stage II sleep often occurs before REM sleep this may explain the gradual increase in B wave activity before REM sleep. However, in this study it was not possible to classify NREM sleep into its different stages. As some eye movement may be present during stage II sleep this may also explain the apparent correlation between eye movement.

Unfortunately during this study blood pressure, heart rate, oxygen saturation or PCO_2 were not measured. These additional parameters may have shed some light on B wave physiology which will be discussed in the introduction to chapter 4.

7. CONCLUSION

Transcranial Doppler proved to be a safe and effective means of monitoring dynamic changes in MCA FV which was compatible with normal sleep. B wave activity was observed and quantified providing a normal baseline for comparison with FV and ICP B wave activity in patients (Chapter 4).

CHAPTER 4

A STUDY OF B WAVE ACTIVITY

A STUDY OF B WAVE ACTIVITY

1. INTRODUCTION

Long term intracranial pressure (ICP) monitoring via a lumber catheter or Ommaya reservoir allows accurate assessment of baseline cerebrospinal fluid (CSF) pressure and detection of spontaneous ICP oscillations, with a frequency of 0.5 - 2 waves per minute, known as B waves. Prominent B wave activity during overnight ICP monitoring was historically considered the most reliable indicator for selecting patients with suspected normal pressure hydrocephalus (NPH) who will improve with shunt surgery. During direct ICP monitoring, as with all invasive procedures, there are associated risks of hemorrhage, epilepsy or infection. Patients with suspected NPH are often elderly and fragile therefore a less invasive means of reliable assessment would be desirable.

This chapter presents data from two clinical studies in patients with suspected normal pressure hydrocephalus. The first study used transcranial Doppler ultrasonography (TCD) during routine overnight ICP monitoring allowing prolonged, on-line, simultaneous recording of cerebral haemodynamic and CSF hydrodynamic changes during sleep. The original objective was to also record simultaneous EEG (electroencephalography), however, an initial pilot study demonstrated that the patients were unable to tolerate the associated movement restrictions and became restless and agitated during the recording period. Therefore EEG was not recorded.

The second study compared the relationship between B wave activity recorded during overnight ICP monitoring and CSF hydrodynamic parameters.

1.1 Aims

The aims of this study were to provide further understanding of the pathophysiology of B wave activity and to determine whether TCD may be used as a diagnostic tool in this patient group.

The following questions were addressed:

- Are B wave type haemodynamic fluctuations, demonstrated with TCD in normal volunteers (Chapter 3), present in patients with suspected NPH?
- Are the properties of the haemodynamic B waves observed in normal volunteers different to those observed in the patient group?
- What are the pathophysiological conditions required for haemodynamic B waves to be transmitted to the CSF?
- Could non-invasive TCD monitoring enhance or replace invasive ICP monitoring?

The second study compared the occurrence of clinically significant B wave activity and hydrodynamic parameters assessed during CSF infusion studies. The aim of this study was to explore the relationship between these parameters and compare the results of the computerised lumber infusion tests with the gold standard of overnight ICP monitoring.

2. ICP FLUCTUATIONS

Although indirect measurements of ICP via the lumbar route were made as early as the 1890s continuous ICP was not introduced to clinical neurosurgical practice until 1951 by Guillaume and Janny [1] in France and by Lundberg in 1960 in Sweden [2]. Lundberg demonstrated the limitations of a signal measurement and concluded that prolonged measurement allowed the detection of pressure fluctuations as well as more accurate assessment of baseline pressure. Lundberg described several types of ICP fluctuation; A, B and C waves, and respiratory and cardiac pulse waves each with specific characteristics. Cardiac pulse waves are the most prominent feature of an ICP trace, induced by the rush of blood into the arteries which dilate

rapidly and transfer expansile energy directly to the surrounding ventricular CSF. Respiratory waves occur at an approximate frequency of 12 per minute (0.2Hz). The respiratory and cardiac pulse waves are present in all ICP recordings and have been explored using MRI (magnetic resonance imaging) [3,4]. A, B and C waves are features of abnormal intracranial hydrodynamics and may be observed in numerous pathological states. C waves are high frequency, high amplitude fluctuations that occur when ICP is continually raised [2]. They are observed in critical states where the cerebral arteries are in a state of paralysis and the prognosis is poor [5].

A and B wave activity may be present in patients with various pathologies [4] including NPH. A waves are characterised by an acute increase in ICP which may be as high as 50-100mmHg, they persist for a variable length of time and cease as spontaneously as they began. These waves occur in states of highly reduced intracranial compliance where increased blood volume associated with vasodilation produces an increase in ICP, which causes a decrease in CPP typically resulting in decreased CBF [6,7,8]. B waves are spontaneous rhythmic fluctuations of irregular shape with a frequency of 0.5 - 2 oscillations per minute (0.008-0.03Hz). Although both A and B waves may feature in the ICP recordings of patients with NPH, the most prominent and consequential fluctuations are B waves. It is now well known that patients who respond well to shunting demonstrate prolonged periods of B wave activity. The presence of B wave activity is considered to be one of the most important prognostic indicators for improvement after shunting [9,10,11,12].

3. B WAVES IN PATIENTS WITH SUSPECTED NPH

Symon et al [13] noted that although patients with dementia and enlarged ventricles often underwent shunting, the results were not entirely satisfactory. He concluded that more reliable differential diagnostic techniques were required and suggested that episodes of pressure waves observed during some prolonged ICP recordings may be of diagnostic importance. Numerous studies since have demonstrated B wave activity is a required

observation for improvement after shunting [9,10,11,12]. Pickard et al performed a series of pre-shunt tests [9] in a group of 26 patients with suspected NPH. Comparison between the pre-operative test results and outcome after shunting demonstrated that the presence or absence of B wave activity was the best predictive indicator. The same author later suggested that B wave activity only became a diagnostic feature if present for more than 5% of the day [11]. In agreement with this finding Børgessen and Gjerris [14] found that the presence of B waves in more than 50% of a 24 hour recording was invariably associated with improvement after shunting. In patients with B wave activity for less than 5% of the recording time, no improvement was seen with shunting. The authors therefore suggested that if B wave activity occurs for between 5-50% of the recording further investigations such as the assessment of the resistance to CSF outflow should be performed.

3.1 The Relationship Between B Wave Activity and CSF Hydrodynamic Compensatory Parameters

Patients often undergo both ICP monitoring and assessment of the CSF compensatory parameters, by computerised infusion test as described in Chapter 2, or other methodology. This has allowed the relationship between the two sets of parameters to be explored, however, it remains controversial whether B wave activity is an indicator of disturbed CSF compensatory parameters. Gjerris et al [15] investigated 150 patients with NPH and 50 patients with high pressure hydrocephalus and demonstrated that in general B wave activity increased with increasing resistance to CSF outflow. The relationship was described as 'obvious but not mandatory' but no correlation coefficient was given. Many authors disagree with these findings [16,17,18,19] and conclude that there is no relationship between these parameters. More recently Drinagl et al [20] compared B wave amplitude and duration with PVI (pressure/volume index) in a group of 25 patients with various pathopysiology. Although no correlation was demonstrated between PVI and B wave duration, a correlation between PVI and B wave amplitude ($r=-0.75$) was shown. This study implied that B waves originate

from fluctuations in CBF and are probably a normal physiological phenomenon, which are amplified in states of low compliance.

3.2 Associations between NPH and Sleep Disorders.

Prominent B wave type fluctuations in the cerebral blood flow in the middle cerebral artery are a normal physiological phenomena during rapid eye movement (REM) sleep [Chapter 3, 21,22,23,24] and, although less obvious, during stage II sleep. In normal sleep REM is seen for approximately 20% of the night, occurring intermittently in periods of variable length. Many NPH patients who respond to shunting demonstrate B wave activity in the ICP for at least 50% of the recording time. This implies that patients with NPH have altered sleep architecture or B wave activity is not confined to specific sleep stages. Overnight studies of ICP and EEG parameters in patients with suspected NPH allowed B wave activity to be assessed during different sleep stages [25]. This study demonstrated B waves were present for 72% of the total recording period and were observed during wakefulness and sleep stages I-IV and REM. Pre shunt B waves were found to be significantly more prominent during REM and stage II sleep compared to wakefulness. Kuchiwaki et al [26] investigated ICP, respiratory movement and sleep stages pre and post shunt in NPH patients. B wave activity was often prolonged, persisting for several hours, accompanied by apnea and disturbed sleep. As a result the patients oscillated between awake and stage I with rare appearances of stage II and REM. Post shunt sleep stages became more stable, and apneas became extremely infrequent. Other studies have also demonstrated an association between sleep disturbance, in particular sleep apnea and NPH [27,28,29].

3.3 The Pathopysiology of B Wave Activity

There is substantial evidence to suggest that these haemodynamic events produce increased blood volume which may provoke B wave fluctuations in ICP when brain compliance is low. Newell et al monitored ICP, cerebral blood flow velocity, ABP (arterial blood pressure) and end tidal CO_2 in head injured patients [6,30]. A good correlation was found between

fluctuations in cerebral blood flow velocity and ICP, demonstrating that B waves are induced by changes in blood volume.

The aetiology of the haemodynamic changes which provokes B wave activity is controversial. Possible mechanisms include fluctuations in arterial PCO_2 [31], activity of a neurogenic oscillator in the brain stem [32,33] or autoregulatory constriction or dilatation of the intracranial vessels [34]. Børgesen et al [31] investigated the relationship between fluctuating PCO_2 and ICP waves in artificially ventilated patients of various aetiology. Although autoregulation was intact, changes in PCO_2 and ICP were not correlated. During A and B wave activity PCO_2 remained almost constant. It was therefore concluded that B wave activity was not induced by changes in PCO_2 and that B waves were not indicative of abnormal respiration.

Experimental models [32,33] have been used to investigate the role of the vasomotor centre and electrophysiological changes during B waves. They demonstrated that B waves were provoked synchronously with oscillations of the sympathetic and phrenic nerve discharges and that the sympathetic nerve discharge precedes the B wave. It was also found that barbiturates suppressed the nerve discharges and the B waves. From these findings it was concluded that B waves must originate from the oscillatory rhythm of the brain stem. It has also been suggested that numerous structures within the brain may contribute to the initialisation of B wave activity.

CSF infusion studies in cats [34] demonstrated that B wave activity correlated with pial vessel oscillations. The oscillations are thought to result from the myogenic autoregulatory mechanism of the smooth muscle vascular walls. The contraction stimuli for these cells is intraluminal pressure induced stretching. The smooth muscle cells then relax and the vessels dilates. This then leads to stretching of the muscle closing the feedback loop. During increased ICP there is further relaxation of the vessel due to a decrease in transmural

pressure. The amplitude of the oscillations increases as transmural pressure falls and reaches a maximum just before autoregulation is exhausted.

4. MATERIALS AND METHODS

4.1 Simultaneous ICP and TCD Monitoring

The relationship between haemodynamic and hydrodynamic fluctuations was assessed in 15 patients (8 males and 7 females, average age 60 years) using transcranial Doppler ultrasonography during routine overnight ICP monitoring (see figure 1). The patients demonstrated the clinical signs and symptoms described in table 1. All patients had suspected normal pressure hydrocephalus, suspected shunt malfunction or BIH (benign intracranial hypertension) and demonstrated ventriculomegaly on CT (computerised tomography) scan or MRI (magnetic resonance image). The procedure required patients to spend at least 1 night in hospital.

ICP was measured via a lumbar drain or via an Ommaya reservoir. This was a clinical decision based on patient state, whether future complications were foreseen and the expected outcome.

For insertion of a lumbar drain patients were put into a lateral recumbent position with a pillow under the head and, if required, a pillow between the knees. After local anaesthesia with 1% lignocaine a large bore cannula was inserted into the subarachnoid space between L3/L4. A flexible silicone lumbar drain was then inserted down along the cannula into the subarachnoid space. After ensuring the drain was positioned correctly, the cannula was carefully removed. In circumstances where cannula insertion proved problematic, patients were supported in a sitting position on the edge of the bed allowing the spine to become convex, expanding the spaces between the vertebrae. The drain was then allowed to fill with CSF. A connector was securely attached to the free end of the drain which was connected to a saline filled 100cm manometer line with a sterile bung in the opposite end to prevent leakage. The drain was secured in position with sterile dressings and was taped perpendicular

to the spine along the small of the back. Although patients were strongly encouraged to remain in bed after the insertion of the lumbar drain, connection to the pressure transducer was delayed until the early evening, minimising the period of restricted movement. To measure CSF pressure via the lumbar drain a three way tap was prepared with a Gaeltec luer lock pressure transducer (Gaeltec, Dunvegan, UK) and a 50cm manometer line (for calibration) secured to two of the connections.

The three way tap and 50cm manometer line was carefully flushed with sterile saline before attaching the 100cm manometer line and lumber drain. This system was then checked to ensure no air bubbles were present. The three way tap was secured to a drip stand, ensuring the pressure transducer was maintained at the same height as the ventricles. The pressure transducer was connected to an amplifier (Gaeltec, Dunvegan, UK). The analogue lumbar CSF pressure signal from the amplifier was acquired, converted (with an analogue-to-digital converter) and stored on two laptop computers each equipped with different software specifically adapted for this purpose. One computer was equipped with the ICM program (Czosnyka, University of Cambridge) [35] which plotted the average ICP every 30 seconds and provided the data required by the clinician for routine diagnostic purposes. The second laptop was equipped with the Biomedical Signal Recorder (Zabolotny, Warsaw University of Technology) which displayed and recorded the dynamic digital signals. This program was used to record both the ICP and TCD signals and provided the data in a flexible format for analysis.

To calibrate the system the three way tap was turned to isolate the patient and connect only the pressure transducer and the 50cm calibration manometer line. With the software in the 'calibration' mode the open end of the 50cm calibration manometer line was positioned at the same height as the pressure transducer. The amplifier was then adjusted to indicate zero and the output voltage from the amplifier for 0mmHg was acquired by the computers. The open end of the 50cm calibration manometer line was then positioned 26cm above the transducer.

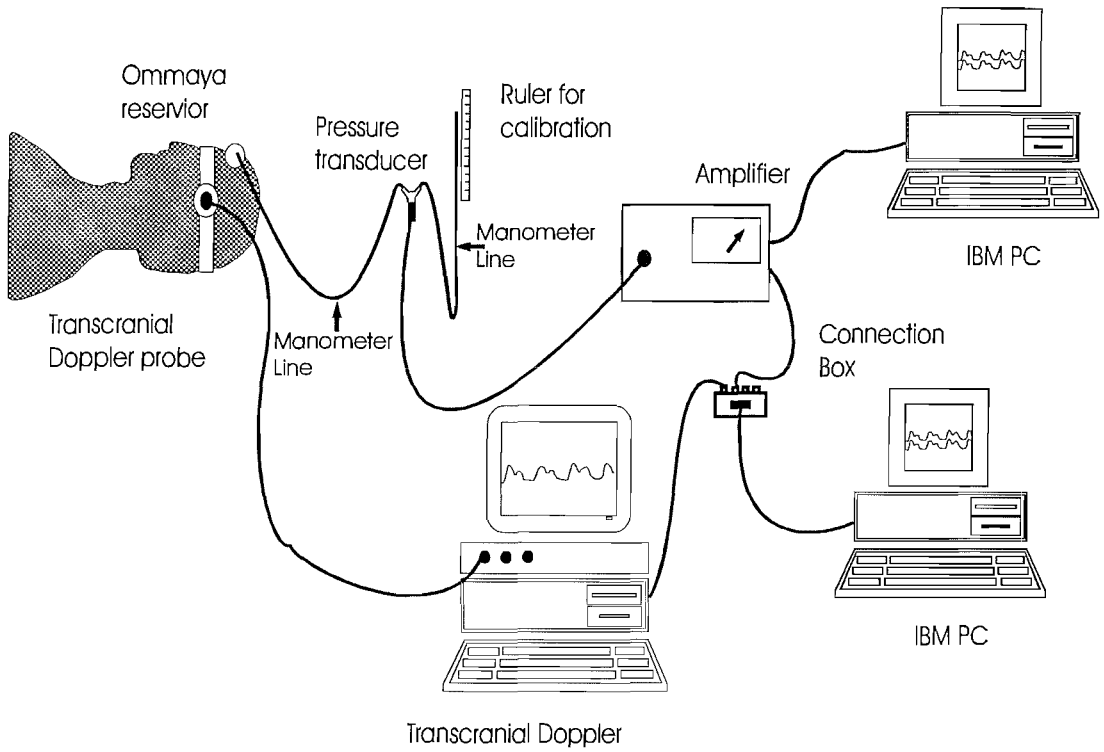

Figure 1. Set-up for overnight ICP and TCD monitoring

Pt no.	Sex	Age	Provisional Diagnosis	Shunt in situ ?	Symptoms*
1	M	61	NPH	N	Dementia, lethargy
2	F	57	NPH	N	Dementia
3	F	34	BIH	N	Ha, Naus, Vom
4	M	75	NPH	N	Gait, Incontinence, Dementia
5	F	68	NPH	N	Gait, Incontinence, Dementia, lethargy
6	M	25	Hydrocephalus	Y	Ha, lethargy
7	M	72	NPH	N	Gait, Incontinence, Dementia
8	F	64	NPH	N	Gait, Incontinence, Dementia
9	F	43	BIH	Y	Ha, Naus, Vom, lethargy
10	F	39	Hydrocephalus	Y	Ha
11	F	78	NPH	N	Gait, Dementia
12	M	73	NPH	N	Gait, Incontinence, Dementia
13	M	62	NPH	N	Dementia, Ha
14	M	69	NPH	N	Gait, Confusion
15	M	82	NPH	N	Gait, Incontinence, Dementia

* Ha = Headache
Naus = Nausea
Vom = Vomiting
Gait = Gait disturbance
Incontinence = Incontinent of urine

Table 1: Details for patients with overnight ICP and TCD monitoring

The amplifier was adjusted to indicate approximately 1/2 to 2/3 scale deflection and the output voltage for 13mmHg was acquired by the computers (26cm H_20 = 13mmHg). After calibration the three way tap was turned to isolate calibration manometer line and connect the patient with the pressure transducer. With the computers in 'monitor' mode the digitised pressure signal was viewed to ensure the pressure pulse waves were clearly visible. If pulse waves were not obvious the patient was asked to cough, producing a large peak in ICP which should be clearly reflected by the digitised pressure signal. No increase of the ICP signal indicated problems with the pressure monitoring system or the position of the lumbar drain.

In many cases where shunt insertion or revision was thought to be the probable outcome ICP was measured via an Ommaya reservoir. If shunting was required then the reservoir and associated connections were used as part of the shunt system. Although insertion of an Ommaya reservoir required surgery, intraventricular CSF pressure measurements were clinically more valuable than less direct techniques and a permanent route for ICP measurement was provided. Under general anesthetic a small incision approximately 4cm was made behind the hairline. The incision penetrated the skin layer, the subcutaneous fat, the fibrous galae aponeurotica and areolar tissue. A small burr hole was then drilled through the hard layer of bone. A star shaped incision was made through the dura forming four flaps which when folded back revealed the subdural space and brain tissue of one hemisphere. A metal cannula was passed through the burr hole and the brain matter to the lateral ventricle and the CSF. A small amount of CSF was drawn up through the cannula to ensure that it was correctly placed. The cannula was then removed and a thin walled silicone catheter passed down the channel. The catheter was then passed through the burr hole and attached to the reservoir which then filled with CSF from the ventricles. The reservoir had a second connector to which a CSF shunt system may be attached if shunting was required. The skin incision was then stapled closing the wound and securing the reservoir under the skin. To measure the pressure a large gauge butterfly needle flushed with saline was inserted into the

reservoir and then connected to the 100cm manometer line and pressure transducer as previously described.

Blood flow velocity in the middle cerebral artery was measured simultaneously with the ICP during the entire night using TCD. The Sci-Med PC Dop (Bristol, UK) equipped with a 2MHz probe was used to insonate a middle cerebral artery via the left or right temporal window. The electronic gain and depth of insonation were adjusted to give a good quality spectrum. As patients underwent prolonged ultrasound exposure the minimum required power was used to reduce any associated risks (see Appendix 2). During the test, the probe position was maintained using an elasticated head band. An observer ensured that the probe position was maintained. Patients were asked to sleep on their backs or the contralateral side to the TCD probe. The analogue flow velocity signal from the TCD was recorded with the ICP signal using the Biomedical Signal Recorder (Zabolotny, Warsaw University of Technology).

4.2 Comparing B Wave Activity and CSF Hydrodynamic Compensatory Parameters.

Computerised CSF infusion tests and overnight ICP monitoring was performed in 47 patients (23 males, 24 females) with an average age of 45 years (range 13 to 80 years) (see table 2). The hydrodynamic compensatory parameters were compared in patients with (n=27) and without (n=20) B wave activity during overnight ICP monitoring. The hydrodynamic compensatory parameters were assessed using the computerised infusion test as described in Chapter 2 [35]. Infusion tests were performed immediately prior to overnight ICP monitoring. The lumbar drain was inserted into the subarachnoid space at L3/L4 and connected to a pressure transducer as described in section 4.1. A lumbar needle inserted at L4/L5 was then connected to an infusion pump. In cases where an Ommaya reservoir had been implanted the infusion test was performed by inserting two needles directly into the reservoir. Pressure was measured via one needle and fluid infused via the other.

Pt no.	Sex	Age	Provisional Diagnosis	Shunt in situ ?	Lumber or Ommaya	Symptoms*
1	M	47	Hydrocephalus	N	L	Ha
2	M	64	NPH	N	L	Gait, Dementia
3	M	64	NPH	N	L	Gait, Incontinence, Dementia
4	M	57	Hydrocephalus	N	L	Ha, Naus
5	F	42	Shunt malfunction	Y	O	Ha, Naus, Vom
6	F	43	shunt malfunction	Y	O	Ha
7	F	13	Shunt malfunction	Y	L	Ha
8	M	65	NPH	N	L	Gait, Dementia
9	M	41	Shunt malfunction	Y	O	Lethargy, Behavioral problems
10	F	14	Shunt malfunction	Y	O	Ha, Naus
11	M	61	NPH	N	O	Gait, Dementia
12	F	22	Shunt malfunction	Y	O	Ha, Naus
13	F	52	Hydrocephalus	N	O	Gait, Dementia
14	M	21	Shunt malfunction	Y	O	Ha
15	F	42	BIH	N	L	Ha, Lethargy
16	F	44	Shunt malfunction	Y	O	Ha, Naus, Behavioral problems
17	F	21	Hydrocephalus	Y	O	Ha
18	F	58	Hydrocephalus	N	L	Ha, Naus, Vom
19	M	41	Hydrocephalus	Y	O	Severe lethargy
20	F	24	Shunt malfunction	Y	L	Ha, Naus, Lethargy
21	F	34	BIH	N	L	Ha, Naus, Vom
22	M	56	NPH	N	O	Gait, Dementia
23	M	57	Shunt malfunction	Y	O	Ha, Gait, Dementia
24	F	30	BIH	N	L	Ha, lethargy
25	F	52	Hydrocephalus	N	O	Gait, Confusion
26	F	57	NPH / Alzheimer's	N		Dementia
27	F	37	Shunt malfunction	Y	O	Ha
28	M	80	NPH	N	L	Gait, Incontinence, Dementia
29	M	78	NPH	N	L	Ha, Gait, Dementia
30	M	72	NPH	N	O	Gait, Incontinence, Dementia
31	F	70	NPH	N	O	Gait, Incontinence, Dementia

* Ha = Headache
Naus = Nausea
Vom = Vomiting
Gait = Gait disturbance

Table 2: Details of patients with CSF infusion tests and overnight ICP monitoring

Pt no.	Sex	Age	Provisional Diagnosis	Shunt in situ ?	Lumber or Ommaya	Symptoms*
32	M	25	Hydrocephalus	N	O	Ha, Naus
33	F	15	Shunt malfunction	Y	L	Ha, Naus, Vom
34	M	16	Hydrocephalus (post HI)	N	O	Ha
35	M	23	Hydrocephalus (assoc with subdural haematoma)	N	O	Ha
36	M	67	NPH	N	L	Gait, Incontinence, Dementia
37	M	30	Shunt malfunction	Y	O	Ha, Lethargy
38	F	41	Hydrocephalus	Y	O	Ha, Lethargy
39	M	53	Shunt malfunction	Y	O	Ha
40	F	45	BIH	N	L	Ha, Naus
41	F	39	BIH	Y	L	Ha
42	F	39	Shunt malfunction	Y	O	Ha, Lethargy
43	M	69	NPH	N	O	Gait, Dementia
44	F	21	BIH	N	L	Ha, Lethargy
45	M	62	NPH	N	O	Gait, Dementia, Incont
46	M	64	NPH	N	L	Gait, Dementia, Incontinence
47	F	31	Shunt malfunction	Y	O	Ha, Naus

* Ha = Headache
Naus = Nausea
Vom = Vomiting
Gait = Gait disturbance
Incontinence = Incontinent of urine

Table 2 continued : Details of patients with CSF infusion tests and overnight ICP monitoring

Off-line analysis of the ICP signal gave a complete set of cerebrospinal compensatory parameters. The resistance to CSF absorption (R_{csf}) was calculated as the pressure change divided by the infusion rate (mmHg/ml/min).

The pressure volume index (PVI) was calculated from the effective volume change. The reference pressure required for the calculation of PVI, was taken as the point at which the ICP-AMP (AMP is the fundamental component of the ICP pulse wave) regression line crosses the ICP axis [36].

On completion of the infusion test the lumbar needle was removed, but the lumbar drain was left in position for overnight ICP monitoring. If the computerised infusion test was performed via an Ommaya reservoir the needle used for fluid infusion was removed and ICP was monitored via the remaining needle. The ICP signal was checked periodically though out the recording period.

5. DATA ANALYSIS

5.1 Simultaneous Overnight ICP and TCD Monitoring.

The ICP and TCD signals were sampled at a frequency of 30Hz and stored on the hard disc of a laptop computer equipped with an analogue to digital converter and the Biomedical Signal Recorder software (figure 2). The data were analysed off-line using a program ICMR (Czosnyka, University of Cambridge) [35] specifically adapted for this purpose. The data was analysed twice. Parameters such as PI (Goslings pulsatility index), RAP, AMP and FVa (amplitude of flow velocity waveform) were calculated during one analysis and output as an ASCII file. The amplitude of the ICP waveform was assessed using the fundamental component waveform of the ICP pulse wave (AMP) to avoid distortion caused by different frequency responses of the pressure transducers used in the study [37,38].

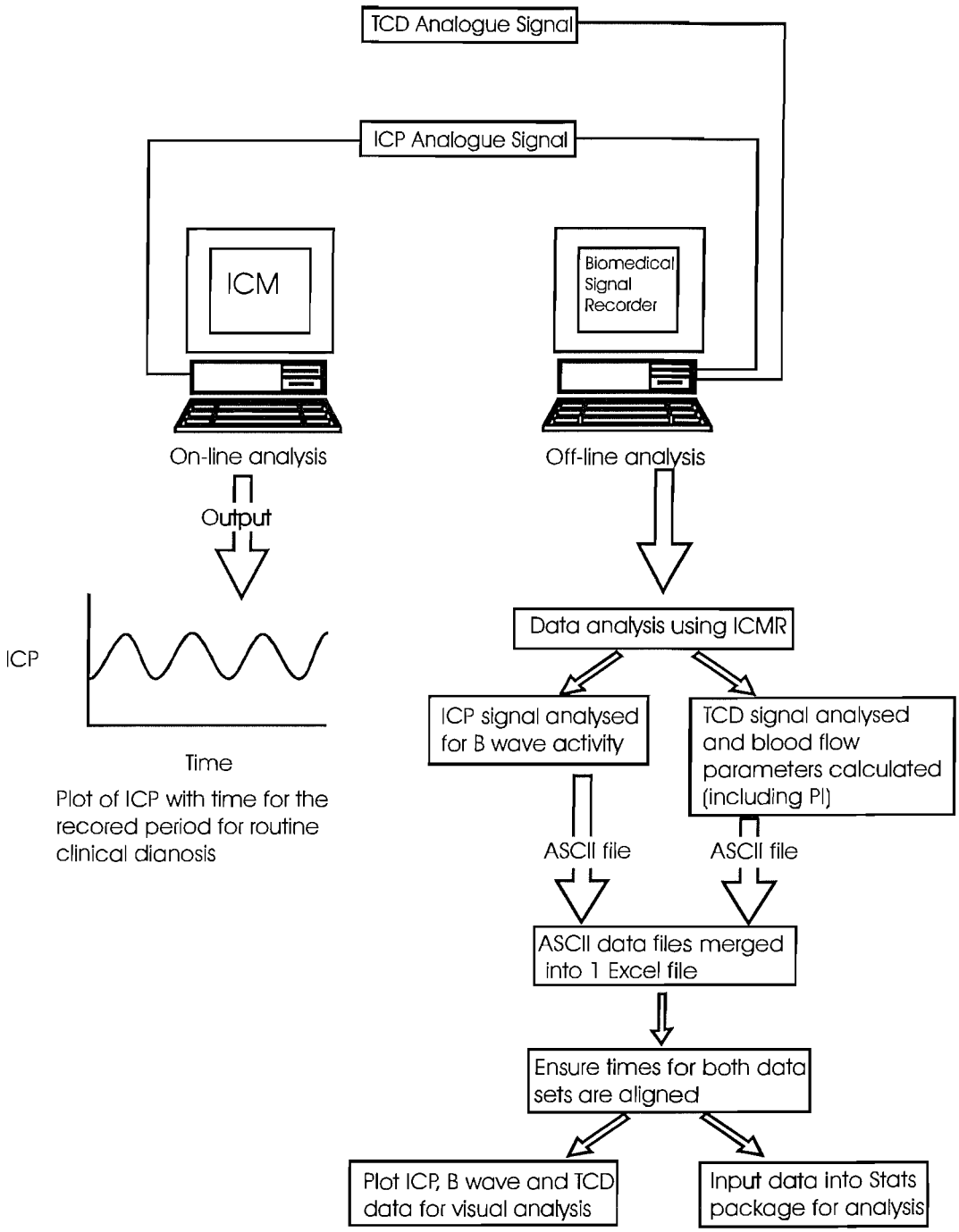

Figure 2: Data analysis flow chart

RAP is the correlation coefficient between the amplitude of the ICP pressure wave (AMP) and mean ICP [37,38]. To determine the amplitude of B wave type fluctuations in the blood flow velocity and ICP signals a second analysis was performed. For this analysis a frequency divider was used to give an effective sampling rate of 12.5Hz. Twenty second epochs of ICP and TCD data were then analysed to assess the amplitude of B waves in the ICP signal (ICP_{Bwave}) and the amplitude of B waves in the TCD signal (FV_{Bwave}).

This data was also output as an ASCII file. The two ASCII files were then merged into one Excel file. After ensuring the times of the two data sets were correctly aligned the data was imported to the software package Statgraphics Plus for statistical analysis and plotted for visual analysis. The patients were divided into subgroups according to the:
(a) degree of correlation between the B wave activity in ICP and TCD signals
(b) degree of ICP B wave activity
The ICP and TCD parameters for these subgroups were compared. In addition the TCD data was compared with the TCD data generated in normal volunteers (see Chapter 3).

Parameters were compared using t-tests.

The ICP signal was input to a second laptop computer equipped with an analogue to digital converter. The software ICM averaged the signal every 30 seconds and plotted the data on-line. This provided a plot of ICP with time for the whole of the recorded period which was then eye-balled. This data was generated solely for routine clinical diagnosis and has not been analysed in this chapter.

5.2 Comparing B Wave Activity and Hydrodynamic Compensatory Parameters.

The ICP signal recorded overnight was analysed as described above. The following parameters were calculated: ICP, AMP, RAP and the amplitude of the ICP B waves (ICP_{Bwave}). The data generated during the computerised CSF infusion tests was analysed as

described in Chapter 2. R_{csf} (resistance to CSF outflow), PVI (pressure volume index) and ICP_{open} (the initial ICP recorded before fluid infusion) were calculated. The ICP and hydrodynamic data was then imported into the software package Statgraphics Plus for statistical analysis. Hydrodynamic parameters were compared in patients with and without clinically significant ICP B wave activity using t-tests.

6. RESULTS

6.1 Simultaneous Overnight ICP and TCD Monitoring

Visual analysis of the recorded signals demonstrated that B wave type fluctuations were present in both the TCD and ICP recordings of some patients as expected. The data was then statistically analysed in three ways. The data are presented as means $\pm$ standard deviation

(a) Patients were divided into two sub-groups according to the degree of correlation between the amplitude of B waves in the ICP signal (ICP_{Bwave}) and the amplitude of B waves in the TCD signal (FV_{Bwave}). High correlation was defined as >0.4 (n=8) and low correlation was defined as < 0.4 (n=7). An example of the ICP and TCD parameters for a typical patient in each sub-group is shown in figures 3a and 3b. The ICP and TCD parameters (mean for recorded period) in these 2 sub-groups were compared as shown in table 3.

TCD and ICP parameters	Good correlation (correlation coeff >0.4) (n=8)	Poor correlation (correlation coeff <0.4) (n=7)	p
ICP (mmHg)	9.82 $\pm$ 7.36	6.12 $\pm$ 8.97	ns
RAP	0.76 $\pm$ 0.15	0.42 $\pm$ 0.31	p=0.008
ICP_{Bwave}(mmHg)	1.02 $\pm$ 0.66	0.90 $\pm$ 0.94	ns
PI	8.78 $\pm$ 1.54	8.52 $\pm$ 2.22	ns
FV (cm/s)	41.19 $\pm$ 11.18	38.76 $\pm$ 9.51	ns
FV_{Bwave} (cm/s)	2.11 $\pm$ 0.59	1.87 $\pm$ 0.67	ns

Table 3: ICP and TCD parameters in patients with good and poor correlation between the amplitude of the ICP B waves (ICP_{Bwave}) and TCD B waves (FV_{Bwave}) (ns = not statistically significant)

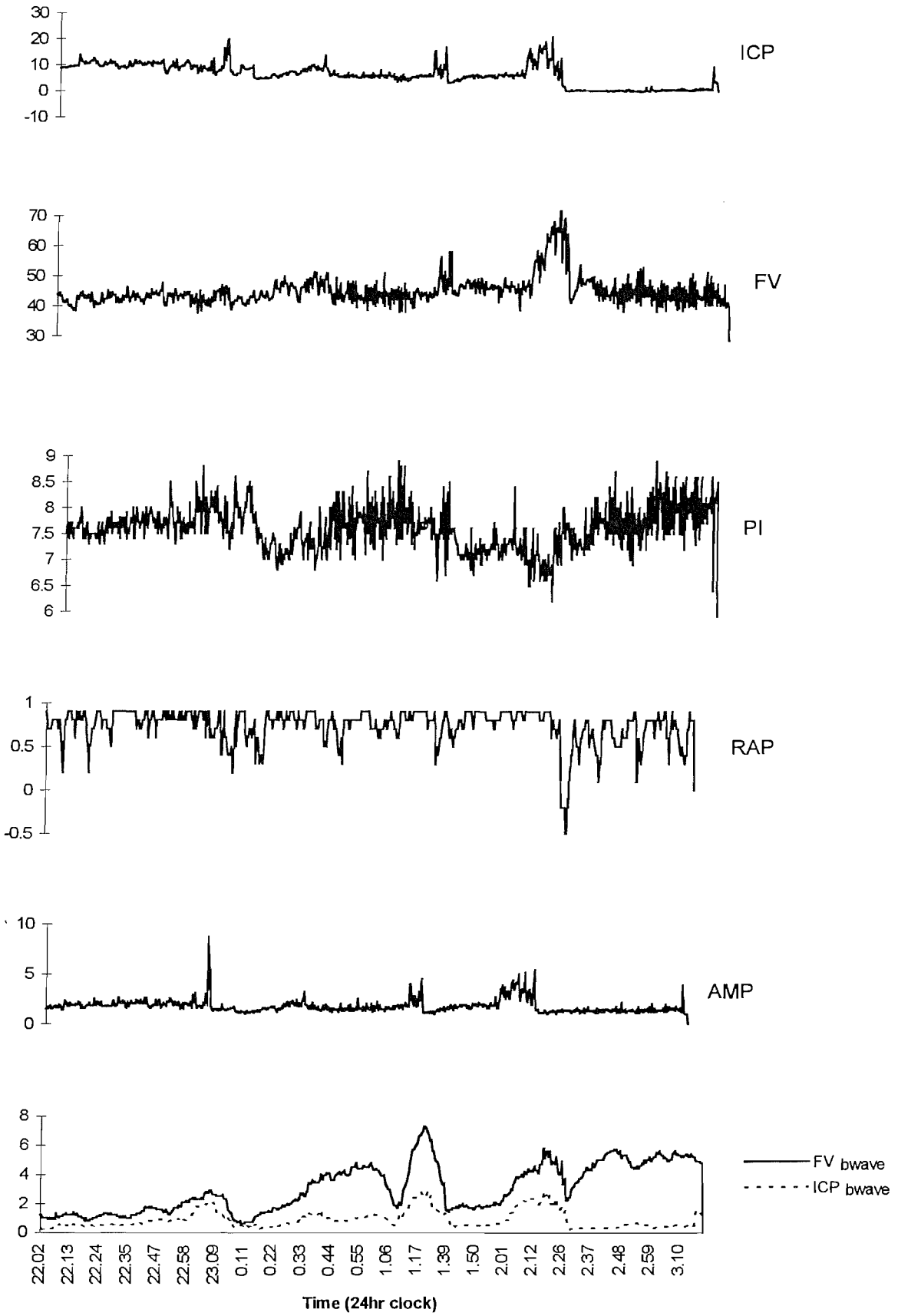

Figure 3a: An example of ICP, FV and derived parameters from a patient with well correlated ICPbwave and Fvbwave activity

ICP (mmHg), FV (cm/s), FVbwave (cm/s), ICPbwave (mmHg), AMP (mmHg)

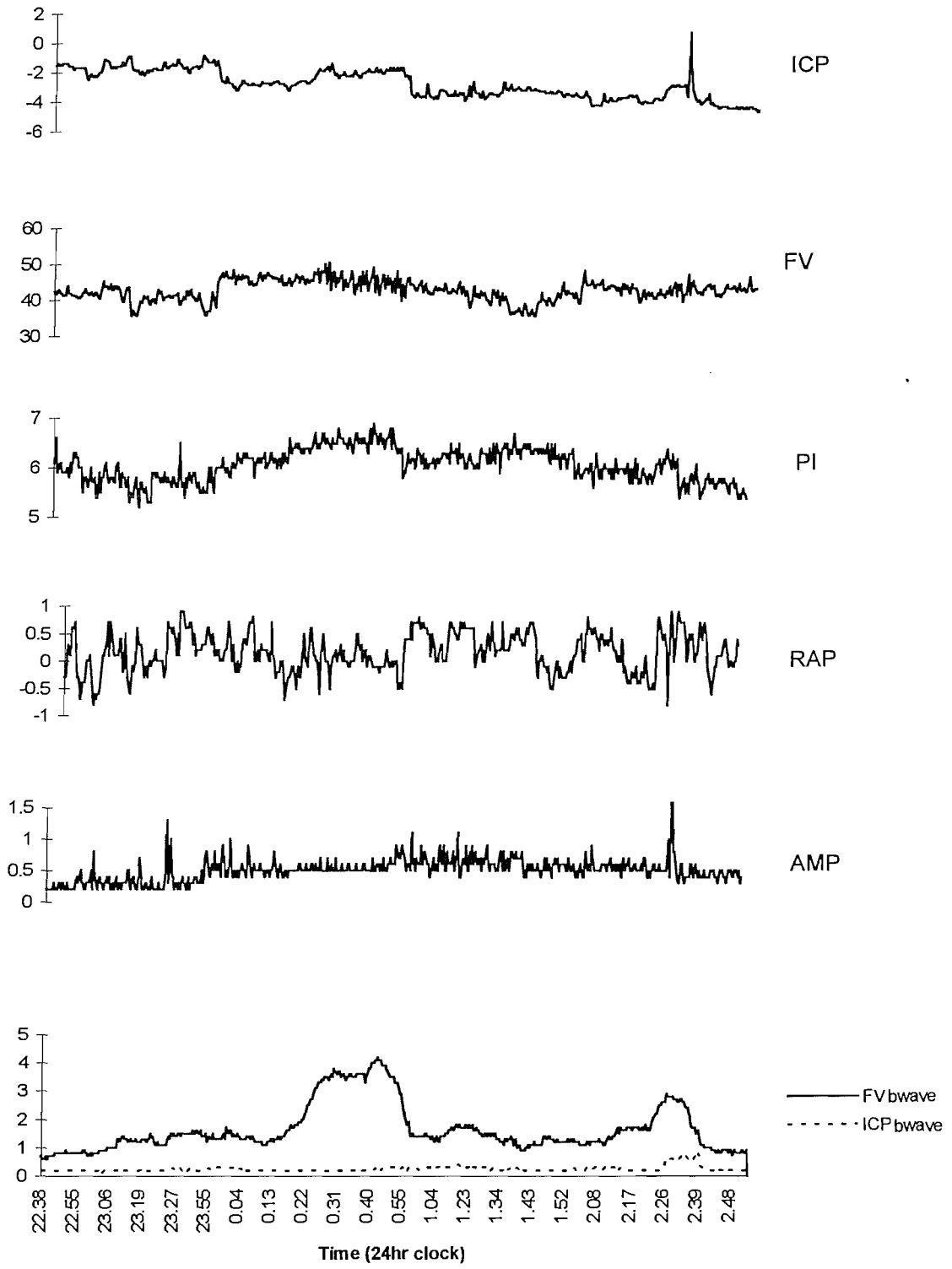

Figure 3b: An example of ICP, FV and derived parameters from a patient with poorly correlated ICPbwave and FVbwave activity

ICP (mmHg), FV (cm/s), FVbwave (cm/s), ICPbwave (mmHg), AMP (mmHg)

Comparison of RAP in the two groups, demonstrated a statistically greater RAP in patients with well correlated ICP_{Bwave} and FV_{Bwave}. As RAP is associated with compliance [38,39] these results suggest that the B wave type fluctuations observed in FV are more likely to be transmitted to the ICP when brain compliance is impaired.

These results also demonstrate that patients with well correlated ICP and FV B wave activity have increased mean ICP, FV and B wave activity compared to patients with poor correlation. However, within these groups a wide inter-patient variability is demonstrated by the large standard deviations and these differences are not statistically different.

(b) Patients were divided into two sub-groups according to the amplitude of B waves in the ICP signal. Patients were considered to have prominent B wave activity if the average amplitude of the ICP B waves (ICP_{Bwave}) was greater than 0.6mmHg (n=10). The remaining patients had ICP_{Bwave} less than 0.6mmHg (n=5). The TCD and ICP parameters were compared for these two groups (see table 4 below).

TCD and ICP parameters	ICP_{Bwave} > 0.6 mmHg (n=10)	ICP_{Bwave} < 0.6 mmHg (n=5)	p
ICP (mmHg)	10.02 ± 8.55	4.24 ± 5.98	ns
RAP	0.77 ± 0.12	0.26 ± 0.20	p<0.0001
ICP_{Bwave}(mmHg)	1.26 ± 0.78	0.37 ± 0.21	p=0.013
PI	0.92 ± 0.17	0.75 ± 0.15	p=0.038
FV (cm/s)	38.44 ± 11.98	43.28 ± 4.23	ns
FV_{Bwave}(cm/s)	2.03 ± 0.70	1.93 ± 0.46	ns

Table 4: ICP and TCD parameters in patients with and without prominent ICP B wave activity (ns= not statistically significant)

Comparison of ICP and TCD parameters in the two groups, demonstrates a statistically greater RAP and PI in patients with prominent B wave activity. As RAP may be associated

with compliance these results suggest that ICP B waves are more prominent when compliance is impaired. Significantly increased PI in patients with prominent B wave activity may suggest a diminished haemodynamic reserve in this group.

(c) The TCD data from the whole patient group (n=15) was then compared with data collected from eight normal volunteers during sleep (see Chapter 3). The B wave frequency and the amplitude of the B wave activity in the TCD signal (FV_{Bwave}) were compared in the 2 groups along with mean FV as shown in table 5.

These results demonstrate that the frequency of B waves in the TCD signal was not significantly different in the patient and normal volunteer groups. However, both the mean FV and the amplitude of the B waves in the TCD signal (FV_{Bwave}) were found to be significantly greater in the normal volunteers compared to the patient group.

TCD parameters	Normal Volunteers (n=8)	Patients (n=15)	p
FV (cm/s)	56.18 ± 10.29	39.47 ± 10.07	p=0.001
B wave frequency (oscillations/minute)	1.47 ± 0.14	1.58 ± 0.23	ns
FV_{Bwave} (cm/s)	3.10 ± 0.39	1.99 ± 0.61	p=0.0001

Table 5: TCD parameters in normal volunteers compared with patients (ns = not statistically significant)

Further analysis of the pooled patient and normal volunteer data demonstrated that the amplitude of B wave activity was positively correlated to mean FV ($r=0.75$, $p<0.05$). This suggests that mean FV should be considered when comparing B wave amplitude.

6.2 Comparing B Wave Activity and Hydrodynamic Compensatory Parameters.

The overnight ICP data was analysed as previously described and the mean and maximum ICP and AMP were calculated along with RAP. This data was tabulated with the hydrodynamic compensatory parameters.

Patients were divided into two sub-groups according to the amplitude of B waves in the ICP signal. Patients were considered to have prominent B wave activity if the average amplitude of the ICP B waves (ICP_{Bwave}) was greater than 0.6mmHg (n=27). The remaining patients had ICP_{Bwave} less than 0.6mmHg (n=20).

Overnight ICP parameters	**Patients with prominent B wave activity in ICP (ICP_{Bwave} > 0.6 mmHg) (n=27)**	**Patients without prominent B wave activity in ICP (ICP_{Bwave} < 0.6 mmHg) (n=20)**	**p**
ICP_{max}	19 ± 13	9.5 ± 15	p<0.022
ICP_{mean}	8.11 ± 6.06	3.48 ± 9.30	p<0.037
AMP_{max}	5.34 ± 3.18	2.41 ± 2.82	p<0.0037
AMP_{mean}	2.38 ± 1.38	1.30 ± 1.42	p<0.015
RAP_{mean}	0.65 ± 0.23	0.34 ± 0.31	p<0.00075
Hydrodynamic compensatory parameters			
R_{CSF}	16.39 ± 9.69	9.04 ± 7.29	p<0.03
PVI	16.63 ± 9.03	25.70 ± 10.20	p<0.03
ICP_{open}	10.19 ± 4.00	4.47 ± 5.00	p<0.006

Table 6: ICP and hydrodynamic compensatory parameters in patients with and without prominent ICP B wave activity.

Table 6 demonstrates that all the parameters compared were significantly different in the two groups. ICP_{max}, ICP_{mean}, AMP_{max}, and AMP_{mean} calculated from the overnight ICP data were significantly greater in patients with prominent B wave activity. The difference in RAP in the two groups was highly significant ($p < 0.00075$) demonstrating, again, that compliance may play a significant role in the propagation of B wave activity. The hydrodynamic compensatory parameters (R_{csf}, PVI and ICP_{open}) calculated from the infusion test data were also significantly greater in patients with clinically significant B wave activity.

7. DISCUSSION

The overnight TCD and ICP recording in patients clearly demonstrated B wave type fluctuations in the cerebral blood flow velocity recordings of all patients. Comparison of the TCD B wave data in patients with normal volunteers demonstrated that there was no significant difference in the frequency of TCD B wave fluctuations. Mean flow velocity was found to be significantly greater in the normal volunteers. This may be an age related finding as the two groups were not aged matched - the average age of the patients was 60 years compared to 31 years in the normal volunteer group. This may explain why the amplitude of TCD B wave activity was greater in the normal volunteers compared to the patients. When the data for both groups was pooled there was a positive correlation between mean FV and TCD B wave amplitude.

These findings demonstrate that TCD may be an effective addition to ICP monitoring to confirm that waves seen in the ICP are not artifact. However, TCD alone could not be used as a diagnostic tool to differentiate normal and pathological states.

TCD and ICP parameters were compared to explore the pathophysiology of ICP B wave activity. RAP and PI were found to be greater in patients with prominent ICP B wave activity. The interpretation and clinical significance of RAP has been explored during CSF infusion tests in hydrocephalic children [37] and during long term monitoring of head injured patients [38,39]. The study in children demonstrated that RAP remains close to zero in a

normal stable system where changes in intracranial volume appear to be compensated for by compression of the vascular bed according to the Monroe-Kelly doctrine. In this situation correlation between the changes in AMP and ICP is low. When adequate compensation can no longer occur AMP increases with ICP producing an increased RAP. This suggests that patients with prominent ICP B wave activity have poor compensatory ability due to a change in compliance.

Increased RAP was also identified in patients with well correlated ICP and TCD B waves. This suggests that changes in compliance are required for transmission of B waves from the haemodynamic to the hydrodynamic systems.

The significance of increased PI in patients with prominent B wave activity must be interpreted with care. A study in rabbits [40] assessing the significance of changes in PI (incorporating some of the data generated in Appendix 1) demonstrated that PI increases when the cerebrovascular resistance decreases due to decreasing CPP. However, when cerebrovascular resistance decreases due to hypercapnia, PI also decreases. As patients with NPH have been reported as having disturbed sleep architecture accompanied by periods of apnea [26], $PaCO_2$ levels may fluctuate during the recording. To interpret the significance of PI, $PaCO_2$ and arterial blood pressure should be measured.

Comparison of hydrodynamic compensatory parameters in patients with and without prominent B wave activity demonstrated that R_{csf} was significantly greater and PVI was significantly lower in patients with prominent B wave activity in overnight ICP recordings. The finding of increased R_{csf} in this group is in agreement with Gjerris et al [15]. As PVI is an indicator of brain compliance this data suggests that patients with prominent ICP B wave activity have reduced brain compliance.

8. CONCLUSIONS

In conclusion the data presented in this chapter has demonstrated that the 'driver' for ICP B wave activity is B wave type fluctuations in the cerebral blood flow velocity. The transmission of the fluctuations in blood flow is dependent on pathophysiological change which appears to be reflected by an increase in the ICP parameter RAP. These findings draw into question the belief that ICP B waves must occur for a certain percentage (5-50%) of the overnight recording to be of clinical significance [11,14]. If a patient undergoing overnight ICP monitoring does not experience REM sleep, the 'driver' flow velocity fluctuations for ICP B wave activity may not be present. This will result in a false negative result. The addition of TCD to overnight recording would be a useful addition for the interpretation of ICP B wave activity.

9. FURTHER STUDIES

Further studies of interest would include overnight ICP, TCD, ABP, ECG and $PaCO_2$ in patients before and after shunting to correlate the change in clinical status with change in physiological parameters. Assessment of ECG and $PaCO_2$ would allow the effects of sleep architecture and sleep apnea to be determined. Non-invasive ABP measurement would complete the physiological picture allowing further exploration of the TCD and ICP parameters

CHAPTER 5

IS THE QUANTIFIED AREA OF HYPERINTENSITY ON MAGNETIC RESONANCE IMAGES A PREDICTOR OF OUTCOME AFTER SHUNTING IN CASES OF SUSPECTED NORMAL PRESSURE HYDROCEPHALUS?

IS THE QUANTIFIED AREA OF HYPERINTENSITY ON MAGNETIC RESONANCE IMAGES A PREDICTOR OF OUTCOME AFTER SHUNTING IN CASES OF SUSPECTED NORMAL PRESSURE HYDROCEPHALUS?

1. INTRODUCTION

Magnetic resonance imaging (MRI) is a versatile clinical and experimental non-invasive technique used in the investigation of neurological disorders. More sensitive in the detection of white matter lesions than computerised tomography (CT) [1] the earliest applications included the assessment of patients with multiple sclerosis and other deep brain changes.

Although not routinely used in the assessment of hydrocephalus, MRI is used as a research tool to investigate the pathophysiology of the condition in vivo. However, in normal pressure hydrocephalus (NPH) the additional information provided by MRI may be valuable for differential diagnosis. MRI techniques for the investigation of NPH include: dynamic studies of cerebrospinal fluid (CSF) flow in the aqueduct, ventricular system [2,3] and CSF shunts [4]; anatomical studies quantifying CSF and ventricular volumes [5,6] and the investigation of white matter hyperintensities [7,8,9,10]. These studies demonstrate the versatility of MRI, but each application requires specific imaging procedures.

This is a retrospective study of MRIs performed pre and post shunt in a group of patients who participated in a detailed study of NPH. Patients underwent rigorous pre and post shunt assessment providing a wealth of clinical data. Regular and comprehensive post operative follow-ups allowed outcome to be assessed reliably. Proton density and T2 weighted MR images were produced in the axial plane at 7mm intervals. Although originally produced for ventricular volume studies, deep white matter and peri-ventricular hyperintensities (PVH) were observed. In this study the occurrence and position of these hyperintensities was investigated and correlated with outcome after shunting.

1.1 Aims

The Southampton NPH study, performed over several years from 1987, is one of the most comprehensive studies of its type. A wealth of clinical and diagnostic data has provided a detailed insight into the pathophysiology of NPH. Detailed follow-up after shunting has allowed data to be correlated with outcome, identifying the factors which indicate good outcome after shunting.

The aim of this study was to use this previously obtained MRI data and quantify white matter changes and to determine whether the:

- degree of white matter hyperintensities (deep white matter changes and PVL) related to outcome after shunting
- position of the white matter changes in each axial slice is significantly related to outcome

The watershed theory (see section 2.2 of this chapter) regarding the position of the deep white matter hyperintensities in relation to the middle cerebral artery was also investigated.

2. MRI HYPERINTENSITIES

The pixel intensity in MRI is predominantly a function of proton density and imaging procedure. Imaging parameters may be manipulated allowing tissue differentiation and enhancement of pathological changes. Proton density however, is a physical material property. Although all mobile protons may contribute to the MR signal, in biological materials the predominant contributors are hydrogen protons in water molecules. Therefore MRI hyperintensities (in T2 weighted images) represent areas with a high concentration of water molecules. Low intensity pixels indicate low mobile proton concentrations such as in bone or air.

Therefore, although an area of hyperintensity in the white matter indicates a pathological increase in water concentration, no insight is provided into the process provoking the tissue change. Visually identical hyperintensities may result from pathologies which induce edema, ischaemia, gliosis, demyelination or degeneration of the white matter. They have also been observed in the white matter of normal elderly subjects. MR images of patients with suspected NPH may demonstrate hyperintensities in the periventricular region and deep in the white matter.

The correlation between signal hyperintensities and pathophysiological changes has been investigated with clinical, post-mortem and experimental investigations. Changes in the relaxation times, the injection of contrast agents and the position and shape of tissue changes all provide clues to the pathological processes occurring within the tissues. Although correlations and associations between MRI, CT and clinical history provides some understanding of the clinical significance of changes on MR images, histological studies are required to demonstrate the associated tissue and cellular changes.

In NPH periventricular and deep white matter hyperintensities are of particular interest.

2.1 Periventricular Hyperintensities.

Clinical studies suggest that the high intensity halo often seen around the lateral ventricles in acute non-compensated hydrocephalus results from the transependymal spread of CSF [7,11,12]. As the hydrocephalus becomes compensated, the interstitial edema is reabsorbed.

A study in dogs demonstrated the MRI changes produced during experimentally induced chronic hydrocephalus [13]. Areas of periventricular hyperintensity on T2 weighted images correlated with expansion of the extracellular space assessed with histology. This provides further evidence to suggest that periventricular hyperintensity may result from transependymal fluid flow rather than tissue degeneration. Although periventricular hyperintensity is a characteristic of hydrocephalus, it is not exclusive to hydrocephalus and may be seen in other pathological states [14].

2.2 Deep White Matter Hyperintensities.

Deep white matter hyperintensities have been demonstrated in many pathological states and, in normal elderly subjects. They may be observed in some, but not all cases of suspected NPH. The pathological basis of deep white matter lesions has been explored in patients diagnosed with Binswangers disease [15] and post-mortem studies of neurologically normal elderly subjects [16]. One neurologically normal patient underwent MR imaging before death providing a baseline to assess image changes induced during post-mortem and fixation procedures. Comparison of the two MR images demonstrated no change in the visual appearance of the MRI features. Areas of hyperintensity were demonstrated in the periventricular area and deep in the white matter of the normal brains. Histology confirmed that the deep white matter hyperintensities correlated with areas of gliosis. In some cases, the area of MR hyperintensity was larger than the area of tissue damage observed. This was explained by the increased water content around the region of gliosis.

Deep white matter changes may result from insufficient blood flow producing regional ischaemia. In the elderly a decrease in perfusion pressure is often observed [17]. Autoregulatory mechanisms are activated to compensate and restore blood flow. If further reductions of flow occur, for example with vascular disease or hypertension, then the vessels may be unable to respond further with the autoregulatory reserve exhausted. The white matter is thought to be more susceptible to such events due to the distribution of blood volume and the vascular bed anatomy.

It is suggested that white matter lesions occur in a watershed zone between the deep medullary and the superficial cortical circulation [10]. In this region the vessels originate from the middle cerebral artery and therefore have a long intraparenchymal course. They are also very thin and particularly sensitive to arteriosclerosis. Therefore disorders such as hypertension which promote arteriosclerosis may advance white matter infarction [18,19,20]. A post-mortem study of 40 formalin fixed brains from neurologically normal subjects over 60 years of age investigated the relationship between MRI hyperintensities, arteriosclerosis and demyelination [20]. The results demonstrated a good correlation between MR hyperintensities and demyelination and gliosis as previously described. A good correlation was also found between

arteriolar thickening and demyelination. The number of hyperintense areas was found to increase with age.

A possible alternative or additional mechanism for the development of deep white matter changes is discussed in the Chapter 6 of this thesis. This hypothesis is based on the mathematical modelling of the physical stresses generated within the cerebral mantle in response to ventricular expansion. Areas of high stress are observed in the white matter in positions which correlate with deep white matter MRI hyperintensities. It is therefore conceivable that areas of high stress combined with the delicate nature of vessels in this area may lead to vascular distortion or destruction and ischaemic events. This is discussed in Chapter 6.

Although the exact process behind the ischaemic events may not be fully understood, the concept of a vulnerable watershed zone in the white matter of patients with NPH will be explored.

3. MRI HYPERINTENSITIES AND THE PATHOPHYSIOLOGY OF NPH

Hyperintensities around the ventricles or deep in the white matter in patients with suspected NPH are a common feature. It is now generally thought that periventricular hyperintensities in the frontal and posterior regions are more likely to result from transependymal CSF flow [7, 12] and hyperintensities in the white matter may be a result of decreasing cerebral perfusion [18, 19, 20].

The association between deep white matter lesions identified using MRI and the pathophysiology of NPH has been investigated by several groups, though a clear picture has not emerged.

Bradley et al [10] demonstrated that deep white hyperintensities were significantly more prevalent in a group of patients with suspected NPH compared to normal controls. A statistical association between deep white matter lesion occurrence and NPH was established. This finding led to the suggestion that the deep white matter changes may be

dependent on ventricular expansion or vice-versa and that the two pathological processes were interdependent. On the basis of this hypothesis the authors suggest that deep white matter changes should not be considered as a negative predictor for outcome after shunting as these tissue changes may be responsible for NPH. In four patients who underwent imaging pre and post shunting no changes in white matter hyperintensities were observed. This is as expected if the hyperintensities are a result of tissue degeneration.

Krauss et al [9] also demonstrated a higher incidence of deep white matter changes and PVL in patients with NPH (all of whom improved post shunt) compared with aged matched controls. The authors demonstrated a correlation between the incidence of both PVLs and DWMLs with ventricular size suggesting a coexistence of NPH and cerebrovascular disease in many patients. They propose that the link between these two disorders is accompanying systemic arterial hypertension rather than causal as suggested by Bradley et al.

4. CORRELATION OF CHANGES IN MRI WITH SYMPTOMS

Although it has been suggested that the typical triad of symptoms seen in NPH may correlate well with tissue changes in the corona radiata [21], a study relating the severity of symptoms with the degree of tissue change has not been performed in this patient group. When MR images of patients with non-Alzheimer's dementia were compared with those in normal elderly subjects, no correlation was found between the incidence of white matter lesions and degree of dementia [22]. However, a more recent study of patients after stroke [23] found significantly larger infarction areas in patients who went on to develop vascular dementia.

5. MRI FOR THE DIFFERENTIAL DIAGNOSIS OF NPH

Several groups have compared MRI hyperintensity occurrence in patients with suspected NPH who did and did not improve with shunting in an attempt to identify an MRI criteria that predicts responsiveness to shunting

Jack et al [7] investigated a group of 54 demented patients retrospectively. Clinical histories were used to classify dementia type. Seventeen patients were considered to have NPH with dementia (assessed with psychometric testing) associated with gait disorder and incontinence. The MRI hyperintensities were classified into periventricular (contiguous with the ependyma) and discrete white matter and were graded according to severity. Patients with NPH had a high incidence of periventricular and white matter changes. The improvement after shunting was assessed in 11 patients. Comparison of MRI features in this small group demonstrated that patients with periventricular hyperintensities, but without discrete white matter changes,demonstrated the best response to shunting.

Krauss et al [8] investigated the effect of white matter lesions on outcome following shunting in rigorously selected patients with NPH. Patients underwent a battery of tests to establish a diagnosis of NPH, including assessment of hydrodynamics and overnight ICP monitoring. All patients underwent MRI scanning before shunting and were followed-up for at least 3 months post-operatively. The results demonstrated a negative correlation between the extent of periventricular and deep white matter lesions with improvement post shunt. However extensive PVL or DWML did not exclude improvement post shunt and the absence of PVL or DWML was not necessarily an indicator for improvement.

6. MATERIALS AND METHODS

6.1 The Patients

Eighteen patients participating in the Southampton NPH research project under went MR imaging pre-shunt, and in the majority of cases (12 patients) post shunt. Before MR imaging all patients had undergone cognitive and clinical assessment and CT scanning. Patients were excluded from the study if the CT scan was not indicative of hydrocephalus or they were in poor general condition with extensive medical problems (figure 1).

As MRI facilities were not available at Southampton General Hospital, patients were transported to the Churchill Clinic, London.

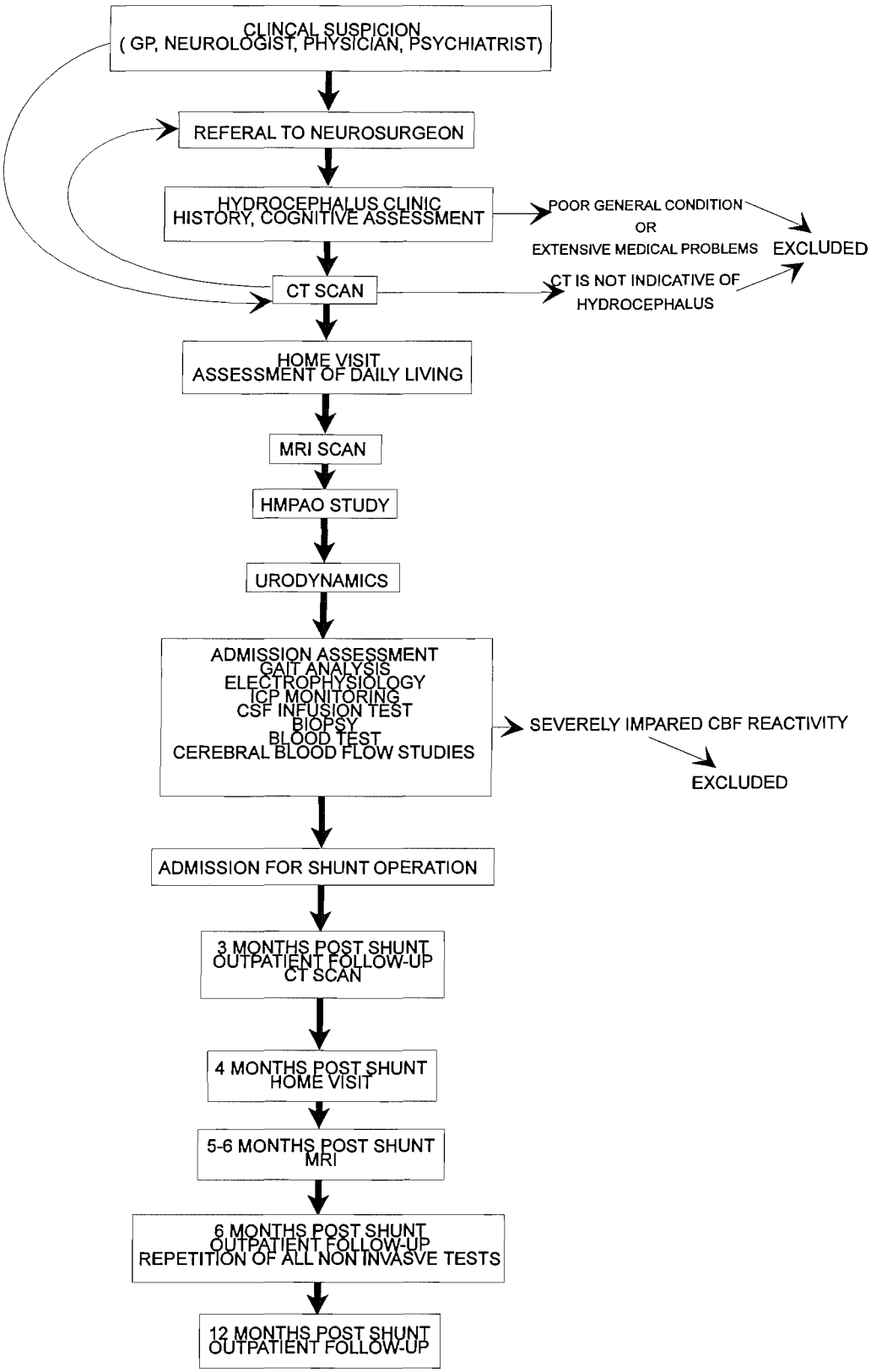

Figure 1. A flow diagram outlining pre and post shunting assessments for patients included in the Southampton NPH Study

Patient Number	Sex	Age When Shunted	Pre shunt History			Post Shunt MRI	Outcome
			Gait Disturbance	Mental Impairment	Incontinence		
1	F	75	18 months	18 months	12 months	*	+
2	F	72	18 months	18 months	3 months	*	+
3	M	73	11 years	0	18 months	*	+
4	M	74	9 years	9 years	0		+
5	F	72	3½ years	0	0	*	+
6	M	74	2 years	2 years	0	*	+
7	M	73	16 years	1 year	2 years	*	-
8	M	72	6 years	6 years	6 years		-
9	M	79	1 year	1year	1 year		-
10	M	78	5 months	0	1 month	*	-
11	M	64	2 years	1 year	0	*	-
12	M	75	18 months	6 months	0		-
13	M	67	8 years	8 years	0		-
14	M	71	1 year	18 months	1 month	*	-
15	M	55	1 year	2 years	0	*	-
16	M	73	10 months	2 years	10 months	*	-
17	F	80	18 months	5 months	1 month	*	-
18	M	Not recorded	Present but duration Not Recorded	Present but duration Not Recorded	Present but duration Not Recorded		-

* Indicates a post shunt MRI was performed

\+ Indicates the patient improved after shunting

\- Indicates no improvement after shunting

Table 1. Summary of Patient Details

A 1.5 Tesla Seimens machine produced T2 and proton density weighted images of sequential 7mm sections in the axial plane. Studies were repeated in the majority of patients 5-6 months after shunting (table1)

6.2 Method

The basic principles of magnetic resonance imaging are not described in this chapter.

6.3 Image Analysis

T2 and proton density weighted images for each patient were available in hard copy form only and therefore required re-digitising to allow computerised image analysis. As the hyperintensities were of main interest, the T2 images were chosen for quantitative analysis. Each image was placed on a light box with a charged video camera in place above. The camera was connected to a PC equipped with 'Frame Grabber' (Rombo Media Pro, Livingstone, Edinburgh) which allowed the digitised camera image to be displayed, acquired and stored. The video camera position was adjusted to ensure that the lens was perpendicular to the light box (preventing unnecessary image distortion). To minimise detail loss which may occur during re- digitisation the camera height above the light box was adjusted to ensure each axial image (and corresponding calibration line) fully occupied the space available on the 'Frame Grabber'. Care was taken to ensure the film, light box and camera lens were dust free. Each axial image was acquired and stored in tagged image file format (tiff) directly onto the main frame computer, networked to the PC (figure 2). All T2 weighted axial images were acquired for each patient pre shunt and where available, post shunt.

The digitised data on the mainframe computer was then accessed via a UNIX workstation. The tiff files were converted to the correct format required by the image analysis program using CaMReS (Cambridge Magnetic Resonance systems, Herchel Smith Department of Medicinal Chemistry, Nick Herrod). Aspect ratio correction was included in this process to prevent image distortion. This process was required as re-digitisation produced rectangular pixels and the monitor used for data analysis has square pixels.

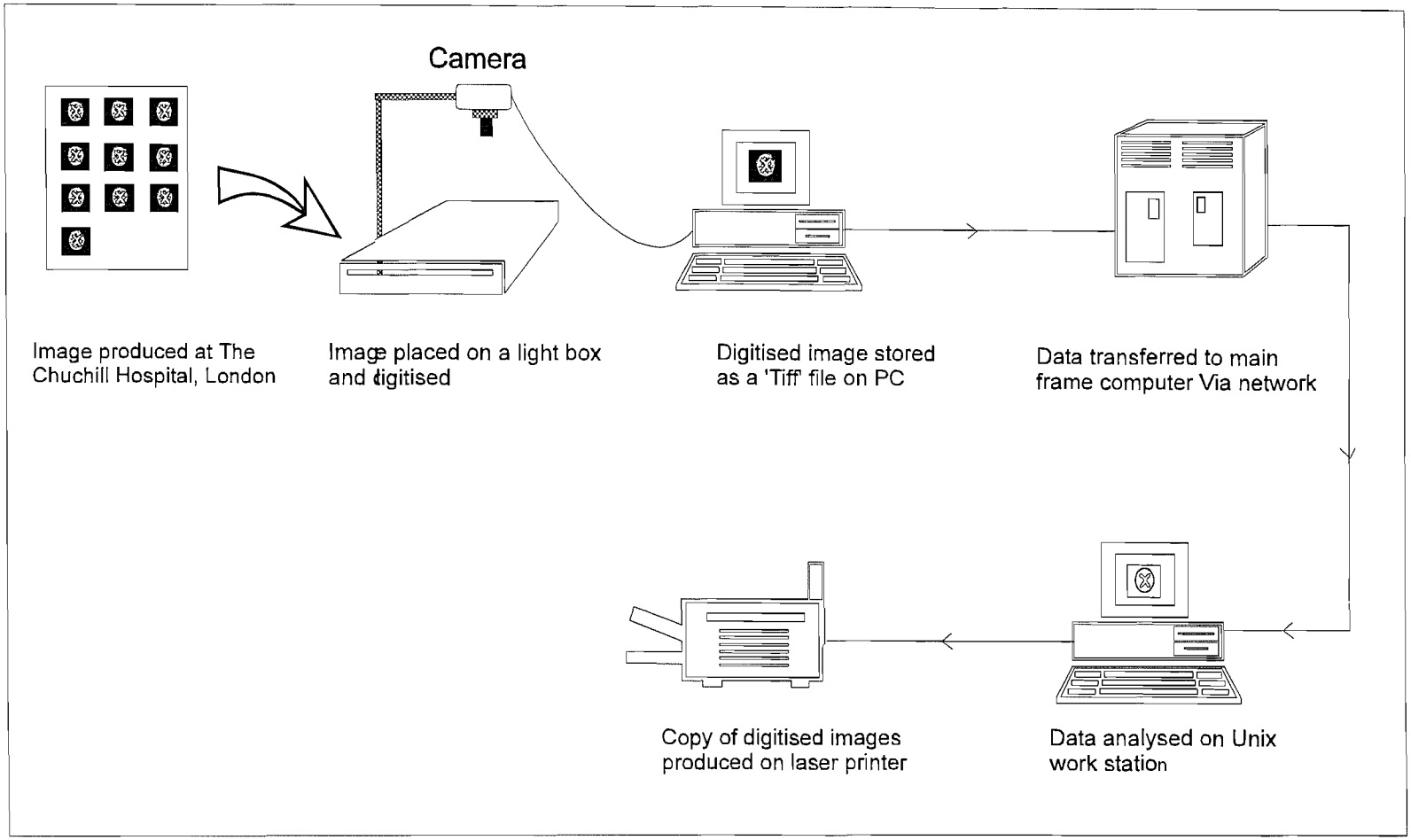

Figure 2. The equipment set-up for image analysis

The converted images were then analysed using CMRview (Herchel Smith department of Medicinal Chemistry).

Unfortunately the image quality was not standardised throughout the study. Some images had low contrast using only a small amount of the available grey scale and the brightness was not optimised. Although CMRview allows the image contrast and brightness to be adjusted it was found that these manoeuvres could change the size of the hyperintensities. Therefore instead of manually changing each image a normalisation procedure was introduced. To normalise an image a representative area (as large as possible) of CSF was selected with the mouse and the average density of the region automatically calculated. An area of bone was then selected in a similar manner. The average density of the lightest and darkest biological areas were then used to 'clip' the image. Therefore the minimum and maximum grey scale values were set to the density of the CSF and bone respectively (figure 3). After normalisation, the image quality was improved without distortion of the hyperintensities. The normalisation theory was based on the estimation that with standard MR settings the density of CSF and bone should appear similar in different subjects assuming no large changes in CSF or bone composition. After normalisation the images in each scan were printed out on a laser printer to allow the position of the hyperintensities to be recorded.

The areas of the hyperintensities were calculated with a semi-automated technique using a combination of boundary defined and interior defined thresholding [18]. Interior defined thresholding was used where ever possible. A small region was drawn with the mouse within a hyperintense area and the intensity of the area determined. The lowest intensity measured in this region was then used as a threshold value. All the pixels with an intensity higher than the minimum are then automatically filled from a predefined seed point positioned inside the hyperintense region. This technique was used when the density of the hyperintense region was obviously different from the surrounding area for example a discrete hyperintensity deep in the white matter. Boundary defined area measurements involve carefully drawing around the region to be measured with the computer mouse then instructing the computer to 'fill' the region and calculate the area in square pixels.

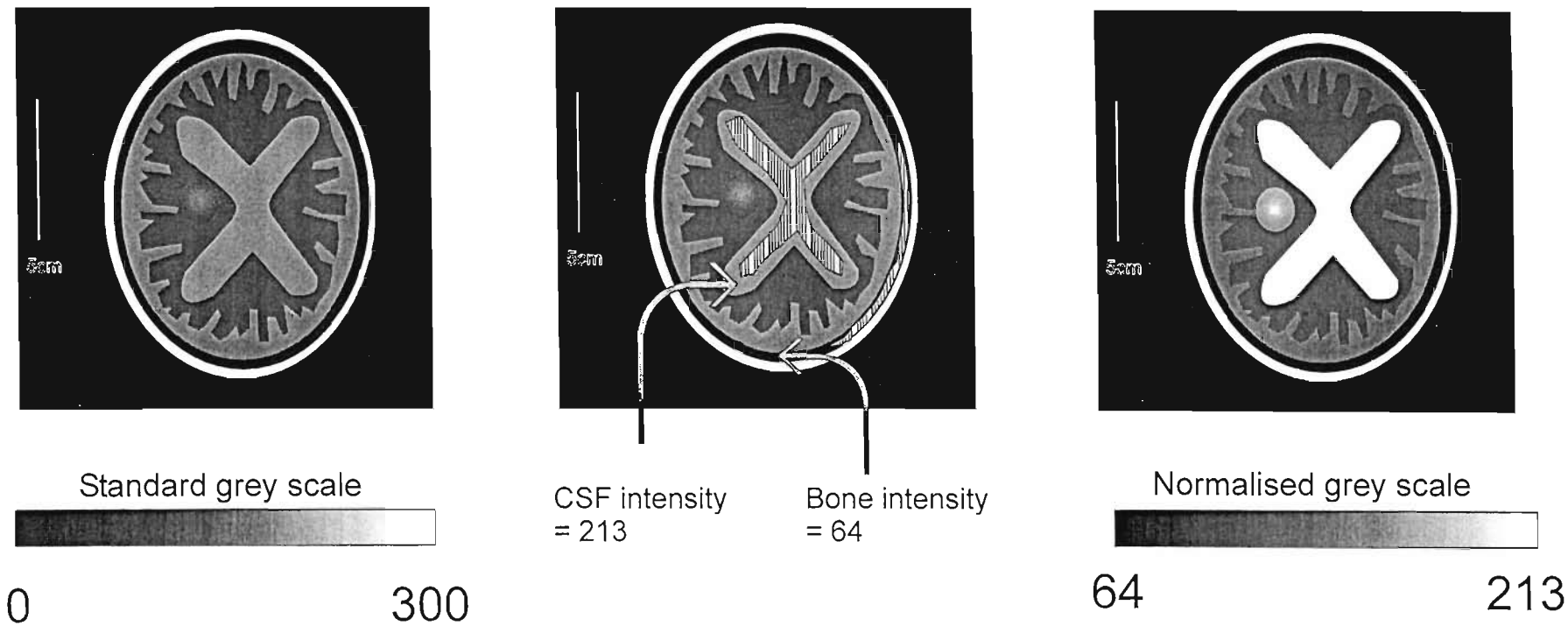

Figure 3. The normalisation procedure

This techniques high dependence on accurate outlining may introduce user dependent error. However where hyperintensities were continuous with the ventricles then boundaries were hand drawn before thresholding the area combining the two techniques.

The area of the thresholded region was calculated in square pixels and a small dot automatically placed at the centre of gravity.

The areas expressed in term of pixels were converted into mm using a conversion factor determined by measuring the 5cm calibration line available on all scans. The position of the hyperintensities were classified according to their location - frontal, body or posterior (figure 4) and according to whether they were continuous or discontinuous with the ventricles. The data was tabulated for each MRI scan allowing the total area of each 'type' of hyperintensity to be calculated for each slice of each MRI scan.

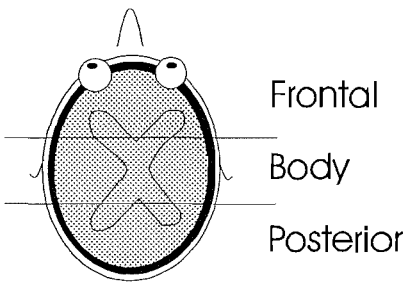

Figure 4. The approximate boundaries used for the classification of hyperintensities into frontal, body and posterior.

Patients' outcome after shunting was assessed by an experienced clinician (JD Pickard). Patients were classified as improved or not improved after shunting based on post shunt assessment of gait, mental impairment, urinary incontinence and social and behavioural factors. Shunt complications and revisions were also taken into consideration. The follow-up period was variable, from 8 months to 33 months depending on the patient state. Six patients improved (3 females and 3 males, average age 73 years, range 72-75 years). No significant improvement was seen in 12 patients (1 female and 11 males, average age 66 years, range 55-80 years).

The data was input into Statgraphics for statistical analysis.

7. RESULTS

To determine the differential diagnostic potential of white matter hyperintensity topography, the area and position of MRI hyperintensities in the pre shunt images were compared in patients who did (n=6) and did not improve (n=12) after shunting. The average area of each type of hyperintensity ± the standard error is presented in table 2.

	Average area of hyperintensity in patients who **improved** after shunting (mm^2) (n = 6)	Average area of hyperintenstiy in patients who did **not improve** after shunting (mm^2) (n = 12)	P
Frontal Continuous	83 ± 78	287±100	n.s.
Frontal Discontinuous	3±2	21±10	n.s.
Body Continuous	11±9	273±87	p<0.05
Body Discontinuous	67±67	199±93	n.s.
Posterior Continuous	417±220	2069±401	p<0.05
Posterior Discontinuous	26±20	35±18	n.s.
Total Continuous	511±286	2629±486	p<0.05
Total Discontinuous	96±88	255±99	n.s.
Total (Total Continuous + Total Discontinuous)	608±364	2884±538	p<0.05

Table 2. The area of each type of hyperintensity for patients who did and did not improve after shunting (compared using a Mann Whitney test)

The area of body continuous, posterior continuous and consequently total continuous and total (continuous + discontinuous) hyperintensities were greater in patients who did not improve after shunting.

To assess the vertical distribution of white matter hyperintensities the total area of all continuous and discontinuous hyperintensities were calculated for each individual pre shunt MRI slice. As each slice was 7mm thick then the number of slices per patient was

variable depending on brain/head size. The area of tissue change per slice was plotted for each patient beginning with slice one at the base of the brain (figure 5)

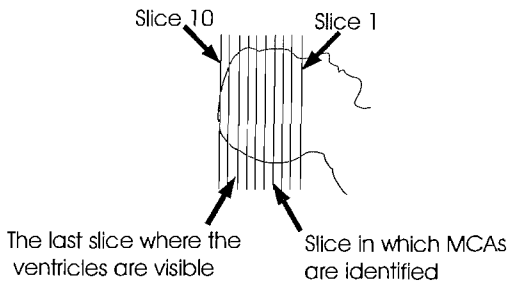

Figure 5. Area of hyperintensity per MRI slice.

Three plots were produced per patient for the continuous, discontinuous and total hyperintense areas for each slice. For each scan the middle cerebral arteries (MCAs) were identified and the slice in which they were located was marked on plots with an asterix (*). The point at which the ventricles were no longer visible at the top of the brain was also assessed. For the majority of patients gross ventricular dilation was seen and the ventricles were visible in all the brain slices. Therefore the last slice in which ventricles were observed was marked on the plots with 2 asterixes (**) (figures 6a, 6b,7a, 7b, 8a, and 8b).

To investigate the 'watershed ' theory for the development of deep white matter lesions, the plots of incontinuous hyperintensities were visually assessed (figures 6a and 6b) to define the distribution of hyperintensities between the base of the brain, the MCAs and the brain apex. No specific pattern was observed and a high patient to patient variability was noted. The area of incontinuous hyperintensity for each slice, between the MCA and the last slice where this type of hyperintensity was observed, was statistically assessed using a regression analysis and analysis of variants. This demonstrated that there was no statistically significant increase in the area of incontinuous hyperintensity as the distance from the MCA increased ($p < 0.05$).

Unexpectedly, visual assessment of the continuous hyperintensity (figures 7a and 7b) and total hyperintensity (figures 8a and 8b) plots revealed increasing areas of hyperintensity from the base of the brain to the apex. A statistical analysis (as described above) was performed, which demonstrated that the area of continuous hyperintensity ($p < 0.001$) and the total area of hyperintensity ($p < 0.001$) in each slice, significantly increased as the distance from the MCA increased.

To determine whether the vertical distribution of hyperintensities could be a possible differential diagnostic indicator, the pattern of the continuous, discontinuous and total hyperintensities was compared for patients who did and did not improve with shunting (figure 6a, 6b, 7a, 7b, 8a and 8b). No specific patterns were observed with continuous hyperintensities identified above and below the MCAs. However it was noted that no discontinuous hyperintensities were seen in 6 of the patients, four of whom improved with shunting. This important observation was then reviewed statistically.

The percentage risk of each type of hyperintensity (frontal continuous, frontal discontinuous, body continuous, body discontinuous, posterior continuous, posterior discontinuous) occurring was calculated for patients who did and did not improve with shunting. The percentage risk difference in the two groups was calculated. This demonstrated that patients who did not improve with shunting had a significantly increased risk of demonstrating all hyperintensities ($p < 0.05$) and a highly significantly increased risk of demonstrating body discontinuous hyperintensities ($p < 0.01$).

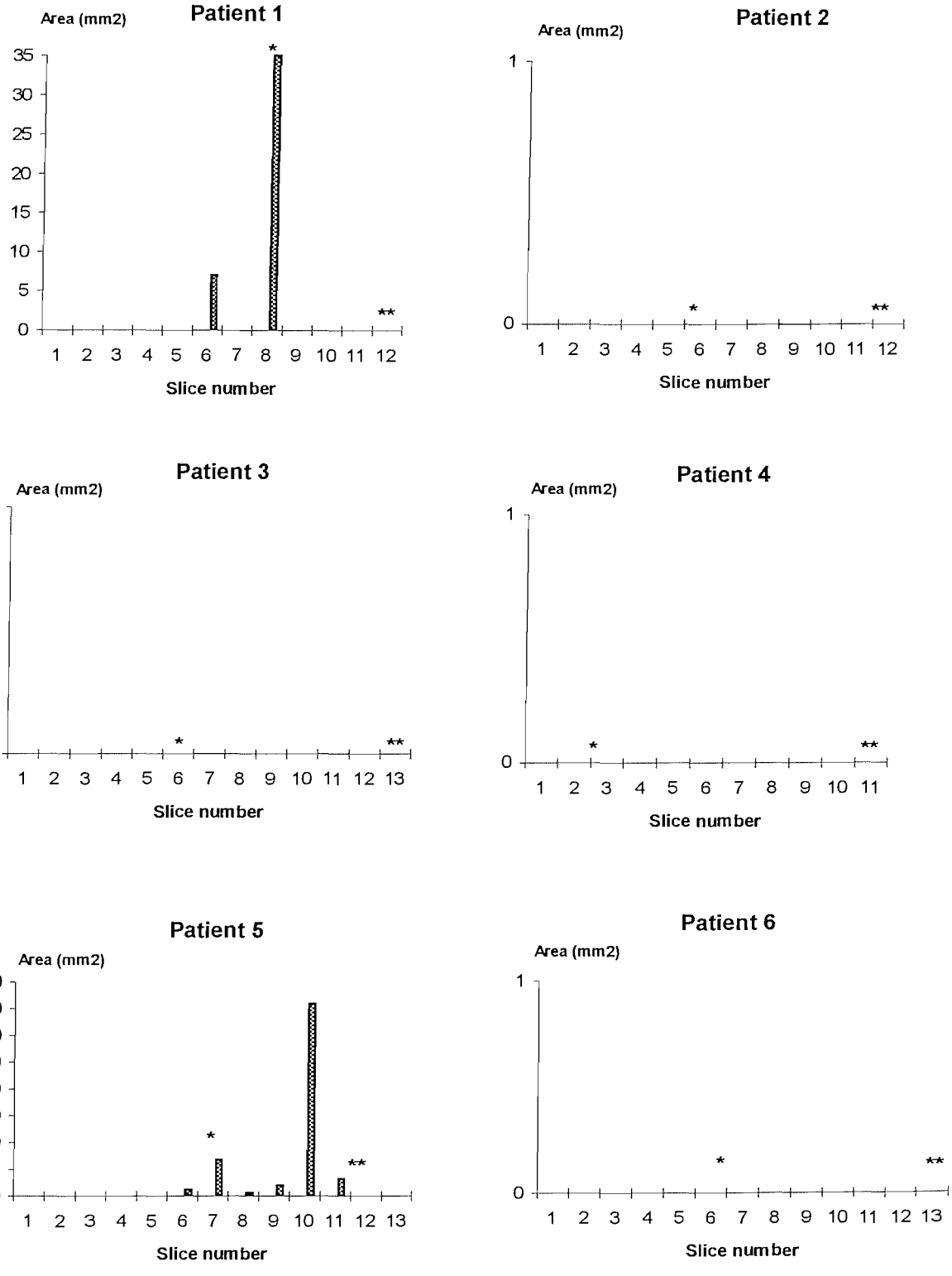

Figure 6a. The area of incontinuous hyperintensities for each MRI slice in patients who did improve with shunting

* indicates the slice in which the MCA was identified

** indicates the slice in which the ventricles were last observed

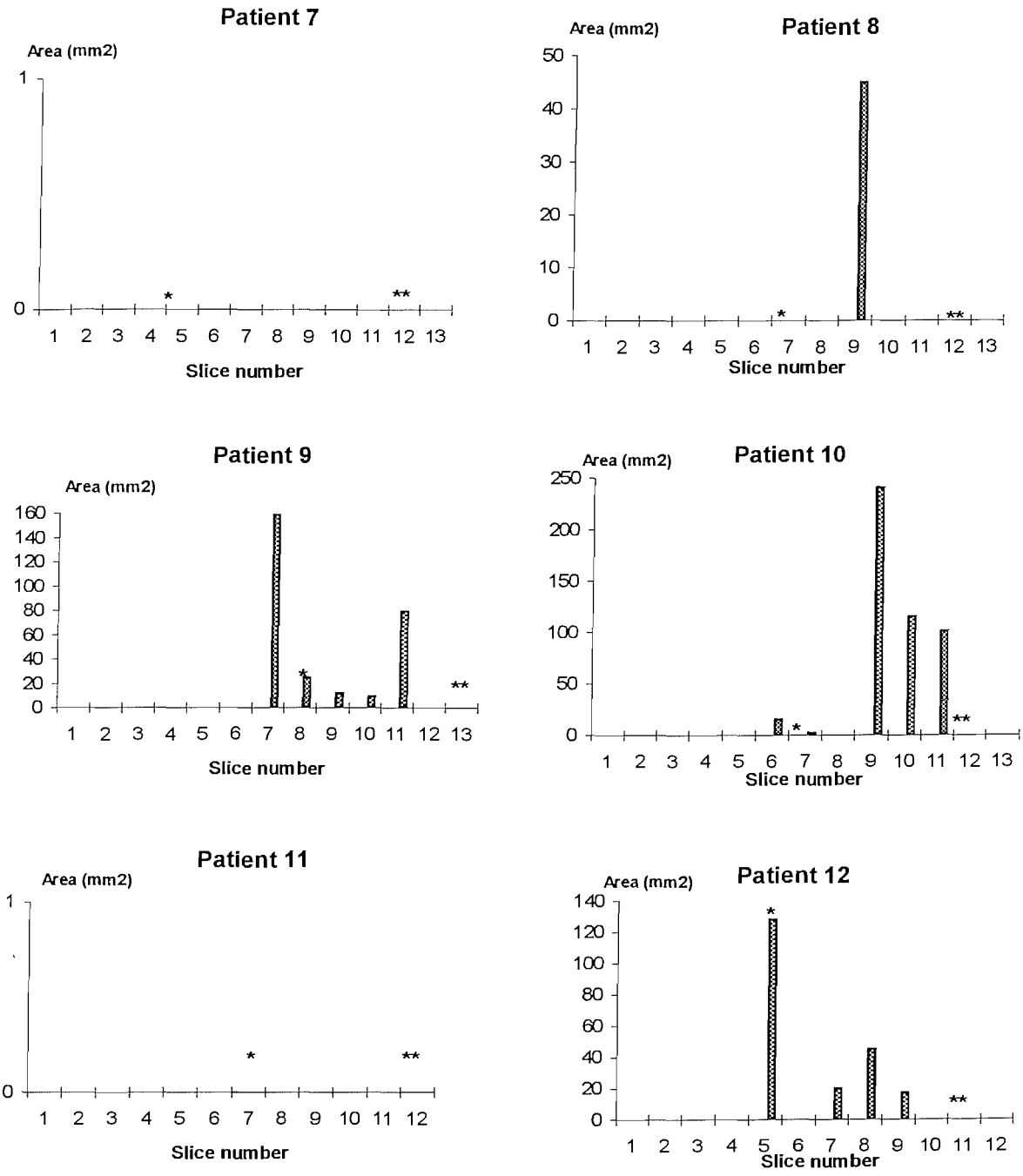

Figure 6b. The area of incontinuous hyperintensities for each MRI slice in patients who did not improve with shunting

* indicates the slice in which the MCA was identified

** indicates the slice in which the ventricles were last observed

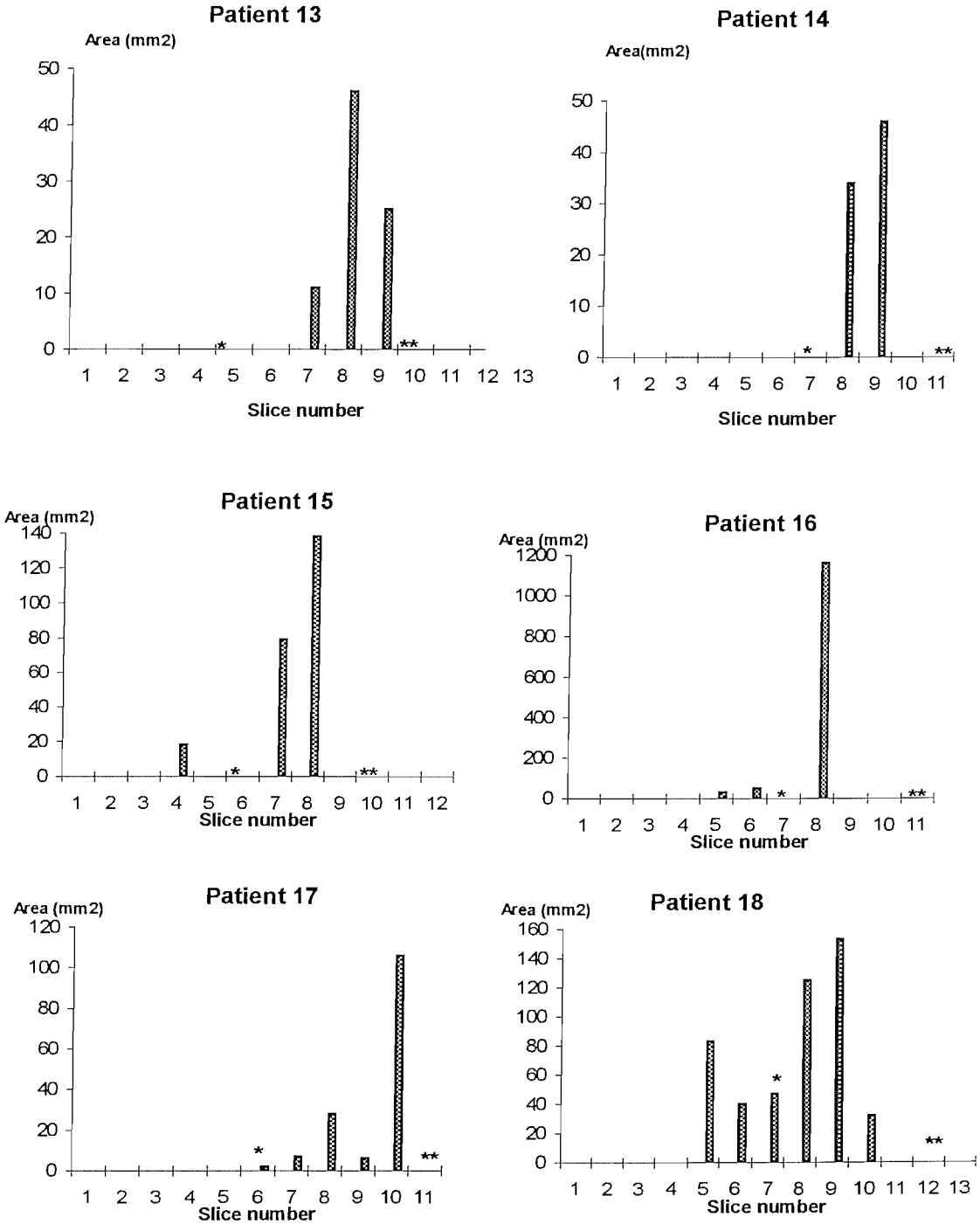

Figure 6 b cont. The area of incontinuous hyperintensities for each MRI slice in patients who did not improve with shunting

* indicates the slice in which the MCA was identified

** indicates the slice in which the ventricles were last observed

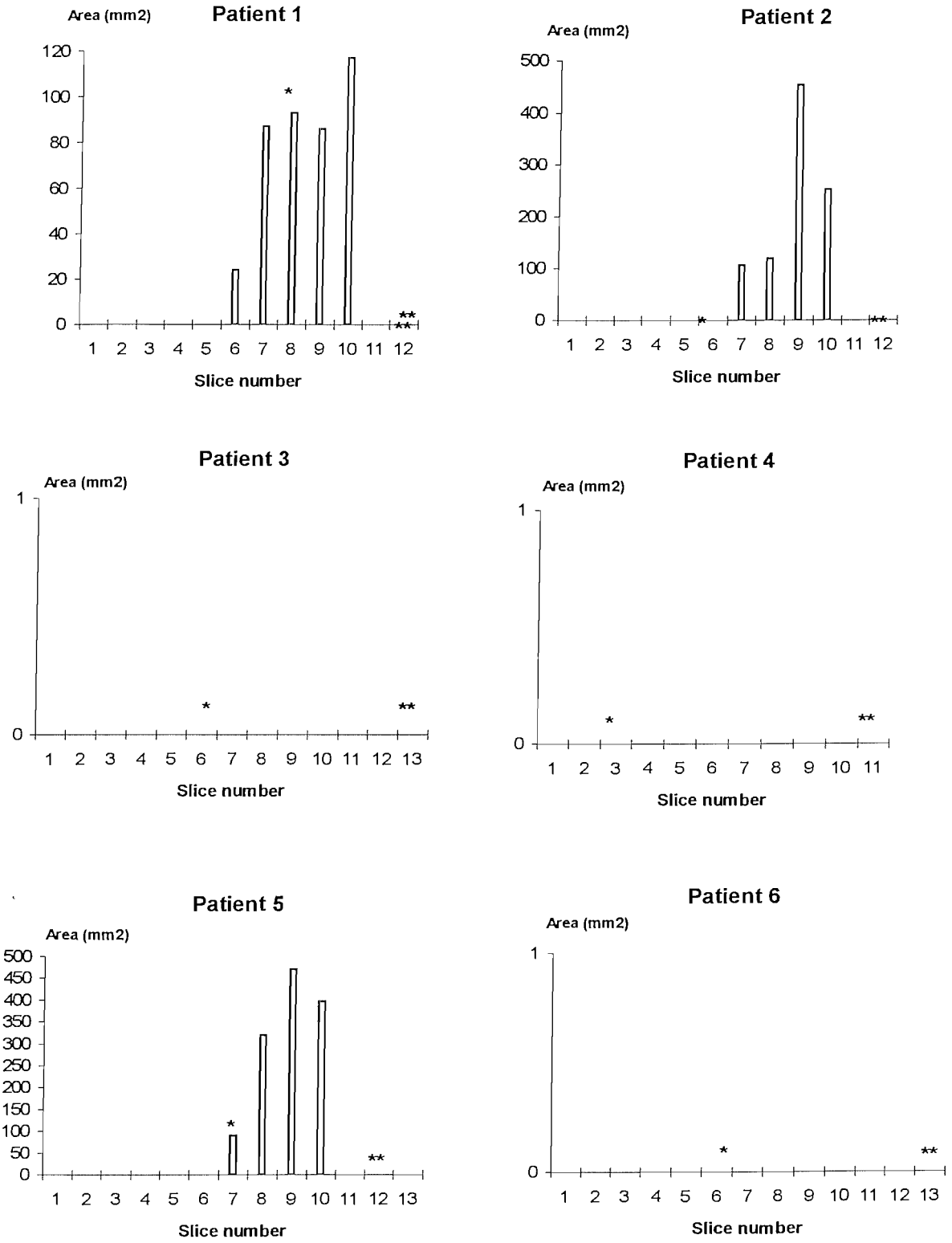

Figure 7 a. The area of continuous hyperintensities for each MRI slice in patients who did improve with shunting
* indicates the slice in which the MCA was identified
** indicates the slice in which the ventricles were last observed

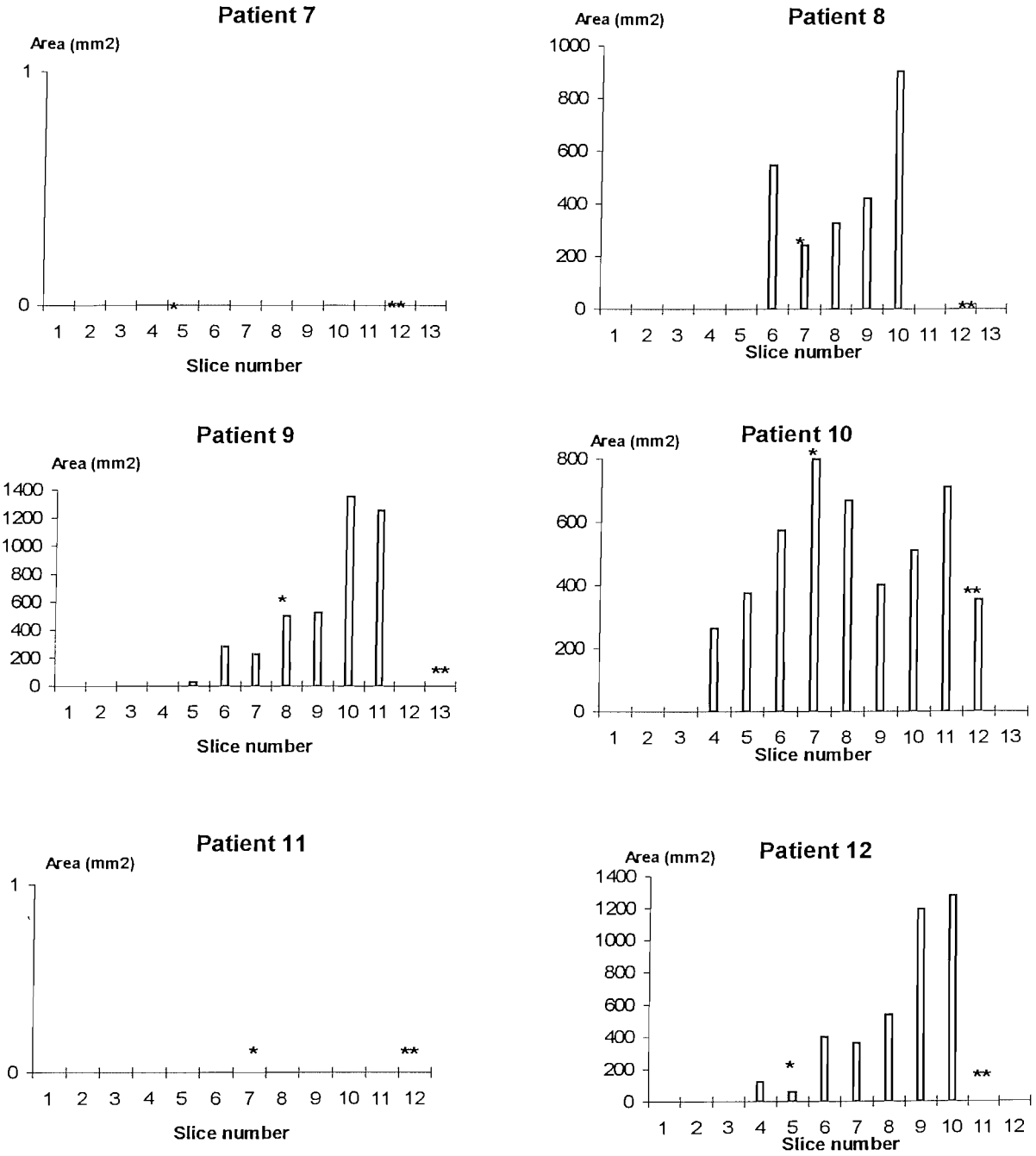

Figure 7 b. The area of continuous hyperintensities for each MRI slice in patients who did not improve with shunting

* indicates the slice in which the MCA was identified

** indicates the slice in which the ventricles were last observed

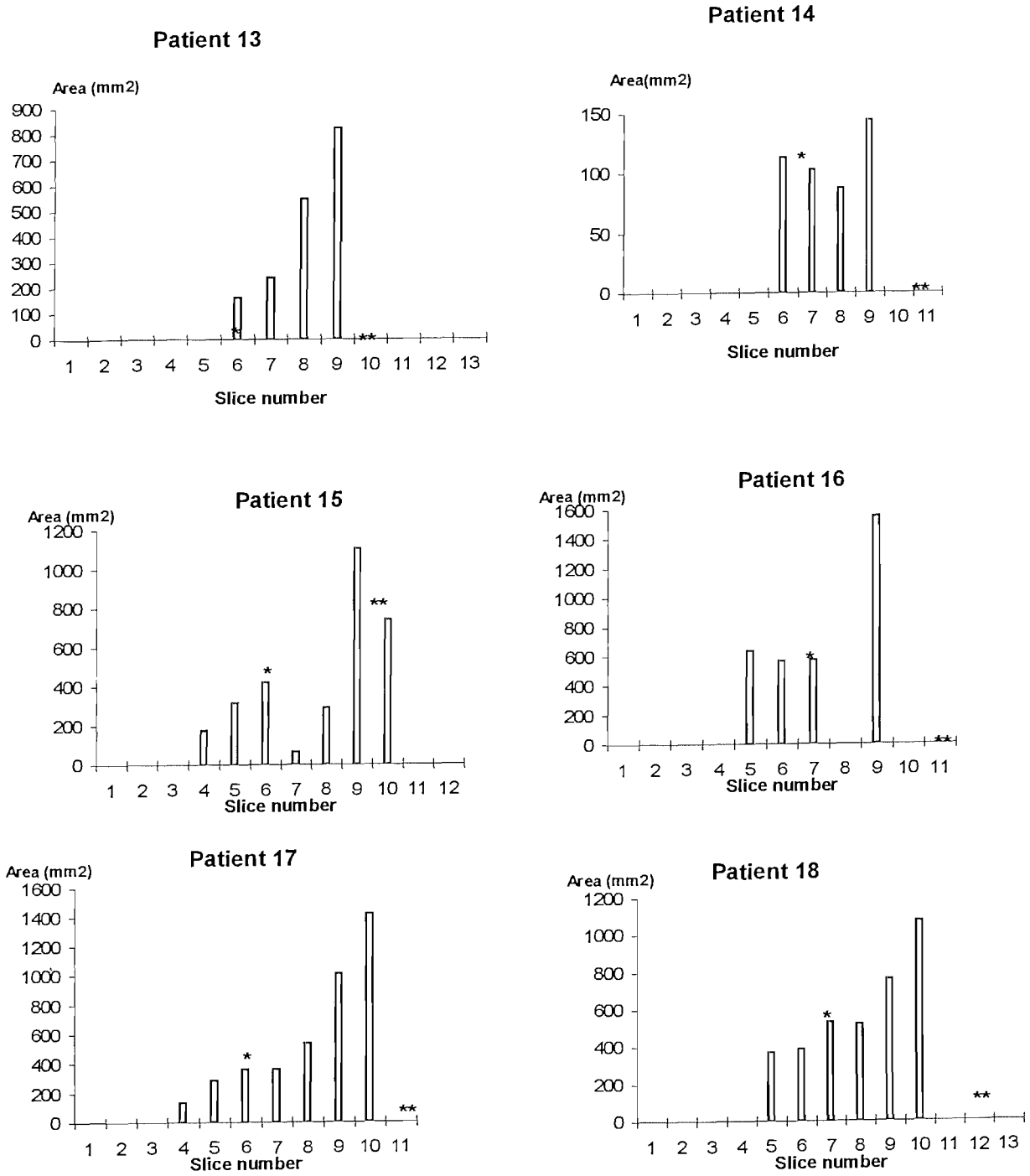

Figure 7 b cont. The area of continuous hyperintensities for each MRI slice in patients who did not improve with shunting
* indicates the slice in which the MCA was identified
** indicates the slice in which the ventricles were last observed

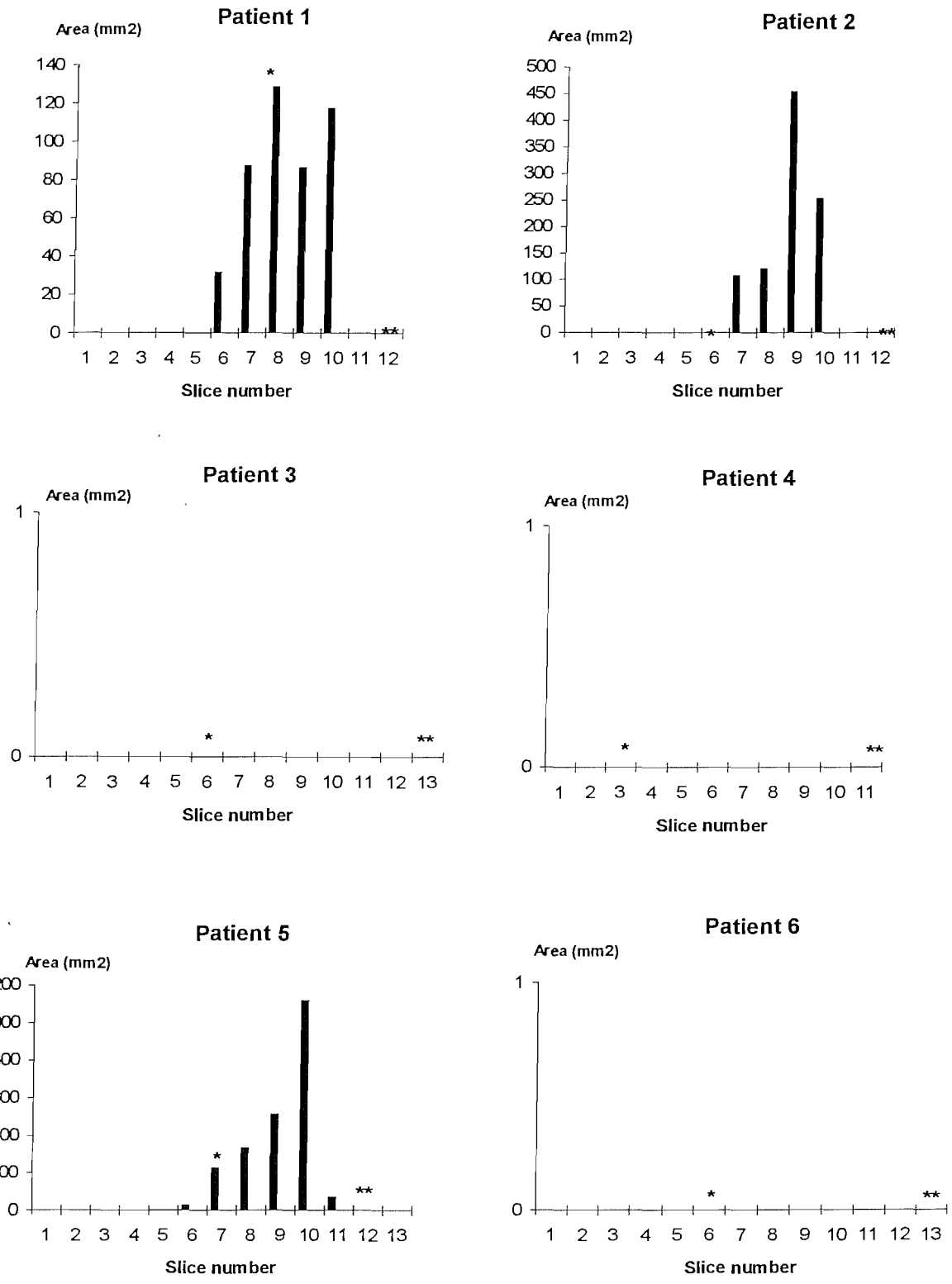

Figure 8 a. The total area of hyperintensities for each MRI slice in patients who did improve with shunting
* indicates the slice in which the MCA was identified
** indicates the slice in which the ventricles were last observed

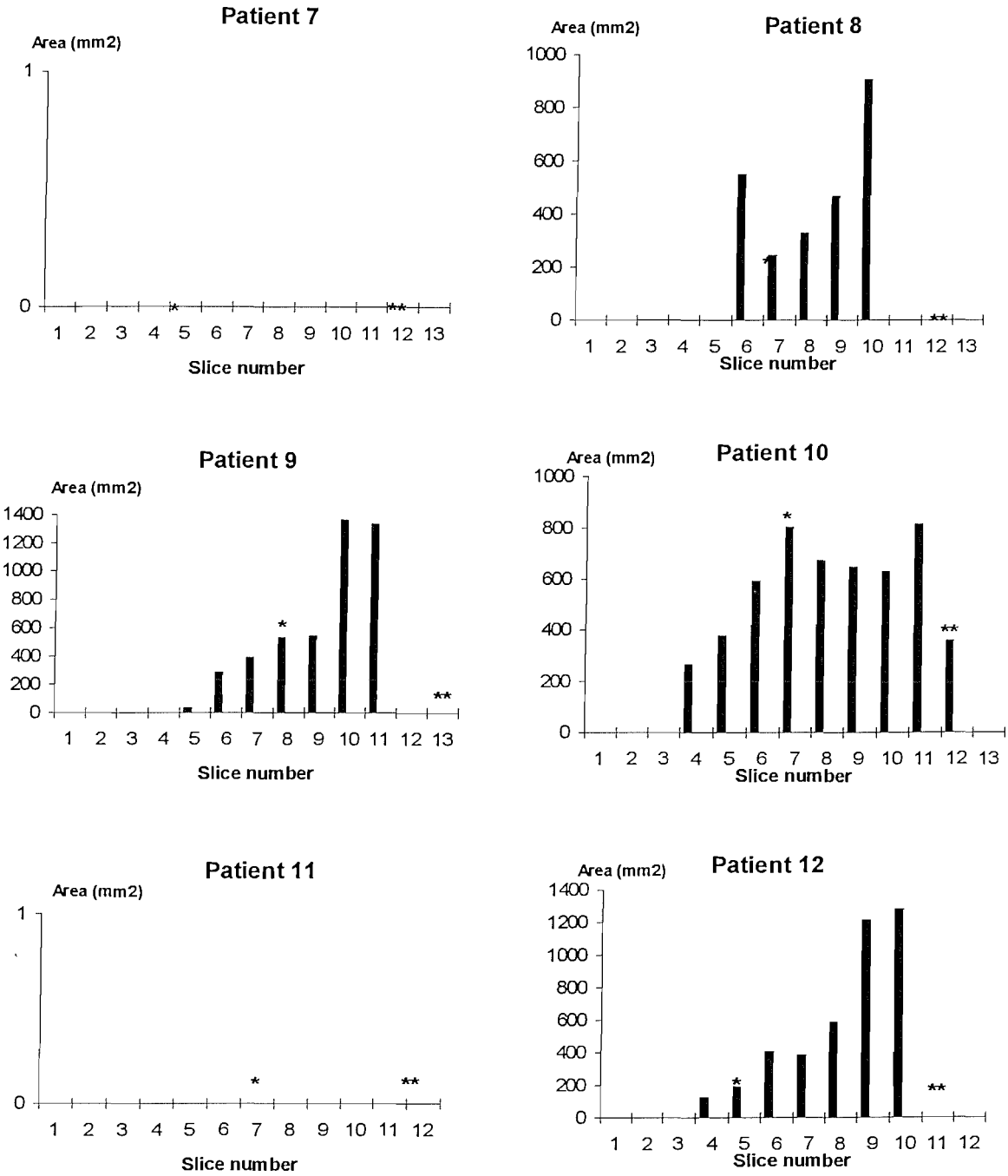

Figure 8 b. The total area of hyperintensities for each MRI slice in patients who did not improve with shunting
* indicates the slice in which the MCA was identified
** indicates the slice in which the ventricles were last observed

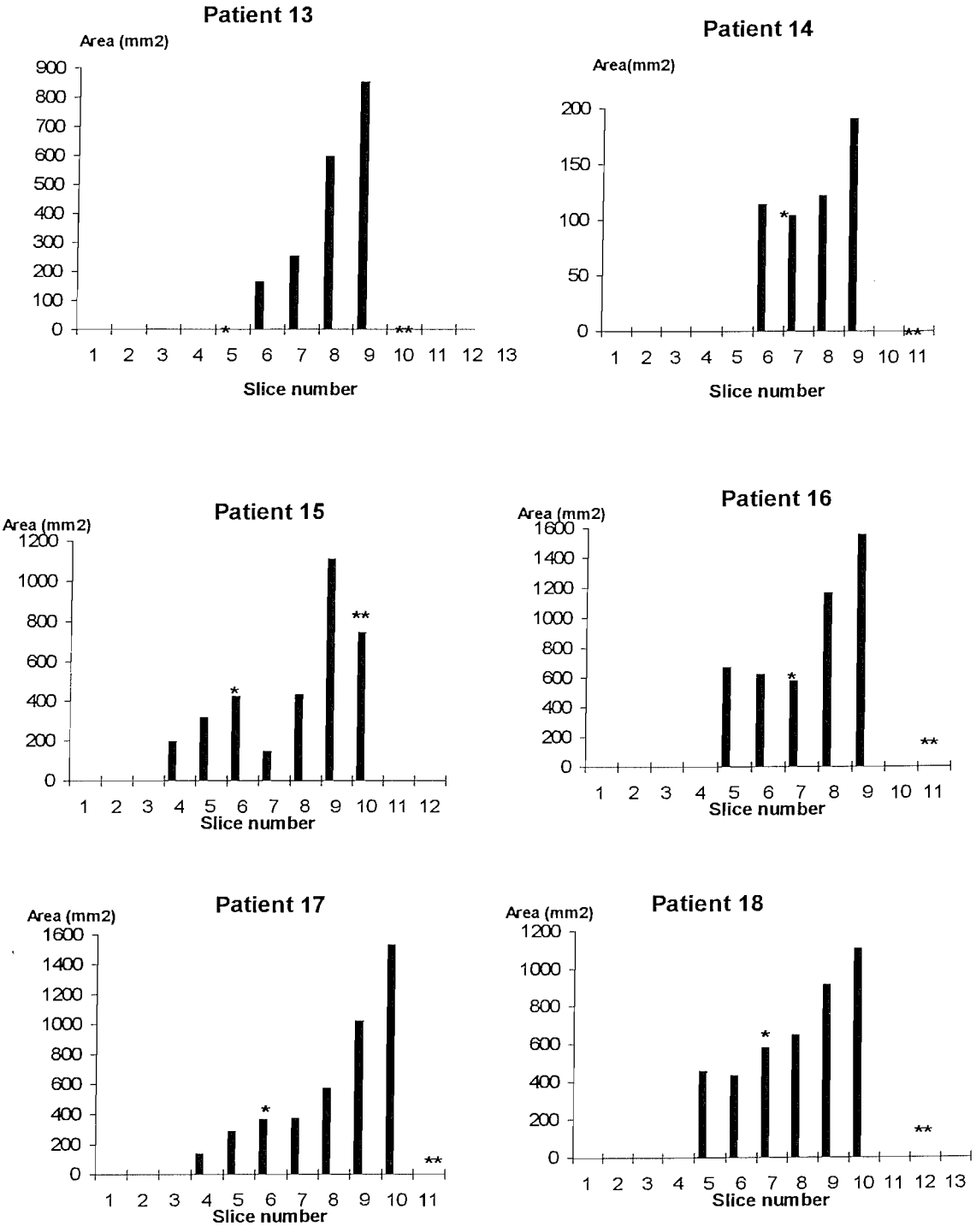

Figure 8 b cont. The total area of hyperintensities for each MRI slice in patients who did not improve with shunting
* indicates the slice in which the MCA was identified
** indicates the slice in which the ventricles were last observed

8. DISCUSSION

8.1 Clinical Discussion

This was a detailed, retrospective analysis of MRI white matter hyperintensities in patients with suspected NPH. The MRI scans were performed pre and post shunt in patients included in the Southampton NPH study, one of the most comprehensive studies of its type. In this analysis, a novel approach was taken allowing the area of white matter hyperintensity to be quantified. The position of each hyperintensity was classified according to proximity to the ventricles ('continuous' or 'discontinuous') and whether it was located in the front, body or posterior of the brain. Hyperintensities classified as 'continuous' or 'body discontinuous' were of particular interest, indicating areas of periventricular lucency and focal white matter lesions respectively.

This study demonstrated a highly significant ($p < 0.01$) increased risk of demonstrating 'body discontinuous' hyperintensities in patients who did not improve after shunting. This result confirmed the findings of a more qualitative study of the same MR images and clinical data [25]. Pickard et al compared CT and MRI parameters, cerebral blood flow, ICP and resistance to CSF outflow in this group of patients to assess indicators of improvement with shunting. They concluded that patients with gait apraxia and mental impairment should be considered for shunting if there are no deep white matter lesions on MRI. However, it was also determined that the presence of deep white matter lesions did not preclude improvement after shunting, but these patients were at significantly greater risks of postoperative complications including stroke and myocardial infarction confirming that they may have a general vascular problem.

Although there are discrepancies in the literature [9,10], this finding is in agreement with other authors [7,8,26] who demonstrated that deep white matter lesions were usually, but not uniquely, a negative indicator for improvement after shunting.

The pathophysiological association between NPH and deep white matter lesions is not clear. It has been suggested that ventriculomegaly may be dependent in some way on

white matter changes [10]. On the assumption that the white matter lesions are caused by infarction, a co-existence between NPH and cerebrovascular disease was suggested [9]. More recently a CT study in 101 patients with suspected NPH demonstrated that cerbrovasular disease (defined as a history of stroke or a CT scan revealing infarcts or hypodense regions) was an important indicator of poor outcome [26a]. The results of this study are in line with this most recent publication.

The vertical plots of white matter incontinuous hyperintensity distribution did not provide evidence for the 'watershed zone' theory. However, statistical analysis demonstrated that there was a highly significant increase in the area of continuous hyperintensities and the total area of hyperintensities, in each slice, as the distance from the MCA increased. This suggests that 'watershed' ischaemia may play a role in periventricular lesions in addition to periventricular biomechanics.

In this study, patients who improved with shunting were less likely to demonstrate PVH (hyperintense regions continuous with the ventricles). Patients who did improve, and did demonstrate PVH, generally demonstrated much smaller regions. This finding is in agreement with Krauss et al [8] who found a negative correlation between extent of PVH and outcome. On the other hand, a better outcome has been described in patients with extensive PVH [7, 27]. This confusing picture may have arisen due to the assumption that signal alterations such as these are caused by increased water concentration in the periventricular tissue resulting from transependymal fluid flow. It may be that these lesions are not specific to NPH and other underlying pathologies such as ischaemic demyelination may cause similar signal alterations. Similar studies assessing periventricular hypodensity on CT have also demonstrated conflicting results. Although early work [28, 29] suggested that periventricular hypodensity on a CT scan should be considered a strong indication for shunting, a more recent CT study [30] suggest that these changes appear to be non-specific and may not be diagnostic indicators for NPH. It therefore remains unclear whether there is a secondary or causal pathophysiological link between NPH and periventricular hyperintensities demonstrated with MRI.

This study has not provided definite preoperative guidelines regarding which patients should undergo shunt surgery, however, overall it appears that patients with minimal disruption to the brain tissue are more likely to improve with shunting and with less risk of complications.

8.2 Technical Discussion

As this was a quantitative study, great care was taken to minimise the degree of bias introduced by poor image quality and application of the protocol [11, 31]. Image quality may be compromised by technical limitations and artefacts which may be introduced during the imaging procedure and during image manipulation, e.g. re-digitising and during analysis. As the analysis is dependent on the visual attributes of the image, the quantitative analysis will be affected.

One of the most apparent sources of detectable artefact in this study was gross anatomical movement. Although all attempts were made to minimise movement during the scan the demented and confused patients were often unable to remain stationary for the required period of data acquisition. These artefacts appear as distinctive curvilinear crescents of signal or 'ghost images' - the superposition of partial images. Patient movement may be reduced with appropriate sedation, however, this was not acceptable for this study where patients were transported long distances (Southampton to London) for MR imaging. To reduce movement effects, scans dominated by this artefact were excluded from the analysis.

A normalisation procedure was introduced to optimise the grey scale and to overcome contrast and intensity variability between scans. Although the image analysis package allowed the image contrast and brightness to be adjusted it was found that these manoeuvres may change the size of the hyperintensities. Therefore instead of manually adjusting the properties of each image, a normalisation procedure was introduced. To normalise an image, a representative area (as large as possible) of CSF was selected with the mouse and the average density of the region automatically calculated. An area of bone

was then selected in a similar manner. The average density of the lightest and darkest biological areas were then used to 'clip' the image. Therefore the minimum and maximum grey scale values were set to the density of the CSF and bone respectively. After normalisation the image quality was improved without distortion of the hyperintensities. The normalisation theory was based on the estimation that with standard MRI settings the density of CSF and bone should appear similar in different subjects assuming no large changes in CSF or bone composition.

Hyperintensities may be easily identified on an MR image, however the boundary of the hyperintensity may be more difficult to establish. Both the edge effect and partial volumes produce hazy lesion outlines. The edge effect occurs at high contrast interfaces and is a product of the Fourier transformation image reconstruction. The resulting image does not duplicate the sharp interfaces which are instead replaced by blurred and accentuated boundaries. Partial volumes occur when the thickness of the MRI slice is greater than the feature of interest. As MR images are 2D representation of 3D slices then each pixel combines the information from a 3D tissue element described as a voxel. A pixel therefore represents the average signal produced by a voxel and provides a good representation if the voxel contents are relatively homogenous. If, however, there are large differences in the tissue properties within a voxel then the average signal is not a good representation of the voxel components. A thresholding technique was used to minimise the edge effect.

A 3D reconstruction of the images was attempted with limited success as the number of scans per patient was inadequate to provide sufficient detail for image analysis. Future work could include 3D reconstruction's which may prove to be the best approach for quantitative assessments. Also, as head size is highly variable it may be appropriate to calculate volume of hyperintensity in relation to brain volume.

9. CONCLUSION

The results of this study demonstrate a high incidence of MRI hyperintense areas on MR images of patients with suspect NPH. The total area of hyperintensity was greater in

patients who did not improve with shunting. These patients also had a greater risk of demonstrating any hyperintensity, in particular body discontinuous hyperintensities. This suggests that patients with minimal disruption to the brain tissue are more likely to improve with shunting.

Evidence for the 'watershed' theory for the development of deep white matter lesions was not provided. However, there was a highly significant increase in the area of continuous hyperintensities and the total area of hyperintensities, in each slice, as the distance from the MCA increased. This suggests that 'watershed' ischaemia may play a role in periventricular lesions in addition to periventricular biomechanics.

CHAPTER 6

THE BIOMECHANICS OF HYDROCEPHALUS: A COMPUTER SIMULATION USING THE FINITE ELEMENT METHOD.

THE BIOMECHANICS OF HYDROCEPHALUS: A COMPUTER SIMULATION USING THE FINITE ELEMENT METHOD.

1. INTRODUCTION

Hydrocephalus is often a reversible process resulting in no neurological deficit - remarkable considering the large increases in cerebrospinal fluid (CSF) volume. This implies that excess fluid may be accommodated without inducing ischaemia, tissue degeneration or other permanent changes. However,as the cranial cavity is a closed system an increase in CSF volume must be accompanied by a reciprocal decrease in blood volume, subarachnoid CSF or brain tissue. Cerebral blood volume may decrease due to compression of the vascular bed containing non-essential venous blood, and the subarachnoid CSF may be displaced. However, together these changes may not be sufficient to account for the total change in ventricular volume. Considering that hydrocephalus may be reversible then it may appear contradictory to suggest that the third volumetric component which may change is the brain tissue. However, it has been suggested that brain tissue may decrease in volume yet stay functionally intact. Hakim [1] postulated that brain tissue is a biphasic material. An analogy was made with an undrained sponge, consisting of a solid phase (the brain tissue) and cavities or pores containing the fluid phase. It was suggested that the cavities were of different types, some containing venous blood and others occupied by interstitial fluid. This implied that ventricular enlargement was partly due to the interstitial fluid being squeezed out from the extracellular space which occupies 20% of the total brain volume.

Hakim was the first to apply the poro-elastic hypothesis to brain tissue in an attempt to answer some of the paradoxical questions surrounding hydrocephalus. Viscous fluid is considered to require a pressure gradient for its expulsion from the pores of what is assumed to be an elastic sponge. Theoretical and experimental studies in human cadavers and explanted brain tissue allowed the biomechanical consequences of CSF-blood-tissue interactions to be investigated. These studies suggested that transmantle pressure gradients

were highly significant, responsible for the initial stages of ventricular dilatation and the generation of stresses and strains within the poro-elastic medium.

A more quantitative approach was then taken, allowing the intracranial biomechanics to be described mathematically [2]. Although the model was highly simplified to an elastic, spherical model allowing the equations to be solved analytically, tangential and radial stress and strain could be calculated. Like all models, parameters which describe the behaviour of the system were required, for example the intraventricular pressure, the resultant ventricular size, subdural stresses and the material properties such as Young's modulus and Poisson's ratio. Changing these parameters allowed the author to model different types of hydrocephalus.

Mathematical models are important in clinical science allowing the calculation of parameters which are impossible to quantify accurately due to ethical, methodological or instrumentation limitations. These parameters describe the mechanical behaviour of a biological system, but often provide a compromise which reflects the technology available at the time. Although Hakim was the first theoretically to apply the poro-elastic theory to hydrocephalus it was not included in a quantitative model. The complex geometry was also excluded.

This single phase elastic model remained unchallenged until Nagashima et al [3,4] proposed a poro-elastic model of a 2 dimensional brain slice. Although this was the first time this approach had been applied to brain tissue, biphasic models had been previously used in other areas of biomechanics [5]. Although this work provided a novel and valuable approach to the questions surrounding hydrocephalus the approach used was flawed (see section 9).

1.1 Aims

The predominant gross anatomical features of hydrocephalus are ventricular dilatation and periventricular edema. Both changes occur in response to abnormal increases in CSF volume. According to Hakim's poro-elastic hypothesis, ventricular dilatation is accommodated partly

by a reduction of extracellular fluid. The cells become more closely packed and the tissue more dense. However edema describes an increase in brain volume due to an accumulation of fluid in expanded extra- or intra-cellular spaces. It remains to be shown whether these conflicting states can be accommodated in the poro-elastic model.

This chapter explores the biomechanics of the stress-strain relationship in brain tissue established during hydrocephalus. A two dimensional model has been developed and appropriate boundary conditions established. Although based on Nagashima's poro-elastic model there are some fundamental differences in the calculations, analysis and interpretation of the results. These will be discussed where appropriate.

2. THE MODEL

The fundamental basis of a mathematical model is the differential equations which describe the dynamic behaviour of the system. These equations may be developed for a specific application, or more commonly existing theoretical models may be adapted for a specific application. This model has been based on equations originally developed by Biot in 1941 [6] to describe the behaviour of soil. Although this may initially appear to be an improbable analogy, the similarities between soil and brain tissue as proposed by Hakim are surprising. The physical similarities are demonstrated in figure 1. Both are deformable porous solids consisting of a solid and a fluid phase. In the case of soil these are mineral grains and water and, in the case of brain tissue, cells and interstitial fluid. Theoretical soil models have been applied in models of cartilage, the pulmonary system and other applications.

The application of these equations has allowed the physical behaviour of the brain tissue during deformation to be described mathematically. The finite element technique is used to solve these equations.

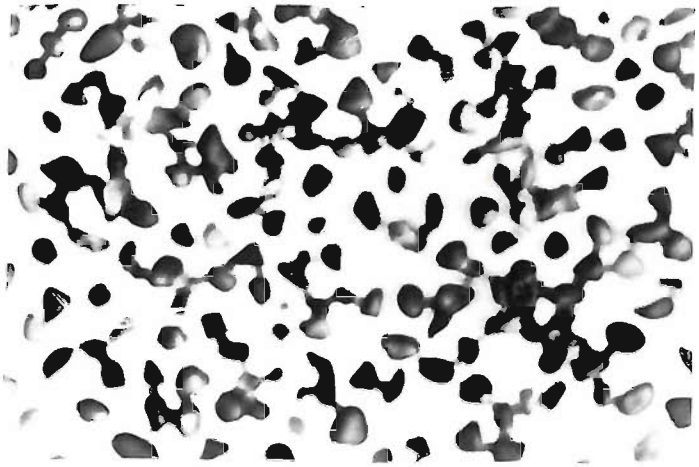

Magnified Soil

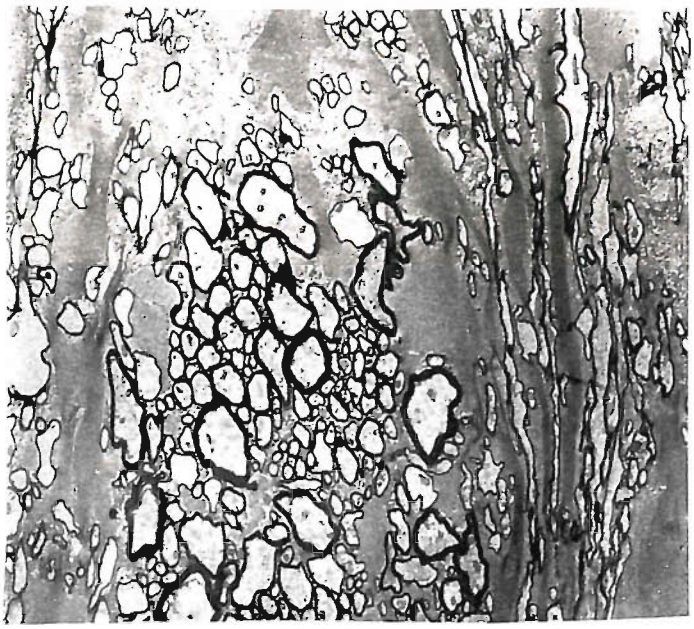

Magnified brain tissue

Figure 1: Photographs of magnified soil and brain tissue, demonstrating the physical similarities

3. THE THEORY OF CONSOLIDATION

The equations which govern the biomechanical behavior of the brain are based on the theory of consolidation, first described for 1 dimensional compression by Terzaghi and Fröhlich [7]. This was later generalised into 3 dimensional terms by Biot in 1941 [6]. The term 'consolidation' is used in soil mechanics to describe the compression of a bi-phasic material which consists of a porous solid phase and an incompressible fluid phase. Deformation of the material results from the flow of fluid within and out of the porous medium. The solid phase remains intact, but the solid/fluid ratio may change. In the biomechanical application of this theory to the brain, the solid porous phase consists of the neurons and glia and the fluid phase is the interstitial fluid, as shown in figure 2.

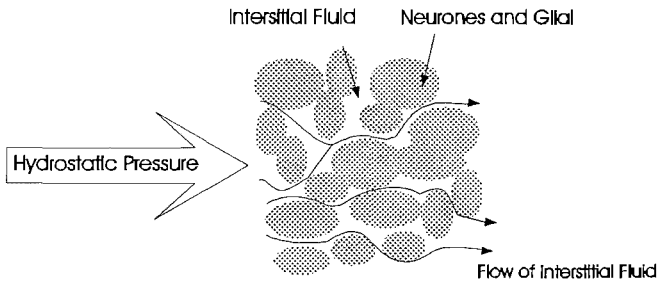

Figure 2: The brain as a poro-elastic medium. A hydrostatic pressure gradient is required to expel the viscous fluid from the cavities of what is assumed to be an elastic sponge

The theory of consolidation is based on the following principles:

1. Terzarghi's Principle of Effective Stress

Terzarghi's theory of effective stress states that the total stress acting on a biphasic material is equal to the sum of the effective stresses acting on the solid phase and the fluid pressure (figure 3).

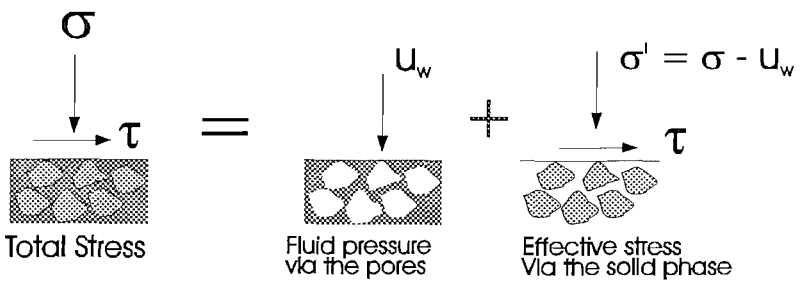

Figure 3: Terzarghi's theory of consolidation, where σ = normal stress, σ'=effective normal stress, τ=shear stress and U_w= fluid pressure adapted from [8]

The effective stress acting on the soil grains cannot be determined directly. It is calculated as the difference between the total stress and the fluid pressure.

2. Hooke's Law and System Equilibrium

The total stress is calculated from system equilibrium and Hooke's Law. A system is described as being in equilibrium when the resultant forces and moments are zero. The normal and shear stresses acting upon a 2 dimensional quadrilateral are shown in figure 4.

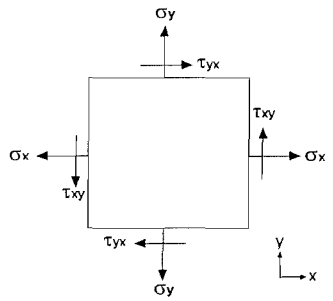

Figure 4 : Normal and shear stresses acting upon a 2 dimensional quadrilateral

For equilibrium:

$$\frac{\partial \sigma_x}{\partial x} + \frac{\partial \tau_{xy}}{\partial y} = 0$$

$$\frac{\partial \tau_{xy}}{\partial x} + \frac{\partial \sigma_y}{\partial y} = 0$$

The stress-strain relationship is described by Hooke's Law as:

$$\begin{Bmatrix} \sigma_x \\ \sigma_y \\ \tau_{xy} \end{Bmatrix} = \frac{E}{1-\upsilon^2} \begin{bmatrix} 1 & \upsilon & 0 \\ \upsilon & 1 & 0 \\ 0 & 0 & \frac{1-\upsilon}{2} \end{bmatrix} \begin{Bmatrix} \varepsilon_x \\ \varepsilon_y \\ \gamma_{xy} \end{Bmatrix}$$

Where E is Young's modulus, υ is Poisson's ratio, ε is normal strain and γ is shear strain.

The strain component of this stress-strain relationship may also be described in terms of displacement

$$\begin{Bmatrix} \varepsilon_x \\ \varepsilon_y \\ \gamma_{xy} \end{Bmatrix} = \begin{bmatrix} \frac{\partial}{\partial x} & 0 \\ 0 & \frac{\partial}{\partial y} \\ \frac{\partial}{\partial y} & \frac{\partial}{\partial x} \end{bmatrix} \begin{Bmatrix} u \\ v \end{Bmatrix}$$

Where u and v are displacements in the x and y direction respectively.

3. Darcy's Law and the Conservation of Mass of Fluid

The pressure component of the total stress (U_w) is calculated using Darcy's Law which states that

$$V = ki$$

where: V= flow rate per unit area i.e. superficial velocity

k= coefficient of permeability

i= the hydraulic gradient

Permeability varies with the fluid density and viscosity, the porosity of the solid phase, shape and arrangement of the solid phase particles and the degree of saturation

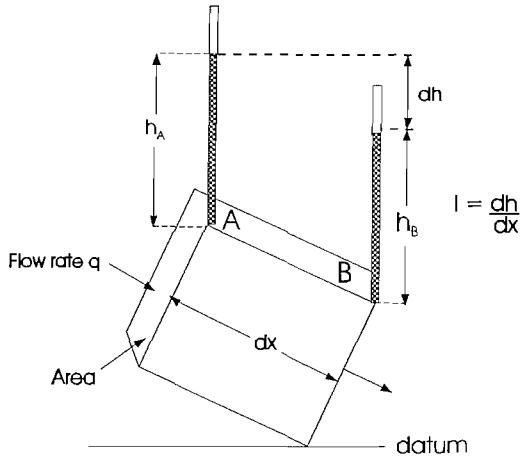

Figure 5: Describing the hydraulic gradient between 2 points A and B in a porous material. The pressure at A= $\gamma_w h_A$ and at B=$\gamma_w h_B$, where γ_w is equal to the bulk modulus of water. Presuming the datum level remains constant the pressure difference between A and B =$h_A - h_B$ = dh.

The hydraulic gradient i is defined above (figure 5) as $\frac{dh}{dx}$ where dh is the pressure difference between points A and B presuming the datum remains constant. In this application

$$h = \frac{u_w}{\gamma_w}$$

where u_w is equal to the pore pressure and γ_w is equal to the bulk modulus of water. Darcy's Law can therefore be re-written as:

$$V = \frac{k}{\gamma_w}\frac{\partial u_w}{\partial x}$$

As the permeability may be different in the different directions then the general form of Darcy's Law may be written as:

$$V_x = \frac{k_x}{\gamma_w}\frac{\partial u_w}{\partial x}$$

$$V_y = \frac{k_y}{\gamma_w}\frac{\partial u_w}{\partial y}$$

If there is no overall volume change of fluid within the system then the conservation of mass may be applied. For no volume change the sum of the component velocities must equal zero:

$$\frac{\partial V_x}{\partial x} + \frac{\partial V_y}{\partial y} = 0$$

substituting the general equations for Darcy's Law into this equation gives :

$$\frac{k_x}{\gamma_w}\frac{\partial^2 u_w}{\partial^2 x} + \frac{k_y}{\gamma_w}\frac{\partial^2 u_w}{\partial^2 y} = 0$$

If there is a time dependent fluid volume change then an additional term $\frac{\partial \varepsilon_v}{\partial t}$ is added which describes the rate of volumetric strain.

$$\frac{k_x}{\gamma_w}\frac{\partial^2 u_w}{\partial^2 x} + \frac{k_y}{\gamma_w}\frac{\partial^2 u_w}{\partial^2 y} + \frac{\partial \varepsilon_v}{\partial t} = 0$$

The reader should note that when these equations are solved (and discussed later in the chapter) compressive pressures are considered positive stresses. This is the opposite to conventional engineering where stress is considered to be positive when tensile (see figure 6). A similar convention is also used for strains.

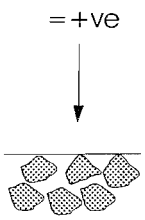

Figure 6: A positive downward fluid pressure producing a positive effective stress

4. THE ENGINEERING MEASURES FOR BIOLOGICAL DAMAGE

Solutions to the consolidation equations provide stress, strain, pressure and displacement relations which may be manipulated and presented in many different forms. It is important to select carefully parameters that may relate to the clinical questions relevant to hydrocephalus. This includes ventricular shape, edema, tissue shearing and pressure distribution:

i)Ventricular shape

Ventricular dilatation on CT is a characteristic feature of hydrocephalus and should therefore be simulated by the model. To determine the change in ventricular size and relative displacement of other areas of the model the nodal displacement is plotted.

ii) Periventricular edema.

Periventricular edema is an increase in tissue volume due to fluid accumulation. In engineering terms, changes in tissue volume with constant shape may be described in terms of volumetric strains where:

$$\text{volumetric strain} = \frac{\text{change in volume}}{\text{original volume}}$$

According to the visco-elastic model, brain parenchyma is incompressible therefore any volume change is achieved by changes in interstitial fluid content. A positive volumetric strain describes tissue compression and a reduction of interstitial fluid. A negative volumetric strain is an increase in volume due to interstitial fluid accumulation and the expansion of the extracellular spaces (figure 7).

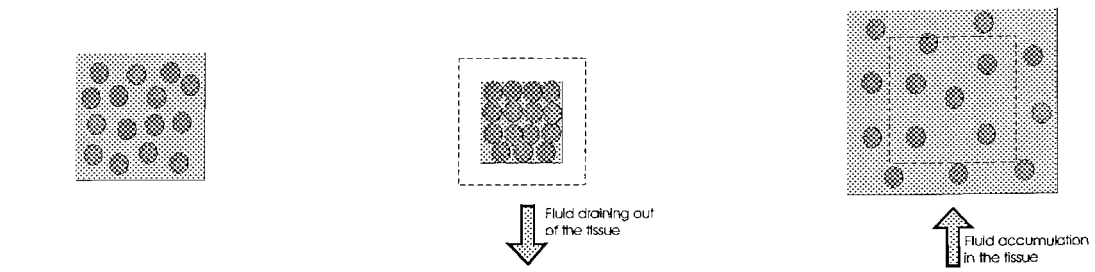

Figure 7: Volumetric Strain

Nagashima et al [3,4] suggested that areas of high pressure could be related to edema. This correlation is confusing considering that fluid will have a tendency to flow away from areas of high pressure to achieve a state of equilibrium.

It remains to be shown whether the visco-elastic model, where tissue compression is achieved by extracellular fluid reduction can also accommodate localised increases of extracellular fluid as seen in edema.

iii) Tissue shearing

Deep white matter hyperintensities are often observed on magnetic resonance images in hydrocephalus, but their aetiology is not fully understood. It has been suggested that ventricular enlargement may lead to tissue distortion and weakening. These changes may produce decreases in blood flow and localised ischaemic events appearing as hyperintense areas on MRI's. It has also been suggested that these changes may be responsible for some of the symptoms related to normal pressure hydrocephalus. It is important therefore to identify any areas of tissue distortion in the simulated model. In engineering terms a change in shape with constant volume is described as shear strain (figure 8).

The brain tissue composed of an incompressible solid phase (parenchyma) and fluid phase (interstitial fluid).

Shear Strain
The tissue changes shape producing shearing, but the parenchymal and interstitial fluid volumes remain constant

Figure 8: Shear Strain

Volumetric strain and shear strain are independent components which may occur simultaneously allowing volumetric and shape changes to be described .

iv) Pore Pressure.

Hydrocephalus is simulated with a transmantle pore pressure gradient. A plot of the nodal pressure demonstrates the pressure distribution throughout the tissue and indicates whether equilibrium has been reached.

5. THE MODEL

5.1 The Finite Element Method

The finite element method (FEM) was developed approximately 40 years ago to provide numerical approximations for physical phenomena. Although most commonly used in engineering, the FEM is a general technique which may be applied to models described by partial differential equations. Complex problems with irregular geometry may be solved, but advanced computing techniques are often required.

To perform a finite element analysis, the structure is geometrically divided into a mesh of small regions (the finite elements) (figure 9). The more elements in an analysis, the more accurate the numerical approximation will be. The behavior of each element is analysed with respect to adjoining elements in the mesh. Therefore the equilibrium, the geometry and the stress-strain relationship of each element must be described.

The process by which partial differential equations are converted into matrix form allowing the analysis of the finite elements is called spatial discretisation. Each element may be assigned specific material properties which are used to calculate element behavior. The results for each element are combined in a global matrix which in effect describes the behavior of the model. With the addition of boundary conditions the global equations may be solved.

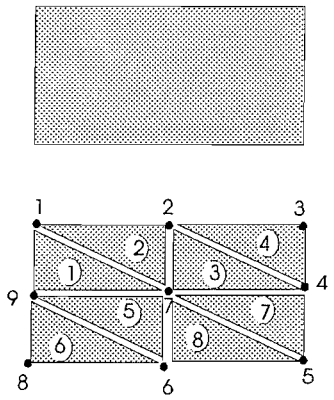

Figure 9: Geometrically dividing a structure into elements. Each element is identified by an element number (1-8 above). The connection between elements is defined by the node numbers (1-9 above).

The global equations are solved over a simulated time period with solutions produced at defined intervals (time steps). This is a dynamic iterative process with a series of solutions generated until the end of the simulated time period and equilibrium is reached. The duration of each time step must be carefully chosen as an incorrect time stepping routine can lead to instability of the analysis and an inaccurate solution.

This is a highly simplified description of a process with many features to be considered. Fortunately computer packages are available which automatically solve the partial differential equations. Although some understanding of the technique is required, detailed mathematical derivations are not.

5.2 The Finite Element Package.

Many finite element packages are available commercially which include a library of pre-programmed elements. The element properties include

a) Element behavior e.g. linear elastic, elasto-plastic, plane strain, consolidation

b) Element shape e.g. triangular, quadrilateral , tetrahedral

c) The number of nodes - the points of mathematical interaction of the elements.

Element selection is determined by the analysis to be performed.

Initial studies were performed using ANSYS [9] a general purpose engineering program. Although ANSYS did not contain an element with consolidation properties, an isoparametric thermal solid was used. Although this element could be adapted to model non-linear porous flow, it was not sufficiently flexible to model consolidation problems. The second approach taken was to use a program developed by Smith and Griffiths [10]. Extensive adaptation was necessary to fulfil the requirements of this study. To do this a full and detailed understanding of the finite element method and the programming language was required. Further problems related to data output were also encountered. These problems proved to be technically too demanding, so alternative avenues were explored.

Finally a finite element package developed at the University of Cambridge Engineering Department was used. The FORTRAN 77 program CRISP (Critical State Program) [11] was written specifically for soil mechanics problems and includes pre-programmed elements for consolidation analysis. The results were exported to a finite element graphics package FEMVIEW [12] for user-friendly data output. Data was input via 2 linked programs, the Geometry Program and the Main Program as described below:

a) The Geometry Program (GPD) contained information regarding the finite element mesh. For simulations with regular geometry the program may automatically generate a mesh from basic spatial information. However, in this application because of the complex irregular geometry, the mesh was created manually. The x-y co-ordinates for each node were input along with the element nodal connectivity. From this data the program drew the mesh and assign element and node numbers.

b)The Main Program (MPD) contained the remaining information required for the analysis including the material properties, boundary conditions, the loading profile, the simulated time of analysis and the number of time steps.

The element selected for the analysis was a six noded triangle with 15 degrees of freedom as shown in figure 10.

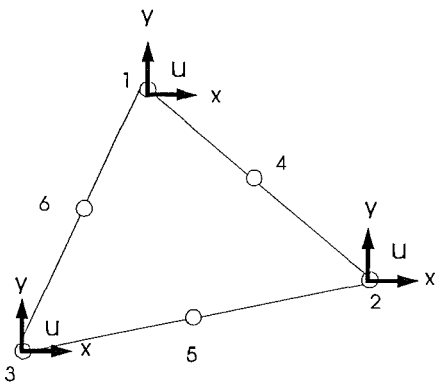

Figure 10: A typical 3 noded triangular element with 15 degrees of freedom.

The position of nodes 1,2 and 3 must be input manually, but the positions of nodes 4, 5 and 6 are automatically calculated. Up to nine degrees of freedom may be specified in the boundary conditions these include X and Y displacements and pore pressure at nodes 1,2 and 3. Nodes 4,5 and 6 have only displacement degrees of freedom which are calculated automatically.

In CRISP, as with other FEM programmes, the differential equations are solved over a simulated time period with solutions produced at a defined series of time steps. However, unlike other FEM programmes, CRISP has a built in sub-routine to ensure that the analysis remains stable. If the time steps defined give an unstable analysis, CRISP automatically adjusts them to give stability and an accurate solution. An experiment was performed to demonstrate this (see Appendix 3).

6. THE COMPUTER SIMULATION

To perform a CRISP simulation the user input data must be provided to describe the Finite Element mesh, material properties and the boundary conditions.

6.1 The Finite Element Mesh.

The mesh geometry is described by the X-Y co-ordinates for each node and the element connectivity (i.e. element - node association). Often meshes may be simulated automatically from minimum input data, but the irregular brain geometry required a manually produced mesh. A horizontal section of brain which included the anterior lateral horns and the atrium of the lateral ventricles (figure 11) was selected from a brain atlas [13]. A simplified version of this slice (figure 12) including only the ventricles and the and white matter was used to produce the mesh. The brain and ventricular outline and the grey matter-white matter boundary were traced onto graph paper and filled with a mesh of 3 noded triangular elements. The mesh was then enlarged and each node and element was numbered. The X-Y co-ordinates for each node and the element connectivity were determined. The grey and white matter elements were assigned different material property zones allowing them to be differentiated during the analysis. The data were input to the GPD file.

As the brain is almost symmetrical half the brain was meshed and subsequently modeled. It is also assumed that the parenchyma is connected to the subarachnoid space which prevents displacement of the outer boundary and midline. This reduced the computing power required to perform the analysis and prevented unnecessary repetition of results. The half brain included 239 nodes and 408 elements (figure 13).

An example of a GPD file is given in Appendix 4.

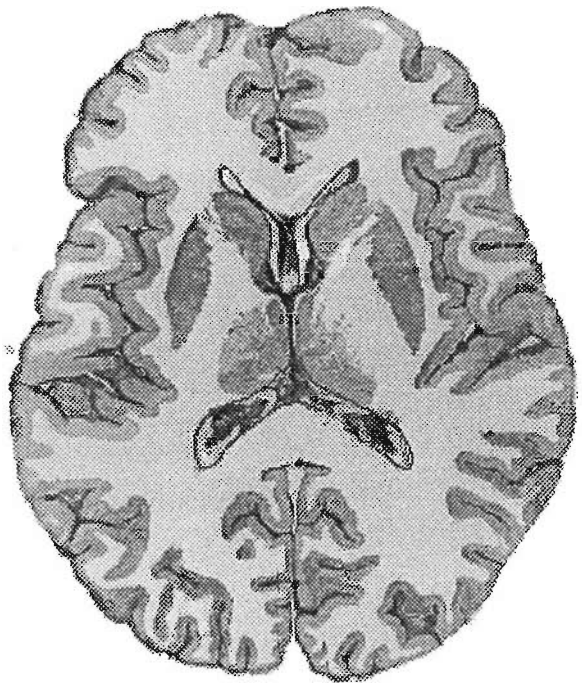

Figure 11: Horizontal section from human brain atlas.

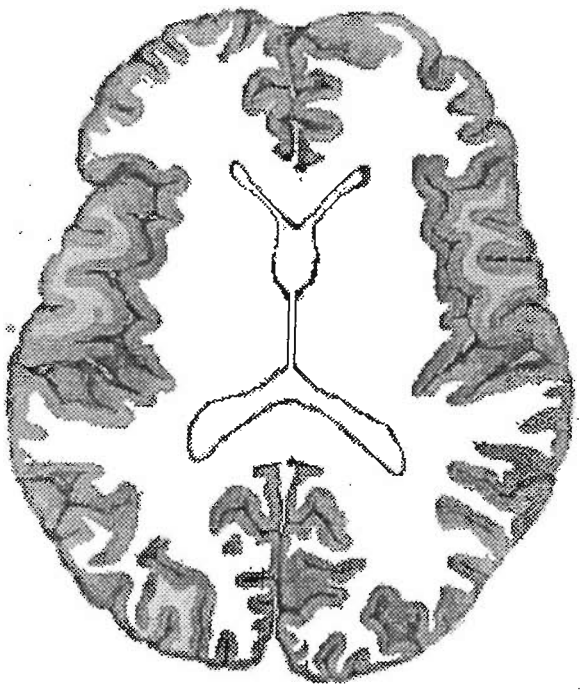

Figure 12. Simplified horizontal section including, grey matter, white matter and ventricles.

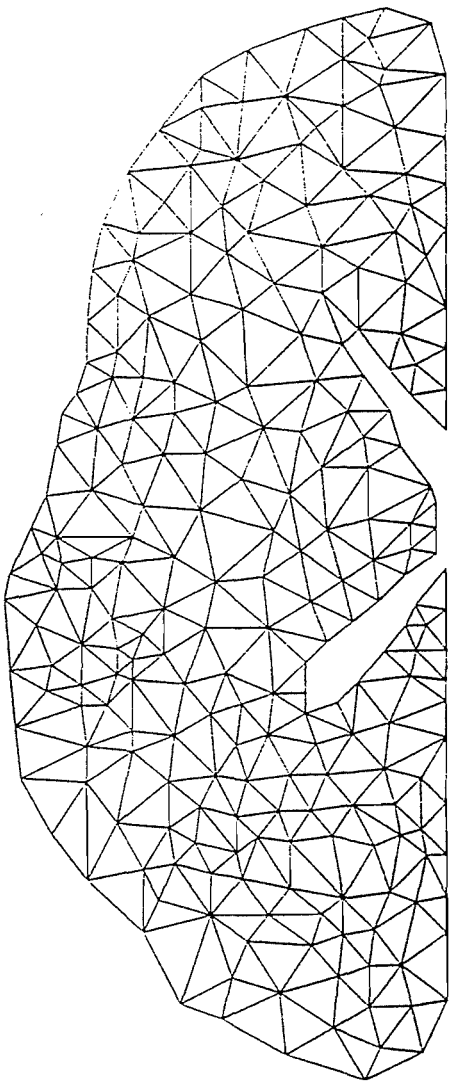

Figure 13: The Finite Element mesh including 239 nodes and 408 elements (element numbers and node numbers are emitted for simplicity)

6.2 The Material Properties

The physical properties of the grey and white matter must be defined including the modulus of elasticity, Poisson's ratio and permeability. These parameters may be determined relatively easily for engineering materials using accepted standard protocols. However, for biological materials the process is more complex. Biomechanical properties change in vitro due to cell death and isolation from other tissues which affect behaviour. These problems combined with possible interperson difference and the changes which may occur with pathology have resulted in widely differing measurements of biological material properties.

An interest in the mechanical properties of brain tissue developed in relation to the study of brain injury associated with skull impact, deformation and fracture. However until the late 1960s very little appropriate experimental data was available.

6.2.1 The modulus of elasticity

The modulus of elasticity describes the ratio of stress to strain for a body obeying Hooke's law [14]. Hooke's Law is used to describe the load/deformation relationship of a material when the load applied is proportional to material deformation i.e. stress α strain. This relationship is linear and once the load is removed the deformation disappears and the material returns to its original state (figure 14A).

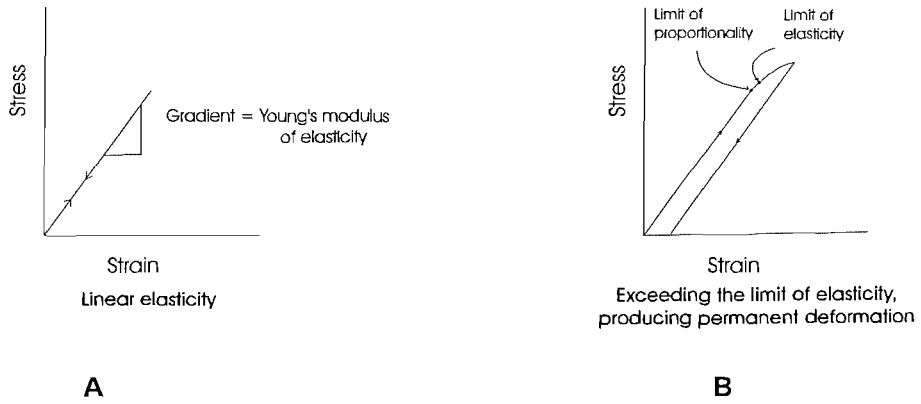

Figure 14A: The stress strain relationship for a material obeying Hooke's law

Figure 14B: Permanent deformation occurs when the elastic limit is exceeded.

The maximum load up to which Hooke's Law may be applied is described as the limit of proportionality and is closely followed by the elastic limit (figure 14B). Once the elastic limit is exceeded some permanent deformation occurs when the load is removed. Some materials may demonstrate a non-linear load deformation relationship, but for this purpose it is assumed that brain tissue has linear elasticity and that permanent deformation does not occur due to exceeding the elastic limit. Although this may be interpreted as an over-simplification of the biomechanics, the theory of consolidation on which the model is based assumes linear elasticity.

One of the first studies of human and primate brain tissue properties was performed in 1969 to provide necessary data for head injury models [15]. In vitro studies were performed on human brain tissue after post-mortum using an engineering based protocol to assess tissue shearing. A vibrating probe was pressed into the revealed cortex with the pia arachnoid in tact. A range of shear moduli of between 6-11x10^3 dynes/cm^2 were measured. Assuming Poisson's ratio to equal 0.25 then the modulus of elasticity may be calculated as 1.5-2.8KN/m^2.

Walsh and Shettini [16] evaluated the elastic response of brain tissue in anaesthetised dogs. A pressure displacement transducer was implanted in to the animal skull leaving the dura intact. As the transducer was depressed into the brain tissue, the depth of insertion and resultant pressure were measured with the transducer system. The elastic modulus was calculated on the basis of the resultant pressure-depth ratio and the geometry of the brain and transducers. The average modulus of elasticity recorded was 3.3 x10^5dynes/cm^2 (33KN/m^2)

The change in material properties when brain tissue is dead and fixed was investigated by Metz et al [17]. The elastic analysis was performed using hypodermic tubing, closed at one end with a rubber membrane. This was inserted into the brain of a rhesus monkey and filled with a known quantity of fluid. The pressure within the probe was recorded. The increase in pressure is dependent on the expansion of the rubber covering the slits in the probe, which in turn is dependent on the tissue properties. This test was performed on live monkeys under

anaesthesia, after death and after the tissue had been fixed with formaline. The elastic modulus in vivo was in the range of $1.0x10^5$ dyne/cm^2 to $3.5x10^5$ dyne/cm^2 (10-35KN/m^2). The values obtained 45 minutes after death were in the same range. In fixed tissue the values increased to 3 - 14 $x10^5$ dynes/cm^2 (30-140KN/m^2).

More recently Guillaume et al [18] investigated the mechanical behaviour of brains under hypergravity. Fresh bovine brains were removed and placed in a skull-like transparent mold. The brain and mold were then centrifuged. Approximately half the brains were perfused with saline solution during centrifugation. The displacements and deformation of the brain tissue were recorded using a camera also placed in the centrifuge. Data obtained from these digitised images were used to perform a finite element analysis. The deformation modelled using FEM allowed Young's modulus (and Poisson's ratio, see next section) to be estimated. In brains that were not perfused $E = 46.8 \pm 31.3$KN/ m^2 (n=35) and $E = 106.4 \pm 73.9$KN/ m^2 (n=34) in perfused brains. These values are higher than those previously reported.

Elastance is a parameter commonly reported in pressure volume studies of the intracranial cavity which may be assessed in humans with minimally invasive techniques. If the lumbar route is used then the cranial cavity remains closed. It was suggested that the elastance coefficient calculated during PV tests may be related to elasticity of the brain tissue. Studies [19,20] have since demonstrated that brain elastance is not related to brain tissue elasticity. Therefore this tool which meets the experimental criteria for accurate measurement i.e. may be performed in vivo in humans with a minimally invasive technique does not provide the required information.

This data is summarised in table 1.

Author	Nature of Study		Parameter	E(KN/m^2)
Fallenstein & Hulce (1969)	Human	- in vitro, post mortum	Shear modulus	1.5 - 2.8
Walsh and Schettini (1976)	Dog	- in vivo	Elastic modulus	33
Metz et al (1970)	Monkey	- in vivo - after death	Elastic modulus Elastic modulus	10 - 35 30 – 140
Guillaume et al (1997)	Bovine	- in vitro, perfused - in vitro, nonperfused	Elastic modulus Elastic modulus	106.4±73.9 46.8±31.3

Table 1 : A summary of the elastic modulus data

The elastic moduli were selected on the basis the experimental evidence and the data selected by Nagashima et al [3,4].

6.2.2 Poisson's ratio

Poisson's ratio (υ) is the constant of proportionality relating the lateral strain to direct strain. For example, if a bar is subjected to a direct stress which produces longitudinal strain then it will extend in the direction of the stress and contract in the lateral direction. The relationship between lateral and direct strain is :

$$\text{Lateral strain} = -\upsilon \times \text{direct strain.}$$

Poisson's ratio is always in the range 0 to 0.5. Nagashima et al [3,4] and Hakim [2] suggest that Poisson's ratio for brain tissue equals 0.5. This however cannot be correct as $\upsilon=0.5$ would produce an infinitely large bulk modulus :

$$K = E/3(1-2\upsilon)$$

where K is the bulk modulus and E is the Young's modulus. As compressibility is the reciprocal of the bulk modulus, an infinitely large bulk modulus implies no material compression and therefore no tissue density changes. If the incompressible solid phase (neurons and glia) were considered in isolation then it would be appropriate for υ to approach 0.5. However, as the Poisson's ratio is used to calculate the total stress (see consolidation

equations- Terzarghi's theory) for the biphasic, undrained, compressible tissue as a whole then $\upsilon=0.25$ is a more realistic estimation.

In the study of bovine brain previously described in the 'modulus of elasticity' section, Guillaume et al [18] also determined Poisson's ratio from the distortion and displacement of the brain when centrifuged. For perfused brain mean $\upsilon = 0.370 \pm 0.188$ and non-perfused brain $\upsilon = 0.326 \pm 0.198$. Although this study demonstrated considerable variability in both perfused and non-perfused brains it confirms the improbability that υ should be considered to be 0.5.

6.2.3 Tissue permeability

Tissue Permeability is the ease at which extracellular fluid can pass through the extracellular spaces and is calculated using Darcy's Law. The permeability of tissue is dependent on many factors including the porosity, the shape of the solid phase particles, the viscosity of the fluid and the degree of saturation.

Very few papers quantitatively explore tissue permeability. For the most, studies explore changes in brain hydraulic conductivity in different pathologies and investigate the affects of other physiological parameters [21]. However, Rosenberg [22] quantified the bulk flow of interstitial fluid. Radioactive labelled sucrose was infused into the ventricles of normal cats for between 1 and 4 hours. The cats were then sacrificed and the brains sectioned. The results demonstrated bulk flow in the white matter with fluid moving from the tissue into the ventricles at a rate of 10.5μm/min.

Although this provides some insight into the rate of fluid movement in the normal brain, in hydrocephalus the situation is very different. Flow is reversed with fluid moving from the ventricles into the tissue. Alternative drainage routes via the perivascular spaces are

established allowing fluid to drain more easily. These microscopic drains cannot be included in the same finite element model as gross anatomical changes. Therefore the tissue permeability input to CRISP must be a total permeability which takes into consideration all routes by which fluid may flow through the tissue. Unfortunately there is no experimental data available for such permeability.

6.2.4 Material property changes with pathology

The material properties become even more complex if pathological states are considered, when the normal anatomy and physiology are usually modified to some extent. Such changes may affect the composition and behaviour and therefore the physical properties of a material. In hydrocephalus there are changes in the distribution of extracellular fluid for example with edema. This is likely to produce an inhomogenous material with the material properties dependent on the physical changes produced by the pathology. A recent study on cats has demonstrated changes in the poro-elastic properties in brains with kaolin induced hydrocephalus [23]. Although the changes were not quantified the authors concluded that the hydrocephalic brain tissue appeared less stiff. This change was attributed to a 'weakening' of the tissue. The time course of these changes was not explored.

Investigation of biomechanical tissue properties are often performed in vitro. However tissue behavior is highly dependent on the properties of the surrounding media. Once tissue is isolated its behavior changes. This is particularly significant for the brain which is enclosed by the skull in a very specific controlled environment. Although this suggests that in vivo studies are preferable they are often very invasive and therefore not ideal. Biomechanical changes have been demonstrated with craniotomy in cats [24]. The study demonstrated that when a closed cavity is opened, intracranial pressure and white and grey matter tissue pressures all decreased. Bolus injection tests [25] into both the tissue and ventricles allowed the tissue compliance and the tissue resistance and the pressure volume index to be calculated respectively. The PVI increased after craniotomy and the tissue compliance in the cortex

decreased. Although no change in fluid content was seen, considerably different results were obtained after craniotomy. This must be considered when using experimental data.

6.2.5 Material Properties selected.

Although the experimental data described above offers some guidance for material property definition, many uncertainties still remain. A series of 1 dimensional finite element studies were performed to provide insight into the affects of changing the material properties. Changes in permeability altered the rate of drainage and therefore the time for equilibrium to be reached. The degree of compression was found to decrease with increasing Poisson's ratio and Young's modulus.

The material properties used for this analysis were selected on the basis of the experimental data described above and on an understanding of hydrocephalus and consolidation. Accordingly the material properties of grey and white matter were differentiated (see table 2).

Property	Grey Matter	White matter
Young's Modulus (KN/m^2)	30	3
Poisson's ratio	0.25	0.25
Permeability(m/s)	$1x10^{-7}$	$1x10^{-4}$

Table 2: A summary of the material properties used in the analysis.

An example of the MPD file is given in Appendix 5.

7. BOUNDARY CONDITIONS

To solve the mathematical equations that describe a theoretical model, variables describing the behavior of the system at the physical boundaries must be defined. These variables or boundary conditions are dependent on the nature of the problem and without them solutions cannot be obtained. To perform a consolidation analysis, the boundary conditions may include prescribed pressures (and the resultant total stress), loads, displacements or fluid flow across boundaries (flux). CRISP however does not allow flux to be prescribed. Therefore, when pressure is not prescribed, the boundary is assumed to be impermeable and the flux is automatically set to zero allowing the equations to be solved. The boundary conditions are applied to the element vertex nodes which lie along the boundary, values at mid-point nodes being calculated automatically by the program.

For engineering problems the boundary conditions are well defined, with unknowns being determined experimentally. Biological models, however, are more complex with numerous factors affecting boundary conditions producing an elaborate conundrum of interactive variables. In the definition of the boundary conditions, the anatomy and physiology were considered with special attention paid to the micro structure and permeability of different structures, the fluid pathways and direction of fluid flow. In addition the pathology and pathophysiology of hydrocephalus must also be considered.

In the biological problem the brain tissue is separated from the intraventricular fluid by the ependyma. When hydrocephalus occurs, the intraventricular pressure increases and exerts a force on the ependyma and brain tissue. The physical affect of the increased pressure is dependent on the properties of the brain tissue and the boundary conditions. When this problem is translated into an engineering consolidation model, the brain tissue becomes a bi-phasic material. The ventricular fluid is modeled as a hydrostatic pressure head and the properties of the ependyma are modeled as boundary conditions rather than an additional material zone. For this model the prescribed boundary conditions include displacements and pressures and the pressure induced total stresses.

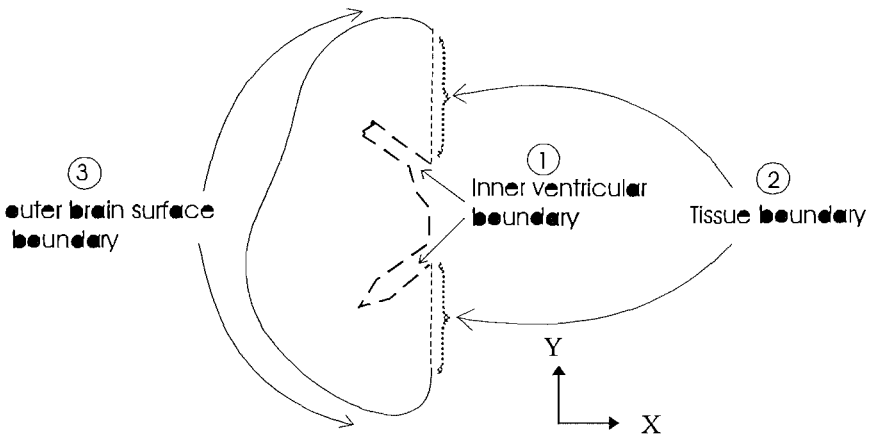

Figure 15: The mesh outline, illustrating the 3 boundary zones where the boundary conditions must be specified.

The 3 zones of the brain mesh where boundary conditions must be specified are demonstrated in figure 15.

(1) Inner ventricular boundary.

For nearly all simulations the intraventricular CSF pressure increases in 20 even steps from 0 to 1.3KNM^{-2} (0-10mmHg) over a simulated period of 100 hours as shown in figure 16. Although this may appear to be a modest pressure increase compared to clinical observations, the transmantle pressure gradient established is sufficient to drive ventricular expansion.

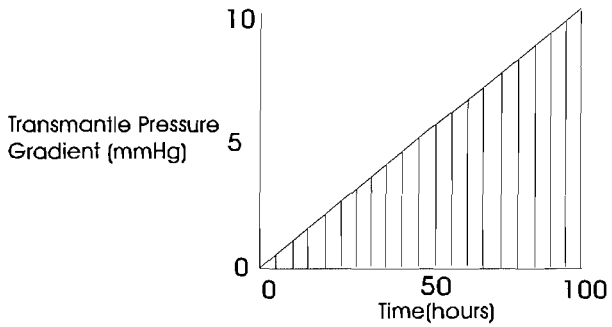

Figure 16: The pressure profile for the ventricular boundary.

The intraventricular CSF (with increasing pressure) and brain tissue interact via the ependyma, a layer of cuboidal cells with open pathways. Although this thin microscopic layer could not be included in a macroscopic study of the brain, its permeability is an important boundary characteristic which affects the simulated brain behavior. Therefore the ependyma is modeled as a hypothetical membrane i.e. its properties are reflected in the boundary conditions, but its physical structure is not included in the mesh.

Translation of the boundary properties into engineering terms, which may be applied to the model, is demonstrated below (figure 17). The intraventricular CSF pressure (Pv) is equal to the total stress (σ) acting on the boundary. According to Terzarghi's principle of effective stress, total stress is equal to the effective stress (σ' acting on the solid phase of the bi-phasic material and the fluid pressure (U_w). CRISP allows σ and U_w to be defined at the boundaries. σ'is automatically calculated ($\sigma' = \sigma - U_w$).

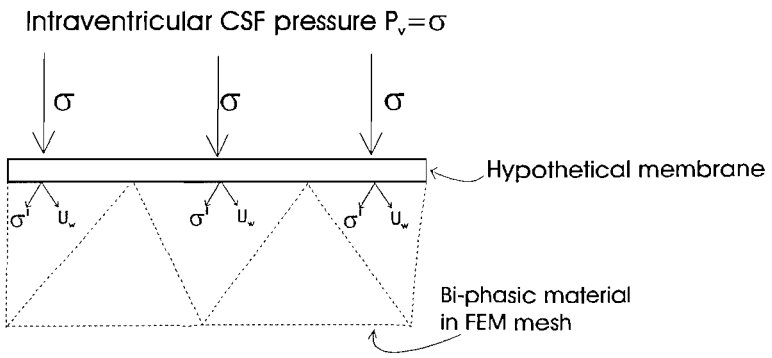

Figure 17: The intraventricular pressure applied as the total stress along a boundary element is divided into effective stress (σ') and fluid pressure (U_w).

The division of the total stress into σ' and U_w is determined by the properties of the hypothetical membrane. If the membrane is impermeable U_w is unspecified and the flux across the boundary is automatically set to zero. If the membrane is permeable then U_w is defined in the range 0 (minimum permeability) to σ (maximum permeability).

Although the displacement of the ventricular walls could be specified, deformation occurs as a result of the change in ventricular pressure. Therefore it would appear more biologically realistic to specify the pressures and resultant stresses producing the displacement and other tissue changes.

(2) The Tissue Boundary.

This boundary is at the line of symmetry and remains constant during the simulations. In a whole brain slice, simulated fluid flow across this region would be the same in both directions. This is the equivalent of no flow, therefore this boundary is assumed to be impermeable and U_w is not defined. Displacement in the x direction is specified as zero allowing unspecified displacement y direction only (see figure 15).

(3) The Outer Brain Surface Boundary.

For all simulations this boundary is fixed with no displacement in the x or y direction. The pressure U_w is either

(i) set to zero implying a permeable boundary and providing a reference for the transmantle pressure, or

(ii) unspecified indicating an impermeable boundary.

In summary the boundary conditions applied are pressures and resultant stresses and displacements.

8. THE SIMULATIONS

The data described in the previous pages was used to formulate the geometric program (GPD) and the material properties program (MPD) which are required to run CRISP. GPD contains the mesh data and MPD contains the material properties, boundary conditions and time stepping for the simulation. Examples of these programs are in Appendices 4 and 5.

Each simulation has different boundary conditions which are described in biological and engineering terms. A diagram of a simple 1 dimensional simulation is used to demonstrate the basic changes.

Before the prescribed boundary conditions are determined, the biological problem must first be translated into an engineering model (figure 18).

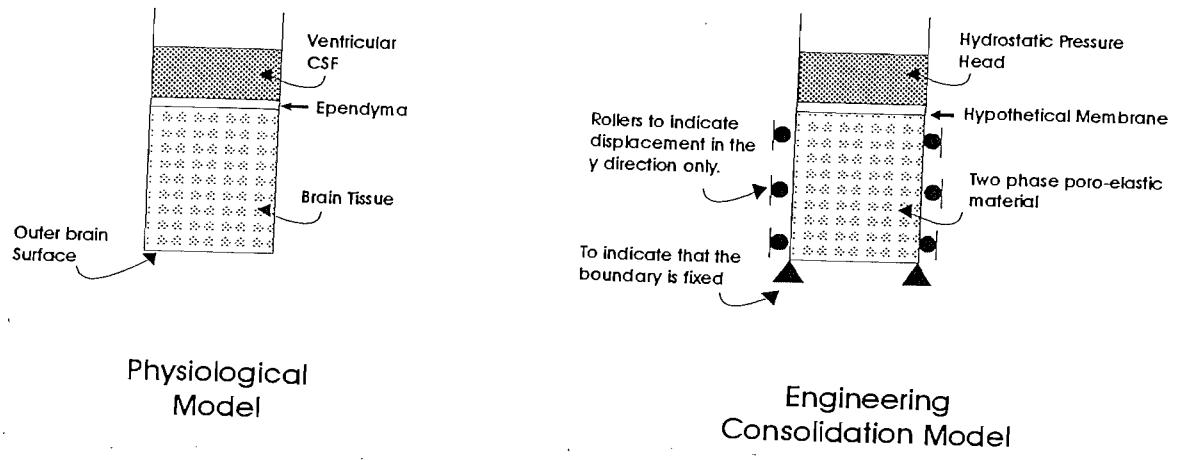

Figure 18: The engineering interpretation of the physiological model in 1 dimension.

The results for each computer simulation are presented in the form of contour plots (figure 19). Four plots are presented for each simulation to demonstrated the parameters of biological importance (see section 4).

The next few pages describe the developmental process which was necessary to establish a viable model which accurately describes the biological system and satisfies the physical engineering criteria. Although many of the models are either biologically or physically incorrect they are included to demonstrate the thought processes and to highlight the many potential problems of applying a quantitative analytical technique to a system with many unknown or unquantified parameters.

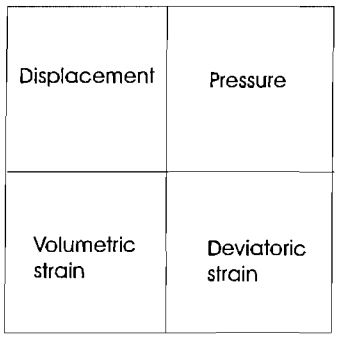

Figure 19: The format of the computer simulated contour plots.

8.1 Simulation 1

Ependymal permeability was not discussed by Hakim [2]. However his original laboratory experiments investigating the interaction of bi-phasic brain tissue, CSF and blood included a thin plastic membrane between the simulated brain tissue and CSF. This implied an impermeable brain-CSF boundary. Therefore, to investigate the bi-phasic poro-elastic model for brain tissue according to Hakim's original work, simulation 1 included an impermeable ependyma.

The intraventricular pressure (P_v) was increased in 20 even steps from 0 to 10mmHg (0 to 1.3KN/M^2) and was specified as a total stress (σ) along the hypothetical membrane. As fluid could not flow across the hypothetical membrane from the ventricles into the brain tissue, U_w was not specified at this boundary. The effective stress (σ') was therefore equal to the total stress i.e. $\sigma = \sigma'$. The outer brain surface was fixed (x and y displacement =0) and permeable ($U_w = 0$). In summary (figure 20) :

(i) Ventricular boundary, σ = 0 to 1.3 KN/M^2, U_w= unspecified

(ii) Outer brain surface boundary, displacement=0, U_w=0

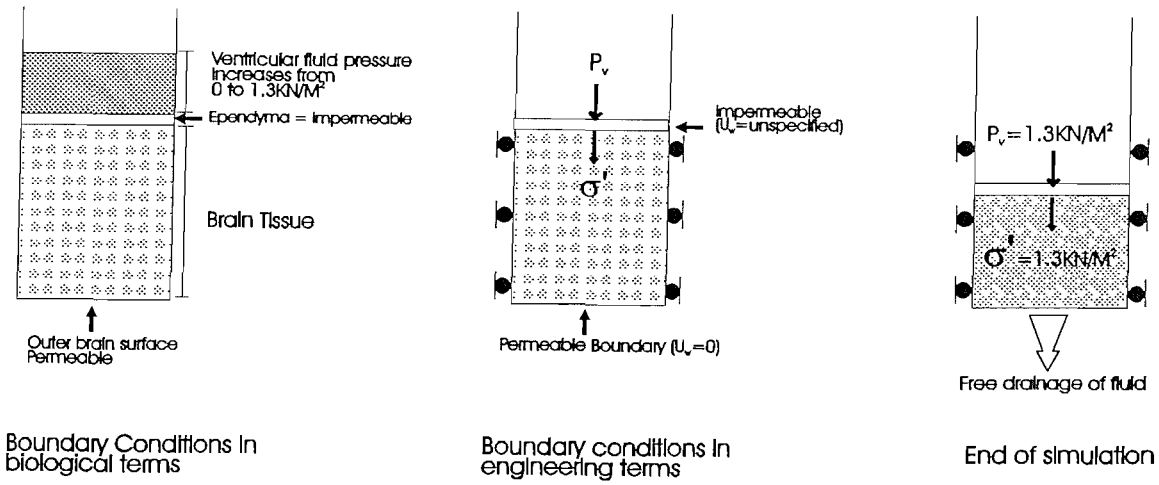

Figure 20: Simulation 1.

The computer simulated results (figure 21) demonstrate ventricular enlargement and tissue density changes. Positive volumetric strain for the majority of the simulated brain slice indicates increased tissue density as a result of fluid flow from the outer brain surface. However two areas demonstrate negative volumetric strain indicating fluid accumulation. These areas correspond with the anterior and posterior horns areas where edema may occur in hydrocephalus. Areas of increased deviatoric strain indicating tissue shearing were seen

(i) in the deep white matter

(ii) at the tissue/ventricular boundary at the anterior and posterior horns. The changes at the ventricular horns may suggest an increase in the ependymal permeability in these small areas. As these small areas are not obvious from the contour plot the deviatoric strain has been plotted for each node around the ventricle (figure 22).

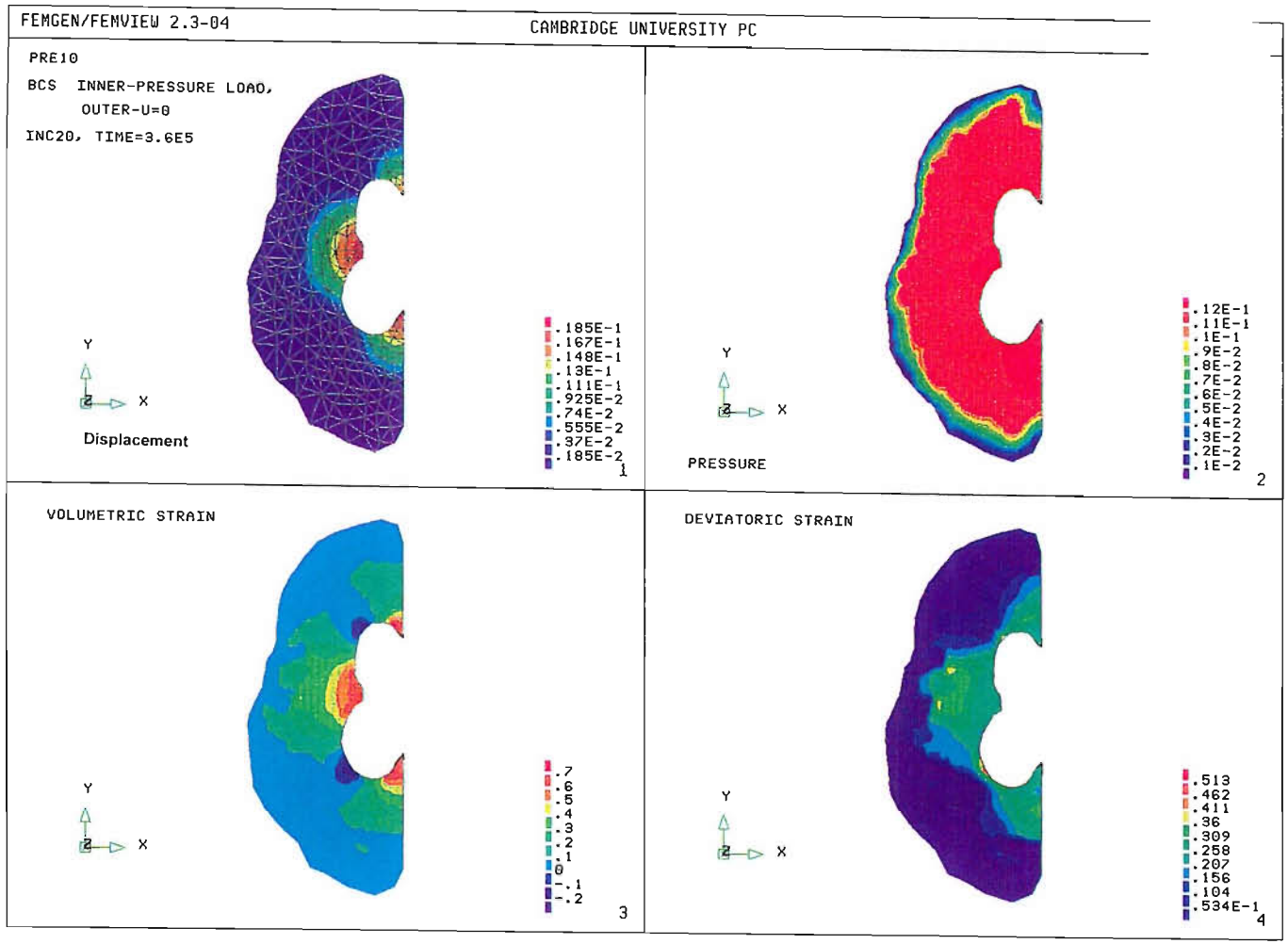

Figure 21: The contour plots of displacement, pressure, volumetric strain and deviatoric strain for simulation 1. Ventricular expansion is demonstrated with negative volumetric strain at the anterior and posterior horns.

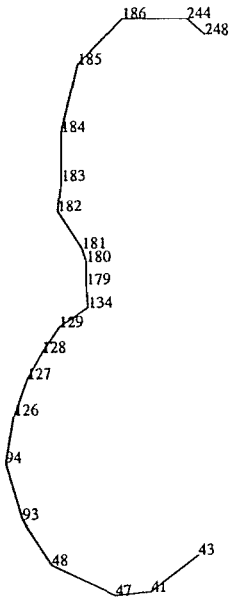

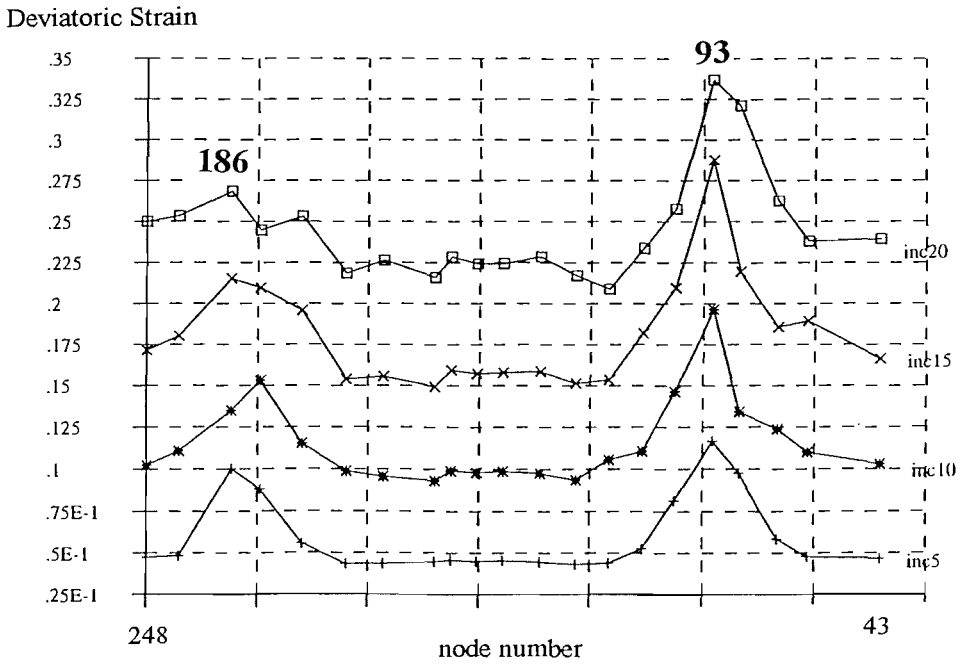

Figure 22a: The node numbers at the ventricular/tissue boundary

22b: The deviatoric strain for each node at the ventricular/tissue boundary at step5 (after 1/4 of the simulation), step 10 (after 1/2 of the simulation), step 15 (after 3/4 of the simulation), and step 20 (end of simulation). Note the peaks occurring at nodes 186 and 93 .

8.2 Simulation 2

Although simulation 1 produced reasonably convincing results the impermeable nature assigned to the ependyma is biologically incorrect in non-pathological states. It is now generally accepted that the ependyma is a permeable layer. A model was created to include this basic anatomical observation.

The intraventricular pressure (P_v) was increased in 20 even steps from 0 to 10mmHg (0 to 1.3KN/M^2), however it was not applied as a total stress. The hypothetical membrane was permeable therefore U_w was specified. As the total stress was not applied $U_w = P_v$. The outer brain surface was fixed (x and y displacement =0) and permeable (U_w = 0). In summary (figure 23) :

(i) Ventricular boundary U_w = 0 to 1.3 KN/M^2

(ii) Outer brain surface boundary, displacement=0, U_w=0

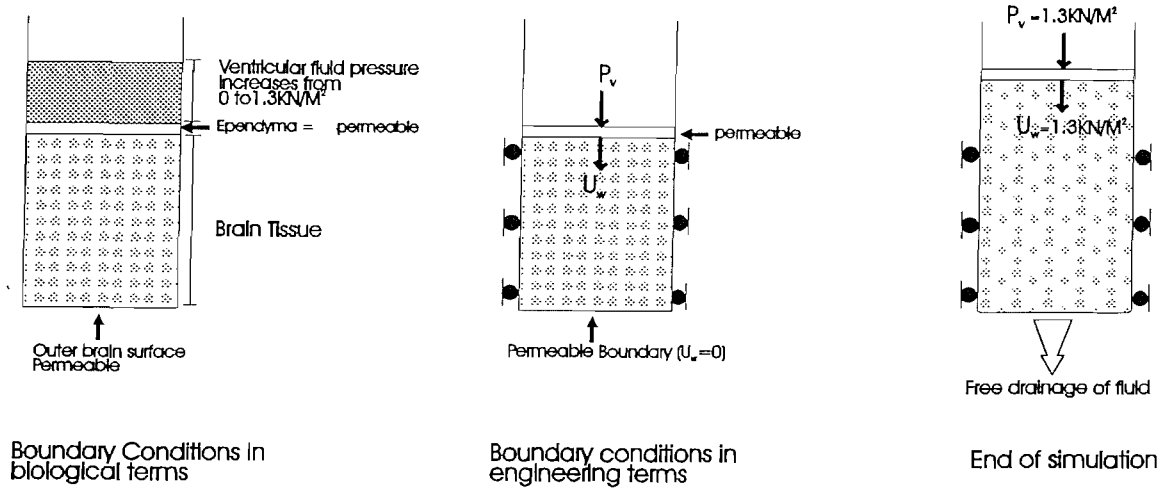

Figure 23: Simulation 2

The computer simulated results (figure 24) demonstrate generalised tissue swelling and ventricular obliteration. This is obviously not representative of the clinical observations therefore this model is biologically incorrect.

The tissue swelling is due to incorrect application of the boundary conditions. This is a result of literally translating the biological problem to an engineering problem. In biological terms the ventricular pressure increases and exerts an effect on the brain tissue. Translating this correctly into engineering terms the intraventricular pressure must be applied as total stress ($P_v=\sigma$). The total stress in then divided into effective stress and pressure depending on the properties of the hypothetical membrane. Applying the intraventricular fluid pressure as tissue fluid pressure U_w only, is the equivalent of injecting fluid into the tissue, therefore the results of the simulation are not surprising. Although obviously incorrect, this simulation was included to emphasise the problems of misinterpretation encountered during this study.

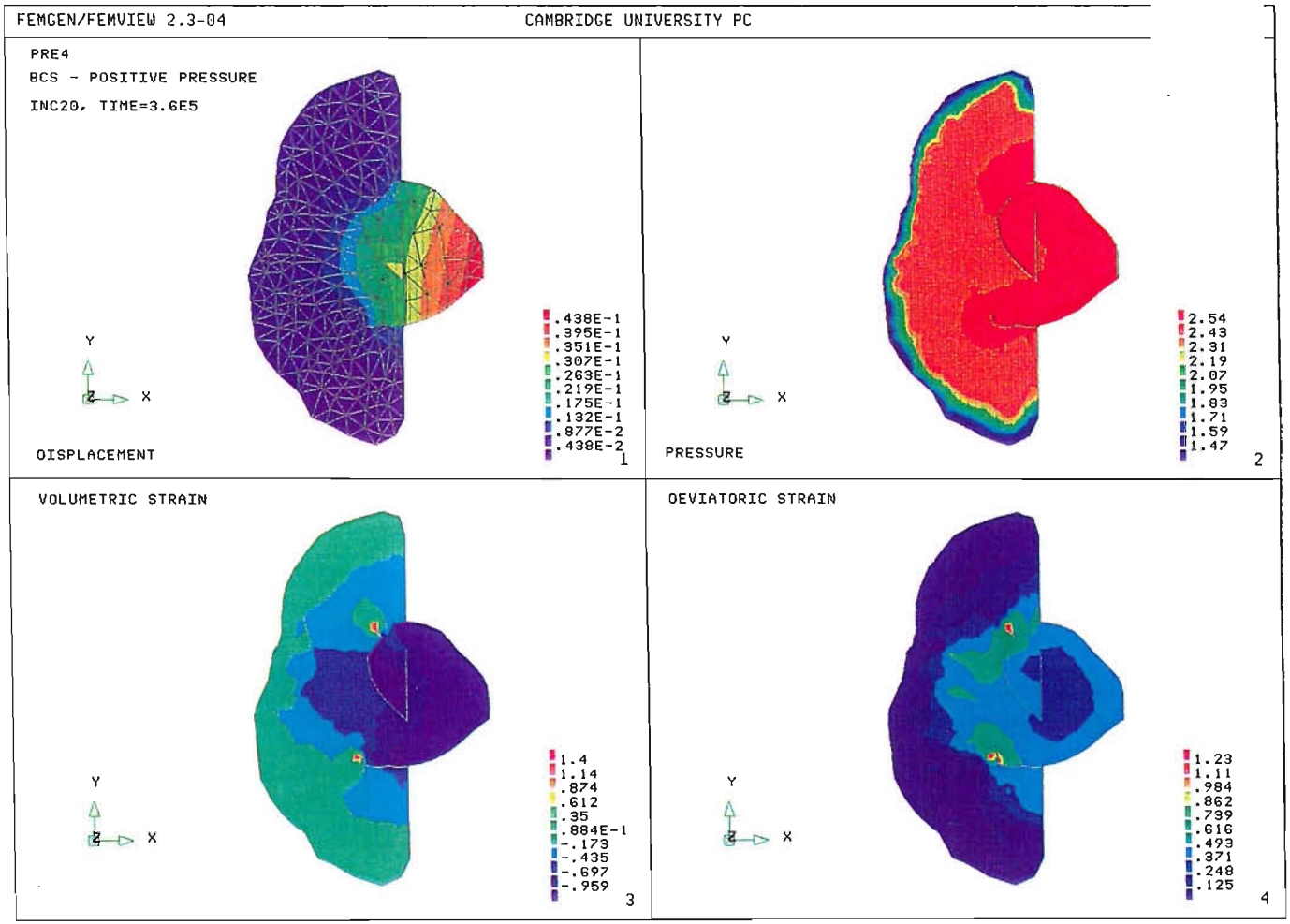

Figure 24: The contour plots of displacement, pressure, volumetric strain and deviatoric strain for simulation 2 demonstrating generalised tissue swelling and ventricular obliteration.

8.3 Simulation 3

The next stage in the model development was to perform a similar simulation, but using a negative 'suction' pressure.

The boundary conditions were the same as simulation 2 but the intraventricular pressure (P_v) was decreased in 20 even steps from 0 to -10mmHg (0 to -1.3KN/M^2).

In summary (figure 25) :

(i) Ventricular boundary U_w = 0 to -1.3 KN/M^2

(ii) Outer brain surface boundary, displacement=0, U_w=0

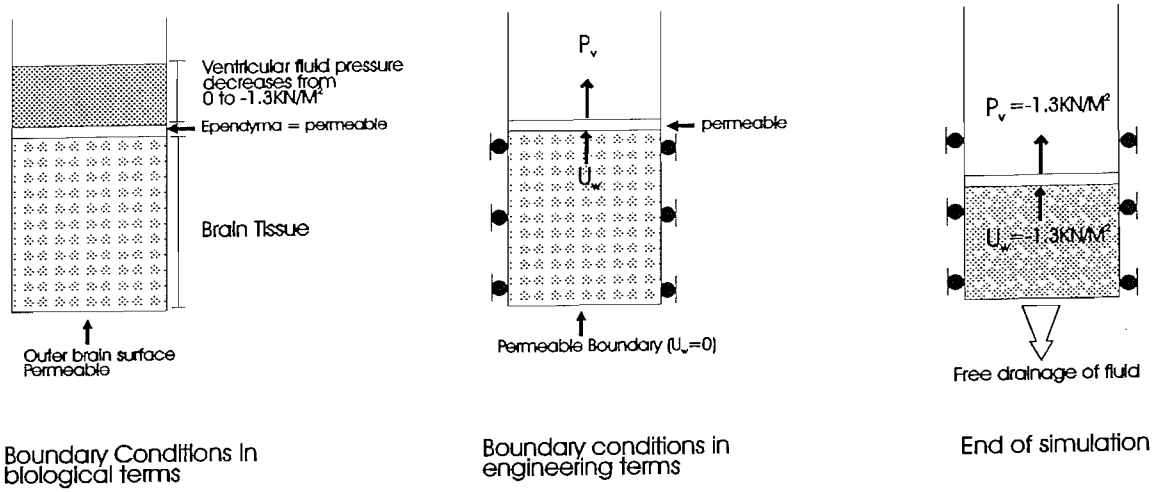

Figure 25: Simulation 3.

The results (figure 26) demonstrate increased ventricular volume with increased brain tissue density. However no areas of negative strain were observed indicating that the 'suction' did not allow for fluid accumulation. For this reason and the lack of biological evidence for negative suction pressure this model is also biologically incorrect.

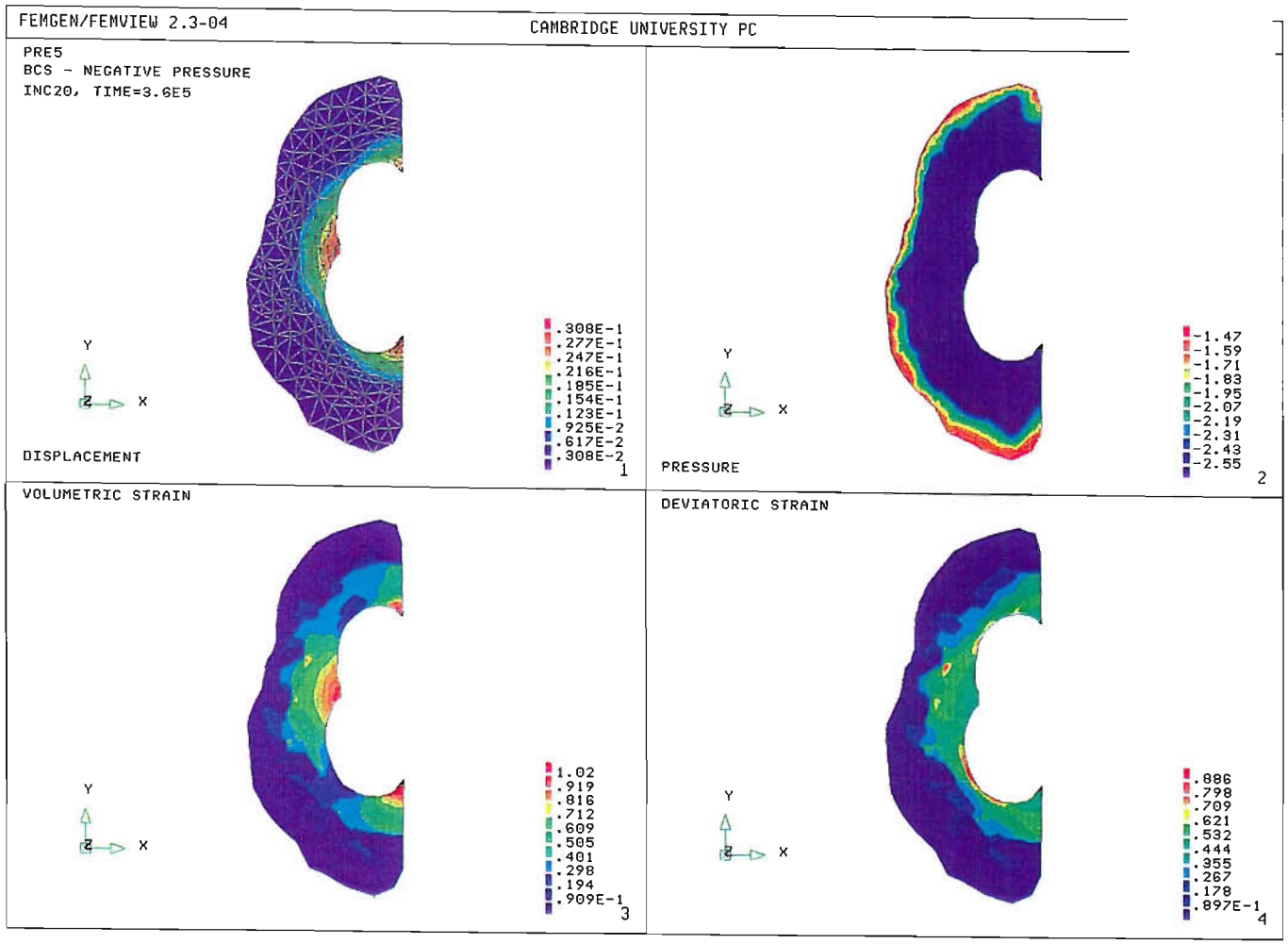

Figure 26: The contour plots of displacement, pressure, volumetric strain and deviatoric strain for simulation 3 demonstrating ventricular enlargement, but no negative volumetric strain.

8.4 Simulation 4

Although the previously described simulations were either biologically incorrect (simulations 1 and 3) or the boundary conditions had been incorrectly applied (simulation 2) they have highlighted some of the potential problems.

Applying the correct boundary conditions to simulation 2 produces the results shown below (figure 27). The intraventricular pressure (P_v) was increased in 20 even steps from 0 to 10mmHg (0 to 1.3KN/M^2) and was applied as a total stress (σ) along the hypothetical membrane. For this simulation the hypothetical membrane was highly permeable therefore at the boundary $U_w = \sigma$ and consequently $\sigma' = 0$. The outer brain surface was fixed (x and y displacement =0) and permeable (U_w = 0). In summary (figure 27) :

(i) Ventricular boundary σ= 0 to 1.3 KN/M^2 , U_w = 0 to 1.3 KN/M^2

(ii) Outer brain surface boundary, displacement=0, U_w. =0

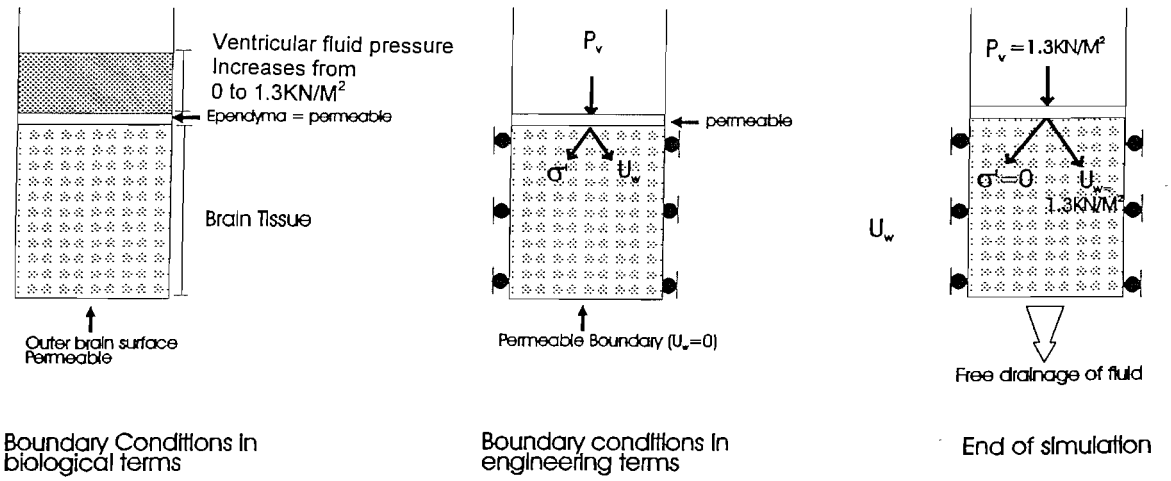

Figure 27: Simulation 4.

The computer simulated results (figure 28) demonstrate a small ventricular enlargement accompanied by tissue density changes. Positive volumetric strain was seen in the majority of

the tissue with 2 areas of negative volumetric strain indicating fluid accumulation as in simulation 1. This simulation is therefore representative of the pathopysiological changes although the ventricular dilation is very modest.

At the end of the simulation $U_w = 1.3$ KN/M^2 at the ependymal membrane and $U_w = 0$ at the outer brain surface. Therefore a pressure gradient is established throughout the tissue. As $U_w + \sigma' = \sigma$ a σ' gradient is implied. At the ependymal boundary $\sigma' = 0$ and at the outer brain surface $\sigma' = 1.3$ KN/M^2. The balance between U_w and σ' determines the material behavior.

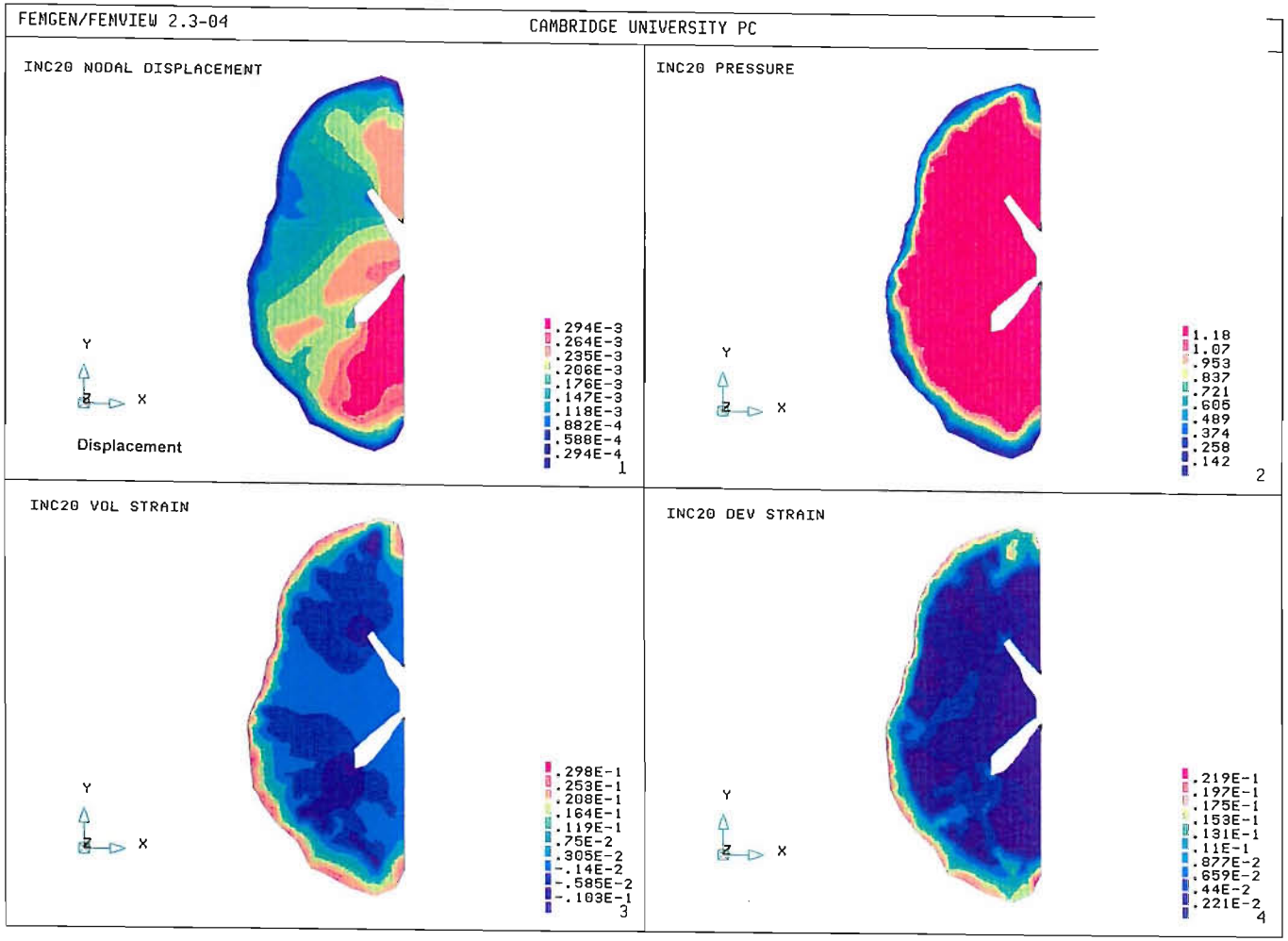

Figure 28: The contour plots of displacement, pressure, volumetric strain and deviatoric strain for simulation 4 demonstrating modest ventricular enlargement and negative volumetric strain

8.5 Simulation 5

In simulation 4 the boundary conditions were applied correctly and the results appeared promising, however the ventricular dilatation was very modest. For simulation 5 the permeability of the ependyma is reduced to a minimum.

The intraventricular pressure (P_v) was increased in 20 even steps from 0 to 10mmHg (0 to 1.3KN/M^2) and was applied as a total stress (σ) along the hypothetical membrane. For this simulation the hypothetical membrane was minimally permeable therefore at the boundary $U_w = 0$ and consequently $\sigma' = 0$ to 1.3 KN/M^2. The outer brain surface was fixed (x and y displacement =0) and permeable ($U_w = 0$). In summary:

(i) Ventricular boundary $\sigma = 0$ to 1.3 KN/M^2 , $U_w = 0$

(ii) Outer brain surface boundary, displacement=0, $U_w = 0$

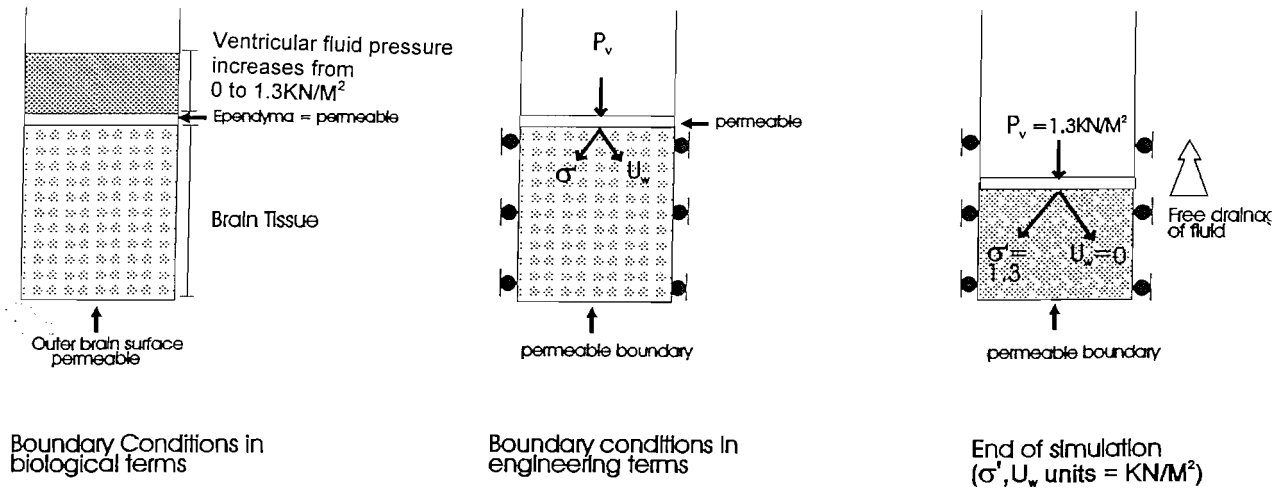

Figure 29 : Simulation 5.

The computer simulated results (figure 30) demonstrate ventricular enlargement comparable to that seen on CT or MRI in hydrocephalic patients. Relatively large areas of negative volumetric strain are seen at the anterior and posterior horns with positive volumetric strain

in the remainder tissue. In an area of the mesh equivalent to the deep white, matter areas of high deviatoric stress are seen indicating areas of possible shearing. These areas may correlate with areas of deep white matter lesions. Areas of increased deviartoric strain were also seen at the tissue/ventricular boundary at the anterior and posterior horns as in simulation1. Unlike simulation 4 the pressure at both boundaries is equal to 0 therefore there is no U_w and σ' gradients are established within the tissue.

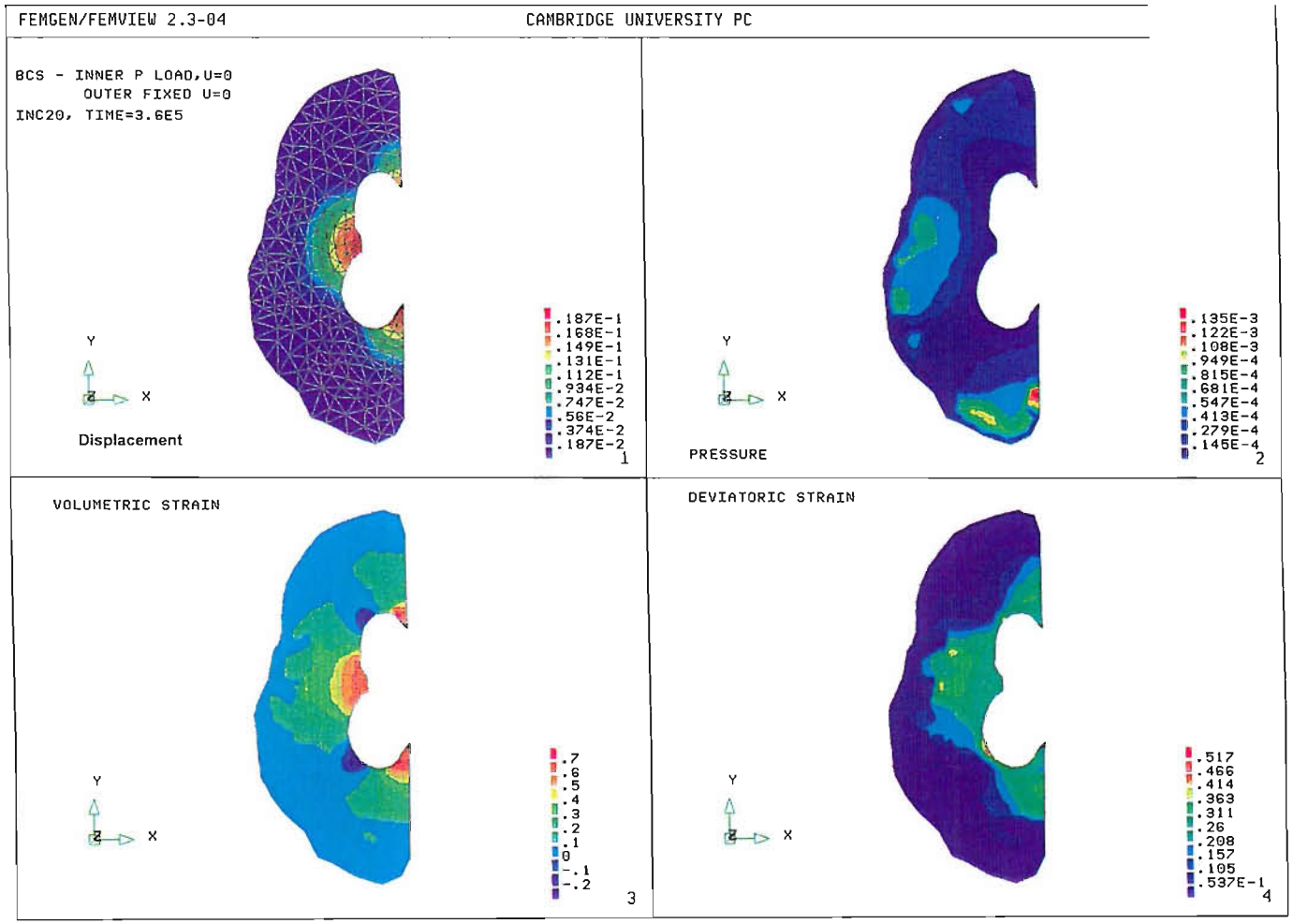

Figure 30: The contour plots of displacement, pressure, volumetric strain and deviatoric strain for simulation 5 demonstrating ventricular enlargement comparable with that seen in clinical images and areas of negative volumetric strain. Areas of high deviatoric strain, indicative of shearing occur deep in the white matter and ventricular/tissue boundary .

8.6 Simulation 6

Extreme permeabilities are modeled in simulations 4 and 5. Permeability was at a maximum in simulation 4 (U_w= 0 to 1.3 KN/M^2) and a minimum in simulation 5 (U_w=0). The actual permeability is probably between these 2 extremes. For this simulation σ was split between σ' and U_w respectively giving U_w= 0 to 0.26 KN/M^2 at the ependyma.

The intraventricular pressure (P_v) was increased in 20 even steps from 0 to 10mmHg (0 to 1.3KN/M^2) and was applied as a total stress (σ) along the hypothetical membrane. For this simulation the hypothetical membrane was moderately permeable with U_w= 0 to 0.26 KN/M^2 at the boundary and consequently σ'= 0 to 1.04 KN/M^2. The outer brain surface was fixed (x and y displacement =0) and permeable (U_w = 0). In summary:

(i) Ventricular boundary σ= 0 to 1.3 KN/M^2, U_w = 0 to 0.26 KN/M^2

(ii) Outer brain surface boundary, displacement=0, U_w =0

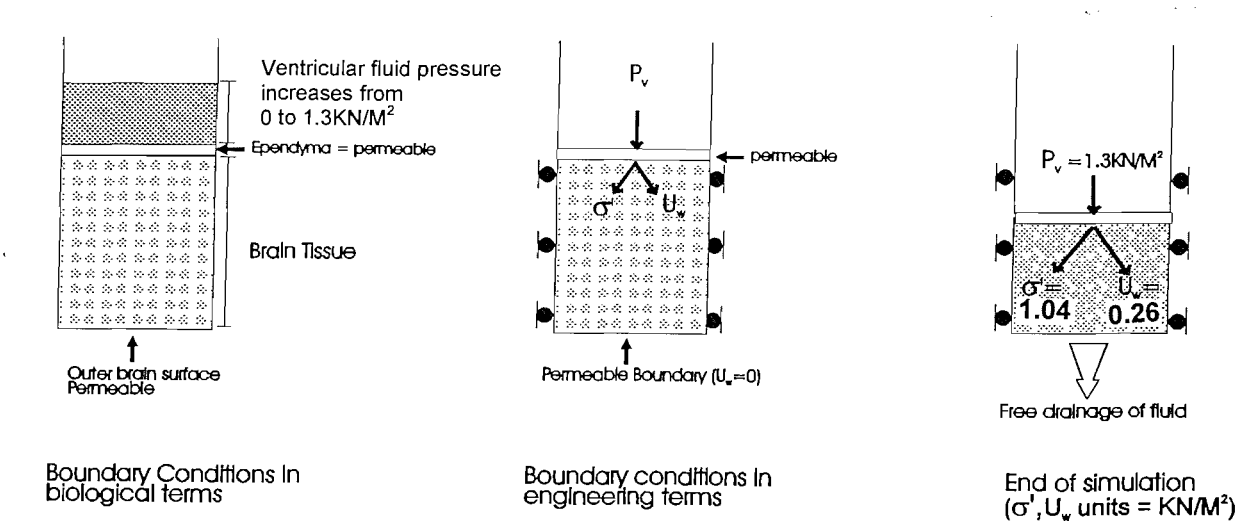

Figure 31: Simulation 6

The computer simulated results (figure 32) demonstrate changes very similar to simulation 5, with less ventricular expansion. Tissue density changes with negative volumetric strain at the ventricular apices is seen. Areas of high deviatoric strain occur in the deep white matter and at the tissue/ventricular boundary.

As the pressure is 4mmHg (0.52 KN/M^2) at the ependyma (at the end of the simulation) and 0 at the outer brain surface, a pressure gradient and therefore a σ' gradient are established through the tissue.

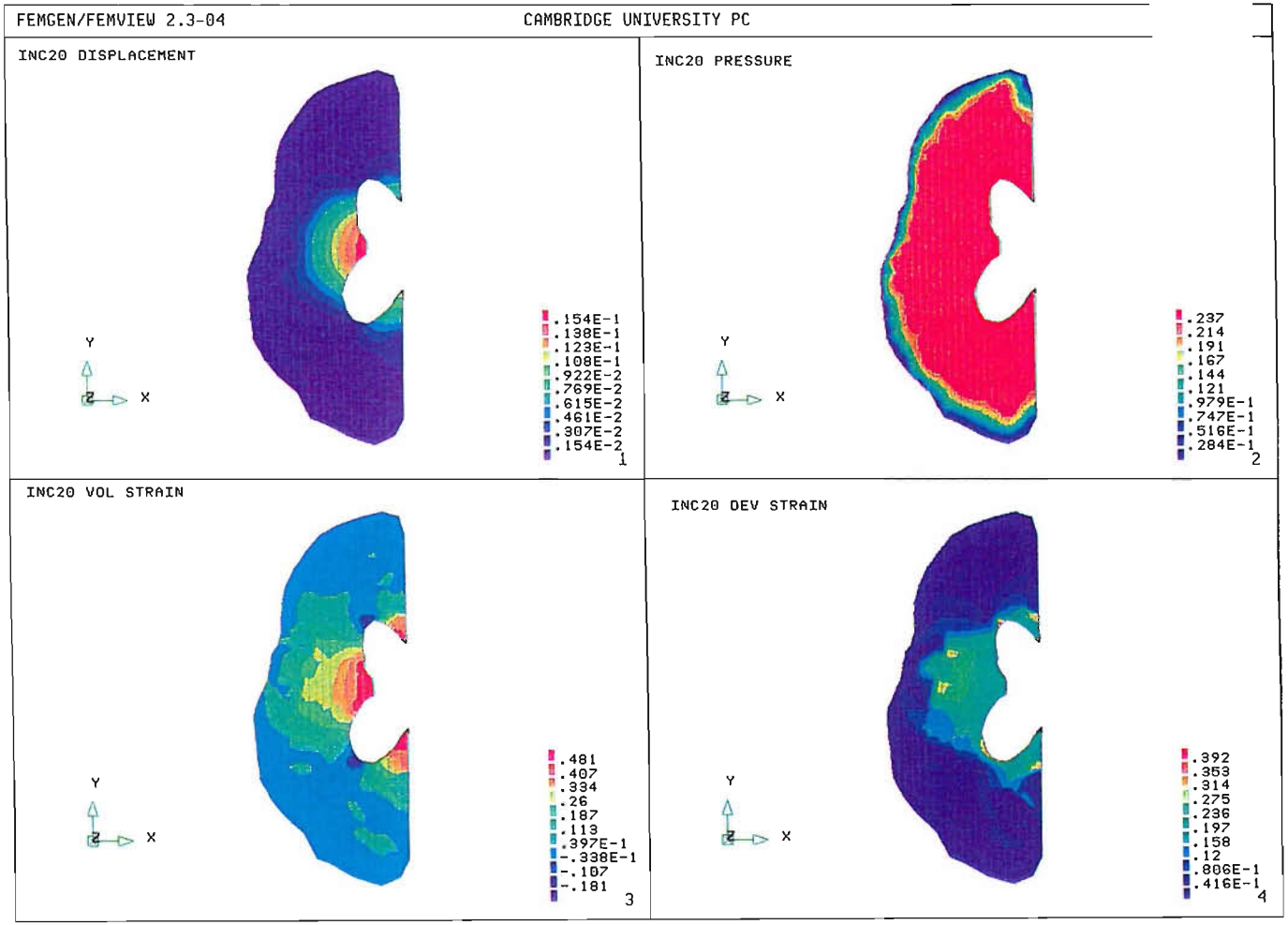

Figure 32: The contour plots of displacement, pressure, volumetric strain and deviatoric strain for simulation 6 demonstrating ventricular enlargement comparable with that seen in clinical images and negative volumetric strain. Areas of high deviatoric strain, indicative of shearing occur deep in the white matter and at the tissue\ventricular boundary.

8.7 Simulation 7 - Changes with Pathology

The boundary conditions and material properties may change during the simulations. The changes demonstrated in simulation 6 are summarised below.

1. Ventricular enlargement.
2. Tissue density changes- decreasing density at the anterior and posterior ventricular horns and increasing in the remaining tissue.
3. Tissue Shearing in the white matter and at the tissue/ventricular boundary. Shearing at the boundary may indicate increased ependymal permeability in these areas.

This simulation is performed in 2 phases in an attempt to include some of the changes described above. The first phase of the 2 phase analysis was performed as for simulation 5:

(i) Ventricular boundary $\sigma = 0$ to 1.3 KN/M^2 , $U_w = 0$

(ii) Outer brain surface boundary, displacement=0, $U_w=0$

For phase 2

(i) σ is maintained at 1.3 KN/M^2.

(ii) The permeability of the hypothetical membrane is increased to a maximum in the areas of high deviatoric strain. Therefore at the apex of the anterior and posterior ventricular horns $U_w = 1.3$ KN/M^2. For the remaining boundary U_w remains equal to 0.

(iii) In areas of positive volumetric strain the tissue becomes more dense. The permeability of these areas are decreased.

Phase 2 was simulated over 100 hours therefore the total simulation time was 200 hours. The contour plot (figure 33) demonstrates

(i) ventricular enlargement and tissue density changes.

(ii) the volumetric strain is more negative than in the 1 phase models indicating an increase in the amount of fluid accumulating in the edematous tissue areas. The area of negative strain is also increased.

(iii) deviatoric strain occurs in the deep white matter as in the 1 phase analysis, but it is decreased in magnitude.

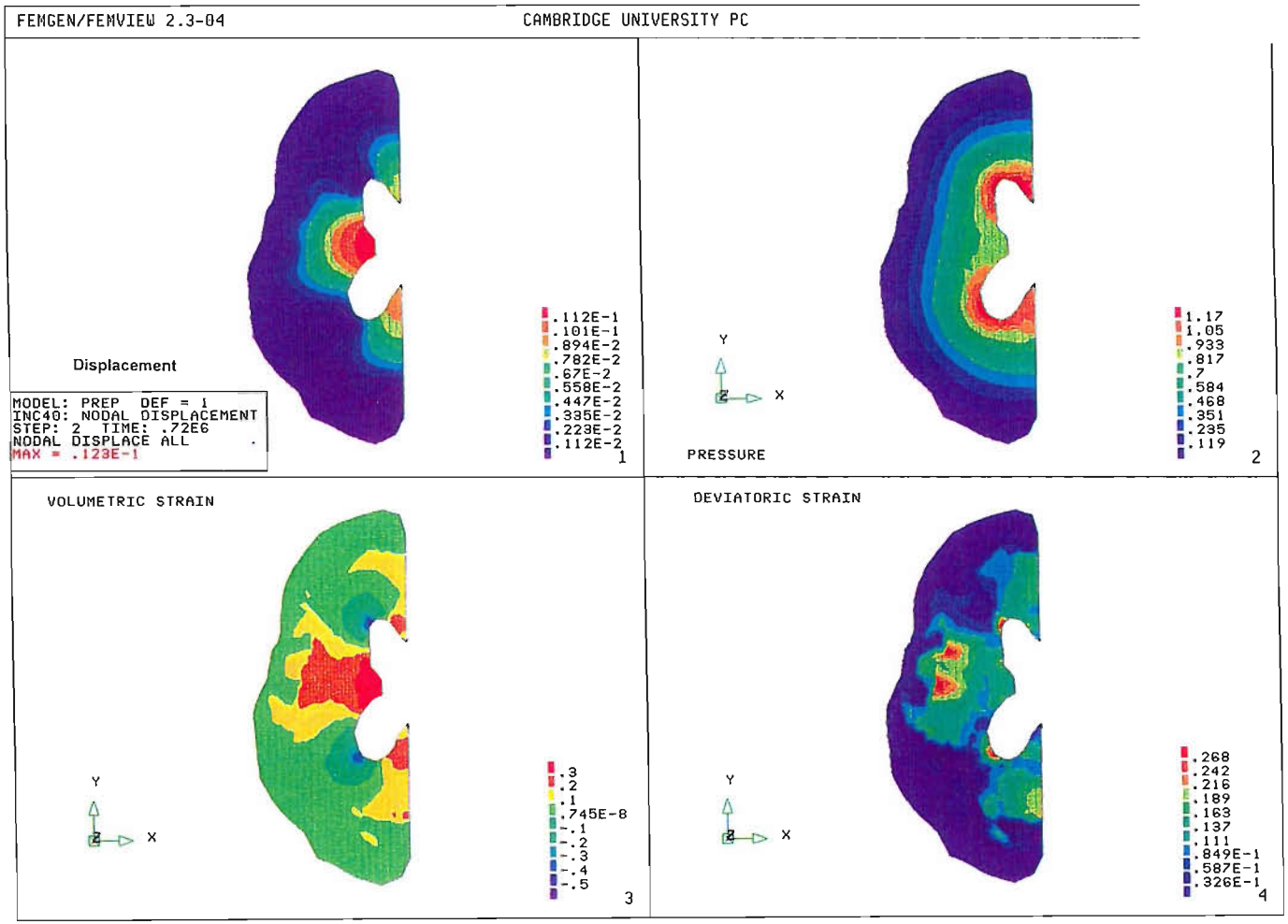

Figure 33: The results from the 2 phase analysis demonstrating dilating ventricles, an increased area of negative volumetric strain and areas of deviatoric strain in the deep white matter.

9. DISCUSSION

A two dimensional finite element model has been established to describe the fundamental gross physical changes which occur during hydrocephalus. Hakims poro-elastic hypothesis was applied, and the theory of consolidation was used mathematically to describe the poro-elastic behavior. The model was used to simulate increasing CSF pressure within the ventricles and the subsequent biomechanical and topographical changes.

The prominent changes simulated with increasing ICP were
(i) ventricular dilatation
(ii) areas of negative volumetric strain, indicating edema, at the anterior and posterior horns
(iii) areas of increased deviatoric strain, indicating tissue shearing points deep in the white matter and at the ventricular apices along the tissue/ventricular boundary.

Comparing these changes to the clinical and pathophysiological characteristics of hydrocephalus, is encouraging. The predominant anatomical features of acute hydrocephalus on CT scan are ventricular dilatation and periventricular edema. Ventricular enlargement is simulated by a reduction in extracellular fluid and edema as the accumulation of extracellular fluid. Both these conflicting states have been accommodated concurrently in the poro-elastic model.

In non-pathological states, interstitial fluid, produced by the brain cells and endothelium, drains into the intraventricular CSF across the ependyma. However, when intracranial pressure is increased, the direction of flow is reversed and fluid accumulates in the white matter. This occurs predominantly around the ventricular horns and only affects the white matter as demonstrated by the simulations. Simulation 1, with an impermeable ependyma also demonstrated areas of negative volumetric strain, which suggests that fluid accumulation may not only be dependent on CSF flow across the ependyma, but also on the geometric changes and the decreasing fluid content of the surrounding tissue.

In hydrocephalus the ependyma may be normal, stretched or torn depending on the degree of ventriculomegaly and the rapidity of dilatation. Areas of increased deviatoric strain at the ventricular apices along the tissue/ventricular boundary may suggest that the ependyma is particularly vulnerable to damage in these regions. Simulation 7 demonstrates that ependymal damage and the resulting increased permeability of these boundary regions produces a larger area of negative volumetric strain.

Other areas of increased deviatoric strain were identified in the deep white matter. In raised pressure hydrocephalus, deep white matter changes are not usually seen on MRI or CT. However in normal pressure hydrocephalus in the elderly, deep white matter lesions are a common feature. It has been suggested that these lesions occur in a watershed zone where the blood vessels are narrow and have a long intraparenchymal course. These vessels are thought to be more sensitive to arteriosclerosis and therefore more prone to ischaemic events. The increased deviatoric strain in the deep white matter suggests that tissue in this area is also more susceptible to shearing which may contribute to deep white matter changes.

Hakim's poro-elastic hypothesis was first applied by Nagashima et al. The theory of consolidation was used mathematically to describe the behavior of the brain tissue and the equations were solved using the finite element method. Although this work provided a valuable start the approach was flawed in 3 main areas:

(i) The selection of Poisson's ratio

Nagashima suggested that the Poisson's ratio for the brain tissue should be close to 0.5 (0.4999). This suggests that brain tissue is almost incompressible, a contradiction since ventricular dilatation is achieved by fluid drainage and tissue compression. If the solid and fluid phases were considered together with no drainage, then tissue compression would not be possible. However in soil mechanics problems, the Poisson's ratio is determined for drained materials. The fluid is therefore removed leaving voids. Therefore the material may be compressed without compressing the individual particles.

(ii) The application of the boundary conditions.

The boundary conditions for the hydrocephalus model are complex. The simulations have demonstrated that the results are highly dependent on the boundary conditions, with small variations producing very different results. Simulation 3 demonstrates that incorrect boundary conditions may produce results which appear correct. It is therefore important to discuss the boundary conditions in detail.

The boundary conditions applied by Nagashima et al were not clearly defined and therefore interpretation of their model is difficult. It appears that displacement was prescribed at the tissue/ventricular boundary. This is biologically incorrect as displacement occurs as a result of the total stress produced by the increasing intraventricular pressure. Although pore pressure was defined for the fluid phase, the permeability of the boundary was not discussed.

(iii) The biological interpretation of the engineering results.

Edema defined as the accumulation of water within tissue is a prominent characteristic of hydrocephalus and should therefore feature in theoretical models. For these simulations, edema is described as negative volumetric strain. As brain cells are incompressible in the acute phase, any change in volume must be due to a change in fluid content. Nagashima suggested that areas of high pressure could be related to edema. Pressure, however, is not related in any way to fluid distribution. However, fluid will have a tendency to flow away from high pressure areas suggesting that this parameter is a poor indicator of edema.

Although the simulated tissue changes appear to correlate exceptionally well with the pathophysiology and anatomy of hydrocephalus, as with any theoretical model, many assumptions and estimations have been made. As yet there is no clinical evidence to support the assumption that brain tissue behaves as a bi-phasic poro-elastic medium. A CT study in patients with hydrocephalus (pre and post shunt) and patients with subdural and epidural hematoma [25] was performed. Patients demonstrating signs of periventricular edema were not included in the study, therefore localised accumulation of fluid was not considered. The results from the patients with hematoma demonstrated that the tissue next to the hematoma

had a higher density than tissue in the same anatomical region contralateral. The results from the hydrocephalic group were,however,more difficult to interpret. Some patients demonstrated density changes soon after shunting, but the results were not consistent enough to provide conclusive evidence for Hakim's hypothesis. This may be a reflection of the limited accuracy of CT for water detection.

The material properties assigned to the brain tissue are important. Unlike engineering problems, these parameters are not readily available, are difficult to assess and may change with pathology. Therefore the values used are a compromise based on experimental studies and our understanding of hydrocephalus. Simulation 7 includes a change in permeability which may occur as a result of tissue density changes.

10. CONCLUSIONS

A two dimensional finite element model has been established to describe the fundamental gross physical changes which occur during hydrocephalus. The model was used to simulate increasing CSF pressure within the ventricles and the subsequent biomechanical and topographical changes.

The prominent changes simulated with increasing ICP were
(i) ventricular dilatation
(ii) areas of negative volumetric strain, indicating edema, at the anterior and posterior horns
(iii) areas of increased deviatoric strain, indicating tissue shearing, points deep in the white matter and at the ventricular apices along the tissue/ventricular boundary.

These tissue changes correlate exceptionally well with the pathophysiology and anatomy of hydrocephalus and provide significant insight into possible biomechanical processes that could produce the anatomical changes identified with neuroimaging.

CHAPTER 7

CONCLUSIONS

CONCLUSIONS

1. SUMMARY OF CONCLUSIONS

The studies described in this thesis used modern engineering and computational techniques to investigate the complex biomechanical interrelationship between cerebrospinal fluid (CSF) hydrodynamics and cerebral haemodynamics and CSF volume and the cerebral mantle in normal pressure hydrocephalus (NPH) and other complex disorders of the CSF circulation.

The 'dynamic' relationship between the CSF hydrodynamics and the cerebral haemodynamics was investigated using CSF infusion studies and overnight intracranial pressure (ICP) monitoring combined with transcranial Doppler ultrasonography (TCD).

The CSF infusion and TCD study presented in Chapter 2 demonstrated that moderate increases in ICP induced during infusion, provoked cerebral haemodynamic changes, in particular an increase in the pulsatility index of the blood flow velocity waveform (PI). Although an increase in PI was seen in all patients, those with elevated resistance to CSF outflow (R_{csf}) demonstrated a significantly greater increase in PI compared to those with normal R_{csf}. This finding was discussed in detail in Chapter 2 and lead to the hypothesis that there may be a difference in the autoregulatory capacity of patients with normal R_{csf} and increased R_{csf}. This study concludes that as the PI behaves differently in the two groups TCD may have the potential to replace direct ICP monitoring during CSF infusion studies, providing a less invasive one needle test. However there was no evidence to suggest that TCD is a good indicator of ICP in this patient group.

The study of B wave activity presented in Chapters 3 and 4 demonstrated that changes in cerebral haemodynamics may affect CSF hydrodynamics in certain patients. Overnight TCD monitoring allowed the identification and quantification of B wave activity in the cerebral circulation of normal volunteers. This demonstrated that haemodynamic B wave activity is a

normal physiological phenomenon and provided a baseline for comparison with the patient group.

Simultaneous overnight ICP and TCD recordings in patients demonstrated that haemodynamic B wave fluctuations were also present in patients. Comparing the fluctuations in the normal volunteers and patients demonstrated that there was no significant difference in the frequency of B waves in the two groups therefore, TCD cannot replace ICP for the assessment of B wave activity.

Hydrodynamic B wave activity was also demonstrated in the ICP recording of some patients. It was concluded that the 'driver' for ICP B waves were B wave fluctuations in the cerebral blood flow velocity. The transmission of the fluctuations in blood flow to the CSF was dependent on changes in the compliance of the cerebral mantle. These findings draw into question the belief that ICP B waves must occur for a certain percentage (5-50%) of the overnight recording to be of clinical significance.

The 'static relationship between the increase in CSF volume and the properties of the cerebral mantle was explored using image analysis and mathematical modeling.

The image analysis study presented in Chapter 5 demonstrated a high incidence of MRI hyperintense areas on MR images of patients with suspect NPH. The total area of hyperintensity was significantly greater in patients who did not improve with shunting. These patients also had a greater risk of demonstrating any hyperintensity. This suggests that patients with minimal disruption to the brain tissue are more likely to improve with shunting.

Evidence for the 'watershed' theory for the development of deep white matter lesions was not provided. However, there was a highly significant increase in the area of hyperintensitity continuous with the ventricles, in each slice, as the distance from the middle cerebral artery increased. This suggests that 'watershed' ischaemia may play a role in periventricular lesions.

Chapter 6 describes a two dimensional finite element model which was established to describe the fundamental gross physical changes which occur during hydrocephalus. The model was used to simulate increasing CSF pressure within the ventricles and the subsequent biomechanical and topographical changes.

The prominent changes simulated with increasing ICP were:
(i) ventricular dilatation
(ii) areas of negative volumetric strain, indicating edema, at the anterior and posterior horns
(iii) areas of increased deviatoric strain, indicating tissue shearing, points deep in the white matter and at the ventricular apices along the tissue/ventricular boundary.

These tissue changes correlated exceptionally well with the pathophysiology and anatomy of hydrocephalus provide significant insight into possible biomechanical processes that may produce the anatomical changes identified with neuroimaging. In particular the location of the areas of increased deviatoric strain, correlated very well with the location of deep white matter lesions described in Chapter 5, providing an additional possible mechanism, for production of these changes in the cerebral mantle.

APPENDIX 1

APPENDIX 1

TRANSCRANIAL DOPPLER DURING INFUSION STUDIES - AN EXPERIMENTAL STUDY TO ASSESS THE HAEMODYNAMIC CHANGES.

1. INTRODUCTION

Chapter 2 describes changes in the transcranial Doppler (TCD) waveform observed during moderate increases in intracranial pressure induced during cerebrospinal fluid (CSF) infusion studies. Different TCD trends were noted in patients with increased resistance CSF outflow (R_{csf}) compared to those with normal R_{csf}. In all patients, an increase in Goslings pulsatility index (PI =(flow velocity systolic - flow velocity diastolic)/flow velocity mean)) was observed with increasing intracranial pressure (ICP). However, in patients with increased R_{csf}, PI rose significantly higher due to the divergent behaviour of flow velocity systolic (FVs) and flow velocity diastolic (FVd). The physiological significance of these changes could not be assessed as a non-invasive means of continuous arterial blood pressure (ABP) measurement was not available. Invasive ABP assessment was not considered acceptable at that time.

This experimental study explores whether these haemodynamic changes are related to the state of the autoregulatory reserve. Infusion tests were performed in autoregulated and non-autoregulated rabbits. Continuous recording of TCD, ICP, ABP and cortical blood flow with laser Doppler flowmetry (LDF) allowed assessment of the cerebral haemodynamic and cerebrovascular changes.

1.1 Aims

This study was performed to explore the cerebral haemodynamic changes during CSF infusions tests using TCD and LDF. The aims of this study were to determine:

- whether the changes in the TCD parameters may be related to the state of autoregulation.

- whether there is any discrepancy between the limits of cerebral autoregulation and cerebrovascular resistance (CVR)
- determine the repeatability of experimental CSF infusion tests.

1.2 Issues and Assumptions

Although the data presented in this appendix has been published as part of a comprehensive study to determine the relationship between PI and CVR [1], there are numerous issues which should be considered, when using the results of this study to interpret the findings in hydrocephalic patients (Chapter 2).

- In this study, three rabbits were autoregulated and five were non-autoregulated. As all the animals were treated similarly, the reason for autoregulatory impairment is not clear. It is assumed that loss of autoregulation was associated with the trauma of surgery or the experimental protocol. Although studies have been reported in the literature, where autoregulation has been 'randomly' impaired during the experimental procedure [2,3], care must be taken when using these results to help interpret the findings in patients where specific pathologies have caused autoregulation to be impaired.

- This study was performed in a group of young healthy rabbits. It is therefore questionable whether the results may be used to interpret data from hydrocephalic patients many of whom are elderly with chronic pathology.

- The study in patients described in Chapter 2 used TCD to insonate the middle cerebral artery (MCA). However the anatomy of the rabbit does not allow easy access to the MCA, therefore the basilar artery was insonated, an approach that has previously been used successfully [4,5]. Although this allowed the assessment of blood flow velocity it assumes that basilar flow behaves in a similar way to MCA flow, which may or may not be correct.

- The pulsatility of the cerebral blood velocity was assessed in the basilar artery using TCD and autoregulation was assessed using a laser Doppler probe positioned on a cerebral hemisphere. This assumes that blood flow in these two distinct areas are linked.

2. AUTOREGULATION

Maintenance of cerebral blood flow (CBF) is complex with a close mutual dependence between cerebral haemodynamics, ICP and blood volumes resulting from unique features of the cerebral circulation. Although blood volume may change in response to changes in other intracranial volumes, for example CSF volume, in a normal human CBF remains constant due to autoregulatory adjustment of CVR, with an adjustment time of 10-20 seconds. Cerebral blood flow is dependent on the cerebral perfusion pressure (CPP) and CVR. Changes in CPP produced by changes in ABP or ICP provoke vessel dilatation or constriction. As resistance is inversely proportional to vessel radius to the forth power, small autoregulatory changes in vessel radius produce large changes in cerebrovascular resistance. According to this concept, cerebral blood flow is calculated as CBF=CPP/CVR when autoregulation is intact [6,7].

In normal healthy humans changes in mean autoregulatory mechanism allows CBF to be maintained if the mean CPP is in the range of 50-150mmHg. When the autoregulatory reserve is exhausted CBF changes proportionally with CPP. In pathological states the reactive mechanisms may be impaired or not function at all exposing the brain to ischaemic events. Therefore the state of the autoregulatory mechanism has significant clinical implications and in some pathologies may be related to patient outcome.

2.1 Autoregulation in Normal Pressure Hydrocephalus

The state of the autoregulatory reserve in NPH has not been widely explored. Meyer et al [8] demonstrated that the vasomotor responsiveness to CO_2 in NPH is impaired and Tanaka et al [9] demonstrated a reduced response to intravenous acetazolamide in patients who improved with shunting.

Numerous techniques have been used to assess CBF in NPH including single photon emission computed tomography [10,11,12], xenon enhanced computed tomography [9,13], positron emission tomography [14] and TCD [15,16]. Studies have demonstrated widespread regional decreases in CBF in patients with NPH, particularly in the frontal regions and subcortical white matter. The autoregulatory mechanism may therefore be engaged in the resting state to maintain sufficient blood flow to the brain. Additional changes in CPP may induce a more rapid decrease in the autoregulatory reserve. It has been suggested that these events may be responsible for the deep white matter changes often observed on MRI scans in suspected NPH.

Other factors which may effect the autoregulatory reserve in NPH and other elderly patients include chronic systemic hypertension and cerebrovascular disease. Prolonged chronic systemic hypertension shifts the CBF/CPP curve towards higher levels of CPP [17]. This protective mechanism provides additional defences against further increases in ABP and CPP which may exceed the upper limit of autoregulation which is accompanied by increasing CBF and decreasing CVR. Stenosis or occlusion of a major or branch vessels may activate haemodynamic mechanisms which result in insufficient CBF. Therefore part of the autoregulatory reserve is expended to maintain normal flow in resting conditions. Further haemodynamic events such as decreasing arterial blood pressure during cardiac arrhythmia during normal sleep, or physiological increases in ICP may result in exhaustion of the autoregulatory reserve.

2.2 Transcranial Doppler Ultrasonography and Autoregulation

Cerebral haemodynamic responses similar to those observed during the clinical infusion tests have been noted in head injured patients [18] and animal models [1,4]. It has been suggested that changes in the TCD waveform during decreasing CPP may reflect the state of the cerebral autoregulatory reserve.

Nelson et al [4] investigated the relationship between FV and cerebral autoregulation in rabbits. Changes in TCD parameters were recorded during increasing ICP induced by lumbar infusion into the subarachnoid space. On the basis of the experimental results and

theoretical modelling three specific haemodynamic phases were described: Phase 1, where FV is maintained during changes in CPP indicating a fully preserved autoregulatory reserve. Phase 2, a transitional period where CPP in the diastolic phase is close to the critical closing pressure producing a decreasing FVd and increasing pulsatility. Phase 3 where the autoregulatory reserve is exhausted, FV and FV amplitude decrease rapidly as a result of diminishing FVs and FVd. Similar haemodynamic events in rabbits have been observed when a reduction in CPP is induced by controlled haemorrhage [4]. Multimodal monitoring in head injured patients [18,19] has demonstrated phase 1 and 2 haemodynamic behaviour. Decreasing FVs, indicative of the exhaustion of the autoregulatory reserve, is thought to occur in the terminal state only and was not observed.

To investigate whether these dynamic changes in the TCD parameters observed during increasing ICP reflect the state of the autoregulatory reserve the dynamic changes in CBF must be assessed. Laser Doppler flowmetry provides continuous on-line CBF measurement.

3. LASER DOPPLER FLOWMETRY

Laser Doppler flowmetry, first described in 1975 by Stern [20], is a continuous, on-line technique for measuring changes in the micro-circulation. A low power infrared laser (of known frequency) is directed into the tissue via a fibre optic. As the photons enter the tissue they are randomly scattered by the cells. The frequency of the photons which interact with moving blood cells is changed according to the Doppler principle. The degree of frequency shift is dependent on the cell velocity. A portion of the scattered light is reflected back to a receiving fibre contained within the same probe. The signal contains numerous frequencies at varying powers. Signal analysis provides the velocities of the moving blood cells and the comparative number of cells moving at each velocity. As the photons are randomly scattered the direction of flow cannot be determined. The sample volume is small ($1mm^3$) and includes the area were the transmitted and receiving beams overlap (see figure 1). The blood flow changes measured in the sample volume can be considered indicative of changes in other areas of the brain only if the tissue is homogenous.

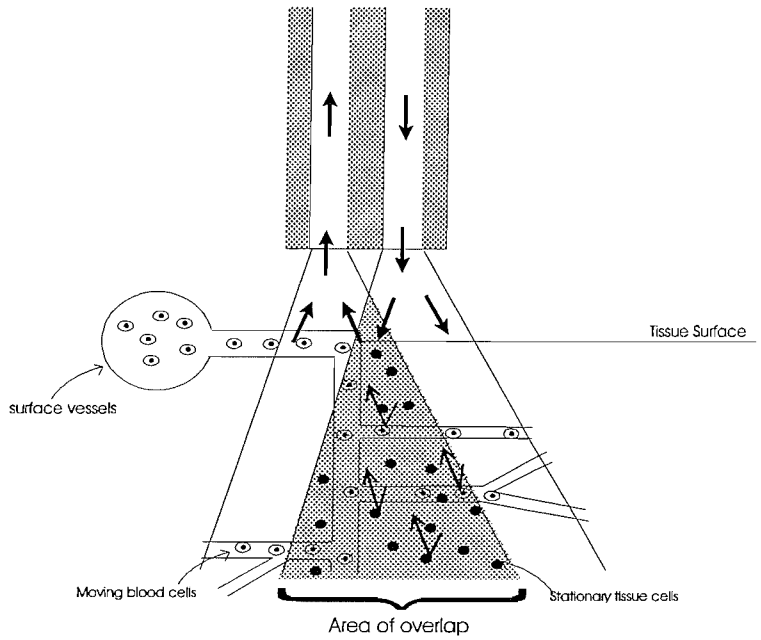

Figure 1: A schematic Diagram of LDF

Unlike ultrasound in TCD, the laser is unable to penetrate the skull, therefore in neurological applications the technique is invasive. A craniotomy or burr hole is required to expose the cortex surface therefore the technique is clinically limited to interoperative [21,22] and intensive care monitoring [23,24].

The data produced by laser Doppler flowmetry correlates well with other more established cerebral blood flow techniques. Autoradiography in rats demonstrated a good correlation between changes in laser Doppler flow and cerebral blood flow but a poor correlation with absolute cerebral blood flow measurements. This finding has been confirmed in other studies using different techniques such as hydrogen clearance [25] and labelled microspheres [26].

Absolute values of cerebral blood flow cannot be obtained with LDF because in zero flow conditions, for example after death, a signal is still observed. This is due Brownian motion (random motion of molecules observed in all materials) that produces a background signal which is always present even after the circulation ceases and is described as the biological zero. The biological zero may be obtained at the end of an

experimental study after an animal is sacrificed. For clinical applications the problem is more complex. A recent study by Richards et al demonstrates that the biological zero may be estimated from the extrapolated TCD flow velocity versus laser Doppler flow regression curve [27]. This parameter may be useful in clinical applications and during experimental studies where the biological zero may change due to factors such as edema [28].

It can be concluded that LDF provides a reliable technique for the continual assessment of changes in cerebral blood flow, an essential parameter for the assessment of autoregulalatory status.

4. MATERIALS AND METHODS

Eight normal New Zealand White rabbits of both sexes (weight from 3.1 to 3.8 kg) were studied under the UK Animals (Scientific Procedures) Act 1986. The animals were prepared using previously described techniques [4,5].

Rabbits were anaesthetised using intravenous alphaxalone/alphadalone (Saffan, 3mg/kg) injected into the marginal ear vein and inhaled 1-3% halothane in 3:1 nitrous oxide/oxygen. A jugular vein was cannulated and a tracheotomy was performed. The rabbits were then given an intravenous infusion of pancuronium (Pavolon, 0.5 mg/kg/hr) and ventilation was controlled using a pump. Halothane was maintained at 1.5%. The rabbits were placed prone on a padded warming blanket maintained at 39°C and supported in a Sphinx position with a purpose-built head frame. Rectal temperature was monitored. The apparatus was set-up as shown in figure 2.

Arterial blood pressure was continuously monitored through a cannula inserted into the dorsal aorta via the femoral artery using a luer-tipped blood pressure transducer. (Gaeltec Ltd., Dunvegan, U.K.) A second cannula was placed in the other femoral artery allowed blood removal for arterial blood gas analysis.

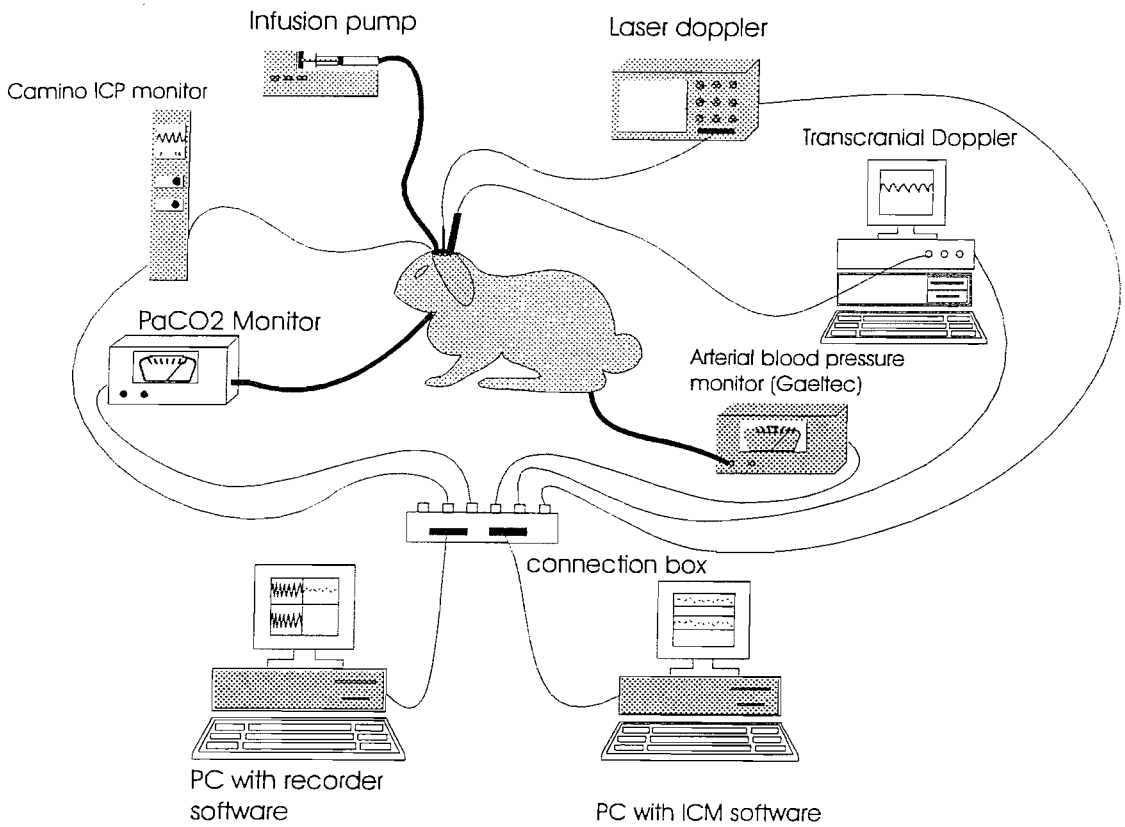

Figure 2: The experimental set-up.

Three burr holes were made for the placement of the transcranial Doppler, laser Doppler and Camino probes (see figure 3)

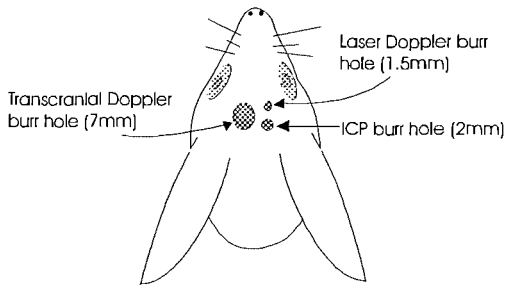

Figure 3: Burr hole placement for transcranial Doppler, laser Doppler and ICP probes.

A small hole was made in the dura via the 2mm burr hole and a fibre-optic catheter connected to a pressure monitor (Model V420, Camino Laboratories, San Diego CA, USA) inserted subdurally for the measurement of intracranial pressure. A narrow bore cannula (O.D. 0.61mm, Portex Ltd., U.K.) was flushed with Hartmann's solution and inserted alongside the fibre-optic catheter. This was connected to a syringe driver for the infusion of Hartmann's solution. Both the Camino probe and the cannula were sealed in position with super glue preventing fluid leakage from intracranial cavity.

Blood flow velocity in the basilar artery was measured using an 8MHz pulsed Doppler ultrasound probe (PCDop 842, SciMed, Bristol, U.K.). For clinical applications a 2MHz probe is used to insonate the cerebral arteries transcranially. However in the rabbit the vessels are relatively narrow and superficial requiring lower depths of insonation (1.7 to 2.2 cm). Because the transcranial properties of the 8MHz probe are poor, a 7mm frontal posterior burr-hole at the bregma is required. The Doppler probe gives an angle of insonation of the basilar artery of approximately 10^{o}. Nelson et al provided [4] angiographic validation for this method. The probe was positioned over the burr hole with the intact dura covered with a layer of ultrasound gel. The probe position and the depth

of insonation was adjusted to ensure the correct vessel was insonated. When a good quality spectrum was obtained, the probe was clamped in position.

Localised capillary perfusion in the cortex was measured using a laser Doppler probe connected to a flowmeter (Moor Instruments, Axbridge, Devon, U.K.). The 1mm probe was positioned epidurally via the remaining burr hole.

The arterial blood pressure, intracranial pressure, flow velocity, laser-Doppler flux and $PaCO_2$ were monitored continuously. The Analogue signals were acquired, amplified (where required), converted (using an analogue to digital converter) and stored on computer hard disc. Two PCs equipped with ICM software (Czosnyka, University of Cambridge, UK.) and the Biomedical Signal Recorder (Zabolotny, Warsaw University of Technology, Poland) were used allowing on-line trends to be plotted (figure 4) as well as recording the data.

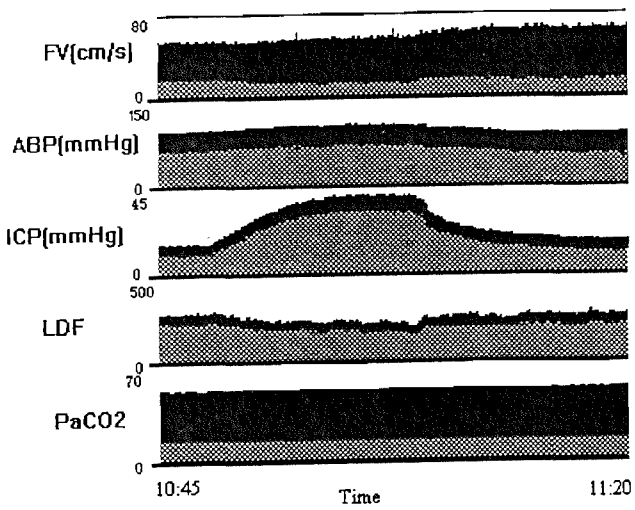

Figure 4: A typical on-line recording demonstrating ICP and the haemodynamic parameters during an infusion.

Before the experiment the blood gases were analysed and the animal stabilised. A baseline ICP was recorded for 10 minutes before the subdural infusion. An infusion rate of 0.1 or 0.05 ml/min was selected. The infusion was continued until an intracranial pressure plateau had been reached and maintained for several minutes. After the infusion the

pressure was allowed to return to a stable baseline before the experiment was repeated. The number of infusions performed in each rabbit was dependent on the animal stability.

Although attempts were made to mimic the clinical infusion tests, the rabbits were found to be intolerant to the laminectomy required for lumbar infusion. The prolonged preparation time (2 hours) and blood loss produced haemodynamic instability. Subarachnoid infusion and pressure monitoring were therefore performed via a craniotomy. Dye studies were performed to ensure this route provided access to the CSF circulatory pathways. Tiluodine blue was infused at the same infusion rate as that used for the infusion studies. The animals were then sacrificed and brain sections taken. In all three rabbits studied dye stained the ventricular cavities and the CSF pathways in the brain and spine. Sections of the brain and spinal tissue are presented in figure 5.

4.1 Data Analysis

The data recorded for each animal was divided into individual infusion tests and analysed using 2 different techniques (figure 6). The Computerised infusion Test Program (Czosnyka, University of Cambridge, UK.) allowed the cerebrospinal compensatory parameters to be calculated, which were then input to Excel for statistical analysis. The ICMR Program (Czosnyka, University of Cambridge, UK.) was used to calculate 1 minute averages of the recorded signals and other parameters such as FVs, FVd, PI and CPP. This data was converted into an ASCII file and input to Statgraphics (Statgraphics 5- Statistical Graphics Corporation, US). Data for CPPs of 50-80mmHg were used for statistical analysis.

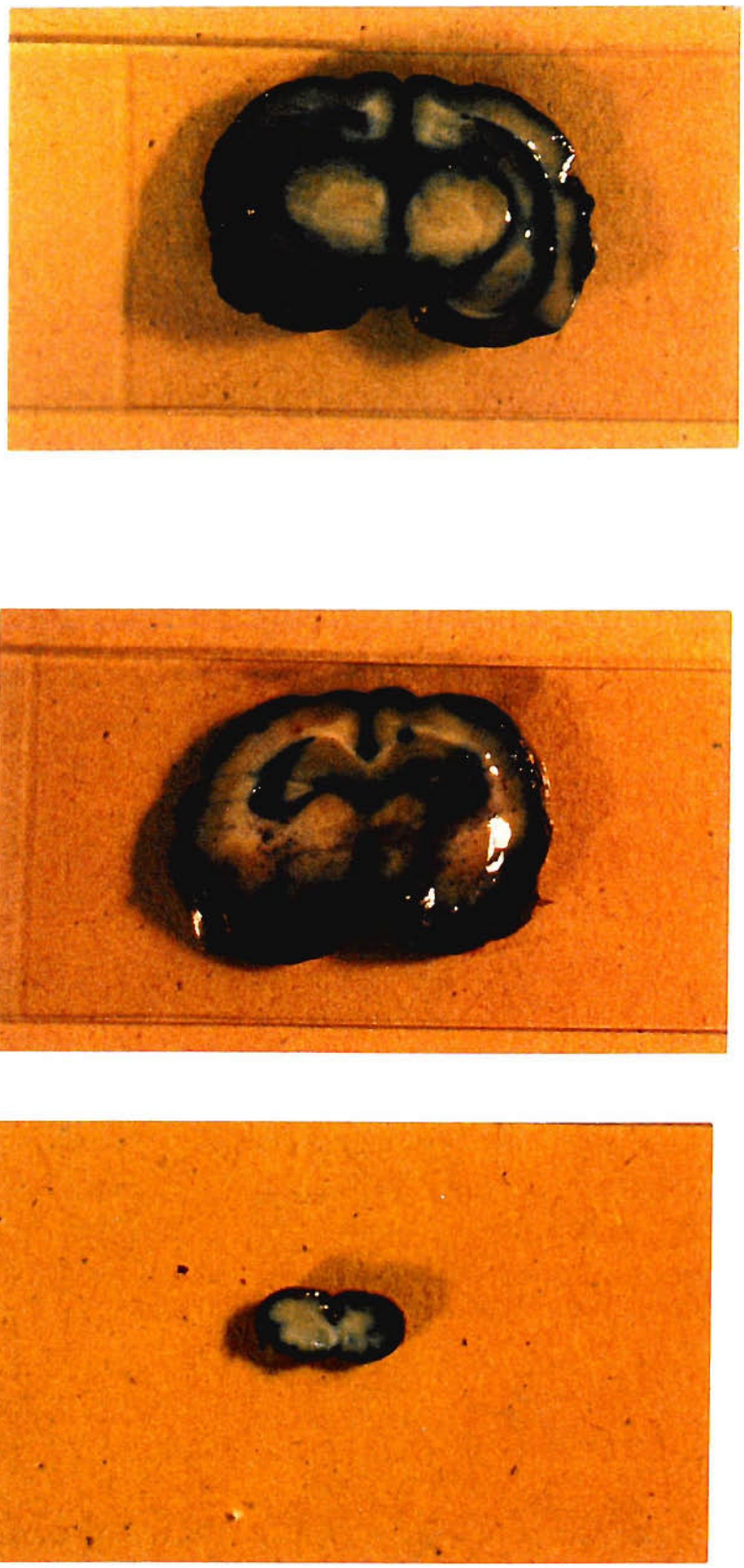

Figure 5: Slices of rabbit brain after dye infusion, demonstrating dye stained ventricles and CSF pathways. At the level of

a) the parietal cortex, including the third ventricle

b) the sensory motor cortex including the lateral ventricle

c) the cervical spine

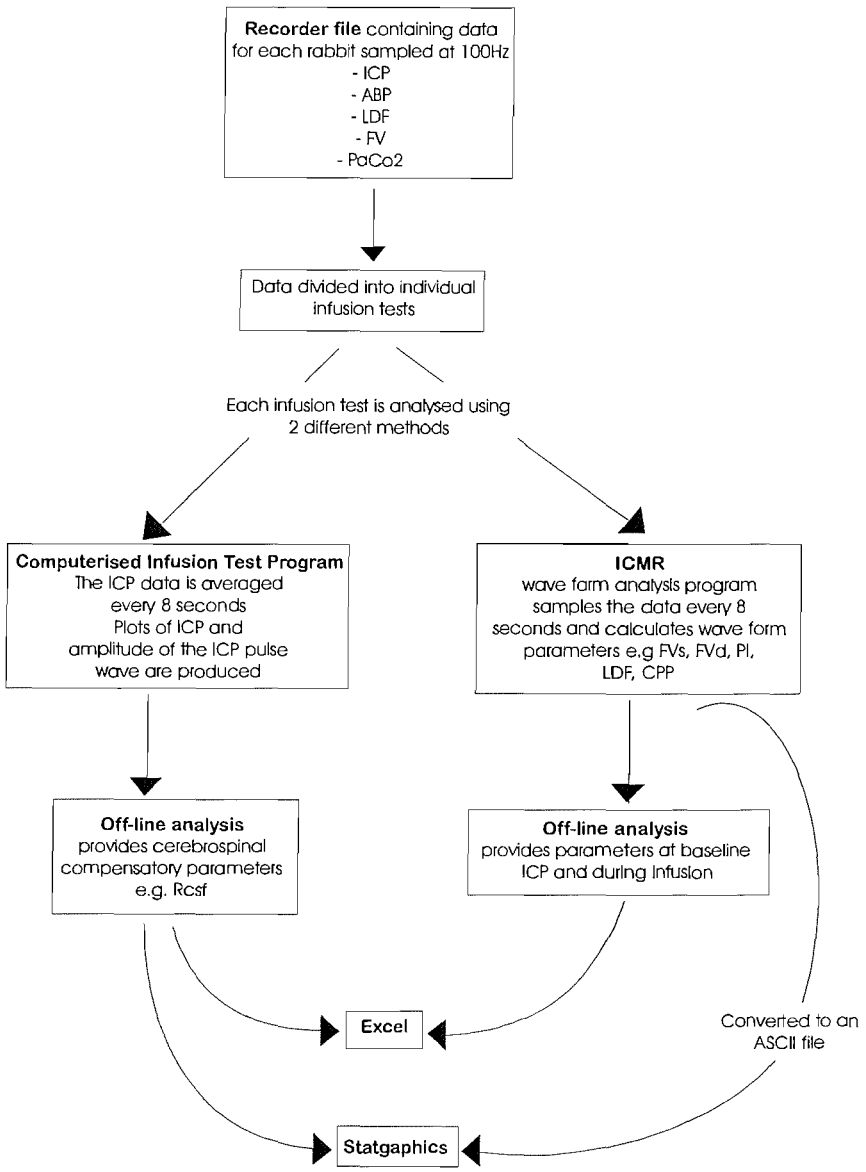

Figure 6: Data analysis procedure using ICMR and the Computerised Infusion Test program.

5. RESULTS

The mean ICP before CSF infusion was 20.1 $\pm$ 5.7 mmHg with a range of 9.1mmHg to 27.8mmHg. During infusion ICP rose to 34.0 $\pm$ 5.1mmHg with a range of 24.5mmHg to 50.5mmHg. The mean R_{csf} was calculated as 194.9 $\pm$ 92.7mmHg/ml/min with a range of 86mmHg/ml/min to 494.7mmHg/ml/min. The average R_{csf} for each animal is shown in table 1 and figure 7. The variability in R_{csf} in subsequent infusion tests is in each animal

is demonstrated in figure 8. The average coefficient of variation for each rabbit was 14%. Comparing the mean R_{csf} between rabbits gave a coefficient of variation of 60%.

Rabbit number	Mean R_{csf} ±SD	Minimum	Maximum
1	123±14	102	132
2	265±24	240	297
3	139±21	115	164
4	186±40	145	271
5	111±18	86	127
6	178±17	157	188
7	452±59	411	494
8	311±65	257	384

Table 1: The mean, minimum and maximum R_{csf} for each animal.

The average arterial blood pressure at baseline ICP was 76.9 ± 22.4mmHg. This did not change significantly during infusion. Figure 9 demonstrates absolute change in ABP during each infusion study.

The spectral pulsatility index calculated as the first harmonic of the FV waveform divided by FV mean was 1.01 ± 0.50 before infusion. It increased significantly during infusion to 1.29 ± 0.71 ($p<0.03$).

To determine whether the haemodynamic changes were related to the state of autoregulation, the rabbits were divided into autoregulating and non-autoregulating animals. The classification was performed on the basis of the laser Doppler recordings of CBF. The Laser Doppler 1 minute averages were corrected for the biological zero and normalised against the baseline value. The normalised LDF data were then plotted as a percentage of the baseline recording with CPP for each rabbit. Rabbits were classified as:
(i) autoregulating when LDF was maintained during decreasing CPP (for CPP<40mmHg) (n=3).
(ii) non-autoregulating when LDF decreased with CPP (n=5)

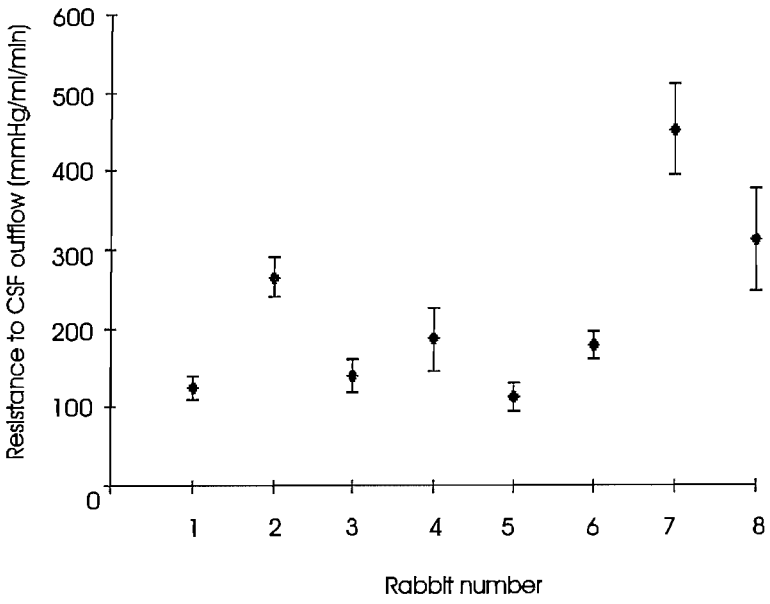

Figure 7: The average R_{csf} for each rabbit ±SD.

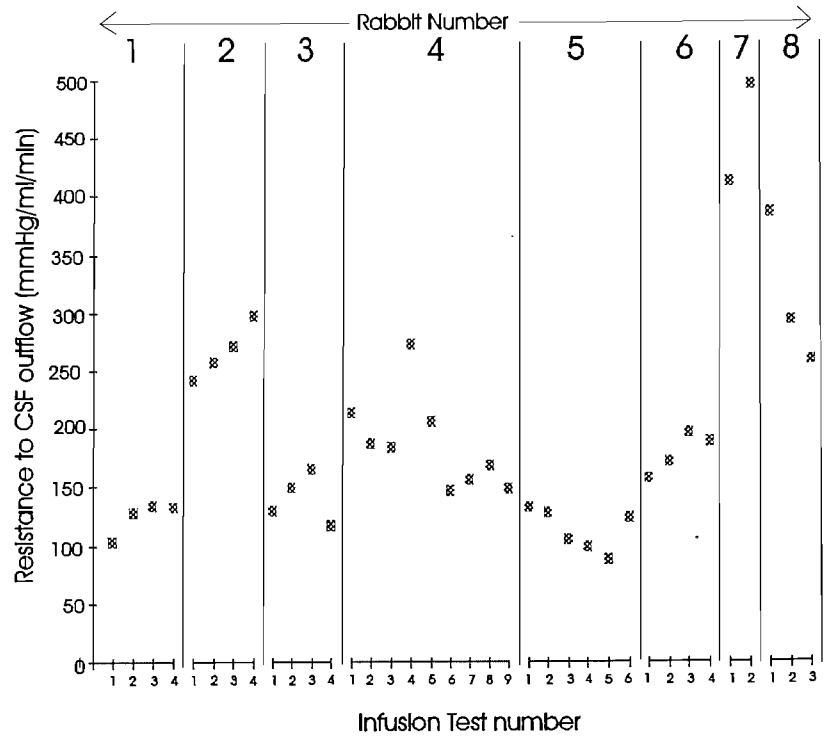

Figure 8: R_{csf} recorded in each CSF infusion tests for each rabbit.

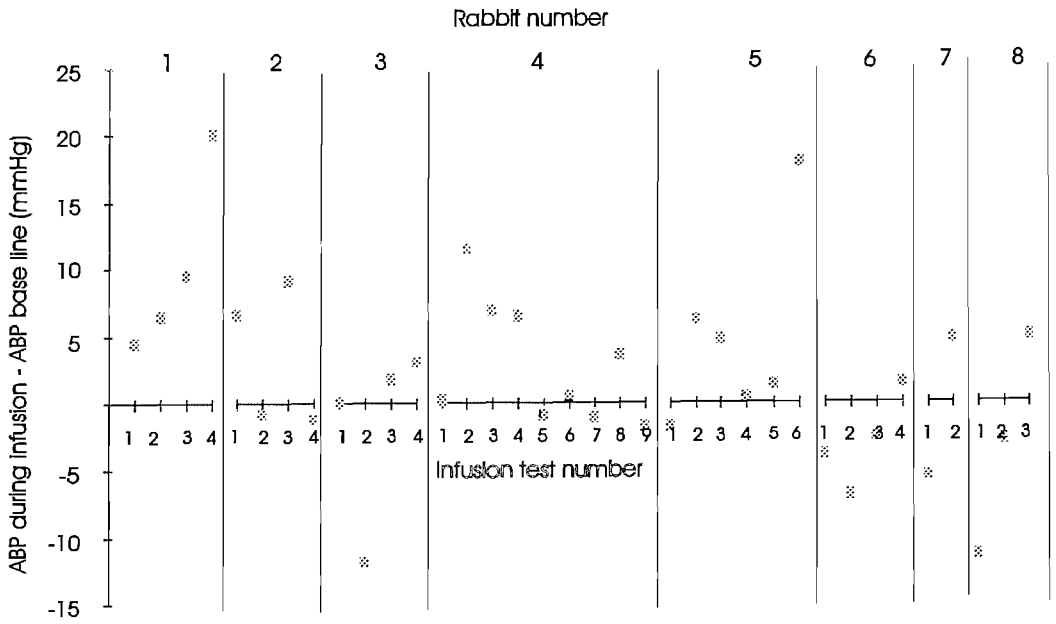

Figure 9: The absolute changes in ABP during each infusion study (ABP during infusion minus ABP at baseline)

In the autoregulating group, LDF and CPP were poorly correlated ($r=-0.059$) demonstrating that LDF was independent of CPP. In the non autoregulating group LDF and CPP were well correlated ($r=0.56$, $p<0.0001$). The LDF/CPP scatter plots for autoregulating and non-autoregulating animals are shown in figures 10 and 11 respectively.

The 1 minute average values of cerebrovascular resistance were calculated as a percentage of the baseline value from CPP and the normalised LDF where CVR% =CPP/LDF%. The CVR%/CPP scatter plot (figure 12) demonstrates decreasing CVR in both autoregulating and non autoregulating animals. According to the equation CBF= CPP/CVR, CVR must decrease proportionally with CPP to maintain CBF. This 'ideal' relationship for the maintenance of CBF is identified on the CVR/CPP scatter plot with a superimposed white line. In the autoregulated group the points are clustered along this 'ideal' line indicating that the changes in CVR and CPP are proportional. However, in the non-autoregulating group the majority of points are above this line demonstrating that the changes in CVR was not sufficient to maintain CBF.

Scatter plots of the TCD parameters FVs, FVd, FV amplitude (FVa) and FV mean (FV) were plotted with CPP for the autoregulated and non-autoregulated animals. In both groups:

(i) FVs demonstrated relatively stable behaviour with decreasing CPP (figure 13).
(ii) FVd decreased with decreasing CPP (figure 14).
(iii) FVa increased with decreasing CPP (figure 15).
(iv) FV decreased with decreasing CPP (figure 16).

The autoregulated and non-autoregulated groups demonstrated similar trends for the above variables. Therefore the spectral pulsatility index trends calculated from the above parameters demonstrated similar parabolic trends in the autoregulated and non-autoregulated groups (figure 17).

The correlation coefficients for CVR and PI with CPP for autoregulating and non autoregulating animals are demonstrated in table 2.

Correlation with CPP	Autoregulated	Non-autoregulated
CVR	r = 0.97 ; p<0.0001	r = 0.90 ; p<0.0001
PI	r = -0.85 ; p<0.0001	r = -0.851 ; P< 0.001

Table 2: The correlation of CVR and PI with CPP for autoregulated and non-autoregulated animals

CVR and PI correlated well with CPP in both groups, with PI increasing and CVR decreasing with decreasing CPP.

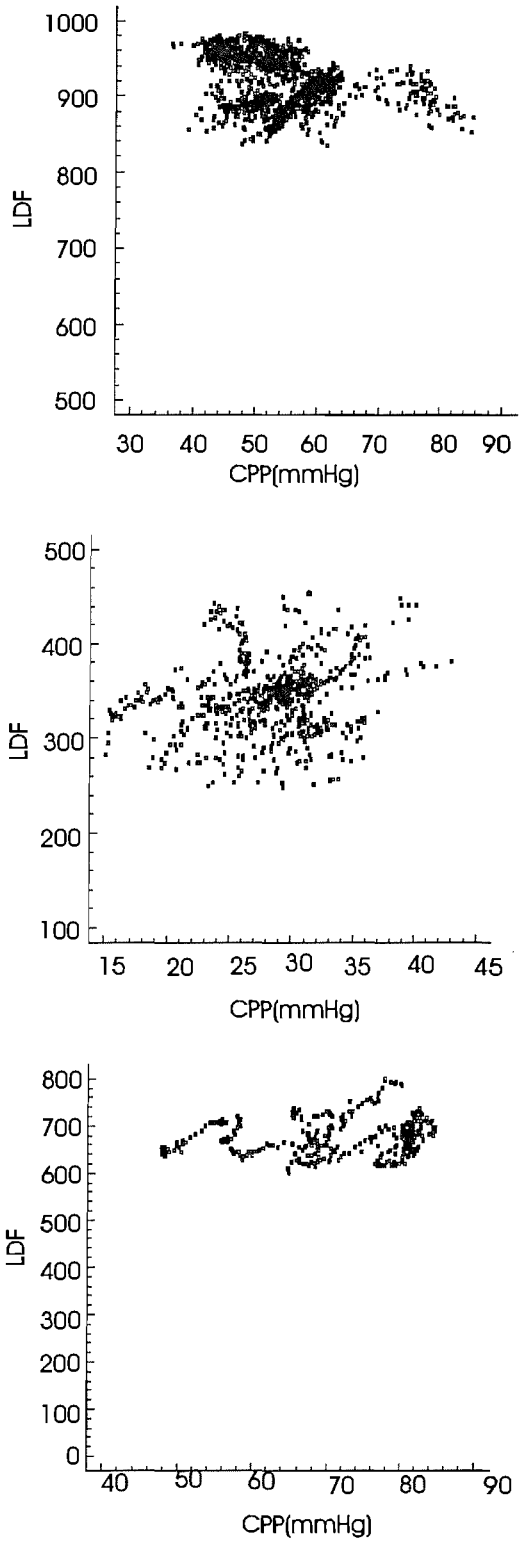

Figure 10: LDF/CPP scatter plot for each autoregulating rabbit.

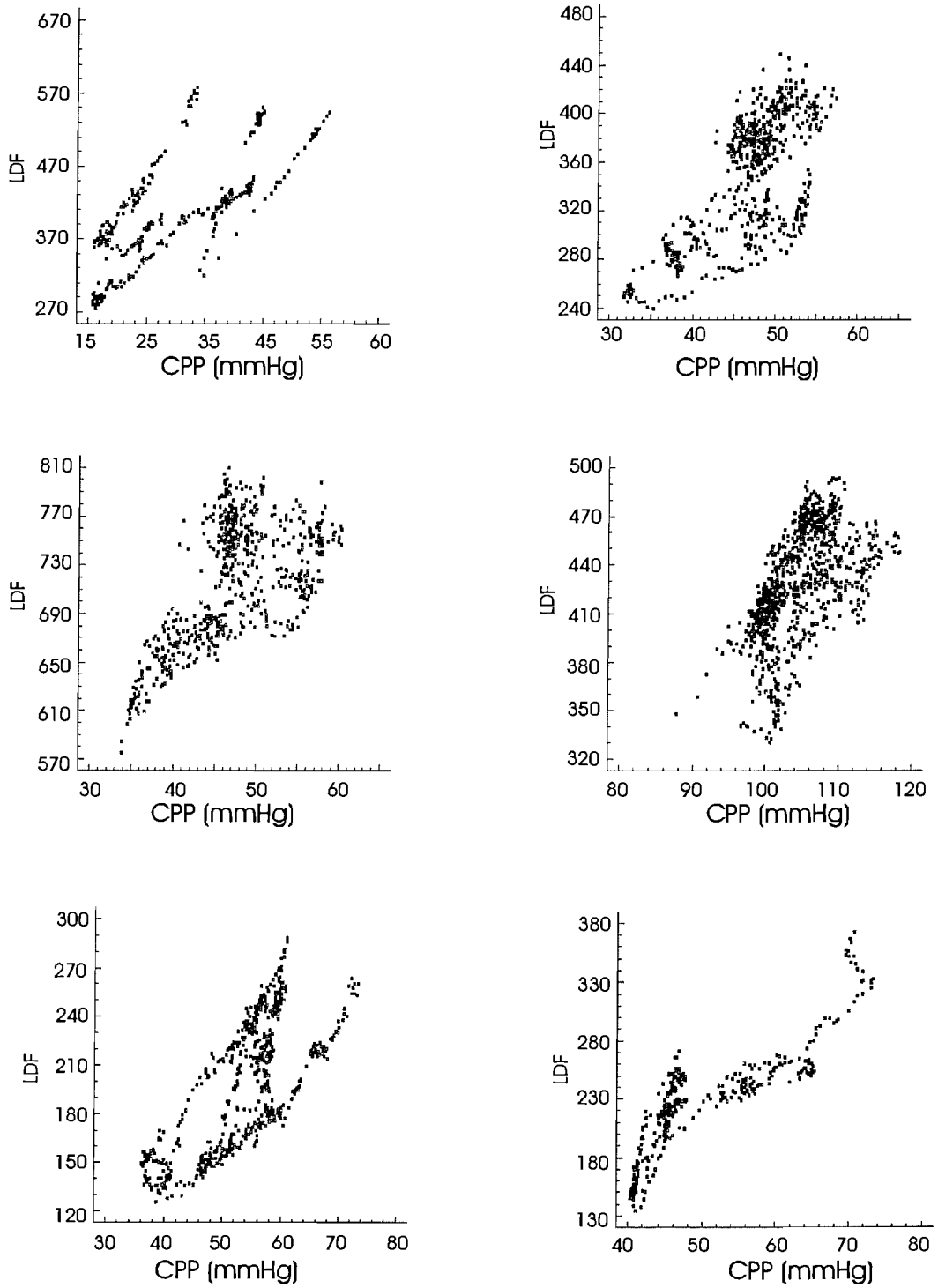

Figure 11 LDF/CPP scatter plot for each non-autoregulating rabbit.

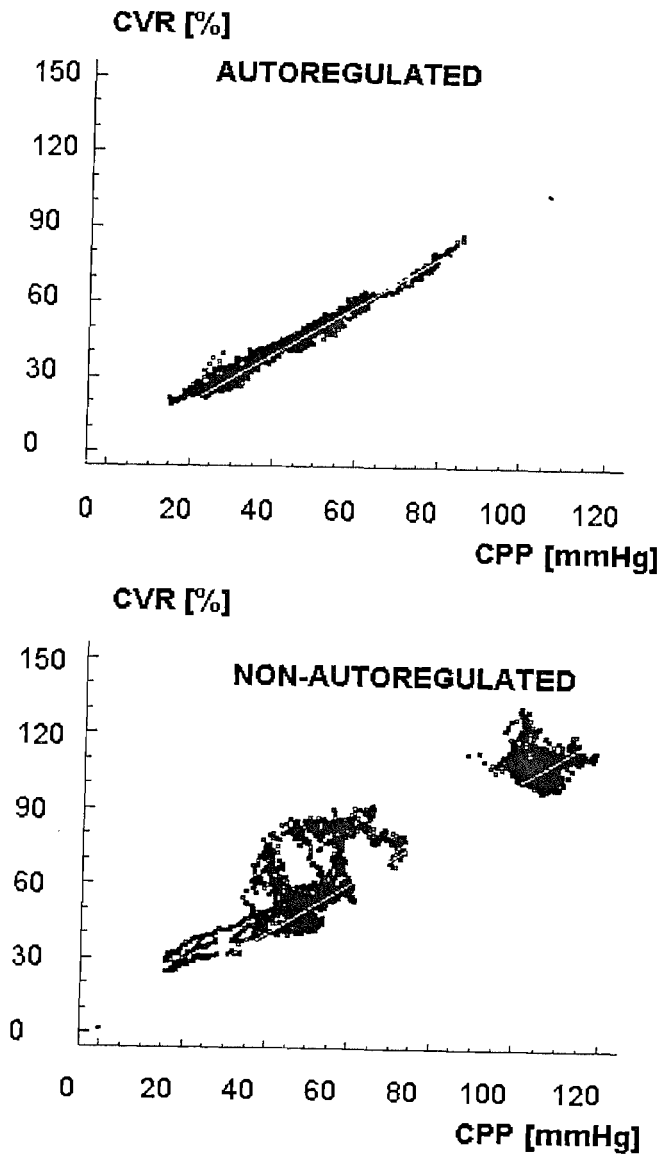

figure 12: The CVR%/CPP scatter plots in autoregulated and non-autoregulated animals. In both groups CVR% decreases with CPP (pooled data for all autoregulating animals and all non-autoregulating animals).

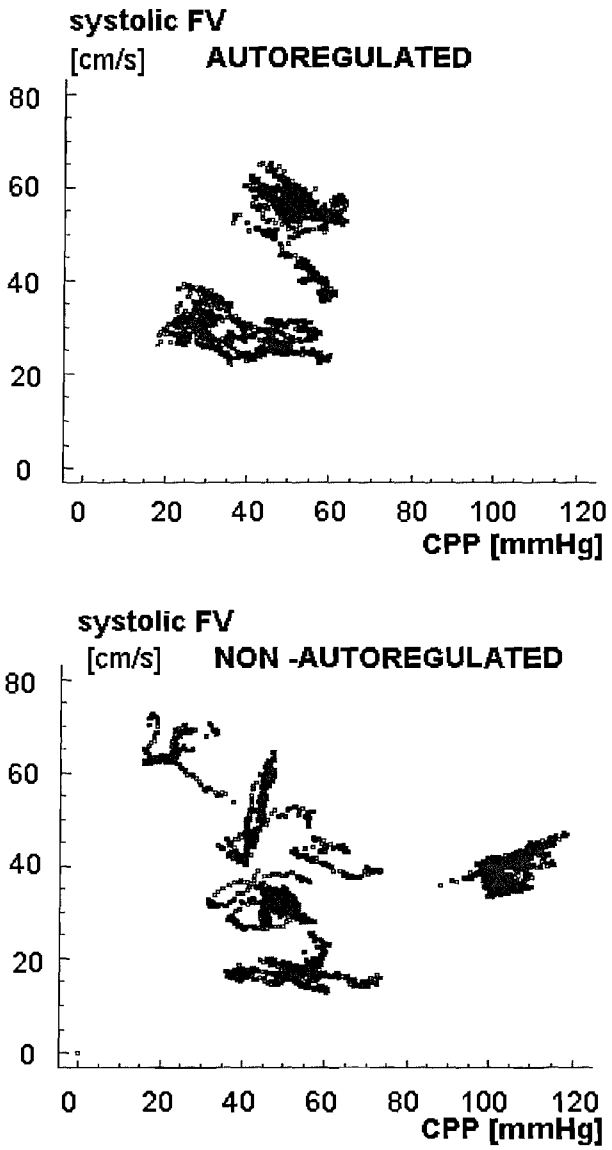

Figure 13: FVs is relatively stable with decreasing CPP in both autoregulating and non-autoregulating animals (pooled data for all autoregulating animals and all non-autoregulating animals).

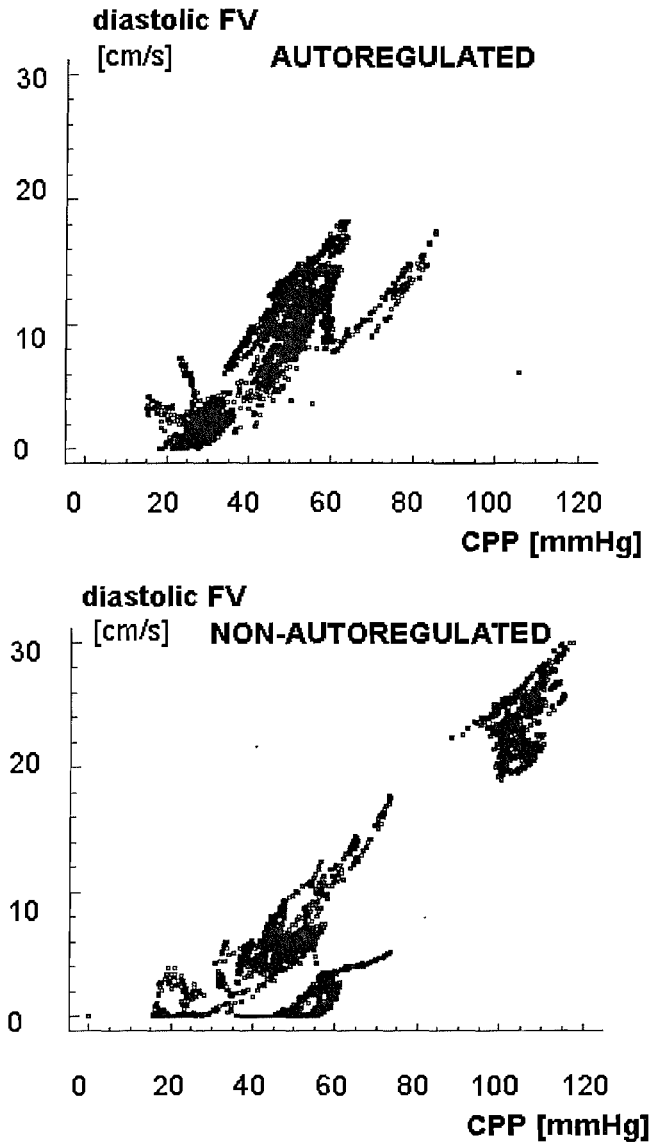

Figure 14: FVd decreases with decreasing CPP in both groups (pooled data for all autoregulating animals and all non-autoregulating animals).

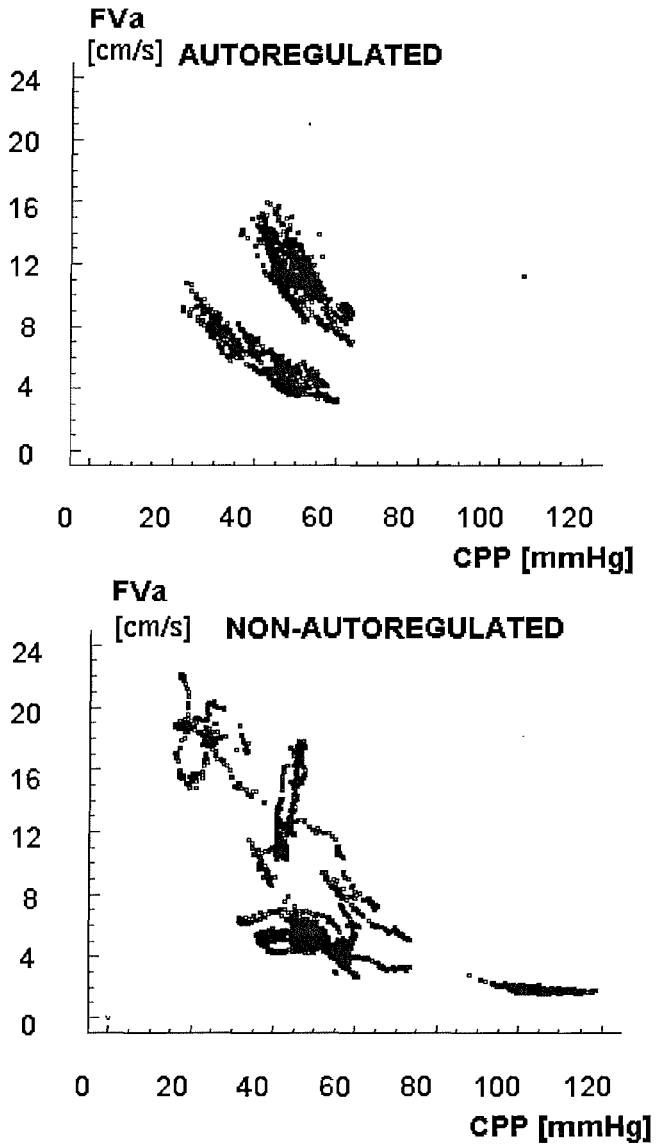

Figure 15: As a result of diverging FVs and FVd, FVa increases with decreasing CPP in both groups (pooled data for all autoregulating animals and all non-autoregulating animals).

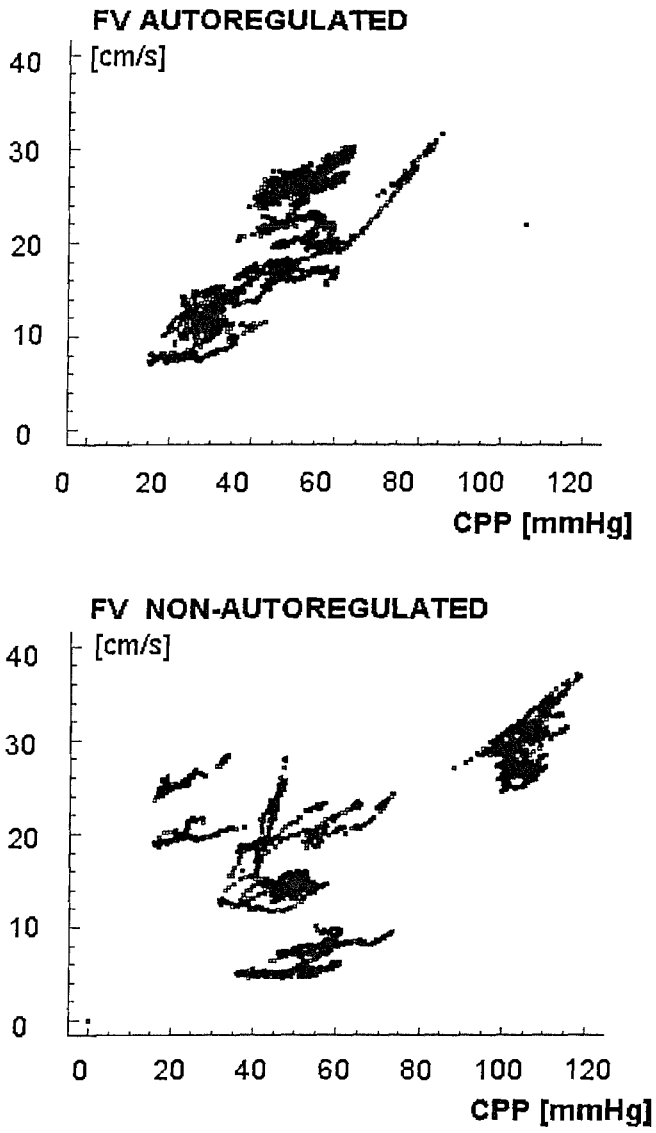

Figure 16: FV decreases with CPP(pooled data for all autoregulating animals and all non-autoregulating animals).

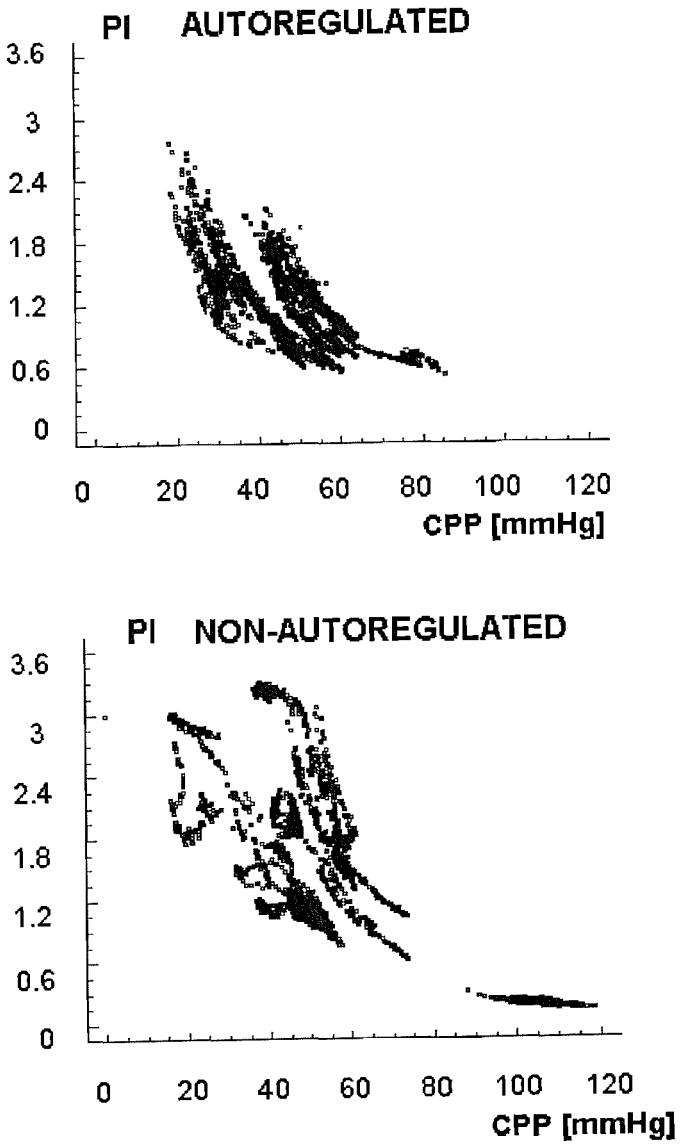

Figure 17: PI decreases with CPP in both groups as a result of the divergent behaviour of FVs FVd and decreasing FV(pooled data for all autoregulating animals and all non-autoregulating animals).

6. DISCUSSION

It has been suggested that the divergent behaviour of FVs and FVd observed during decreasing CPP is related to the state of cerebral autoregulation [1,4,18]. This study using TCD combined with LDF has allowed this hypothesis to be explored.

PI and CPP correlated well in both autoregulated and non-autoregulated animals. In both groups PI increased hyperbolically with decreasing CPP, confirming the findings of previous studies [18,19]. The comparable PI/CPP trends in the 2 groups demonstrates that changes in PI are not related to the state of autoregulation. Considering that it is generally accepted that PI is dependent on CVR, this finding appears surprising and adds to the complicated and contradictory findings related to PI.

However if PI is solely dependent on CVR and CVR is well correlated with CBF then a difference in PI behaviour in the autoregulated and non-autoregulated groups would be expected. As PI followed similar trends in both groups this implies other variable physical parameters in addition to CVR effect, and in some cases dominate PI behaviour. This would suggest that although changes in PI reflect cerebrovascular reactivity, the reactivity is not necessarily associated with changes in CVR.

Although this parameter has been successfully applied as a diagnostic indicator its physiological significance is not fully understood. This finding fuels the growing suspicion that PI is a complex phenomena which should be interpreted with care.

6.1 Reproducibility of Infusion Test Results.

The average resistance to CSF outflow for all the infusion tests was 217$\pm$ 132 mmHg/ml/min. This findings are comparable with previously reported R_{csf} in rabbits [29,30,31].

The reproducibility of a test is an important means of assessing its reliability. An investigation which demonstrates high variability in repetitive studies may be of limited clinical value. A study of the reproducibility of measurements of resistance to CSF

outflow using lumbo-ventricular and lumbo-lumbar perfusion tests has been performed in patients with suspected abnormal CSF outflow [32]. The results demonstrated good repeatability with identical values of R_{csf} obtained in patients with NPH.

An earlier study had demonstrated a variation in the conductance to CSF out flow of less than 5% [33] where 15 minutes was allowed between tests.

The increased variability of R_{csf} seen in this study compared to the clinical studies described above may be due to several factors. The animals were anaesthetised for prolonged periods and often became unstable towards the end of the experiments. This may have produced changes in cerebral blood volume which is presumed to constant during CSF infusion studies.

7. CONCLUSION.

This study suggests that changes in PI produced during intracranial hypertension does not reflect the state of cerebral autoregulation. However considering the issues and assumption associated with this experiment (described in section 1.2) care must be taken when interpreting this data or extrapolating it to explain findings in patients.

APPENDIX 2

APPENDIX 2

THE SAFETY OF TRANSCRANIAL DOPPLER

1. INTRODUCTION

Transcranial Doppler (TCD) has emerged as a multi-purpose non-invasive monitoring technique [1] widely used in neurosurgical units. As clinical research progresses continuous monitoring of TCD both intraoperatively and in intensive care has become more common. Patients may therefore be exposed to static and focused ultrasound energy for prolonged periods and any risk of hazard associated with ultrasound exposure may increase [2]. Although diagnostic ultrasound techniques have a good safety record [3], the radiation advisory bodies suggest that the benefits from the procedure must be considered in the context of the associated risks.

In most clinical applications patients usually benefit from the investigations. However the use of TCD in normal volunteers for research purposes is increasing. These studies are performed to provide a normal baseline for comparison with clinical data. The volunteer may undergo prolonged periods of exposure to ultrasound energy but stands to gain little from the examination. Therefore, the risk of associated hazards must be assessed.
A study was planned to investigate cerebral blood flow velocity in normal volunteers during sleep requiring up to 8 hours of ultrasound exposure (see Chapter 3). During the study design, basic calculations suggested that volunteers may be at risk from thermal bio-effects resulting from the absorption of ultrasound energy in the temporal bone (see section 1.3). The aim of this study was to investigate the possible hazards and to determine acceptable exposure levels.

1.1 Biological Effects Following Exposure to Diagnostic Ultrasound.

Although high doses of ultrasound energy can change biological tissue, these effects are presumed to be dose dependent. Therefore, as the dose administered decreases, the probability of detecting changes also decreases. At very low dosages, biological variability is so great that it becomes difficult to determine whether a change is a natural fluctuation or actually caused by ultrasound.

Many different ultrasound induced bio-effects have been reported in the literature: chromosome damage, sister chromatid exchange effects, changes in the cellular surface, effects on the immune system, blood and blood coagulation and embryonic growth and development [2,4]. However the experiments have often been unrepeatable and no firm conclusions may be drawn. The British Institute of Radiology working group [2] concluded that a clearer picture will evolve only if long term, properly conducted research is performed and an adequate database is established.

The dominant mechanisms for ultrasound induced changes in biological tissue arecavitation and heating [5].

Cavitation may occur if the ultrasound field interacts with microscopic gas bubbles. It is probable that such bubbles occur in biological tissue [2]. Under suitable conditions, bubbles up to a few micrometers may begin to oscillate giving rise to mechanical damage in the surrounding tissue. When the acoustic pressure, amplitude, frequency and bubble size are appropriate, bubbles may expand and rapidly collapse. The high temperatures which may be produced in the collapsing bubbles may create potentially toxic chemicals such as free radicals. Air cavities larger than the resonance size are not affected in the same way. Attempts to demonstrate cavitation activity in mammals have suggested that it may only occur with ultrasonic powers of hundreds of Wcm^{-2} [6].

Hyperthermia induced by ultrasound exposure has been investigated in both therapeutic and diagnostic ultrasound. If exposures are sufficiently high, the resultant temperature

increase may produce biological effects. Although these effects are therapeutic in the treatment of tumours or ocular disease, in routine diagnostic ultrasonography they should be avoided. The degree of heating is dependent on the tissue and ultrasound properties, including the absorption coefficient and ultrasound power.

Both cavitation and thermal mechanisms become more significant in certain circumstances [6].

Cavitation may be important where:

(i) gassy fluids are exposed

(ii) small gas-filled spaces are exposed

(iii) the tissue temperature is higher than normal

Heating of the biological tissue may be important where:

(i) The tissue has a high protein content

(ii) A high intensity, continuous wave beam is used

(iii) A high temporal average intensity pulsed beam is used.

(iv) Bone is included in the insonation pathway.

(v) Perfusion of blood is poor.

During transcranial Doppler examinations, insonation of the cerebral arteries usually occurs via the temporal window - an area of thin bone above the zygomatic arch. Bone, with a high coefficient of absorption [4], is a prominent feature in the insonation path, therefore, thermally induced hazards may be of importance in this application [8]. As gas filled spaces or gassy fluids are not a prominent feature in the TCD propagation pathway, then it is unlikely that cavitation will occur. Therefore, the risks of biological changes as a result of ultrasound induced hyperthermia are considered.

To assess the risks of thermal bio-effects, the acoustic output of the device and transducer must be determined. Parameters of interest when considering thermal effects include:

(i) The total ultrasonic temporally - averaged power (mW), which relates directly to transport of ultrasound energy into the tissue.

(ii) The pressure and intensity - the beam shape characteristics describe the spatial extent of ultrasound power within a medium and hence the spatial variation of intensity. The intensity at any moment is a function of acoustic pressure:

$$i = \frac{p^2}{\rho c}$$

where i is the intensity, p equals the acoustic pressure at the particular instance and ρc is a characteristic of acoustic impedance. If a continuous single frequency wave is generated then p varies sinusoidally with time and the temporal average intensity (I) is calculated by averaging i :

$$I = \frac{p_0^{\,2}}{2\rho c}$$

where p_0 is the pressure amplitude. The total time averaged power of a directed ultrasound field is equal to the time averaged intensity over the traverse section of the whole beam. Within the transverse section there are maxima of the time averaged intensity. These spatial peaks are valuable indicators of potential bio-effects.

Other intensities of thermal importance are spatial - average temporal - average (SATA) intensity and spatial - peak temporal - average (SPTA) intensity (figure 1). Other intensities that may have to be considered for other assessments are the spatial - peak temporal - peak (SPTP) intensity, spatial - peak pulse- average (SPPA) intensity and spatial - average pulse- average (SAPA) intensity.

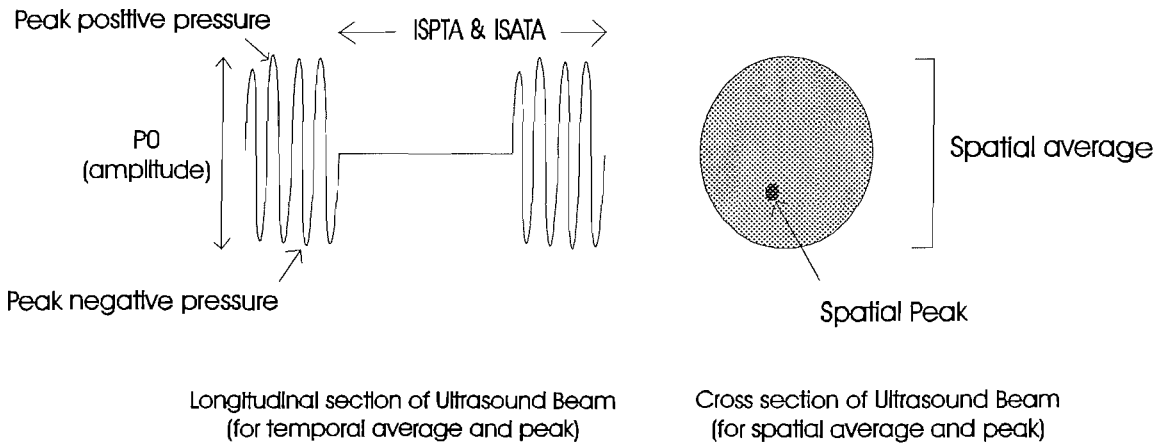

Figure 1: Diagrammatic representation of ultrasound pressures and intensities

(iii) The beam shape - 6dB beam area (mm^2)

(iv) Duty time - the ratio of the on time of the pulse to the total time

(v) Exposure time (s)

The Sci-Med TCD was tested at the National Physical Laboratory. The values shown in table 1 were measured in water.

Acoustic Output Parameter	
Centre frequency	2.0 MHz ±5%
Peak-positive acoustic pressure	400 kPa ±16%
Peak-negative acoustic pressure	-350 kPa ±16%
Spatial-peak temporal -peak intensity	10.5 W cm^{-2} ±29%
Spatial-peak temporal-average intensity	470 mW cm^{-2} ±29%
Spatial-average temporal -average intensity	230 mW cm^{-2} ±29%
-6 dB beam area	20.4 mm^2 ±28%
Pulse duration	10.7 µs ±5%
Pulse repetition rate	10.28 kHz ±3%
Total power	81 mW±33%

Table 1: The acoustic output parameters for the Sci-Med TCD

Comparing these results with the currently acceptable exposure parameters [6] (table 2) demonstrates that the Sci-Med acoustic pressures and intensities are low and total power is within the average range, however the duty cycle period indicates increased pulse duration and/or repetition time. Although the power is within the average range theoretical considerations suggest that local heating could occur in clinical conditions. The possible heating of the bone and tissue must therefore be considered.

Acoustic Output Parameter	
Peak-positive acoustic pressure	0.1-7.4 MPa
Peak-negative acoustic pressure	0.1-3.9 MPa
Spatial-peak temporal peak intensity	0.036-1100 Wcm^{-2}
Duty Time	0.001 s
Average power	0.1-80 mW

Table 2: Exposure parameters currently considered to be acceptable

1.2 Thermal Mechanisms in the Human Body

Body temperature is maintained stable with only a few degrees of fluctuation. However temperature is not constant throughout the body with a core temperature of approximately 37°C and a skin temperature of between 31.5°C and 35°C. The body produces heat by metabolism and muscular contraction, therefore these temperatures may vary depending on activity. Responses to rising body temperature include sweating, dilatation of blood vessels and increase in cardiac output which increase heat dissipation [9]. Shivering to generate heat occurs in response to a decreasing body temperature. These mechanisms however may not be adequate to maintain temperature in extreme conditions. A sustained core temperature of 42°C is barely compatible with life and an increase to 43°C results in death.

Changes in temperature affect the cell production rate. Maximum cell production occurs at 37°C and at higher or lower temperatures there are fewer cells produced [8,9]. At

28°C there is almost no cell growth. At sustained moderately increased temperatures (+4°C) there is an increased incidence of cell death due to thermal damage and at higher temperatures (44 - 46°C) there is a rapid coagulation of protein. Studies in vitro and in vivo suggest that there is a logarithmic relationship between time and temperature for thermal death. For example at 40°C very long exposures of between 5 and 100 hours are required for thermal induced cell death [10].

Elevated temperatures produce a wide range of biological effects. A review of the lowest reported thermal exposures producing teratogenic effects [10] is shown in the graph below (figure 2). The solid lines represent multiple data points relating to a single effect, and the dashed line represents the lowest temperatures for observed thermally induced biological changes. Exposure times and temperatures below this limit may be considered to be safe. Above this limit there is an increased probability of thermal damage. To ensure that exposure is maintained below this limit, the duration or temperature may be altered. Although this data provides a guide for determining whether a biological effect due to hyperthermia is likely, it is not ideal as the threshold for teratogenic effects may differ from the threshold for tissue changes in adults. However this data does provide the first guidelines relating temperature and time of exposure accordingly this threshold will be used in this study.

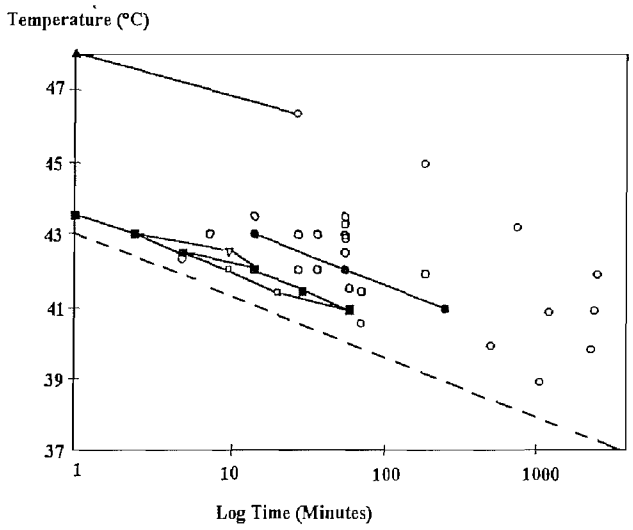

Figure 2: A Graph summarising the lowest reported thermal exposures producing teratogenic effects [10]

1.3 The Mechanism of Ultrasound Induced Hyperthermia

As ultrasound energy passes through the body, it is either reflected or absorbed and converted into thermal energy. The rate of heat production rate is described by the equation :

$$qv = 2\alpha I$$

Where qv is the heat production rate per unit volume, α is the coefficient of absorption and I is the local time averaged intensity.

This equation assumes that the insonated material is homogenous and that the ultrasound field is uniform. However, there is variation in heat production along the path of the propagating ultrasound beam as a result of inhomogenous tissue characteristics and nonuniform ultrasound field.

The absorption coefficient (α) is dependent on the ultrasound frequency and the macromolecular composition of the tissue. For soft tissues the absorption coefficient increases with protein content. Bone however, is a structurally complex connective material consisting of calcified collagen, adipose, blood vessels and other components producing unique acoustic properties. Its absorption coefficient is much greater than soft tissue (excluding lung), which may lead to heat generation in the bone and surrounding tissue.

There is no evidence to suggest that temperature increases of up to 1°K would be biologically harmful [3]. It is therefore important to determine whether the Sci-Med Transcranial Doppler could produce temperatures greater than this. Carstensen et al [11] compared a theoretical model as a predictor of temperature with experimental models. As a reasonable correlation was found between these 2 models the theoretical model was used to estimate temperature increases.

The theoretical model states

$$T = \frac{0.319 fW}{Kd}$$

where f = Percentage of energy absorbed

W = Total Power

K = Thermal conductivity

d = Diameter of the disc

The average value of f has been shown to be 80% with a possible maximum of 99% [6]. The average thermal conductivity for bone has been shown to be $0.38 Wm^{-1}K^{-1}$ [12]. The diameter of the ultrasound transducer is $1.5 \times 10^{-2} M$ and the total power is $81mW \pm 33\%$. To determine the worst case scenario the total power W = 81mW + 33% = 117mW was used .

Worst Case calculation where: f = 99% and W=117 mW

T =0.319 x 0.99 x 0.117/ 0.38 x 0.015

T = 6.48°C

Case where: f = 99% and W = 81mW

T = 4.48°C

Case where: f = 88% and W = 55mW

T = 2.71°C

From these examples it can be seen that considerable heating is possible. On the basis of these results, more complex experimental studies were performed.

1.4 Aim

Statements from national and international bodies agree that the risk of any procedure should be considered in the context of the diagnostic benefits and alternative procedures available. This implies that where no diagnostic information is gained efforts should be made to ensure that minimum risk exists.

Therefore the aims of this study are:

- to determine the 'worst case' possible temperature increases which may result from long term exposure to transcranial Doppler ultrasonography.

- to determine which ultrasound powers may be used for the long term evaluation of cerebral blood flow in normal volunteers to prevent temperatures increasing above the threshold demonstrated in figure 2.

2. METHODS AND MATERIALS

Ultrasound induced hyperthermia was measured in human bone in vitro. During TCD examinations the ultrasound beam passes through layers of skin, muscle, bone, dura matter, arachnoid, pia mater and brain tissue. However as the absorption coefficient of bone is much greater than that of soft tissues, a model using a human bone sample was considered to be valid. Experimental conditions were established to mimic 'worst case' physiological conditions.

Clinical TCD examinations are more difficult to perform in elderly Caucasian females. This is thought to result from a thickening of the temporal bone. In such cases more ultrasound energy is absorbed by the bone increasing the risks of hyperthermia. Therefore to satisfy a 'worst case' requirement a temporal bone from a 90 year old female (cause of death, acute myocardial infarction) was investigated. A second bone from a 66 year old male (cause of death, ischemic heart disease) was also used. Both bones were removed from cadavers and stored in formalin.

As the temporal bones were not fresh a series of experiments were performed on a rabbit skull to assess the effects of different treatment processes. Initially the fresh skull was insonated with ultrasound, and the temperature increase noted. The skull was then stored in formalin, soaked in Milton and autoclaved. After each process the temperature increase during ultrasound exposure was noted. A significant change in the temperature increase was only observed after autoclaving. This may be due to changes in the bone composition induced during the autoclaving procedure, for example the removal of fat

traces and the breakdown of tissues such as blood vessels. Therefore the human bone used in this experiment was not autoclaved.

2.1 The Hardware

The Hardware used in the experimental set-up is shown in figure 3. Temperature changes were measured with 2 thermocouples (Physistemp Instruments Inc., New Jersey, USA). The ultrafine T type thermocouples (IT-23) were selected with the following parameters:

- diameter 0.009 of an inch (minimising thermal disruption)
- accuracy of 0.1°C (within the physiological range)
- time constant of 0.005 seconds

A thermocouple is an electric circuit consisting of 2 dissimilar metals, in this case copper and constantan. A thermoelectric potential is produced at the junction of the conductors when exposed to temperature changes. Two thermocouples were required to measure differential and reference temperatures. A specific amplifier and power supply were designed and built to complete the thermocouple set-up. Calibration of the system allowed absolute temperatures to be measured. The analogue output from the amplifier was converted (with an analogue-to-digital converter) and input into an IBM PC equipped with the specifically adapted ICM Biomedical Signal Recorder software(Czosnyka, University of Cambridge, UK). The data was acquired at a frequency of 50Hz using and automatically stored on hard disc. Data over a 10 second period was averaged then plotted on the computer screen (figure 4). Both the differential and reference temperatures were plotted 'on-line' during the experiments. The example recording in figure 4 demonstrates five experimental insonations over a 6 hour period. A gradual increase in bone temperature (Tdif) can be seen at the beginning of each insonation, followed by a short period of equilibrium. The bone temperature decreased after the ultrasound is turned off. The reference temperature (Tref) was stable throughout the 6 hour recording period.

The TCD tested was a Sci-Med PC Dop 842 (Bristol, UK) equipped with a 2MHz probe. This machine is used routinely in clinical and experimental applications.

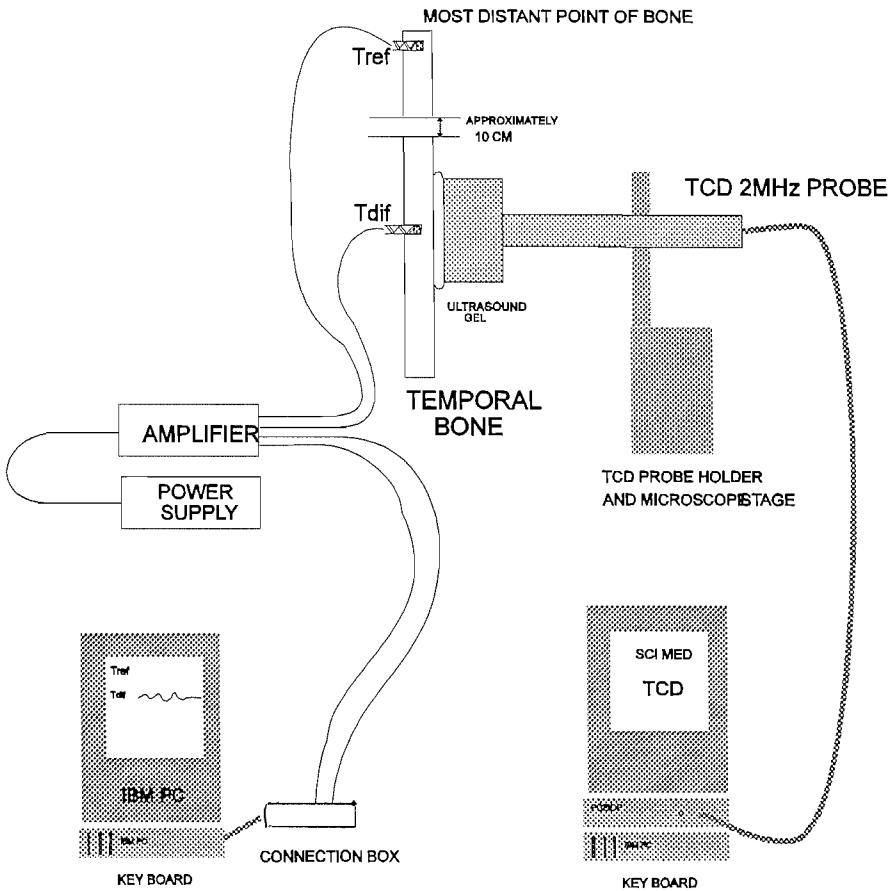

Figure 3: The experimental set-up

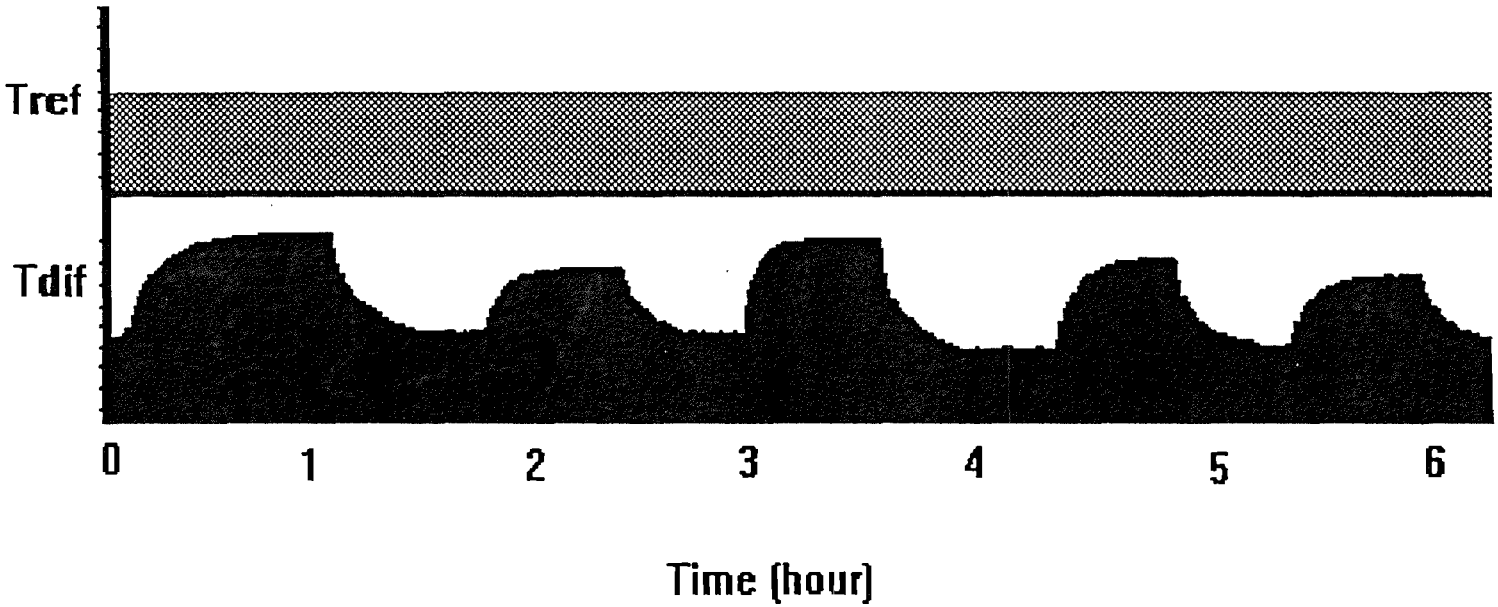

Figure 4: The differential temperature (Tdif) and reference temperature (Tref) as recorded and plotted during 5 experimental insonations performed over a 6 hour period

2.2 Preliminary Studies

To establish the most suitable experimental set-up with an accurate means of detecting temperature changes a preliminary study was performed on beef bone. As the thermal conductivity of the thermocouple is much greater than the bone, an experiment was performed to determine whether the thermocouple removed heat from the system. A small hole was drilled in the bone which was then insonated with the 2MHz probe on maximum power for approximately 30 minutes. The thermocouple was then inserted into the hole and the temperature recorded. Assuming that the air surrounding the bone was still, minimising convection, the temperature recording was a good approximation of the localised temperature without the thermocouple in situ. The thermocouple position was maintained and the bone insonated for a further 30 minutes. The temperature was then recorded. The second temperature with the thermocouple in situ was then compared to the approximation of temperature with-out the thermocouple (table2):

Temperature - no thermocouple (°C)	Temperature - with thermocouple (°C)
32.0	31.9
32.3	32.3
32.2	32.2
31.6	31.6
31.6	31.4
32.0	32.0

Table 3: Bone temperature with and without the thermocouple in situ

There was no significant difference between the two states, therefore it was concluded that the thermocouple conducted an insignificant amount of heat from the system.

2.3 Static Studies- with no Simulated Perfusion

The apparatus was set-up as shown in figure 3. Two small holes of depth 1.5mm were drilled into the temporal bone with an adapted hypodermic needle and a dental drill. The hole for the thermocouple Tdif was drilled in the thin temporal region and the hole for Tref at the most distant point from Tref. The ultrasound probe was then positioned on the

opposite side on the bone and aligned with the Tdif thermocouple. A 2mm spacer was used between the probe and the bone ensuring that this distance remained constant for each set-up. The 2mm gap was then filled with conducting gel. The temperature change at the site of the thermocouple was dependent on the alignment of the ultrasound probe with the thermocouple. To ensure that the probe and thermocouple were aligned to give the maximum temperature increase and satisfy the 'worst case' conditions, the probe was mounted on to an adapted microscope stage. The position of the ultrasound was accurately and methodically adjusted in the X-Y plane until the 'hot-spot' (the point of greatest heat production) was determined. Figure 5 demonstrates how the 'hot-spot' was established during one investigation. A similar procedure using temperature sensitive liquid crystal paint was used by Duck et al [7]. During the investigations air movement was minimised to avoid convection of heat from the bone. After each recording the temperature was allowed to return to the pre-test temperature before the next test was commenced. The temperature increase was measured for ultrasound powers of 40%, 70% and 100%

The tests were then repeated for a second hole drilled in the temporal region of bone 13cm from the first hole and for one hole in the second temporal bone (bone 2).

To determine the repeatability of the tests, one test with power equal to 100% was performed eight times. The mean temperature increase was 5.5 ± 0.19°C with a coefficient of variance of 3.5%. On this basis each test was performed only 3 times.

To investigate the effect of the depth of insonation on temperature increase hole 1 in bone 1 was insonated with a power of 70% for depths of 3, 5 and 7cm.

As the maximum temperature increase was recorded in bone 2 this was used in the model with simulated perfusion.

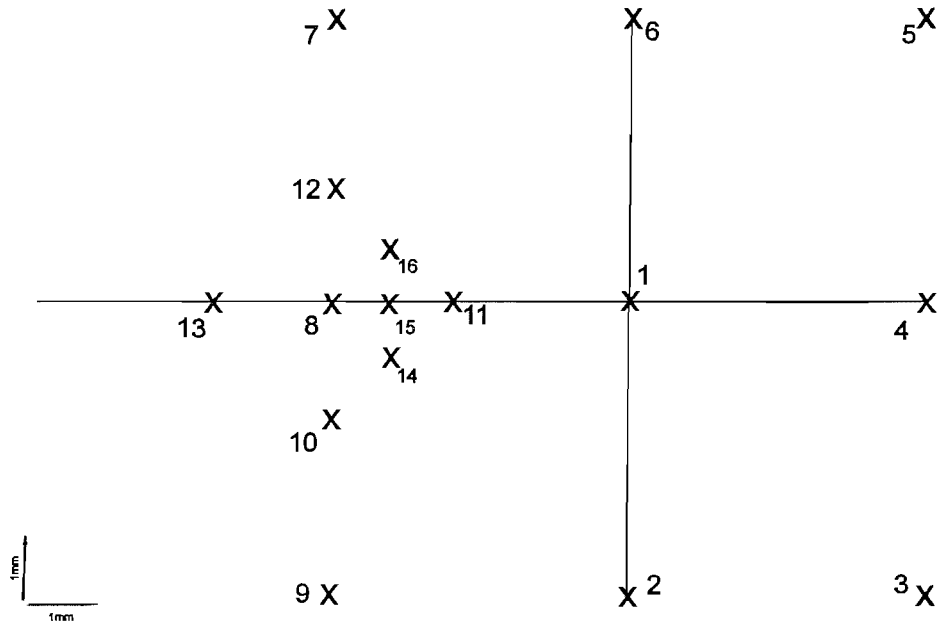

Each X represents the position of the 2MHz ultrasound transducer for one temperature measurement. The transducer was initially moved in 5 mm steps (positions 1-9). The point with the highest temperature change was localised and the positioning refined

Position number	Temperature (°C)
1	2.8
2	3.7
3	4.5
4	3.5
5	3.4
6	4.3
7	4.5
8	4.7
9	3.5
10	4.4
11	4.8
12	3.4
13	2.9
14	4.5
15	4.9
16	4.2

Figure 5: Procedure for locating the 'hot-spot'

2.4 Model with Simulated Perfusion

To determine the effects of simulated perfusion on temperature increase the apparatus was set-up as shown in figure 6. The same procedure to find the 'hot-spot' was performed as described above. Changes in experimental set-up were performed in steps:

I) Thermocouple and silicone glue

ii) Thermocouple + silicone glue + sponge.

iii) Thermocouple + silicone glue + sponge + flow through the sponge

The temperature increase for set-up i) and ii) was assessed for an ultrasound power of 70% to determine the effects of the changes in the experimental set-up. The exposed area of the thermocouple hole was covered sparingly with a small amount of silicone rubber fluid compound (RS 692-542) with a thermal conductivity of 0.334$Wm^{-1}K^{-1}$ which is in the same range as human bone (0.23-0.5$Wm^{-1}K^{-1}$). This prevented the perfusate water, bathing the thermocouple and removing heat from within the thermocouple cavity. The 1cm thick dense sponge was used to simulate the flow through the capillaries in the normal brain. To calculate the flow rate of water through the sponge in ml/100g/min (to correlate with data available for blood flow through tissue) the sponge was soaked in water then weighed. The sponge was then attached to the bone and covered with a layer of thin plastic to minimise the decrease of temperature due to evaporation. To ensure the flow across the sponge was reasonably constant black ink was added to the water and its path observed. The distribution of the ink demonstrated that after some adjustment the flow through the sponge was even suggesting that the flow at the point of the thermocouple was representative of that through the whole sponge. Flow through the sponge was regulated using a small clip to restrict flow through the plastic tubing from the water bath to the sponge. The flow rate was measured using an electronic balance as shown in figure 6. Flow rates of 5ml/100g/min 50ml/100g/min and 70ml/100g/min were selected. The water was equilibrated to room temperature. The change in temperature (at thermal equilibrium) was recorded at each flow rates for powers of 25%, 70% and 100%.

The data were analysed using Statgraphics and presented as means $\pm$ standard deviations.

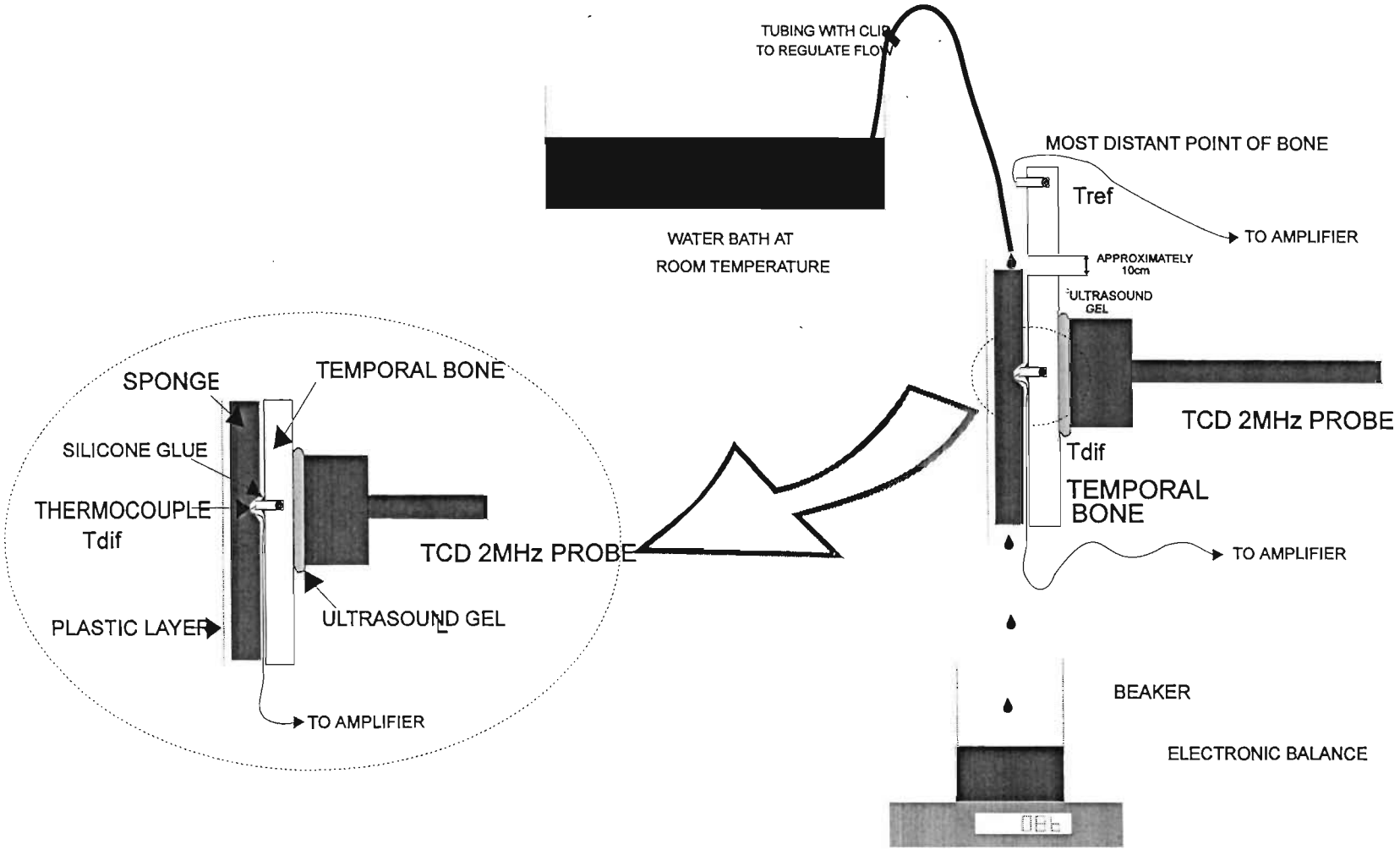

Figure 6: The experimental set-up for model with simulated perfusion

3. RESULTS

3.1 Model with no Simulated Perfusion

The importance of accurate probe placement was demonstrated by the variability in temperatures recorded during the establishment of the 'hot-spot'. For the example in figure 5 the average temperature recorded was 4 ± 0.68°C with a coefficient of variation of 17%. For other set-ups the coefficient of variation increased up to 20%.

The heating effect of three ultrasound powers 40%, 70% (used most commonly for clinical applications) and 100% was determined. As expected, heat production was dependent on the ultrasound power with a maximum temperature increase of 6.3°C observed in bone 2 when exposed to 100% power and a minimum of 1.9°C observed in bone 1 when exposed to 40% power (figure 7). The temperature increase observed in holes 1 and 2 in bone 1 were within the same range, however the temperature increases in bone 2 were slightly higher. This difference may represent normal variability due to small differences in bone structure, or bone composition. During these experiments all TCD parameters were constant and the depth of insonation was maintained at 5cm.

The effect of the depth of insonation is demonstrated in figure 8. These studies were performed at a power of 70% with a new set-up. Although the temperature appears to decrease with increased depth of insonation the temperature is not significantly different at 3 and 7cm.

The temperature increases for 40% power were more substantial than expected therefore for the flow model the minimum power assessed was decreased to 25%.

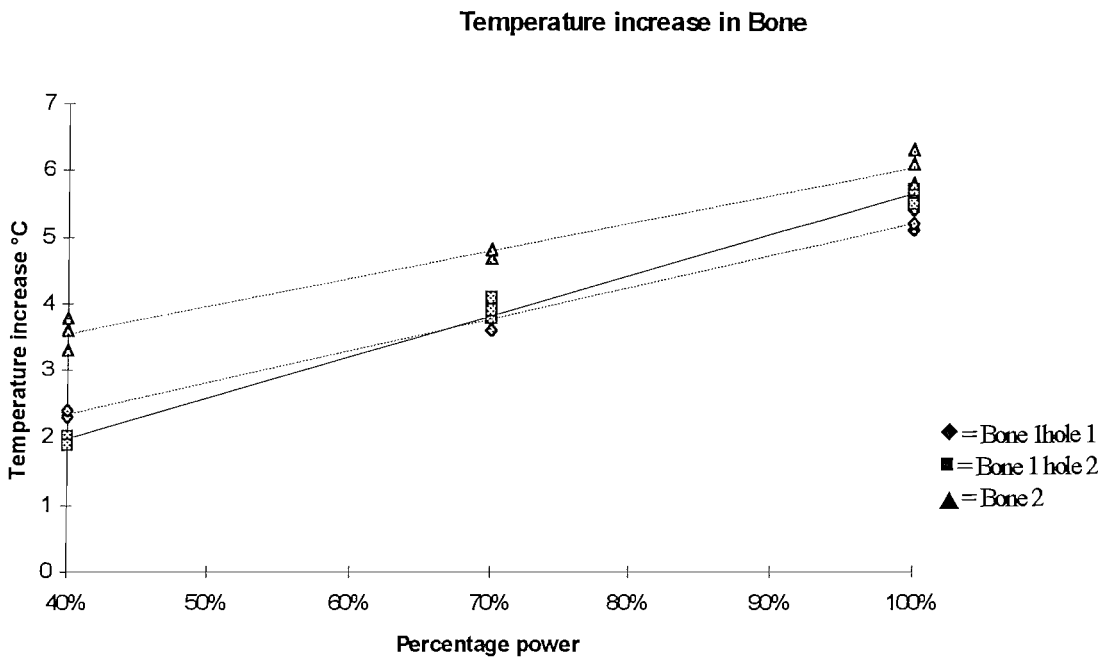

Figure 7: The temperature increase for bones 1 and 2 when insonated with the ultrasound probe set at 40%, 70%, 100% of total power (no simulated perfusion)

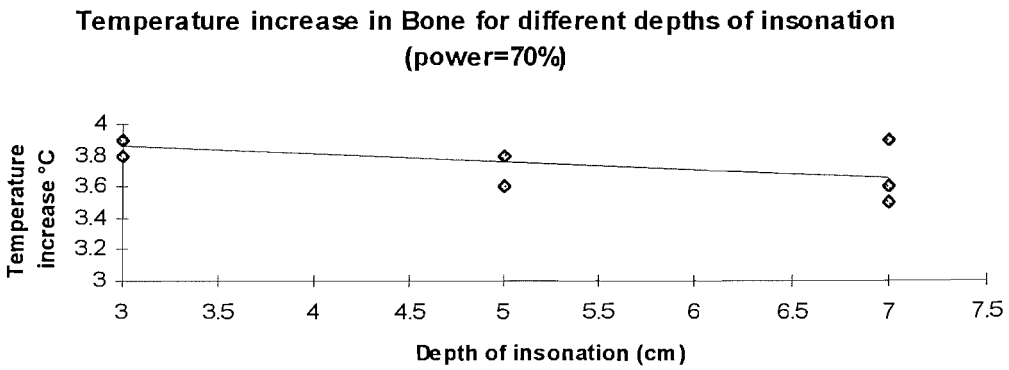

Figure 8: The effect of depth of insonation on temperature increase (no simulated perfusion)

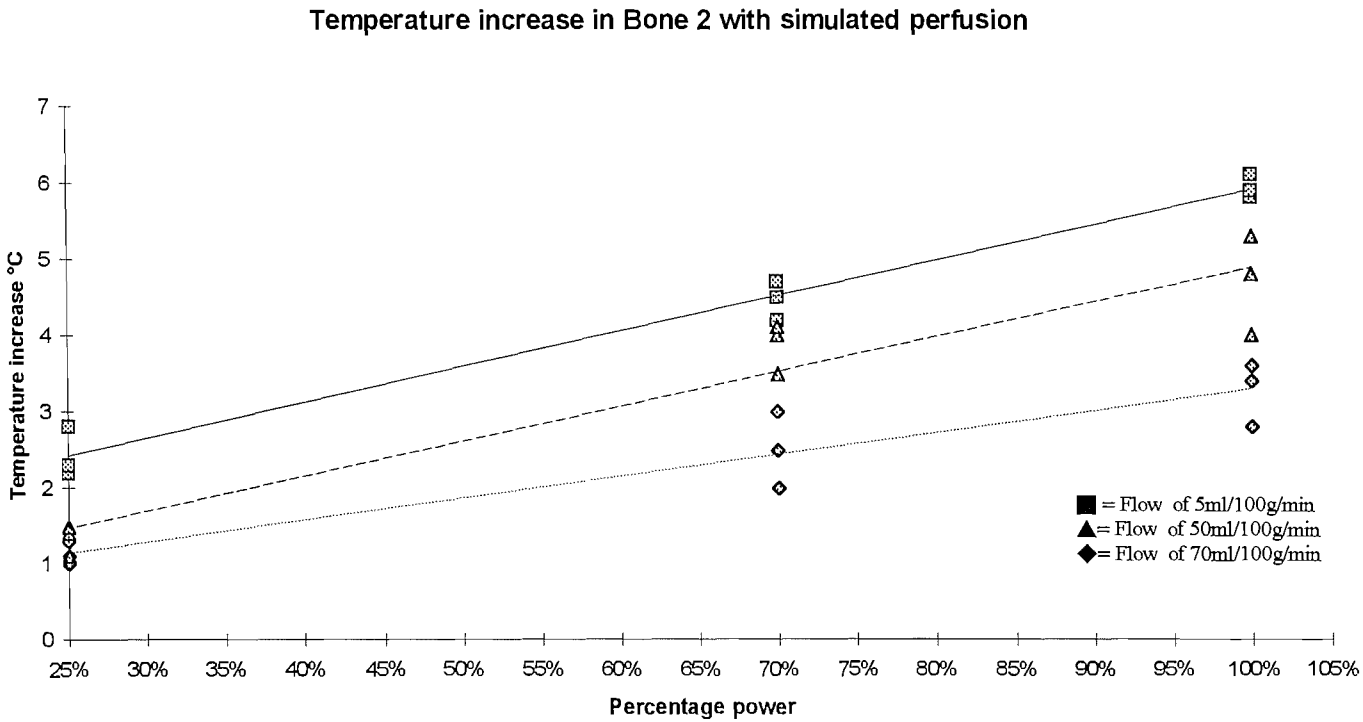

Figure 9: The temperature increase measured in bone 2 during simulated perfusion

3.2 Model with simulated perfusion

The temperature increases measured at 5, 50 and 70ml/100g/min at 25%, 70% and 100% power are presented in figure 9. For the flow model the temperature increase was determined at 70% power for the experimental set up (silicone glue, sponge and plastic layer) with no flow 4.57±0.35°C. This was not significantly different from the temperature increase at 5ml/100g/min.

The table below (table 4) shows the average temperature increase recorded at each flow rate for powers of 25%, 70% and 100%.

Flow rate	Power		
	25%	70%	100%
5ml/100g/min	2.43±0.32	4.47±0.25	5.93±0.15
50ml/100g/min	1.33±0.15	3.87±0.32	4.70±0.66
70ml/100g/min	1.13±0.15	2.50±0.50	3.26±0.42

Table 4 The mean temperature increase (±SD) recorded at each flow rate, for powers of 25%, 20% and 100%.

The maximum temperature recorded was 6.1°C when flow equalled 5ml/100g/min and the insonating power was 100%.

4. DISCUSSION

The model without perfusion allowed the method for 'hot-spot' identification to be established. The transducer was moved by a small distances in a controlled manner to identify the transducer - thermocouple alignment which gave the greatest temperature increase. This process demonstrated temperature increases with a coefficient of variation of up to 20% over a small area of bone, emphasising the importance of correct alignment of the ultrasound transducer and the thermocouple. For bone 1 where the temperature increase was measured in 2 locations of the temporal bone, the second hole was drilled

3cm from the first hole to minimise any thermal interference. No significant difference in temperature was found in the 2 points. A greater temperature increase was observed in bone 2 with a maximum temperature increase of 6.3°C. Therefore to satisfy the 'worst-case' scenario this bone was chosen for the perfusion model. During these studies the thermocouples were wedged in place in the drilled holes. No glue was used to minimise the disruption of the thermal system.

For the perfusion model silicone rubber fluid was used to seal the thermocouple cavity. This combined with the sponge and plastic layer appeared to have an insulating effect. The temperature increase for ultrasound power 70% with and without the glue and sponge was 4.57 ± 0.35°C and 4.27 ± 0.12°C respectively.

As the volunteers are normal without cerebrovascular or cardiovascular disease which may effect blood flow to the brain the perfusion is assumed to be at least 50ml/100g/min. For a simulated flow rate of 50ml/100g/min the maximum temperature increases observed were 5.3°C at 100% power, 4.1°C at 70% power and 1.5°C at 25% power.

To determine the acceptable level of exposure these results were compared to the temperatures plotted in figure 2. Although this data (figure 2) provides a guide for determining whether a biological effect due to hyperthermia is likely, it is not ideal as the threshold for teratogenic effects may differ from the threshold for tissue changes in adults. This data does however provide the first guidelines relating temperature and time of exposure therefore this threshold will be used in this study. Considering the length of exposure will be up to 8 hours (480mins) the data in figure 2 suggests that the temperature should not increase above 39°C. Assuming body temperature is 37°C then an increase of up to 2°C is acceptable. At this level of exposure the volunteer is exposed to a minimal risk of hyperthermia induced bio-effects. Considering the experimental data from the perfusion model the ultrasound power which produced less than a 2°C increase in temperature was 25%. The maximum temperature recorded for 25% power with a simulated perfusion of 50ml/100g/min was 1.5°C, and therefore within the safety guidelines.

Therefore this study suggests that after the initial placement of the transcranial Doppler probe, the power is decreased to 25% of the maximum. This however may be used as a guideline only and not an absolute threshold. This study was performed in vitro with a very simplified model. No additional layers such as skin, muscle, dura, arachnoid and cerebrospinal fluid were included. Each of these may provide both additional insulation and other heat removing mechanisms. Also it was assumed that the bone samples in vitro would have the same thermal properties as temporal bones in vivo.

Other sources of experimental error include:
(i) performing the investigations in air. Although attempts were made to prevent air movement and therefore the convection of heat from the system without insulation some degree of convection must occur. Ultrasound experiments in vitro are normally performed in water which provides a more stable and controllable testing environment. However in this case where flowing water was used to simulate perfusion this was not possible.
(ii) variability of the distance of the ultrasound transducer from the bone. Although a 2mm spacer was used at the initial transducer placement this could not be maintained as the transducer was moved over the curved surface of the temporal bone.
(iii) biological variation.
(iv) the depth of the hole. Theoretical models suggest that the temperature in the bone is dependent on depth at which it is measured. These experiments were performed in a very thin section of bone (approximately 3mm) at a depth of approximately 1.5mm.

In summary these results from the experimental model suggest that powers of up to 25% may be used in normal volunteers for up to 8 hours with minimum risk of thermal bio-effects. However as with all in vitro experiments with many potential errors, too much emphasis should not be placed on this threshold. The experiments do however indicate that thermal effects are a possible hazard. Operators should be aware of such risks and exposure minimised in clinical applications and more importantly in the study of normal volunteers

APPENDIX 3

APPENDIX 3

An experiment was performed to determine the effect of the number of time steps on the FE simulation results. A simulation was run three times maintaining all parameters except for the number of time steps. The number of time steps was set to 20 for the first simulation, 100 for the second and 1000 for the third. Displacement, pressure, volumetric strain and deviatoric strain were plotted for 2 nodes (numbers 179 and 93) for each simulation.

The results demonstrate that the number of time steps (20, 100 or 1000) did not affect the simulation results.

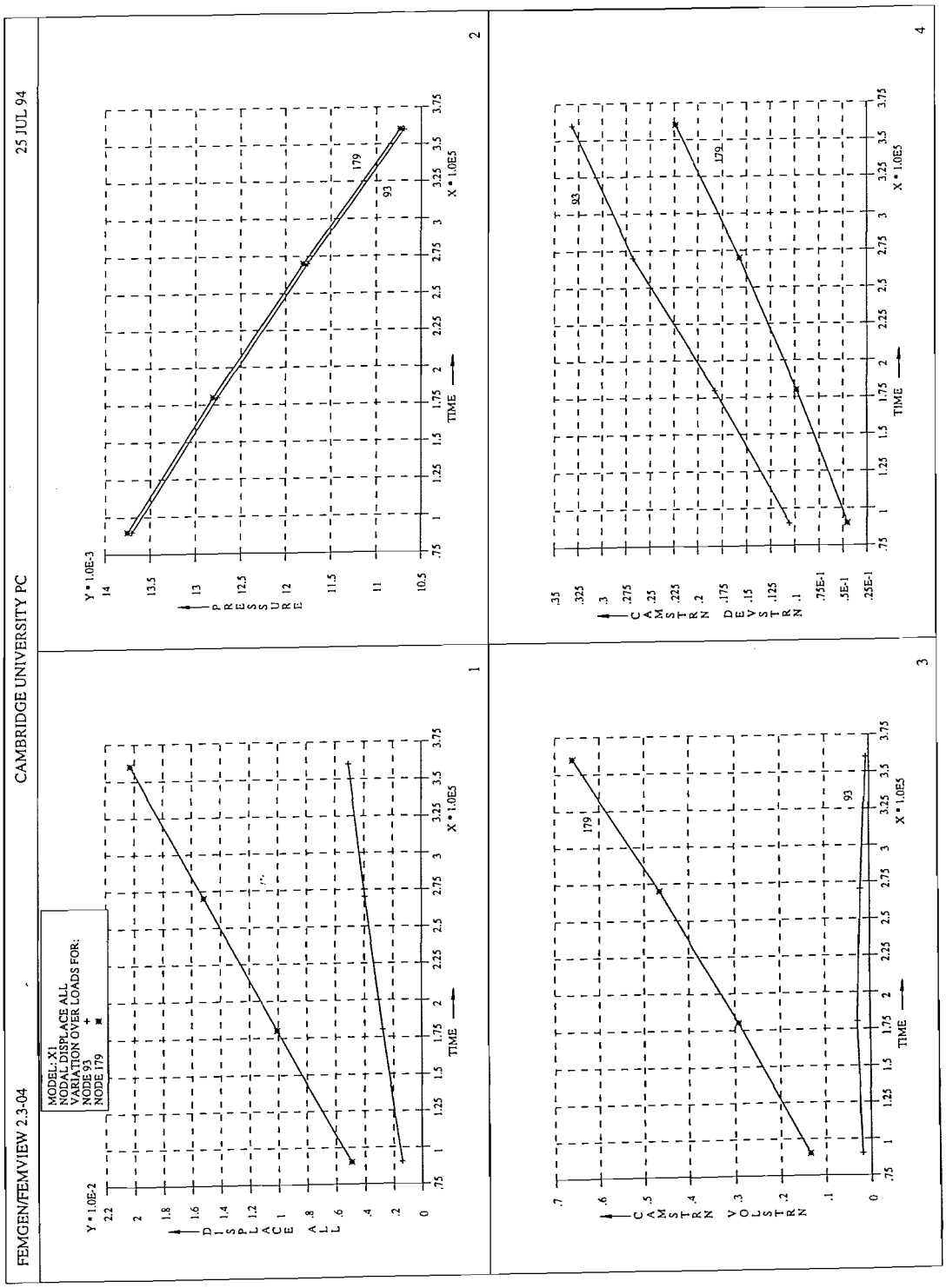

The results of a 20 step simulation

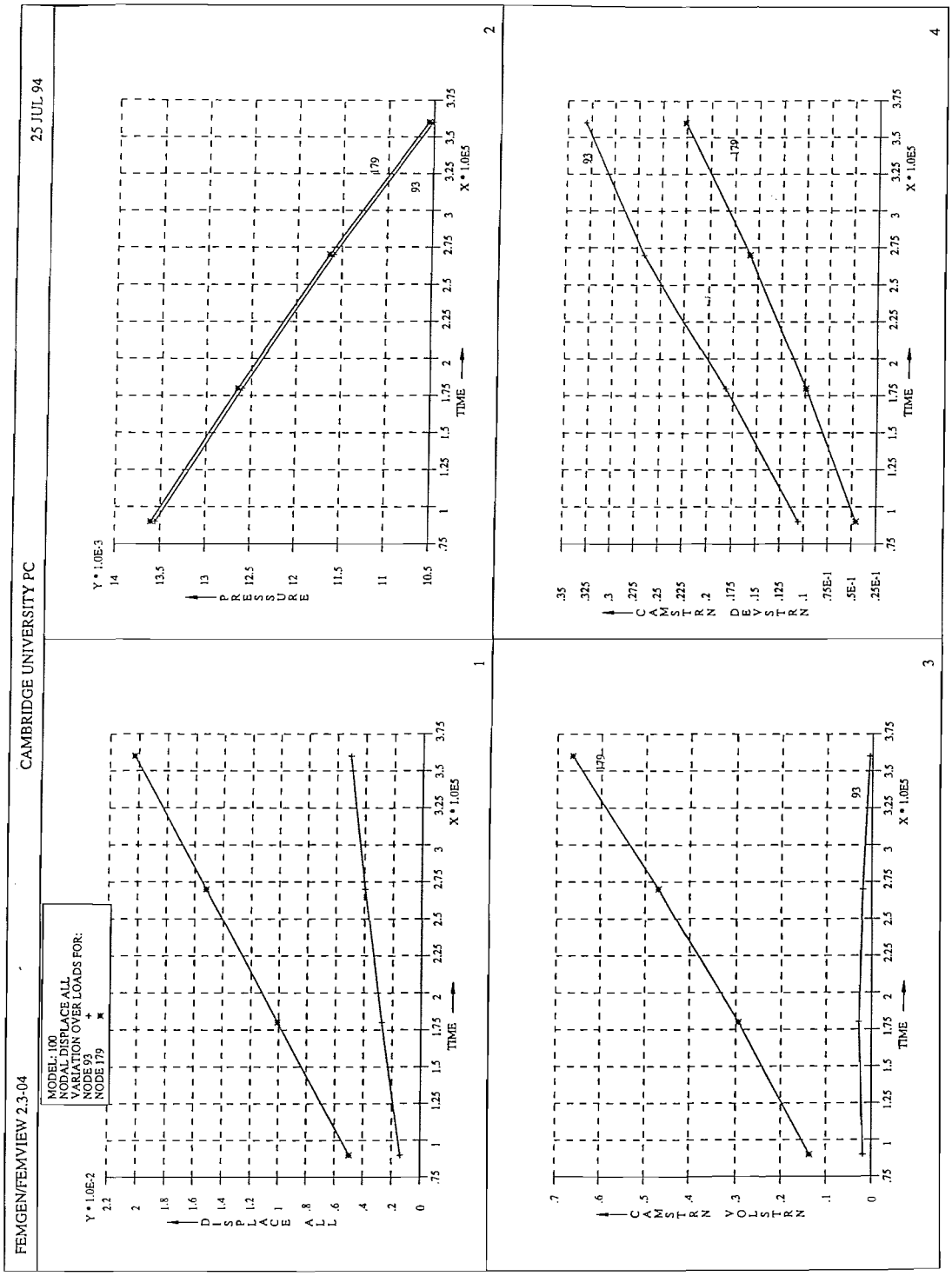

The results of a 100 step simulation

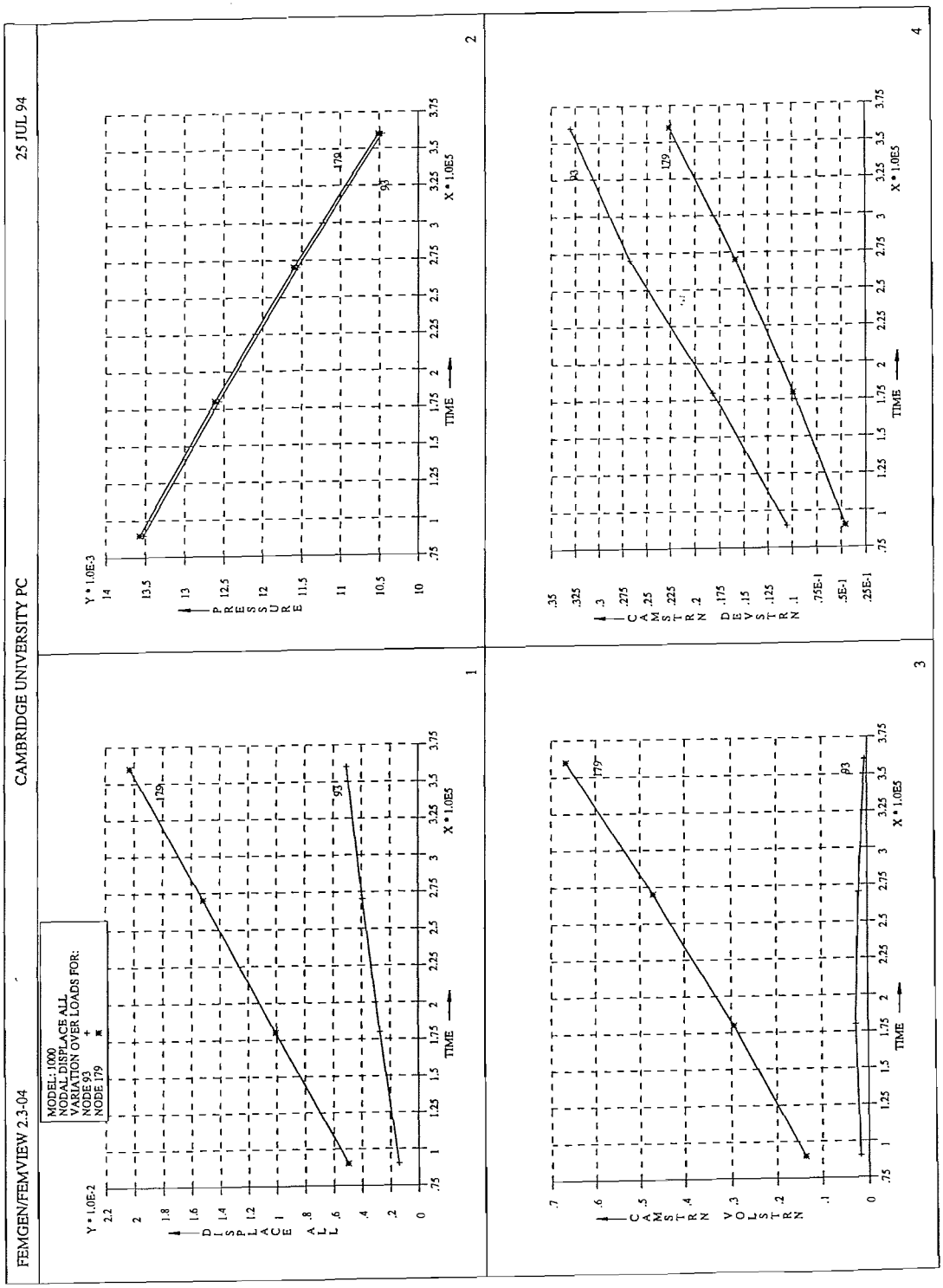

The results of a 1000 step simulation

APPENDIX 4

APPENDIX 4

An example of a GPD file

```
*** HYDROCEPHALUS 1 BRAIN MESH - 23 AUG 93- LAST REV. 18.4.94
C-----UPDATED TO CONTAIN ADDITIONAL PARAMETERS 16TH OCTOBER 1993
     24500
  242  410    3    3    2    0
  253  411
C-----DEBUGGING OPTION
    0    0    0    0    0    0    0    0    0    0
C-----CURVED SIDES
    0    0    0    0
C----LIST OF NODE NUMBERS
C NODE  X    Y
     1        0.09000        0.02000
     2        0.08500        0.01000
     3        0.07400        0.00500
     4        0.05900        0.01000
     5        0.04700        0.01700
     6        0.03900        0.02000
     7        0.03200        0.03400
     8        0.08300        0.01900
     9        0.07700        0.01100
    10        0.06800        0.01500
    11        0.05800        0.02200
    12        0.04900        0.02500
    13        0.04500        0.03700
    14        0.05200        0.03200
    15        0.05600        0.03700
    16        0.06400        0.03100
    17        0.07500        0.01900
    18        0.08100        0.02700
    19        0.09000        0.03300
    20        0.08400        0.03900
    21        0.09000        0.04000
    22        0.09000        0.04800
    23        0.08600        0.04800
    24        0.09000        0.05800
    25        0.09000        0.07100
    26        0.09000        0.07800
    27        0.09000        0.08200
    28        0.09000        0.08800
    29        0.09000        0.09600
    30        0.09000        0.10400
    31        0.08500        0.05300
    32        0.08100        0.05200
    33        0.08000        0.05800
    34        0.08500        0.06300
    35        0.07800        0.06500
    36        0.07200        0.07200
```

37	0.06700	0.06400
39	0.07900	0.07400
40	0.08300	0.08300
41	0.07300	0.08200
42	0.07800	0.08800
43	0.08200	0.09300
44	0.08400	0.09700
45	0.08400	0.08800
46	0.08600	0.09300
47	0.06900	0.07800
48	0.06300	0.07600
49	0.06500	0.07000
50	0.06000	0.06400
51	0.05800	0.05700
52	0.06400	0.05700
53	0.06800	0.05200
54	0.07600	0.05000
55	0.07000	0.04000
56	0.07900	0.04100
57	0.07600	0.03400
58	0.07000	0.03300
59	0.07500	0.02700
60	0.06600	0.03700
61	0.06000	0.04200
62	0.06000	0.05100
63	0.05400	0.05200
64	0.05100	0.04400
65	0.04500	0.04500
66	0.04200	0.05100
67	0.03800	0.04700
68	0.03500	0.04000
69	0.03200	0.04600
70	0.02100	0.04400
71	0.01400	0.05300
72	0.00800	0.06400
73	0.00700	0.07400
74	0.02100	0.06300
75	0.03000	0.06900
76	0.03800	0.07200
77	0.03700	0.06300
78	0.02700	0.05500
79	0.03700	0.05400
80	0.04300	0.05800
81	0.05000	0.04900
82	0.05000	0.05600
83	0.05200	0.06300
84	0.04600	0.06400
85	0.02100	0.07000
86	0.02000	0.07800
87	0.02500	0.07800
88	0.03000	0.08300
89	0.04000	0.08200
90	0.04500	0.07600
91	0.05100	0.07800

92	0.05700	0.08000
93	0.06300	0.08000
94	0.06300	0.08600
95	0.05600	0.07200
96	0.05000	0.07000
97	0.03000	0.07300
98	0.01300	0.08100
99	0.00600	0.08500
100	0.01400	0.08600
101	0.02000	0.08200
102	0.02700	0.08400
103	0.02700	0.08900
104	0.02000	0.09000
105	0.01100	0.09400
106	0.00500	0.09900
107	0.00600	0.10400
108	0.01000	0.11300
109	0.01300	0.11900
110	0.01500	0.12900
111	0.01500	0.10100
112	0.01200	0.10800
113	0.01600	0.10600
114	0.01500	0.11100
115	0.02200	0.10700
116	0.02800	0.10600
117	0.02200	0.10100
118	0.02600	0.09500
119	0.03600	0.09700
120	0.03200	0.09200
121	0.03000	0.08700
122	0.03600	0.08800
123	0.04400	0.09300
124	0.04800	0.08400
125	0.05600	0.09300
126	0.06700	0.09000
127	0.07200	0.09400
128	0.07700	0.09800
129	0.08200	0.10300
130	0.06400	0.09800
131	0.07000	0.10200
132	0.07600	0.10600
133	0.08300	0.10800
134	0.08800	0.10700
135	0.08300	0.11300
136	0.07500	0.11400
137	0.06700	0.11200
138	0.06200	0.10800
139	0.05500	0.10300
140	0.04600	0.10200
141	0.03800	0.10700
142	0.03000	0.11100
143	0.02200	0.12000
144	0.02800	0.12500
145	0.03200	0.11700

146	0.03600	0.12700
147	0.04300	0.11600
148	0.05100	0.12200
149	0.04400	0.12700
150	0.02300	0.13200
151	0.01600	0.13500
152	0.01900	0.13900
153	0.02100	0.14500
154	0.02600	0.14200
155	0.03200	0.14200
156	0.03800	0.14100
157	0.03000	0.13400
158	0.02700	0.14700
159	0.03300	0.15400
160	0.04100	0.15800
170	0.04300	0.14900
171	0.04600	0.13700
172	0.03800	0.13500
173	0.05500	0.13200
174	0.06200	0.13100
175	0.06000	0.11900
176	0.05700	0.11200
177	0.06600	0.12400
178	0.07500	0.12400
179	0.08800	0.11200
180	0.08800	0.11700
181	0.08100	0.12000
182	0.08100	0.12800
183	0.07900	0.13500
184	0.07400	0.14200
185	0.07000	0.14800
186	0.07300	0.15100
187	0.07400	0.13000
188	0.07100	0.13500
189	0.06500	0.14100
190	0.05200	0.14000
191	0.05100	0.15500
192	0.02100	0.15300
193	0.02200	0.16300
194	0.02700	0.15800
195	0.03000	0.16500
196	0.04100	0.17000
197	0.03100	0.17000
198	0.02400	0.17200
199	0.02900	0.18200
200	0.03600	0.17600
201	0.04100	0.18300
202	0.03500	0.19000
203	0.04300	0.20000
204	0.04300	0.19400
205	0.05100	0.19500
206	0.05000	0.18400
207	0.04700	0.17500
208	0.04300	0.18600

```
   209        0.04800        0.16600
   210        0.05200        0.17000
   211        0.05700        0.16000
   212        0.06600        0.16700
   213        0.06600        0.15800
   214        0.07300        0.16300
   215        0.08000        0.17000
   216        0.07500        0.17700
   217        0.06300        0.17500
   218        0.05500        0.18000
   219        0.06200        0.18700
   220        0.05900        0.19600
   221        0.05200        0.20500
   222        0.06300        0.20900
   223        0.07000        0.21100
   224        0.07800        0.21300
   225        0.08700        0.21000
   226        0.09000        0.20000
   227        0.09000        0.18800
   228        0.07000        0.20300
   229        0.07500        0.20700
   230        0.07800        0.20100
   231        0.07700        0.19800
   232        0.08000        0.19000
   233        0.07000        0.19400
   234        0.06500        0.19000
   235        0.07000        0.18200
   236        0.08200        0.18100
   237        0.08300        0.17500
   238        0.09000        0.17900
   239        0.09000        0.17000
   240        0.08600        0.16500
   241        0.08200        0.16000
   242        0.09000        0.15500
   243        0.08100        0.15000
   244        0.07900        0.14300
   245        0.08400        0.14400
   246        0.09000        0.14700
   247        0.09000        0.13900
   248        0.08300        0.13800
   250        0.09000        0.13100
   251        0.06200        0.15000
   252        0.06900        0.02500
   253        0.07200        0.05800
C---------RECORD H OPTIMISATION PROCEDURE
    1
C
C-------- RECORD I - (FRONTAL ASSEMBLY SEQUENCE OF ELEMENTS)
  142  143  140  141  144  390  145  146  389  136
  137  138  388  147  387  148  134  135  139  385
  386  149  150  152  383  384  131  132  128  130
  127  126  129  125  378  124  151  382  391  153
  395  154  133  379  375  376  373  374  372  392
  393  394  155  156  157  158  398  396  397  121
```

```
   122  123  119  120  370  371  380  399  381  400
   401  402  405  117  118  116  115  365  364  366
   367  369  349  350  347  348  403  404  406  407
   114  409  408  410  113  362  363  361  368  351
   352  344  345  346  112  110  111  109  357  358
   359  353  356  343  354  108  360  107  104  105
   106  355  339  340  102  103  101  337  338  335
   336  100   99  334  332  333  330  331  329  341
    98  321  322  342  320  325  326  327  328  323
   324  317  319  318  315  316  307  308  305  306
   314  309  310   93   96   97  285  286  284  287
    92  288  289  296  303  304  290  291  302  311
   312  260  261  313  300  301  299  297  298  294
   295  292  293  258  259  257   94   95  282  281
   283  262  263   91  275  276   90  277  278  279
   280   89  274  273   88  270  271   87  272   86
    84   85  242  243  256  241  240  264  265  411
   254  255  268  269  266  267  252  253   82  251
   250   81   83   79   80   77  248  249   78  247
    76   69   70   68   71   72   73   74   75  246
   244  245  236  237  227  228   66   67   65  238
   239  231  232  229  230   64  226   59   60  233
   234  191  192  235  186  187  185  190  177  223
   224  225   62   63   58   61   57  221  222  189
   193  175  176  184  183  188  172  173  214  215
   218  219  220  212  213   55   56  194  195   14
    15  211  216   51  217   50  196   54  210   53
   209   52   16  197   13   17   48   49  198  199
   170  171  174  169  166  168  165  167  163  164
   162  161  160  159    1  178  182   12  181   11
    18    2    4  180    3   10  179    5    6    7
     8    9   19   20   24   25  200  202   47  201
    45   46   44   21   22   23  205  206  203  204
    42   43   41   40   39   26  207  208   27   28
    36   37   38   34   31   29   35   30   33   32
C
C-------- RECORD J - (ELEMENT NODAL CONNECTIVITY)
C  KEL ITYP IMAT   N1   N2   N3   N4
     1    3    1   25   35   34
     2    3    1   25   34   24
     3    3    1   34   31   24
     4    3    1   34   33   31
     5    3    1   24   31   22
     6    3    1   31   23   22
     7    3    1   22   23   21
     8    3    1   23   20   21
     9    3    1   20   23   56
    10    3    1   23   32   56
    11    3    1   32   54   56
    12    3    1   54   32  253
    13    3    1   53   54  253
    14    3    1  253   52   53
    15    3    1   52   62   53
    16    3    1   62   55   53
```

17	3	1	53	55	54
18	3	1	55	56	54
19	3	1	55	57	56
20	3	1	57	20	56
21	3	1	21	20	19
22	3	1	20	18	19
23	3	1	18	20	57
24	3	1	57	55	58
25	3	1	55	60	58
26	3	1	19	18	1
27	3	1	1	18	8
28	3	1	17	8	18
29	3	1	17	9	8
30	3	1	8	9	2
31	3	1	1	8	2
32	3	1	2	9	3
33	3	1	3	9	10
34	3	1	3	10	4
35	3	1	10	9	17
36	3	1	10	17	252
37	3	1	252	11	10
38	3	1	4	10	11
39	3	1	4	11	5
40	3	1	11	12	5
41	3	1	14	12	11
42	3	1	11	16	14
43	3	1	11	252	16
44	3	1	5	12	6
45	3	1	6	12	13
46	3	1	13	12	14
47	3	1	13	14	15
48	3	1	15	64	13
49	3	1	15	61	64
50	3	1	64	61	63
51	3	1	64	63	81
52	3	1	13	7	6
53	3	1	7	13	68
54	3	1	13	67	68
55	3	1	69	68	67
56	3	1	7	68	69
57	3	1	70	7	69
58	3	1	70	69	78
59	3	1	70	78	74
60	3	1	70	74	71
61	3	1	69	79	78
62	3	1	79	77	78
63	3	1	79	80	77
64	3	1	74	78	75
65	3	1	71	74	72
66	3	1	72	74	85
67	3	1	74	75	85
68	3	1	85	73	72
69	3	1	73	85	86
70	3	1	85	87	86

71	3	1	85	97	87
72	3	1	87	97	88
73	3	1	88	97	76
74	3	1	76	89	88
75	3	1	76	90	89
76	3	1	86	98	73
77	3	1	99	73	98
78	3	1	98	86	101
79	3	1	99	98	100
80	3	1	98	101	100
81	3	1	101	102	104
82	3	1	102	103	104
83	3	1	104	100	101
84	3	1	100	104	105
85	3	1	99	100	105
86	3	1	99	105	106
87	3	1	105	111	106
88	3	1	106	111	107
89	3	1	107	111	112
90	3	1	107	112	108
91	3	1	108	112	114
92	3	1	108	114	109
93	3	1	109	114	143
94	3	1	114	115	142
95	3	1	115	116	142
96	3	1	114	142	143
97	3	1	142	145	143
98	3	1	109	143	110
99	3	1	110	143	150
100	3	1	110	150	151
101	3	1	151	150	152
102	3	1	152	150	154
103	3	1	150	157	154
104	3	1	154	157	155
105	3	1	155	157	156
106	3	1	156	157	172
107	3	1	152	154	153
108	3	1	153	154	158
109	3	1	153	158	192
110	3	1	192	158	194
111	3	1	194	158	159
112	3	1	192	194	193
113	3	1	194	195	193
114	3	1	193	195	198
115	3	1	195	197	198
116	3	1	198	197	199
117	3	1	199	197	200
118	3	1	197	196	200
119	3	1	196	209	207
120	3	1	209	210	207
121	3	1	207	201	196
122	3	1	201	200	196
123	3	1	200	201	199
124	3	1	199	201	202

125	3	1	202	201	208
126	3	1	208	204	202
127	3	1	202	204	203
128	3	1	204	205	203
129	3	1	208	206	204
130	3	1	204	206	205
131	3	1	205	206	220
132	3	1	206	219	220
133	3	1	206	218	219
134	3	1	203	205	221
135	3	1	205	220	221
136	3	1	221	220	222
137	3	1	220	228	222
138	3	1	220	233	228
139	3	1	220	234	233
140	3	1	222	228	223
141	3	1	223	228	229
142	3	1	223	229	224
143	3	1	224	229	225
144	3	1	229	230	225
145	3	1	225	230	226
146	3	1	230	231	226
147	3	1	231	232	226
148	3	1	226	232	227
149	3	1	232	236	227
150	3	1	232	235	236
151	3	1	235	216	236
152	3	1	236	238	227
153	3	1	238	236	237
154	3	1	237	239	238
155	3	1	237	240	239
156	3	1	240	237	215
157	3	1	240	242	239
158	3	1	240	241	242
159	3	2	29	30	44
160	3	2	44	46	29
161	3	2	28	29	46
162	3	2	43	46	44
163	3	2	43	45	46
164	3	2	46	45	28
165	3	2	42	45	43
166	3	2	42	40	45
167	3	2	45	27	28
168	3	2	45	40	27
169	3	2	40	26	27
170	3	2	40	39	26
171	3	2	39	25	26
172	3	2	41	40	42
173	3	2	41	39	40
174	3	2	39	35	25
175	3	2	36	35	39
176	3	2	41	36	39
177	3	2	47	36	41
178	3	2	35	33	34

179	3	2	31	32	23
180	3	2	33	32	31
181	3	2	32	33	253
182	3	2	33	35	253
183	3	2	35	37	253
184	3	2	37	35	36
185	3	2	36	49	37
186	3	2	49	36	48
187	3	2	48	36	47
188	3	2	253	37	52
189	3	2	37	50	52
190	3	2	49	50	37
191	3	2	49	95	50
192	3	2	48	95	49
193	3	2	50	51	52
194	3	2	51	62	52
195	3	2	51	63	62
196	3	2	63	61	62
197	3	2	62	61	55
198	3	2	61	60	55
199	3	2	61	15	60
200	3	2	15	16	60
201	3	2	14	16	15
202	3	2	60	16	58
203	3	2	16	252	58
204	3	2	252	59	58
205	3	2	58	59	57
206	3	2	57	59	18
207	3	2	59	17	18
208	3	2	252	17	59
209	3	2	64	65	13
210	3	2	65	67	13
211	3	2	65	66	67
212	3	2	69	67	79
213	3	2	66	79	67
214	3	2	66	80	79
215	3	2	66	81	80
216	3	2	65	81	66
217	3	2	64	81	65
218	3	2	80	81	82
219	3	2	63	82	81
220	3	2	51	82	63
221	3	2	50	83	51
222	3	2	82	51	83
223	3	2	82	83	84
224	3	2	80	82	84
225	3	2	80	84	77
226	3	2	78	77	75
227	3	2	85	75	97
228	3	2	75	76	97
229	3	2	75	77	76
230	3	2	76	77	84
231	3	2	76	84	90
232	3	2	84	96	90

233	3	2	96	84	83
234	3	2	83	95	96
235	3	2	50	95	83
236	3	2	95	48	92
237	3	2	91	95	92
238	3	2	95	91	96
239	3	2	90	96	91
240	3	2	48	93	92
241	3	2	92	93	94
242	3	2	125	92	94
243	3	2	125	124	92
244	3	2	91	92	124
245	3	2	90	91	124
246	3	2	89	90	124
247	3	2	101	86	87
248	3	2	101	87	102
249	3	2	87	88	102
250	3	2	88	121	102
251	3	2	121	103	102
252	3	2	122	121	88
253	3	2	122	88	89
254	3	2	122	89	123
255	3	2	123	89	124
256	3	2	123	124	125
257	3	2	125	94	126
258	3	2	125	126	130
259	3	2	126	127	130
260	3	2	139	125	130
261	3	2	139	140	125
262	3	2	123	125	140
263	3	2	119	123	140
264	3	2	119	122	123
265	3	2	122	119	120
266	3	2	121	122	120
267	3	2	103	121	120
268	3	2	120	118	103
269	3	2	104	103	118
270	3	2	104	118	117
271	3	2	104	117	111
272	3	2	111	105	104
273	3	2	111	117	113
274	3	2	111	113	112
275	3	2	113	114	112
276	3	2	113	115	114
277	3	2	113	117	115
278	3	2	116	115	117
279	3	2	116	117	118
280	3	2	116	118	119
281	3	2	116	119	141
282	3	2	116	141	142
283	3	2	119	140	141
284	3	2	140	147	141
285	3	2	141	145	142
286	3	2	141	147	145

287	3	2	140	176	147
288	3	2	140	139	176
289	3	2	176	139	138
290	3	2	139	130	138
291	3	2	130	131	138
292	3	2	130	127	131
293	3	2	127	128	131
294	3	2	131	128	132
295	3	2	128	129	132
296	3	2	131	132	137
297	3	2	129	133	132
298	3	2	133	129	134
299	3	2	133	134	179
300	3	2	133	179	135
301	3	2	135	132	133
302	3	2	132	135	136
303	3	2	137	132	136
304	3	2	137	138	131
305	3	2	137	175	138
306	3	2	138	175	176
307	3	2	137	177	175
308	3	2	137	178	177
309	3	2	178	137	136
310	3	2	178	136	181
311	3	2	181	136	135
312	3	2	181	135	180
313	3	2	180	135	179
314	3	2	181	182	178
315	3	2	182	187	178
316	3	2	187	177	178
317	3	2	177	187	188
318	3	2	187	182	183
319	3	2	183	188	187
320	3	2	188	183	184
321	3	2	189	188	184
322	3	2	189	174	188
323	3	2	174	177	188
324	3	2	174	175	177
325	3	2	173	175	174
326	3	2	173	148	175
327	3	2	148	176	175
328	3	2	147	176	148
329	3	2	149	147	148
330	3	2	146	147	149
331	3	2	146	145	147
332	3	2	144	145	146
333	3	2	143	145	144
334	3	2	150	143	144
335	3	2	150	144	157
336	3	2	157	144	146
337	3	2	157	146	172
338	3	2	172	146	149
339	3	2	172	149	171
340	3	2	171	149	173

341	3	2	149	148	173
342	3	2	173	174	189
343	3	2	190	173	189
344	3	2	190	189	251
345	3	2	251	189	185
346	3	2	189	184	185
347	3	2	251	185	213
348	3	2	185	186	213
349	3	2	251	213	211
350	3	2	251	211	191
351	3	2	191	190	251
352	3	2	170	190	191
353	3	2	170	171	190
354	3	2	171	173	190
355	3	2	172	171	156
356	3	2	156	171	170
357	3	2	170	159	156
358	3	2	159	155	156
359	3	2	155	159	158
360	3	2	154	155	158
361	3	2	159	170	160
362	3	2	194	159	195
363	3	2	195	159	160
364	3	2	160	196	195
365	3	2	197	195	196
366	3	2	196	160	209
367	3	2	160	191	209
368	3	2	160	170	191
369	3	2	191	211	209
370	3	2	209	211	210
371	3	2	210	211	212
372	3	2	210	212	217
373	3	2	210	217	218
374	3	2	210	218	207
375	3	2	206	207	218
376	3	2	206	201	207
378	3	2	206	208	201
379	3	2	218	217	219
380	3	2	211	213	212
381	3	2	213	186	214
382	3	2	217	235	219
383	3	2	219	235	234
384	3	2	219	234	220
385	3	2	234	235	233
386	3	2	235	232	233
387	3	2	233	232	231
388	3	2	233	231	228
389	3	2	228	231	230
390	3	2	230	229	228
391	3	2	217	216	235
392	3	2	212	216	217
393	3	2	212	215	216
394	3	2	216	215	237
395	3	2	216	237	236

```
  396    3    2  212  214  215
  397    3    2  214  241  215
  398    3    2  215  241  240
  399    3    2  213  214  212
  400    3    2  214  186  241
  401    3    2  186  243  241
  402    3    2  241  243  242
  403    3    2  243  186  244
  404    3    2  244  245  243
  405    3    2  243  246  242
  406    3    2  246  243  245
  407    3    2  246  245  247
  408    3    2  245  248  247
  409    3    2  245  244  248
  410    3    2  247  248  250
  411    3    2  120  119  118
C================== End of GPD file ==================
```

APPENDIX 5

APPENDIX 5

An example of an MPD file

```
HYDROCEPHALUS 3/ MAIN PROG FILE / 17TH OCT 93
C----LAST REVISED 8-7-94------
C----INNER BOUNDARY-- PRESSURE LOADING=1.3, U NOT SPECIFIED
C----OUTER BOUNDARY--FIXED, U=0
C-----LINK CODE NUMBER-------
25400
C----RECORD C1---
0  2  1  1  20  0  1  0  2
C-----RECORD C2---last 6 numbers rel to output option in record I
C-----NB: MIDSIDE NODE NUMBERING STARTS AT 751
1  1  1  1  253  751  1405  1 411
C----RECORD C3
0
C---RECORD D---MATERIAL PROPERTIES----
C---P(7) unit wt of water -- P(8) unit wt of tissue
1  1  30  30  0.25  0.25  12  0  10.0  10.18  1.0E-7  1.0E-7  0  0
2  1  3   3  0.25  0.25  1.2  0  10.0  10.22  1.0E-4  1.0E-4  0  0
C---RECORD F --- INSITU STRESS OPTION ---
0 0
C---RECORD I --- 1011 FOR EACH INCREMENT----
C---REPEAT I TO M FOR ECH INCREMENT BLOCK
1  1  20  0  -24  0  110  0  0  1  3.6E5  0  0
1011  1011  1011  1011  1011   1011  1011  1011  1011  1011
1011  1011  1011  1011  1011   1011  1011  1011  1011  1011
C---RECORD L -- FOR PRESSURE LOADING
C--N---E1----E2----x/2     x/4          0         x        x/2        x/4
159      30       44      0    1.3      0      1.3      0      1.3
162      44       43      0    1.3      0      1.3      0      1.3
165      43       42      0    1.3      0      1.3      0      1.3
172      42       41      0    1.3      0      1.3      0      1.3
177      41       47      0    1.3      0      1.3      0      1.3
187      47       48      0    1.3      0      1.3      0      1.3
240      48       93      0    1.3      0      1.3      0      1.3
241      93       94      0    1.3      0      1.3      0      1.3
257      94       126      0   1.3      0      1.3      0      1.3
259      126      127      0   1.3      0      1.3      0      1.3
293      127      128      0   1.3      0      1.3      0      1.3
295      128      129      0   1.3      0      1.3      0      1.3
298      129      134      0   1.3      0      1.3      0      1.3
299      134      179      0   1.3      0      1.3      0      1.3
313      179      180      0   1.3      0      1.3      0      1.3
312      180      181      0   1.3      0      1.3      0      1.3
314      181      182      0   1.3      0      1.3      0      1.3
318      182      183      0   1.3      0      1.3      0      1.3
320      183      184      0   1.3      0      1.3      0      1.3
346      184      185      0   1.3      0      1.3      0      1.3
```

```
348     185     186     0   1.3     0     1.3     0     1.3
403     186     244     0   1.3     0     1.3     0     1.3
409     244     248     0   1.3     0     1.3     0     1.3
410     248     250     0   1.3     0     1.3     0     1.3
C-----MOVEMENT IN Y PLANE ONLY
159     30      29      1       1       0       0       0
161     29      28      1       1       0       0       0
167     28      27      1       1       0       0       0
169     27      26      1       1       0       0       0
171     26      25      1       1       0       0       0
2       25      24      1       1       0       0       0
5       24      22      1       1       0       0       0
7       22      21      1       1       0       0       0
21      21      19      1       1       0       0       0
26      19      1       1       1       0       0       0
148     226     227     1       1       0       0       0
152     227     238     1       1       0       0       0
154     238     239     1       1       0       0       0
157     239     242     1       1       0       0       0
405     242     246     1       1       0       0       0
407     246     247     1       1       0       0       0
410     247     250     1       1       0       0       0
C-----NO MOVEMENT IN X OR Y PLANE
31      1       2       1       1       0       0       0
31      1       2       2       1       0       0       0
32      2       3       1       1       0       0       0
32      2       3       2       1       0       0       0
34      3       4       1       1       0       0       0
34      3       4       2       1       0       0       0
39      4       5       1       1       0       0       0
39      4       5       2       1       0       0       0
44      5       6       1       1       0       0       0
44      5       6       2       1       0       0       0
52      6       7       1       1       0       0       0
52      6       7       2       1       0       0       0
57      7       70      1       1       0       0       0
57      7       70      2       1       0       0       0
60      70      71      1       1       0       0       0
60      70      71      2       1       0       0       0
65      71      72      1       1       0       0       0
65      71      72      2       1       0       0       0
68      72      73      1       1       0       0       0
68      72      73      2       1       0       0       0
77      73      99      1       1       0       0       0
77      73      99      2       1       0       0       0
86      99      106     1       1       0       0       0
86      99      106     2       1       0       0       0
88      106     107     1       1       0       0       0
88      106     107     2       1       0       0       0
90      107     108     1       1       0       0       0
90      107     108     2       1       0       0       0
92      108     109     1       1       0       0       0
92      108     109     2       1       0       0       0
98      109     110     1       1       0       0       0
```

```
98      109     110     2       1       0       0       0
100     110     151     1       1       0       0       0
100     110     151     2       1       0       0       0
101     151     152     1       1       0       0       0
101     151     152     2       1       0       0       0
107     152     153     1       1       0       0       0
107     152     153     2       1       0       0       0
109     153     192     1       1       0       0       0
109     153     192     2       1       0       0       0
112     192     193     1       1       0       0       0
112     192     193     2       1       0       0       0
114     193     198     1       1       0       0       0
114     193     198     2       1       0       0       0
116     198     199     1       1       0       0       0
116     198     199     2       1       0       0       0
124     199     202     1       1       0       0       0
124     199     202     2       1       0       0       0
127     202     203     1       1       0       0       0
127     202     203     2       1       0       0       0
134     203     221     1       1       0       0       0
134     203     221     2       1       0       0       0
136     221     222     1       1       0       0       0
136     221     222     2       1       0       0       0
140     222     223     1       1       0       0       0
140     222     223     2       1       0       0       0
142     223     224     1       1       0       0       0
142     223     224     2       1       0       0       0
143     224     225     1       1       0       0       0
143     224     225     2       1       0       0       0
145     225     226     1       1       0       0       0
145     225     226     2       1       0       0       0
C---PORE PRESSURES OUTER SURFACE
31      1       2       3       1       0       0       0
32      2       3       3       1       0       0       0
34      3       4       3       1       0       0       0
39      4       5       3       1       0       0       0
44      5       6       3       1       0       0       0
52      6       7       3       1       0       0       0
57      7       70      3       1       0       0       0
60      70      71      3       1       0       0       0
65      71      72      3       1       0       0       0
68      72      73      3       1       0       0       0
77      73      99      3       1       0       0       0
86      99      106     3       1       0       0       0
88      106     107     3       1       0       0       0
90      107     108     3       1       0       0       0
92      108     109     3       1       0       0       0
98      109     110     3       1       0       0       0
100     110     151     3       1       0       0       0
101     151     152     3       1       0       0       0
107     152     153     3       1       0       0       0
109     153     192     3       1       0       0       0
112     192     193     3       1       0       0       0
114     193     198     3       1       0       0       0
```

```
116     198     199     3       1       0       0       0
124     199     202     3       1       0       0       0
127     202     203     3       1       0       0       0
134     203     221     3       1       0       0       0
136     221     222     3       1       0       0       0
140     222     223     3       1       0       0       0
142     223     224     3       1       0       0       0
143     224     225     3       1       0       0       0
145     225     226     3       1       0       0       0
C--- END OF MPD FILE !!!!! AT LAST---------
```

REFERENCES

(listed for each Chapter and Appendix)

1. REFERENCES - CHAPTER 1

1. Del Bigio MR. Epidemiology and direct economic impact of hydrocephalus: A community based study. *Canadian Journal of Neurological Sciences*. 1998;25:123-126

2. McComb JG. Recent research in to the nature of cerebrospinal fluid formation and absorption. *Journal of Neurosurgery* 1983;59:369-383

3. Welch K. secretion of cerebrospinal fluid by choroid plexus of the rabbit. *American Journal of Physiology*. 1963;205:617-624

4. Cserr HF. Convection of brain interstitial fluid. In: (eds) Shapiro K, Marmarou A, Portnoy H. *Hydrocephalus*. New York: Raven, 59-68, 1984

5.Cutler RWP, Page L, Galicich, Watters GV. Formation and absorption of cerebrospinal fluid in man. *Brain* 1968;91:707-720

6. Weller RO. Pathology of cerebrospinal fluid and interstitial fluid of the CNS: Significance for Alzheimer disease, prion disorders and multiple sclerosis. *Journal of Neuropathology and Experimental Neurology*. 1998;57:885-894

7. Nyberg-HansenR, Torvik A, Bhatia R. On the pathology of experimental hydrocephalus. *Brain Research* 1975;95:343-350

8. Kiefer M, Eymann R, von Iling S, Muller A, Steudel WI, Booz KH. The ependyma in chronic hydrocephalus. *Childs Nervous System*. 1998;14:263-270

9. Bruni JE, Del Bigio MR, Clattenburg RE. Ependyma: normal and pathological. A review of the literature. *Brain Research*. 1985;356:1-19

10. Torvik A, Stenwig AE, Finseth I. Pathology of experimental obstructive hydrocephalus. *Acta Neurolpathologica*. 1981;54:143-147

11. Wikkelso C, Anderson H, Blomstrand C, Matousek M, Svendsen P. Computed tomography of the brain in the diagnosis and prognosis in normal pressure hydrocephalus. *Neuroradiology*. 1989;31:160-165

12. Del Bigio MR, Crook CR, Buist R. Magnetic resonance imaging and behavioral analysis of immature rats with kaolin-induced hydrocephalus. *Experimental Neurology*. 1997;148:256-264

13. Del Bigio MR. Neuropathological changes caused by hydrocephalus. *Acta Neuropathologica*. 1993;85:573-585

14. Rubin RC, Hochwald GM, Tiell M, Mizutani H, Ghatak N. Hydrocephalus: I. Histological and ultrastructural changes in the pre-shunted cortical mantle. *Surgical Neurology*. 1976;5:109-114

15. Weller RO, Shulman K. Infantile hydrocephalus: Clinical, histological and ultrastructural study of brain damage. *Journal of Neurosurgery*. 1972;36:255-265

16. Hakim S, Adams RD. The special clinical problem of symptomatic hydrocephalus with normal cerebrospinal fluid pressure. Observations on cerebrospinal fluid dynamics. *Journal of Neurological Sciences*. 1965;2:117-126

17. Conner ES, Foley L, Black PM. Experimental normal-pressure hydrocephalus is accompanied by increased transmantle pressure. *Journal of Neurosurgery*.1984;61:322-327

18. Bradley WG , Whittemore AR, Watanabe AS, Davis SJ, Teresi LM, Homyka M. Association of deep white matter infarction with chronic communicating hydrocephalus: Implications regarding the possible origin of normal pressure hydrocephalus. *American Journal of Radiology*. 1991;12: 31-39

19. Clarfield AM. The reversible dementias: Do they reverse? *Annals of Internal Medicine*. 1988;109: 476-486

20. Gleason PL, Black PM, Matsumae M. The neurobiology of normal pressure hydrocephalus. *Neurosurgery Clinics of North America*. 1993;4:667-675

21. M Anderson. Normal pressure hydrocephalus. *British Medical Journal Clinical Research*. 1986;293:837-838

22. Vanneste JA. Three decades of normal pressure hydrocephalus: Are we wiser now? *Journal of Neurology, Neurosurgery and Psychiatry*. 1994;57:1021-1025

23. Pickard JD. Normal pressure hydrocephalus - to shunt or not to shunt. In: (eds) Warlow C, Garfield J. *Dilemmas in the Management of the Neurological Patient*. Edinburgh: Churchill Livingstone, 207-214, 1984

24. Larsson A, Wikkelso C, Bilting M, Stephensen H. Clinical parameters in 74 consecutive patients shunt operated for normal pressure hydrocephalus. *Acta Neurologica Scandinavica*. 1991;84:475-482

25. Pickard JD. Adult communicating hydrocephalus. *British Journal of Hospital Medicine*. 1982;27:35-44

26. Fisher CM. The clinical picture in occult hydrocephalus. *Clinical Neurosurgery*. 1977;24: 270-84

27. Caruso R, Cervoni L, Vitale AM, Salvati M. Idiopathic normal-pressure hydrocephalus in adults: result of shunting correlated with clinical findings in 18 patients and a review of the literature. *Neurosurgical Review*. 1997;20:104-107

28. Gjerris F, Borgesen SE, Schmidt j, Sorensen PS. Resistance to CSF outflow in patients with normal pressure hydrocephalus. In (eds) Gjerris F, Borgesen SE, Sorensen *PS .Outflow of Cerebrospinal Fluid*. Munksgaard: Copenhagen, 329-338, 1989.

29. Sussman JD, Sarkies N, Pickard JD. Benign intracranial hypertension. In (ed) Cohadon P. *Advances and Technical Standards in Neurosurgery Vol 24*. Springer Verlag, Berlin, 1998.

30. Drake JM, Saint-Rose CH (eds). *The Shunt Book*. Oxford: Blackwell Science, 23-92, 1995

2. REFERENCES- CHAPTER 2

1. Pickard JD. Normal pressure hydrocephalus - to shunt or not to shunt. In: (eds) Warlow C, Garfield J. *Dilemmas in the Management of the Neurological Patient.* Edinburgh: Churchill Livingstone, 207-214, 1984

2. Larsson A, Wikkelso C, Bilting M, Stephensen H. Clinical parameters in 74 consecutive patients shunt operated for normal pressure hydrocephalus. *Acta Neurologica Scandinavica.* 1991;84:475-482,

3. Weiner HL, Constantini S, Cohen H, Wisoff JH. Current treatment of normal pressure hydrocephalus: comparison of flow regulated and differential pressure valves. *Neurosurgery.* 1995;37: 877-884

4. Vanneste J. van Acker R. Normal pressure hydrocephalus: did publications alter management? *Journal of Neurology, Neurosurgery & Psychiatry.* 1990;53:564-68

5. Katzman R, Hussey F. A simple constant/infusion manometric test for measurement of CSF absorption. *Neurology.* 1970;20: 534-44

6. Kosteljanetz M. Intracranial Pressure: cerebrospinal fluid dynamics and pressure-volume relations (thesis). *Acta Neurologica Scandinavica.* 1987;75 (suppl 111):1-23

7. Marmarou, A, Shulman, K, Rosende RM. A non-linear analysis of CSF system and intracranial pressure dynamics. *Journal of Neurosurgery.* 1978;48: 332-44

8. Davson H, Hollingworth G, Segal MB. The mechanism of drainage of the cerebrospinal fluid. *Brain.* 1970;93:665-78

9. Ekstedt, J. CSF hydrodynamic studies in man. Method of constant pressure CSF infusion. *Journal of Neurology, Neurosurgery and Psychiatry*. 1977;40:105-19

10. Portnoy HD, Croissant PD. Pre-and post operative cerebrospinal fluid absorption studies in patients with myelomeningocele shunted hydrocephalus. *Child's Brain*. 1978;4: 47-64

11. Børgesen SE, Gjerris F, Srensen SC. The resistance to cerebrospinal fluid absorption in humans. *Acta Neurologica Scandinavica*. 1978;57:88-96

12. Gjerris F, Børgesen SE, Hoppe E, Boesen F, Nordenbo AM. The conductance to outflow of CSF in adults with high pressure hydrocephalus. *Acta Neurochirurgica (Wien)*. 1982; 64: 59-67

13. Gjerris, F, Srensen, PS, Vorstrup, S, Paulson, OB. Conductance to cerebrospinal fluid outflow, intracranial pressure and cerebral blood flow in patients with benign intracranial hypertension. *Annals of Neurology*. 1985;17: 158-62

14. Czosynka M, Wollk-Laniewski D, Darwaj P. Software for neurosurgery intensive care. In: (eds) Hoff JT and Betz, AL. *Intracranial Pressure VII*. Berlin: Springer Verlag, 84-87, 1989

15. Czosnyka M, Whitehouse H, Smielewski P, Simac S, Pickard JD. Testing of cerebrospinal compensatory reserve in shunted and non-shunted patients: a guide to interpretation based on an observational study. *Journal of Neurology, Neurosurgery & Psychiatry*. 1996;60:549-58

16. Børgesen, SE, Gjerris, F. The predictive value of conductance to outflow of CSF in normal hydrocephalus. *Brain*. 1982;105: 65-86

17. Børgesen SE, Albeck, MJ, Gjerris F, Czosnyka M, Laniewski P. Computerised infusion tests compared to conventional lumbar-ventricular perfusion for measurement of resistance to CSF outflow. *Acta Neurochirurgica (Wien)*.1992;119:12-16

18. Sullivan HG, Miller JD, Griffith RL, Carter W, Rucker S. Bolus versus steady-state infusion for determination of CSF outflow resistance. *Annals of Neurology*. 1979;5: 228-38

19. Delwel EJ, de Jong DA, Avezaat CJ, van Eijndhoven JH. CSF Dynamics in patients with suspected normal pressure hydrocephalus. In: (eds) Hoff JT and Betz, AL. *Intracranial Pressure VII*. Berlin: Springer Verlag, 379-382, 1989

20. Kosteljantetz M, Westergaard L, Kaalund J, Nehen AM. The significance of outflow resistance measurements in the prediction of outcome after CSF-shunting in patients with normal pressure hydrocephalus. In: (eds) Hoff JT and Betz, AL. *Intracranial Pressure VII*. Berlin: Springer Verlag, 383-385, 1989

21. Vorstrup S, Christensen J, Gjerris F, Sorenson PS, Thomsen AM, Paulson OB. Cerebral blood flow in patients with normal pressure hydrocephalus before and after shunting. *Journal of Neurosurgery*. 1987;66: 379-387

22. Vanneste J, Augustijn P, Tan WF, Dirven C. Shunting normal pressure hydrocephalus: the predictive value of combined CT and clinical data. *Journal of Neurology Neurosurgery and Psychiatry*. 1993;56:251-256

23. Maksymowicz W, Czosnyka M, Zabolotny W, Koszewski W. Communicating hydrocephalus versus brain atrophy- is a reliable differentiation possible. *Acta Neurochirurgica*. 1998;71:

24. Boon AJ, Tans JT, Delwel EJ, Egler-Peerdeman SM, Hanlo PW, Wurzer JA, Avezaat CJ, de Jong DA, Gooskens RH, Hermans J. Does CSF outflow resistance predict the response to shunting in patients with normal pressure hydrocephalus. *Acta Neurochirurgica.* 1998;71:331-333

25. Kontos HA. Validity of cerebral arterial blood calculations from velocity measurements. *Stroke.* 1989;20:1-3

26. Evans DH, Barrie WW, Asher MJ, Bentley S, Bell PR. The relationship between ultrasonic pulsatility index and proximal arterial stenosis in a canine model. *Circulation Research.* 1980;46:470-475

27. Giller CA, Hodges K, Batjer HH. Transcranial Doppler pulsatility in vasodilation and stenosis. *Journal of Neurosurgery.* 1990;72:901-906

28. Legarth J, Nolsoe C. Doppler blood velocity waveforms and the relation to peripheral resistance in the brachial artery. *Journal of Ultrasound in Medicine.* 1990;9:449-453

29. Risberg, J, Lundberg, N, Ingvar DH. Regional cerebral blood volume during acute transient rises of the intracranial pressure (plateau waves). *Journal of Neurosurgery.* 1969;31:303-310

30. Nelson RJ, Czosnyka M, Pickard JD, Maksymowicz W, Perry S, Martin JL, Lovick AH. Experimental aspects of cerebrospinal haemodynamics: The relationship between blood flow velocity wave form and cerebral autoregulation. *Neurosurgery.* 1992;31:705-710

31. Czosnyka M, Guazzo E, Iyer V, Kirkpatrick P, Smielewski P, Whitehouse H, Pickard JD. Testing of cerebral autoregulation in head injury by waveform analysis of blood flow velocity and cerebral perfusion pressure. *Acta Neurochirurgica.* 1994;[Suppl] 60:468-71

32. Chan KH, Miller D, Piper IR. Cerebral blood flow at constant cerebral perfusion pressure but changing arterial and intracranial pressure: Relationship to autoregulation. *Journal of Neurosurgical Anaesthesiology*. 1992;4:188-193

33. Pople IK, Quinn MW, Bayston R, Hayward RD. The Doppler pulsatility index as a screening test for blocked ventriculo-peritoneal shunts. *European Journal of Paediatric Surgery*. 199;1 [Suppl 1]:27-29

34. Quinn MW, Pople IK. Middle cerebral artery pulsatility in children with blocked cerebrospinal fluid shunts. *Journal of Neurology, Neurosurgery and Psychiatry*. 1992;55:325-327

35. Chadduck WM, Crabtree HM, Blankenship JB, Adametz J. Transcranial Doppler ultrasonography for the evaluation of shunt malfunction in paediatric patients. *Child's Nervous System*. 1991;7:27-30

36. Hanlo PW, Gooskens RH, Nijhuis IJ, Faber JA, Peters RJ, van Huffelen AC, Tulleken CA, Willemse J. Value of transcranial Doppler indices in predicting raised ICP in infantile hydrocephalus. A study with review of the literature. *Child's Nervous System*. 1995;11:595-603

37. Newell DW. Transcranial Doppler ultrasonography. *Neurosurgery Clinics of North America*. 1994;5:619-31

38. Hanlo PW, Peters RJ, Gooskens RH, Heethaar RM, Keunen RW, van Huffelen AC, Tulleken CA, Willemse J. Monitoring intracranial dynamics by transcranial Doppler - a new Doppler index: trans systolic time. *Ultrasound in Medicine & Biology*. 1995;21:613-21

39. Gruzhas E, Vilcinis R, Klumby L, Shidishki J. Transcranial Doppler indicators of cerebrospinal system visco-elastic properties. *Acta Neurochirurgica*. 1998;71:

40. Qureshi AI, Razumovsky AY, Williams MA, Ulatowoski JA, Hanley DF. Cerebral haemodynamics in patients with normal pressure hydrocephalus. Conference proceedings: Tenth International Symposium on Intracranial Pressure and Neuromonitoring in Brain Injury. Virginia USA, May 1997

41. Reid A, Marchbanks RJ, Bateman DE, Martin AM, Brightwell AP, Pickard JD. Mean intracranial pressure monitoring by non-invasive audiological technique: a pilot study. *Journal of Neurology, Neurosurgery and Psychiatry*. 1989;52: 610-612

42. Moss SM, Marchbanks RJ, Burge DM. Long term assessment of intracranial-pressure using the Tympanic Membrane Displacement technique. *European Journal of Paediatric Surgery*. 1991;1 [Suppl 1]: 25-26

43. Samuel M, Burge DM, Marchbanks RJ. Quantitative assessment of intracranial pressure by the tympanic membrane displacement audiometric technique in children with shunted hydrocephalus. *European Journal of Paediatric Surgery*. 1998;8:200-207

44. Samuel M, Burge DM, Marchbanks RJ. Tympanic membrane displacement testing in regular assessment of intracranial pressure in eight children with shunted hydrocephalus. *Journal of Neurosurgery*. 1998;88:983-995

45. Czosnyka M, Batorski L, Laniewski P, Maksymowicz W, Koszewski W, Zaworski W. A computer system for the identification of cerebrospinal compensatory model. *Acta Neurochirurgica (Wien)*. 1990;105:112-116

46. Eksted J. CSF hydrodynamic studies in man. *Journal of Neurology, Neurosurgery and Psychiatry*. 1978;41:345-353

47. Goh D, Minns RA, Pye SD. Transcranial Doppler (TCD) ultrasound as a non-invasive means of monitoring cerebro-haemodynamic changes in hydrocephalus. *European Journal of Paediatric Surgery*. 1991;1:14-17

48. Iacopino DG, Zaccone C, Molina D, Todaro C, Tomasello F, Cardia E. Intraoperative monitoring of cerebral blood flow during ventricular shunting in hydrocephalic paediatric patients. *Child's Nervous System*. 1995;11:483-486

49. Nadvi SS, Du Trevou MD, Van Dellen JR, Gouws E. The use of transcranial Doppler ultrasonography as a method of assessing intracranial pressure in hydrocephalic children. *British Journal of Neurosurgery*. 1994;8:573-577

50. Chan KH, Miller DM, Dearden NM, Andrews PJD, Midgley S. The effects of changes in cerebral perfusion pressure upon middle cerebral artery blood flow velocity and jugular bulb venous oxygen saturation after severe brain injury. *Journal of Neurosurgery*. 1992;77:55-61

51. Czosnyka M, Richards H, Pickard JD, Harris N, Iyer V. Frequency dependent properties of cerebral blood transport - an experimental study in anaesthetised rabbits. *Ultrasound in Medicine and Biology*. 1994;20:391-399

52. Czosnyka M, Richards H, Kirkpatrick P, Pickard JD. Assessment of cerebral autoregulation with ultrasound and laser Doppler waveforms - an experimental study in anaesthetised rabbits. *Neurosurgery*.1994;35:287-292

53. Meyer JS, Tachibana H, Hardenberg JD, Dowell RE, Kitagawa Y, Morttel KF. Normal pressure hydrocephalus influence on cerebral haemodynamic and cerebrospinal fluid pressure- chemical autoregulation. *Surgical Neurology*. 1984;21:195-203

54. Tanaka A, Kimura M, Nakayama Y, Yoshinaga S, Tomonaga M. Cerebral blood flow and autoregulation in normal pressure hydrocephalus. *Neurosurgery*. 1997;40:1161-1165

55. Strandgaard S, Jones JV, Mackenzie ET, Harper AM. Upper limit of cerebral blood autoregulation in experimental renovascular hypertension in the baboon. *Circulation Research*. 1975;37:164-167

56. Short D. The vascular fault in chronic hypertension with particular reference to the role of medial hypertrophy. *Lancet*. 1966;1:1302-1304

57. Xie P, Chapleau , Mc Dowell T, Hajduczok G, Abbond FM. Mechanisms of decreased barroreceptor activity in chronic hypertensive rabbits. *Journal of Clinical Investigation*. 1990;86:625-630

58. Kinoshita K, Katayama Y, Hirayama T, Maejima S, Takashi T. Changes in jugular oxygen saturation associated with intracranial pressure waves.*Acta Neurochirurgica*. 1998;71:

59. Orbist W, Langfitt T, Jaggi J, Cruz J, Gennarelli G. Cerebral blood flow and metabolism in comatosed patients with acute head injury. *Journal of Neurosurgery*. 1984;61:241-253

60. Robertson C. Comparison of methods for ICP waveform analysis with intracranial hypertension in head injured patients. In: (eds) Avezaat CJJ, van Eijndhoven JHM, Maas AIR, Tans JTJ. *Intracranial Pressure VIII*. Berlin: Springer Verlag, 348-355, 1993

61. Rafferty C. Changes in jugular bulb oxygen saturation and associated changes in intracranial pressure. In: (eds) Avezaat CJJ, van Eijndhoven JHM, Maas AIR, Tans JTJ. *Intracranial Pressure VIII.* Berlin: Springer Verlag, 418-423, 1993

62. Pickard JD. Adult communicating hydrocephalus. *British Journal of Hospital Medicine* 1982;27:35-43

63. Pickard JD, Teasdale G, Matheson M, Lindsey K, Galbrith S, Wyper D, Macpherson P. Intraventricular pressure waves - the best predictive test for shunting in normal pressure hydrocephalus. In (eds) Shulman K, Marmarou A, Miller JD, Becker DB, Hochwald GM, Brock M. *Intracranial Pressure IV.* Berlin: Springer Verlag, 489-500, 1980

64. Goh D, Minns RA, Pye S, Steers J. Continuous intraventricular pressure and simultaneous cerebral blood flow velocity (CBFV) measurements during sleep in hydrocephalic children. The Eighth International Symposium on Intracranial Pressure 1991; Rotterdam (Abst 221).

65. Newell DW, Strooss R, Aaslid R, Reulen HJ. Spontaneous fluctuations in cerebral blood flow as a cause of B-waves. The Eighth International Symposium on Intracranial Pressure 1991; Rotterdam (Abst 127).

66.Czosnyka Z, Czosynka M, Copeman J, Smielewski P, Piechnik S, Whitehouse H, Pickard JD. Autoregulation of cerebral blood flow in patients with suspected normal pressure hydrocephalus. Abstract submitted to Brain 99, 1999

67. Czosnyka M. Smielewski P. Kirkpatrick P. Menon DK. Pickard JD. Monitoring of cerebral autoregulation in head-injured patients. *Stroke.* 1996;27:829-834.

3. REFERENCES - CHAPTER 3

1. Pickard JD, Teasdale G, Matheson M, Lindsey K, Galbrith S, Wyper D, Macpherson P. Intraventricular pressure waves - the best predictive test for shunting in normal pressure hydrocephalus. In (eds) Shulman K, Marmarou A, Miller JD, Becker DB, Hochwald GM, Brock M. *Intracranial Pressure IV*. Berlin: Springer Verlag, 489-500, 1980

2. Symon L, Dorsch NWC. Use of long term intracranial pressure measurement to assess hydrocephalic patients prior to shunt surgery. *Journal of Neurosurgery*. 1975; 42:258-73

3. Pickard JD. Adult communicating Hydrocephalus. *British Journal of Hospital Medicine*. 1982;27:35-44

4. Graff-Radford NR, Godersky JC, Jones MP. Variables predicting outcome in symptomatic hydrocephalus in the elderly. *Neurology*. 1989;39:1601-1604

5. Rechtshaffen A, Kales A. *A manual of standardized terminology, techniques and scoring system for sleep stages of human subjects*. Public Health Service, U.S. Government Printing Office, Washington D.C. 1968

6. Kushinsky W. Coupling of function, metabolism, and blood flow in the brain. *Neurosurgical Review*. 1991, 14:163-168

7. Kety SS. The measurement of cerebral blood flow by means of inert diffusable tracers. *Keio Journal of Medicine*. 1994;43:9-14

8. Sakia F, Meyer JS, Karacan I Derman S, Yamamoto M. Normal human sleep: regional cerebral hemodynamics. *Annals of Neurology*. 1980;7:471-478

9. Townsend RE, Prinz PN, Orbst WD. Human cerebral blood flow during sleep and waking. *Journal of Applied Physiology*. 1973;35:620-625

10. Meyer JS, Amano T, Karacan I. Changes in LCBF measured by CT scan during REM and non-REM human sleep. Journal of Cerebral Blood Flow and Metabolism 1981;(suppl 1):S465-466

11. Masden PL, Holm S, Vorstrup S, Friberg L, Lassen NA, Wildschiødtz G. Human regional cerebral blood flow during rapid eye movement sleep. *Journal of Cerebral Blood Flow and Metabolism.* 1991;11:502-507

12. Braun AR, Balkin TJ, Wesensten NJ, Carson RE, Varga M, Baldwin P, Selbie S, Belenky G, Herscovitch P. Regional cerebral blood flow throughout the sleep-wake cycle. An $H_2{}^{15}O$ PET study. *Brain.* 1997;120:1173-1197

13. Maquet P, Degueldre C, Delfiore G, Aerts J, Peter J-M, Luxen A, Franck G. Functional Neuroanatomy of human slow wave sleep. *The Journal of Neuroscience.* 1997;17:2807-2812

14. Maquet P, Peters J-M, Aerts J, Delfiore G, Degueldre C, Luxen A, Franck G. Functional neuroanatomy of rapid eye-movement sleep during dreaming. *Nature.* 1996;383:163-166

15. Aaslid R, Markwalder T, Nornes H. Non-invasive transcranial Doppler ultrasound recording of flow velocity in basal cerebral arteries. *Journal of Neurosurgery.* 1982;57: 769-774

16. Fischer AQ, Taormina MA, Akhtar B, Chaudhary BA. The effect of sleep on intracranial hemodynamics: A transcranial Doppler study. *Journal of Child Neurology.* 1991;6:155-158

17. Klingelhöfer J, Sander D. Transcranial Doppler Ultrasonography during Sleep. In: (eds) Babikian V, Wechsler L. *Transcranial Doppler Ultrasonography.* Butterworth-Heinemann, 1999.

18. Droste DW, Berger W, Schuler E, Krauss JK. Middle cerebral artery blood flow velocity in healthy persons during wakefulness and sleep: a transcranial Doppler study. *Sleep*. 1993;16: 603-609

19. Mautner D, Haberl RL, Dirnagl U, Villringer A, Schmiedk P, Einhaupl K. B-waves in healthy persons. *Neurological Research*. 1989;11: 194-196

20. Anthony MY, Levene MI, Evans DH, Cyclic variations in cerebral blood flow velocity. *Archives of Disease in Childhood*. 1991;66:12-16

21. Ferrarri F, Kelsall AWR, Rennie JM, Evans DH. The relationship between cerebral blood flow velocity fluctuations and sleep state in normal newborns. *Paediatric Research*.1994;35:50-54

22. Abin HJ, Tilikete S, Barrucand D. Alcohol intake, cigarette smoking and sleep disturbance. *Archives of Internal Medicine*. 1996;156:1028

23. Lobo LL, Tufik S. Effects of alcohol on sleep parameters of sleep deprived healthy volunteers. *Sleep*. 1997;20:52-59

24. Lin AS, Uhde TW, Slate SO, McCann UD. Effects of intravenous caffeine administered to healthy males during sleep. *Depression and Anxiety*. 1997;5:21-28

25. Klingelhofer J, Hajak G, Matzander G, Schulz-Varszegi M, Sander D, Ruther E, Conrad B. Dynamics of cerebral blood flow velocities during normal human sleep. *Clinical Neurology and Neurosurgery* 1995;97:142-148

26. Hajak G, Klingelhofer J, Schulz-Varszegi M, Matzander G, Sander D, Conrad B Ruther E. Relationship between cerebral blood flow velocities and cerebral electrical activity in sleep. *Sleep*. 1994;17:11-19

4. REFERENCES - CHAPTER 4

1. Guillaume J, Janny P. Manometrie intracranienne continue. Interet de la methode et emprimiers resultats. *Revue Neurologique*. 1951;84:131-42

2. Lundberg N. Continuous recording of ventricular fluid pressure in neurosurgical practice. *Acta Psychiatrica et Neurologica Scandinavica*. 1960;36 (Suppl 149)

3. Schroth G, Klose U. Cerebrospinal fluid flow II. Physiology of respiratory-related pulsations. *Neuroradiology* 1992;35:10-15

4. Schroth G, Klose U. Cerebrospinal fluid flow. I Physiology of cardiac-related pulsations. *Neuroradiology* 1992;35:1-9

5. Gaab MR, Heissler. ICP monitoring. *Critical Reviews in Biomedical Engineering* 1984;11:189-250

6. Newell DW, Aaslid R, Stoos R, Seiler R, Reulen HJ. Evaluation of haemodynamic responses in head injury patients with transcranial Doppler monitoring. *Acta Neurochirurgica (Wien)* 1997;139:804-817

7. Norne H, Magnes B, Aaslid R. Observations of intracranial pressure plateau waves. In: (eds) Lundberg N, Ponten U, Brock M. *Intracranial Pressure II*. Springer. Berlin Heidelberg, New York .421-426, 1975

8. Rosner MJ, Becker DP. Origin and evolution of plateau waves: experimental observations and a theoretical model. *Journal of Neurosurgery*. 1984;60:312-324

9. Pickard JD, Teasdale G, Matheson M, Lindsay K, Galbraith S, Wyper D, Macpherson P. Inracranial pressure waves - the best predictive test for shunting in normal pressure

hydrocephalus. In (eds) Shulman K, Marmarou A, Miller JD, Becker DB, Hochwald GM, Brock M. *Intracranial Pressure IV.* Berlin: Springer Verlag, 498-500, 1980

10. Symon L, Dorsch NWC. Use of long term intracranial pressure measurement to assess hydrocephalic patients prior to shunt surgery. *Journal of Neurosurgery.* 1975;42:258-73

11. Pickard JD. Adult communicating hydrocephalus. *British Journal of Hospital Medicine.* 1982;27:35-44

12. Graff-Radford NR, Godersky JC, Jones MP. Variables predicting outcome in symptomatic hydrocephalus in the elderly. *Neurology.* 1989;39:1601-1604

13. Symon L, Dorsch NWC. Pressure waves in so-called low-pressure hydrocephalus. *The Lancet.* December 16th 1972, 1291-1292

14. Børgesen SE, Gjerris F. The predictive value of conductance to outflow of CSF in normal pressure hydrocephalus. *Brain.* 1982;105:65-86

15. Gjerris F, Børgesen SE, Schmidt K, Sorensen PS, Gyring J. Measurement of conductance to cerebrospinal fluid outflow by the steady-state perfusion method in patients with normal or increased intracranial pressure. In: (eds) Miller JD, Teasdale GM, Rowan JO, Galbraith SL, Mendelow AD. *Intracranial pressure VI.* Berlin. Springer Verlag. 411-416. 1986

16. Miller JD, Pickard JD. Intracranial volume/pressure in patients with head injury. *Injury* 1974;52:265-268

17. Sahuquillo J, Rubio E, Codina A, Molins A, Guitart LM, Poca MA, Chasampi A. Reappraisal of the Intracranial pressure and cerebrospinal fluid dynamics in patients with the

so-called normal pressure hydrocephalus syndrome. *Acta Neurochirurgica (Wein).* 1991;112:50-61

18. Castel JP, Dartigues JF, Vandendriesche M. Pathological intracranial pressure waves in Arnold Chiari malformations. In: (eds) Shulman K, Marmarou A, Miller JD, Becker DB, Hochwald GM, Brock M. *Intracranial Pressure IV.* Berlin: Springer Verlag. 569-574. 1980

19. Wilkinson H, Schuman N, Ruggiero J. Nonvolumetric methods of detecting impaired intracranial compliance or reactivity. *Journal of Neurosurgery.* 1979;50:758-767

20. Drinagl U, Garner C, Haberl R, Mautner D, Schmiedek P, Einhaupl KM. Correlation between B waves and intracranial pressure-volume relationships. In: (eds) Hoff JT, Betz AL. *Intracranial pressure VII.* Berlin. Springer Verlag Heidlberg , 213-216,1989

21. Droste DW, Berger W, Schuler E, Krauss JK. Middle cerebral artery blood flow velocity in healthy persons during wakefulness and sleep: a transcranial Doppler study. *Sleep.* 1993;16: 603-609

22. Mautner D, Haberl RL, Dirnagl U, Villringer A, Schmiedk P, Einhaupl K. B-waves in healthy persons. *Neurological Research.* 1989;11:194-196

23. Anthony MY, Levene MI, Evans DH. Cyclic variations in cerebral blood flow velocity. *Archives of Disease in Childhood.* 1991;66:12-16

24. Ferrarri F, Kelsall AWR, Rennie JM, Evans DH. The relationship between cerebral blood flow velocity fluctuations and sleep state in normal newborns. *Paediatric Research* 1994;35:50-54

25. Krauss JK, Droste DW, Bohus M, Regel JP, Scheremet, Riemann D, Seeger W. The relationship of intracranial pressure B waves to different sleep stages in patients with suspected normal pressure hydrocephalus. *Acta Neurochirugica (Wien)* 1995;136:195:-203

26. Kuchiwaki H, Kaegeyama N, Hirai N, Takada S, Inao S, Terashima N, Shiguri H. A biological rhythm in a patient with normal pressure hydrocephalus - comparative studies in pre and post operative patients by a polygraphy. *Brain & Nerve.* 1984;36:911-916

27. Kristensen B, Malm J, Rabben OK, Rabben T. The association of idiopathic adult hydrocephalus syndrome with sleep apnea. In: (eds) Nagai H, Kamiya K, Ishii S. *Intracranial Pressure IX.* Springer-Verlag, 1994

28. McNamara ME, Millman RP, Epstein MH, Fogel BS. The association of normal pressure hydrocephalus with obstructive sleep apnea. *Journal of Geriatric Psychiatry and Neurology.* 1992;5:238-240

29. Kristensen B, Malm J, Rabben T. Effects of transient and persistent cerebrospinal fluid drainage on sleep disordered breathing in patients with idiopathic adult hydrocephalus syndrome. *Journal of Neurology, Neurosurgery and Psychiatry.* 1998;654:497-501

30. Newell DW, Aaslid R, Stooss R. Reulen. Spontaneous fluctuations in cerebral blood flow as a cause of B Waves. In : (eds) Avezaat CJ, van Eijndhoven JHM, Tans JTJ *Intracranial Pressure VIII.* Berlin. Springer. 424-427, 1993

31. Børgesen SE, Espersen JO. The correlation between A-waves and B-waves and arterial CO2 tension. In: (eds) Miller JD, Teasdale GM, Rowan JO, Galbraith SL, Mendelow AD. *Intracranial pressure VI.* Berlin. Springer Verlag. 1986

32. Maede M, Takahashi K, Miyazaki M, Ishii S. The role of the central monoamine system and the cholinoceptive Pontine area on the oscillation of ICP " pressure waves". In: (eds) Miller JD, Teasdale GM, Rowan JO, Galbraith SL, Mendelow AD. *Intracranial pressure VI.* Berlin. Springer Verlag. 1986

33. Higashi S, Yamamoto S, Hashimoto M, Fujii H, IIto H, Kogure Y, Tokuda K. The role of vasomotor centre and adrenergic pathway in B waves. In (eds) JT Hoff, AL Betz *Intracranial pressure VII.* Berlin, Springer Verlag. 220-224, 1989.

34. Auer LM, Sayama I Intracranial pressure oscillations caused by oscillations in cerebrovascular volume. *Acta Neurochirurgica.* 1983;68:93-100

35. Czosnyka M, Whitehouse H, Smielewski P, Simac S, Pickard JD. Testing of cerebrospinal compensatory reserve in shunted and non shunted patients: a guide to interpretation based on an observational study. *Journal of Neurology, Neurosurgery and Psychiatry* 1996;60:549-558

36. Czosnyka M, Batorski L, Laniewski P, Maksymowicz W, Kosewski W, Zaworski W. A computerised system for the identification of the cerebrospinal compensatory parameter. *Acta Neurochirurgica (Wien)* 1990; 105:112-116

37. Czosnyka M. Wollk-Laniewski P. Batorski L. Zaworski W. Analysis of intracranial pressure waveform during infusion test. *Acta Neurochirurgica.* 1988;93:140-5

38. Czosnyka M. Guazzo E. Whitehouse H. Smielewski P. Czosnyka Z. Kirkpatrick P. Piechnik S. Pickard JD. Significance of intracranial pressure waveform analysis after head injury. *Acta Neurochirurgica.* 1996;138:531-41

39. Czosnyka M. Price DJ. Williamson M. Monitoring of cerebrospinal dynamics using continuous analysis of intracranial pressure and cerebral perfusion pressure in head injury. *Acta Neurochirurgica.* 1994;126:113-9

40. Nelson RJ. Czosnyka M. Pickard JD. Maksymowicz W. Perry S. Martin JL. Lovick AH. Experimental aspects of cerebrospinal haemodynamics: the relationship between blood flow velocity waveform and cerebral autoregulation. *Neurosurgery.* 1992;31:705-9. Discussion pages 709-10, 1992.

5. REFERENCES - CHAPTER 5

1. van Swieten JC, van den Hout JHW, van Ketel BA, Hijdra A, Wokke JHJ, van Gijn J. Periventricular lesions in the white matter on magnetic resonance imaging in the elderly. *Brain*. 1991;114:761-774

2. Kunz U, Heintz P, Ehrenheim C, Stolke D, Dietz H, Hundeshagen H. MRI as the primary diagnostic instrument in normal pressure hydrocephalus. *Psychiatry Research*. 1989;29:287-288

3. Schroth G, Klose U. MRI of CSF flow in normal pressure hydrocephalus. *Psychiatry Research*. 1989;29:289-290

4. Frank E, Buonocore M, Hein L. The use of magnetic resonance imaging to assess slow fluid flow in a model cerebrospinal fluid shunt system. *British Journal of Neurosurgery*. 1990;4:53-58

5. Condon BR, Patterson J, Wyper D, Hadley DM, Teasdale G, Grant R, Jenkins A, Macpherson P, Rowan J. A quantitative index of ventricular and extraventricular intracranial volumes using MR imaging. *Journal of Computer Assisted Tomography*. 1986;10(5):784-792

6. Holodny AI, Waxman R, George AE, Rusinek H, Kalnin A, de Leon ME. Differential diagnosis of normal-pressure hydrocephalus and Alzheimer disease: Significance of perihippocampal fissures. *American Journal of Neuroradiology*. 1998;19:813-819

7. Jack CR, Mokri B, Laws ER, Houser OW, Baker HL, Petersen RC. MR findings in normal pressure hydrocephalus: Significance and comparison with other forms of dementia. *Journal of Computer Assisted Tomography*. 1987;11: 923-931

8. Krauss JK, Droste DW, Vach W, Regel JP, Orszagh M, Borremans JJ, Tietz A, Seegar W. Cerebrospinal fluid shunting in idiopathic normal-pressure hydrocephalus of the elderly: effect of periventricular and deep white matter lesions. *Neurosurgery*. 1996;29:292-299

9. Krauss JK, Regel JP, Vach W, Orszagh M, Jungling FD, Bohus M, Droste DW. White matter lesions in patients with idiopathic normal pressure hydrocephalus and in an aged-matched control group: A comparative study. *Neurosurgery*. 1997;40:491-495

10. Bradley WG, Whittemore AR, Watanabe AS, Davis SJ, Teresi LM, Homyka M. Association of deep white matter infarction with chronic communicating hydrocephalus: Implications regarding the possible origin of normal pressure hydrocephalus. *American Journal of Radiology*. 1991;12: 31-39

11. Bradley WG, Pathopysiological Correlates of Signal alteration. In: (eds) Brant-Zawadzki M, Norman D. *Magnetic Resonance Imaging of the Central Nervous System*. New York: Raven Press, 1987

12. Vanneste J. Three decades of normal pressure hydrocephalus: Are we wiser now? *Journal of Neurology, Neurosurgery and Psychiatry*. 1994;57: 1021-1025

13. Drake JM, Potts G, Lemaire C. Magnetic resonance imaging of Silastic-Induced canine hydrocephalus. *Surgical Neurology*. 1989;31: 28-40

14. Zimmerman RD, Flemming CA, Lee BC, Saint-Louis LA, Deck MD. Periventricular hyperintensity as seen by magnetic resonance: prevalence and significance. *American Journal of Neuroradiology*. 1986;146:443-450

15. Revesz T, Hawkins CP, du Boulay EPGH, Barnard RO, McDonald WI. Pathological findings correlated with magnetic resonance imaging in subcortical arteriosclerotic encephalopathy (Binswangers disease). *Journal of Neurology, Neurosurgery and Psychiatry*. 1989;52: 1337-1344

16. Marshall VG, Bradley WG, Marshall CE, Boohpat T, Rhodes RH. Deep white matter infarction: correlation of MR imaging and histopathological findings. *Radiology*. 1988;167:517-522

17. Kawamura J, Meyer JS, Ichijo M, Kobari M, Terayma Y, Weathers S. Correlations of leuko-araiosis with cerebral atrophy and perfusion in elderly normal subjects and demented patients. *Journal of Neurology, Neurosurgery and Psychiatry*. 1993;56:182-187

18. Kirkpatrick JB, Hayman LA. White- matter lesions in MR imaging of clinically healthy brains of elderly subjects: Possible pathologic basis. *Radiology*. 1987;162: 509-511

19. Munoz DG, Hastak SM Harper B, Lee D, Hachinski VC. Pathologic correlates of increased signals of the centrum ovale on magnetic resonance imaging. *Archives Neurology*. 1993;50:492-497

20. van Swieten JC, van den Hout JHW, van Ketel BA, Hijdra A, Wokke JHJ, van Gijn J. Periventricular lesions in the white matter on magnetic resonance imaging in the elderly. *Brain*. 1991;114:761-774

21. Hakim S, Venegas JG, Burton JD. The physics of the cranial cavity, hydrocephalus and normal pressure hydrocephalus: mechanical interpretation and mathematical model. *Surgical Neurology*. 1976;5:187-210

22. Brant- Zawadzki M, Fein G, van Dyke C, Kiernan R, Davenport L. MR imaging of the ageing brain : Patchy white-matter lesions and dementia. *American journal of Neuroradiology*. 1985;6: 675-682

23. Lui CK, Miller BL, Cummings JL, Mehriner CM, Goldberg MA, Howng SL, Benson DF. A quantitative MRI study of vascular dementia. *Neurology*. 1992;42:138-143

24. A van Dam, JD Foley. *Fundamentals of Interactive Computer Graphics*. Reading, Mass. Addison Wesley Publishing Company. Chapter 11, 1982

25. Pickard JD, Newton H, Greene A, Richards HK, Lovick AH, Lang DA, Hoare RD. A prospective study of idiopathic normal pressure hydrocephalus - guidelines for outpatient investigation. *Journal of Neurology, Neurosurgery and Psychiatry*. 1992;55:517-518

26. Kristensen B, Malm J, Fagerlund M, Hietala S-O, Johansson B, Ekstedt J, Karlsson T. Regional cerebral blood flow, white matter abnormalities, and cerebrospinal hydrodynamics in patients with idiopathic adult hydrocephalus syndrome. *Journal of Neurology, Neurosurgery and Psychiatry*. 1996;60:282-288

26a. Boon AJ, Tans JTJ, Delwel EJ, Egeler-Peerdeman SM, Hanlo PW, Wurzer HAL, Hermans J. Dutch normal pressure hydrocephalus study: the role of cerebrovascular disease. *Journal of Neurosurgery*. 1999;90:221-226.

27. Kertesz A, Black SE, Tokar G, Benke T, Carr T, Nicholson L. Periventricular and subcortical hyperintensities on magnetic resonance imaging. *Archives of Neurology*. 1988;45:404-408

28. Mori K, Handa H, Murrata T, Nakano Y. Periventricular lucency in computed tomography. *Journal of Computer Assisted Tomography*. 1980;4:204-209

29. Borgesen SE, Gjerris F. The predictive value of conductance to outflow of CSF in normal pressure hydrocephalus. *Brain*. 1982;105:65-86

30. Wikkelso, Anderson H, Blomstrand C, Matousek M, Svendsen P. Computed tomography of the brain in the diagnosis of and prognosis in normal pressure hydrocephalus. *Neuroradiology*. 1989;31:160-165

31. Plante E, Turkstra L. Sources of error in the quantitative analysis of MRI scans. *Magnetic Resonance Imaging*. 1991;9:589-595

6. REFERENCES - CHAPTER 6

1. Hakim S. Biomechanics of Hydrocephalus. *Acta Neurologica Latinoamericana*. 1971;1:1-194

2. Hakim S, Venegas JG, Burton JD. The Physics of the Cranial Cavity, Hydrocephalus and Normal Pressure Hydrocephalus: Mechanical Interpretation and Mathematical Model. *Surgical Neurology*. 1976.;5: 187-210

3. Nagashima T, Tamaki N, Matsumoto S and Seguchi Y: Theoretical Model for Hydrocephalus: Application of the Finite Element Method. In: (eds) JD Miller, GM Teasdale, JO Rowan, SL Galbraith and AD Mendelow. *Intracranial Pressure VI*. Berlin. Springer Verlag, 441-446. 1986

4. Nagashima T, Tamaki N, Matsumoto S, Horwitz B and Seguchi Y: Biomechanics of Hydrocephalus: A new Theoretical Model. *Neurosurgery*. 1987;21:898-904

5. Simon BR, Wu J S-S, Carlton MW, Kazarian LE, France EP, Evans JH, Zienkiewicz OC. Poroelasticdynamic structural models of rehsus spinal motion segments. *Spine*. 1985;10:494-507.

6. Biot MA: General Theory of Three Dimensional Consolidation. *Journal of Applied Physics* 1941;12:1244-1258

7. Terzaghi K, Frolich OK. *Theorie der Setzung von Tonschichten*. Vienna. Dentike. 1936.

8. Bolton M. *A Guide to Soil Mechanics*. Cambridge UK. MD & K Bolton, 1991

9. ANYSYS User Manual, ANSYS Inc.

10. Smith IM, Griffiths DV. *Programming the Finite Element method*. London: John Wiley and sons. 286-294, 1982.

11. Britto AM and Gunn MJ. *Critical State Soil Mechanics via Finite Elements*. Ellis Horwood. 1987.

12. FEMGV 5.0: Femsys Ltd, 158 Upper New Walk, Leicester, UK.

13. Roberts M, Hanaway J. *Atlas of the Human Brain in section*. Philadelphia. Lea and Febiger, 1970

14. Pitt V.H. (editor) *Penguin Dictionary of Physics*. 1983

15. Fallanstein GT, Hulce VD. Dynamic mechanical properties of human brain tissue. *Journal of Biomechanics*. 1969;2:217-226

16. Walsh EK, Schettini A. Elastic behavior of brain tissue in vivo. *American Journal of Physiology*. 1976;230:1059-1062

17. Metz H, McElhaney J, Ommaya AK. A comparison of the elasticity of live dead and fixed brain tissue. *Journal of Biomechanics*. 1970;3:453-458

18. Guillaume A, Osmont D, Gaffie D, Sarron JC, Quandieu P. Effects of perfusion on the mechanical behavior of the brain-exposed to hypergravity. *Journal of Biomechanics*. 1997;30:383-9

19. Chopp M, Portnoy HD, Branch C. Hydraulic Model of the cerebrovascular bed: An aid to understanding the volume pressure test. *Neurosurgery*. 1983;13:5-11

20. Walsh EK, Schettini A. Brain Tissue Elasticity and CSF elastance. In (eds) Hoff JT, Betz AL. *Intracranial pressure VII.* Berlin. Springer-Verlag, 271-274, 1989.

21. Wallenfang W. Fries G. Jantzen J.P. Bayer J. Trautmann F. Pathomechaninim of brain edema in experimental intracerebral mass haemorrhage. *Acta Neurochirurgica.* 1988,Suppl. 43:182-185

22. Rosenberg GA, Kyner WT, Estrada E. Bulk flow of brain interstitial fluid under normal and hyperosmolar conditions. *American Journal of Physiology.* 1980;238:F42-49

23. Zee CM. Shapiro K. The visoelasticy of normal and hydrocephalic tissue. In (eds) Hoff JT, Betz AL. *Intracranial pressure VII.* Berlin. Springer-Verlag, 263-265, 1989.

24. Hatashita S, Hoff JT. The effect of craniotomy on the biomechanics of the normal brain. *Journal of Neurosurgery* . 1987;67 : 573-578

25. Penn RD, Bacus JW . The brain as a sponge: A computed tomographic look at Hakim's hypothesis. *Neurosurgery.* 1984;14: 670-675

7. REFERENCES - APPENDIX 1

1. Czosnyka M, Richards H, Kirkpatrick P, Pickard JD. Assessment of cerebral autoregulation with ultrasound and laser Doppler waveforms - an experimental study in anaesthetised rabbits. *Neurosurgery*. 1994;35:287-292

2. Piper IR, Chan KH, Miller JD. Pulsatile cerebral perfusion pressure: significance for cerebral blood flow. *Journal of Neurosurgical Anesthesiology*. 1994;6:223-225

3. Miller JD. Stanek A. Langfitt TW. Concepts of cerebral perfusion pressure and vascular compression during intracranial hypertension. *Progress in Brain Research. 1972;35:411-32*

4. Nelson RJ, Czosnyka M, Pickard JD, Maksymowicz W, Perry S, Martin JL, Lovick AH. Experimental aspects of cerebrospinal haemodynamics: The relationship between blood flow velocity wave form and cerebral autoregulation. *Neurosurgery*. 1992;31:705-710

5. Nelson, RJ, Perry S, Hames TK, Pickard JD. Transcranial Doppler ultrasound studies of cerebral autoregulation and subarachnoid haemorrhage in the rabbit. *Journal of Neurosurgery*. 1990;73:601-610

6. Miller JD, Stanek A, Langfitt TW. Cerebral blood flow regulation during experimental brain compression. *Journal of Neurosurgery*.1973;39:186-96

7. Purves MJ. *The Physiology of the Cerebral Circulation*. Cambridge UK. Cambridge University Press. 1972

8. Meyer JS, Tachibana H, Hardenberg JD, Dowell RE, Kitagawa Y, Morttel KF. Normal pressure hydrocephalus influence on cerebral haemodynamic and cerebrospinal fluid pressure- chemical autoregulation. *Surgical Neurology*. 1984;21:195-203

9.Tanaka A, Kimura M, Nakayama Y, Yoshinaga S, Tomonaga M. Cerebral blood flow and autoregulation in normal pressure hydrocephalus. *Neurosurgery*. 1997;40:1161-1167

10. Graff-Radford NR, Rezai K, Godersky JC, Eslinger P, Damasio H, Kirchner PT. Regional cerebral blood flow in normal pressure hydrocephalus. *Journal of Neurology, Neurosurgery and Psychiatry*. 1987;50:1589-1596

11. Larsson A, Bergh AC, Bilting M, Arlig A, Jacobsson L, Stephensen H, Wikkelso C. Regional cerebral blood flow in normal pressure hydrocephalus: diagnostic and prognostic aspects. *European Journal of Nuclear Medicine*. 1994;21:118-123

12. Kristensen B, Malm J, Fagerlund M, Hietala SO, Johansson B, Ekstedt J, Karlsson T. Regional cerebral blood flow, white matter abnormalities and cerebrospinal fluid hydrodynamics in patients with idiopathic adult hydrocephalus syndrome. *Journal of Neurology, Neurosurgery and Psychiatry*. 1996;60:282-288

13. Shimoda M, Oda S, Shibata M, Masuko A, Sato O. Change in regional cerebral blood flow following glycerol administration predicts result from shunting in normal pressure hydrocephalus. *Acta Neurochirurgica*. 1994;129:171-176

14. Kling P, Fischer J, Brinker T, Heissler HE, Burchert W, Berding G, Knapp WH, Samii M. PET and CBF studies of chronic hydrocephalus: A contribution to surgical indication and prognosis. *Journal of Neuroimaging*. 1998;8:205-209

15. Lee EJ, Hung YC, Chang CH, Pai MC, Chen HH. Cerebral blood flow velocity and vasomotor reactivity before and after shunting surgery in patients with normal pressure hydrocephalus. *Acta Neurochirurgica*. 1998;140:599-605

16. Droste DW, Krauss JK. Simultaneous recording of cerebral spinal fluid pressure and middle cerebral artery flow velocity in patients with suspected symptomatic normal pressure hydrocephalus. *Journal of Neurology, Neurosurgery and Psychiatry*. 1993;56:75-79

17. Strandaard S, Jones JV, Mackenzie ET, Harper AM. Upper limit of cerebral blood autoregulation in experimental neurovascular hypertension in the baboon. *Circulation Research*. 1975;37:164-167

18. Czosnyka M, Guazzo E, Iyer V, Kirkpatrick P, Smielewski P, Whitehouse HE, Pickard JD. Testing of cerebral autoregulation in head injury by waveform analysis of blood flow velocity and cerebral perfusion pressure. *Acta Neurochirurgica*. 1994;suppl. 60:468-471

19. Chan KH, Miller DM, Dearden NM, Andrews PJD, Midgley S. The effects of changes in cerebral perfusion pressure upon middle cerebral artery blood flow velocity and jugular bulb venous oxygen saturation after severe brain injury. *Journal of Neurosurgery*. 1992;77:55-61

20. Stern MD. In vivo evaluation of microcirculation by coherent light scattering. *Nature*. 1975;254:56-58

21. Rosenblum BR, Bonner RF, Oldfield EH. Intraoperative measurement of cortical blood flow adjacent to cerebral AVM using laser Doppler velocimetry. *Journal of Neurosurgery*. 1987;66:396-399

22. Fasano VA, Urciuli R, Bolognese P, Mostert M. Intraoperative use of laser Doppler in the study of cerebral microvascular circulation. *Acta Neurochirurgica*. 1988;95:40-48

23. Haberl RL, Villringer A, Dirnagl U. Applicability of laser Doppler flowmetry for cerebral blood flow monitoring in neurological intensive care. *Acta Neurochirurgica*. 1993;suppl 59:64-68

24. Steinmeier R, Bondar I, Bauhuf C. Assessment of cerebral haemodynamics in comatose patients by laser Doppler flowmetry - preliminary observations. *Acta Neurochirurgica*. 1993;suppl 59:69-73

25. Haberl RL, Heizer ML, Ellis EF. Laser-Doppler assessment of brain microcirculation: effect of local alterations. *American Journal of Physiology*. 1989;256: H1255-H1260

26. Eyre JA, Essex TJH, Flecknell PA, Bartholomew PH, Sinclair JI. A comparison of measurements of cerebral blood flow in the rabbit using laser Doppler spectroscopy and radionuclide labelled microspheres. *Clinical Physics and Physiological Measurement*. 1988;9:65-74

27. Richards HK, Czosnyka M, Kirkpatrick PJ, Pickard JD. Estimation of laser Doppler flux biological zero using basilar artery flow in the rabbit. *American Journal of Physiology*. 1995;268:H213-217

28. Wahlberg E, Olofsson P, Swedenborg J, Fagrell B. Effects of local hyperaemia and edema on the biological zero in laser Doppler fluxmetry (LD). *International Journal of Microcirculation: Clinical Experiments*. 1992;11:157-165

29. Shapira Y, Artru AA, Lam AM. Changes in the rate of formation and resistance to reabsorption of cerebrospinal fluid during deliberate hypotension induced with adenosine or haemorrhage. *Anesthesiology*.1992;76:432-439

30. Foxworthy JC, Artru AA. Cerebrospinal fluid dynamics and brain tissue composition following intravenous infusions of hypertonic saline in anaesthetised rabbits. *Journal of Neurosurgical Anestheasiology*. 1990;2:256-265

31. Donato T, Shapira Y, Artru A, Powers K. Effects of mannitol on cerebrospinal fluid dynamics and brain tissue edema. *Anesthesia and Analgesia.* 1994;78:58-66

32. Schmidt JF, Borgesen SE, Gjerris F. Reproducibility of measurements of resistance to CSF outflow. In (eds) Gjerris F, Borgesen SE, Sorensen PS. *Outflow of Cerebrospinal Fluid, Alfred Benzon Symposium 27.* Copenhagen, 224-229, 1989

33. Borgesen SE. Conductance to outflow of CSF in normal pressure hydrocephalus. Acta Neurochirurgica. 1984;71:1-45.

8. REFERENCES - APPENDIX 2

1. Aaslid R, Markwalder T, Nornes H. Non-invasive transcranial Doppler ultrasound recording of flow velocity in basal cerebral arteries. *Journal of Neurosurgery*. 1982;57:769-774

2. Wells PNT (ed). The Safety of Diagnostic Ultrasound. *British Journal of Radiology Supplement No 20.* Published by: The British Institute of Radiology London 1987.

3. American Institute of Ultrasound in Medicine Bioeffects Committee. Bioeffects considerations for the safety of diagnostic ultrasound. *Journal of Ultrasound in Medicine*. 1988;7 (supplement).

4. Barnett SB, Rott H-D, Ter Haar GR, Ziskin MC, Maeda K. The sensitivity of biological tissue to ultrasound. *Ultrasound in Medicine and Biology*. 1997;23:805-812

5. Williams R. *Ultrasound: Biological Effects and Potential Hazards*. London; Academic Press, 1983.

6. Suslick K. *Ultrasound its Chemical, Physical and Biological effects*. Wiley-VCH 1988.

7. Duck A, Starritt HC. A study of the heating capabilities of diagnostic ultrasound beams. *Ultrasound in Medicine and Biology*. 1994;20:481-492

8. Barnett SB, Kossoff G, Edwards MJ. Is diagnostic ultrasound safe? *The Medical Journal of Australia*. 1994;160:33-37

9. Barnett SB, Ter Haar GR, Ziskin MC, Nyborg WL, Maeda K, Bang J. Current status of research on biophysical effects of ultrasound. *Ultrasound in Medicine and Biology*.1994;20: 205-218

10. National council on Radiation Protection and Measurements. Exposure criteria for medical diagnostic ultrasound: I. Criteria based on thermal mechanisms. NCRP report number 113, 1992

11. Carstensen E, Child S. Ultrasonic heating of the skull. *Journal of the Acoustical Society of America*. 1990;87:1310-1317

12. Duck F. *Physical Properties of Tissue*. London. Academic Press, 1990.